Max-Planck-Institut
für Meteorologie

MAX-PLANCK-GESELLSCHAFT

International Max Planck Research School
on Earth System Modelling

Riverine and coastal ocean contributions to global and regional oceanic cycling of carbon and nutrients

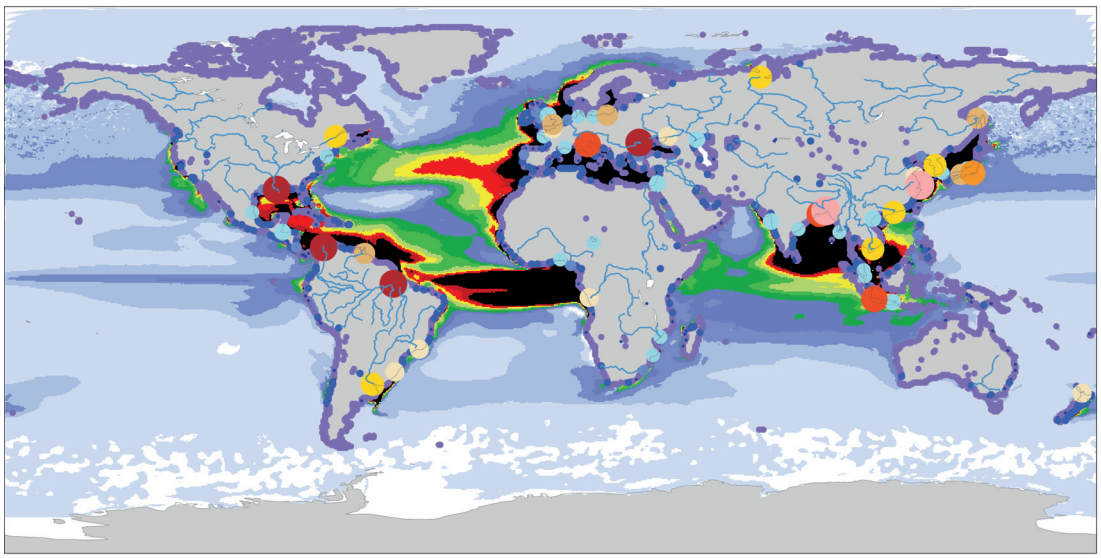

Fabrice Lacroix

Hamburg 2020

Berichte zur Erdsystemforschung
Reports on Earth System Science

225
2020

Hinweis

Die Berichte zur Erdsystemforschung werden vom Max-Planck-Institut für Meteorologie in Hamburg in unregelmäßiger Abfolge herausgegeben.

Sie enthalten wissenschaftliche und technische Beiträge, inklusive Dissertationen.

Die Beiträge geben nicht notwendigerweise die Auffassung des Instituts wieder.

Die "Berichte zur Erdsystemforschung" führen die vorherigen Reihen "Reports" und "Examensarbeiten" weiter.

Notice

The Reports on Earth System Science are published by the Max Planck Institute for Meteorology in Hamburg. They appear in irregular intervals.

They contain scientific and technical contributions, including Ph. D. theses.

The Reports do not necessarily reflect the opinion of the Institute.

The "Reports on Earth System Science" continue the former "Reports" and "Examensarbeiten" of the Max Planck Institute.

Anschrift / Address

Max-Planck-Institut für Meteorologie
Bundesstrasse 53
20146 Hamburg
Deutschland

Tel./Phone: +49 (0)40 4 11 73 - 0
Fax: +49 (0)40 4 11 73 - 298

name.surname@mpimet.mpg.de
www.mpimet.mpg.de

Layout

Bettina Diallo and Norbert P. Noreiks
Communication

Copyright

Riverine and coastal ocean contributions to global and regional oceanic cycling of carbon and nutrients

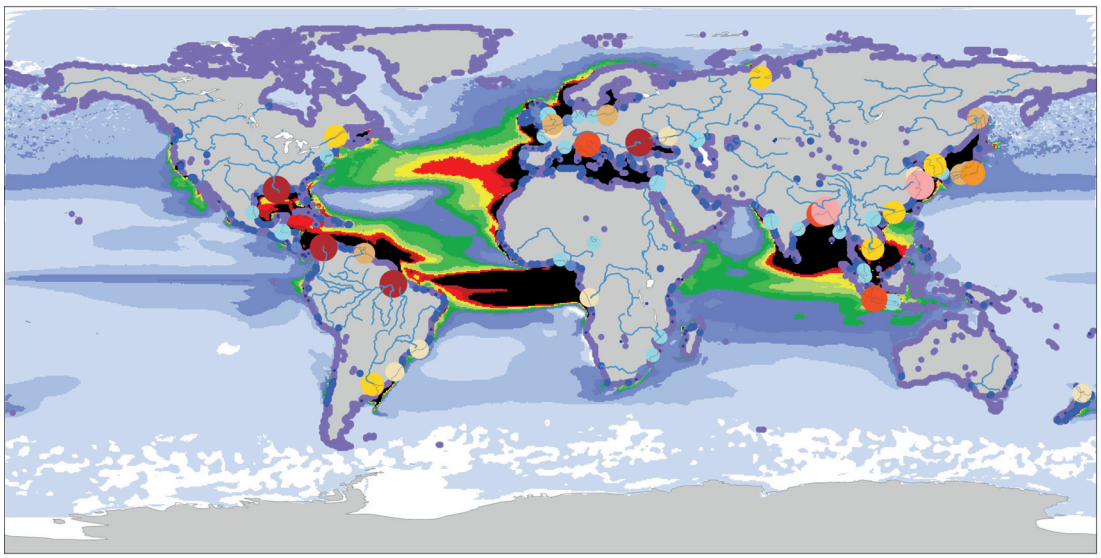

Fabrice Lacroix

Hamburg 2020

Fabrice Lacroix
from Quebec City, Canada

Max-Planck-Institut für Meteorologie
The International Max Planck Research School on Earth System Modelling
(IMPRS-ESM)
Bundesstrasse 53
20146 Hamburg

Université Libre de Bruxelles
Department of Geoscience, Environment and Society (DGES)
Avenue Franklin Roosevelt 50
1050 Bruxelles
Belgien

Tag der Disputation: 08.07.2019

Folgende Gutachter empfehlen die Annahme der Dissertation:
Dr. Tatiana Ilyina
Prof. Dr. Pierre Regnier

The figure on the front age presents major river flows on land, increases of riverine phosphate inputs to the ocean during the 20th century represented by dots on the coastline, and the perturbation net primary production in the ocean.

Berichte zur Erdsystemforschung / Max-Planck-Institut für Meteorologie 225
Reports on Earth System Science / Max Planck Institute for Meteorology 2020

ISSN 1614-1199

UNIVERSITÉ LIBRE DE BRUXELLES

Abstract

Department Geoscience, Environment & Society (DGES)

Doctor of Sciences

Riverine and coastal ocean contributions to global and regional oceanic cycling of carbon and nutrients

by Fabrice Lacroix

Résumé français

Les rivières sont une source importante de components biogéochimiques pour les océans. Les flux de ces composés affectent particulièrement les régions côtières des océans qui sont importantes pour les activités biologique à l'échelle global. Jusqu'à présent, les modèles globaux biogéochimiques des océans ont représenté de manière inadéquate, ou même complètement ignorés les flux de carbone, de nutriments et d'alcalinité provenant des rivières. En particulier, aucun modèle n'a considéré les apports fluviaux de la période préindustrielle, et les flux organiques ont été fortement simplifiés selon leur composition biogéochimique et leur réactivité dans l'océan. Les océans côtiers et leur contribution au cycle du carbone global restent incompris, et jusqu'à présent peu de recherches ont été réalisées sur cet aspect important, et en appliquant des modèles globaux. Finalement, les perturbations anthropogènes des apports fluviaux lors du 20^{e} siècle et leurs conséquences sur l'état physique et biogéochimique des océans côtiers n'ont pas été analysées dans un modèle global qui prenne en compte la circulation tridimensionnelle de l'océan. Ainsi, l'objectif principal de cette thèse a été d'intégrer les apports biogéochimiques des rivieres et ameliorer la representation du cycle du carbone dans la zone cotiere dans un model océanique global.

Dans une première étape, mon travail a visé à combler les lacunes en terme de connaissances concernant les implications à long terme des apports biogéochimiques fluviaux pour le cycle océanique du carbone, en tenant compte de la période préindustrielle. J'ai estimé la contribution des rivières dans les apports préindustrielle et leur distribution spatiale en utilisant les données prédites d'un Modèle du Système Terre, en utilisant une hiérarchie de modèles avancés qui permettent d'estimer l'érosion chimique et le transfert de matériel organique des écosystèmes terrestres à l'océan. Les apports fluviaux ont été ajoutés dans le modèle de biogéochimique océanique HAMOCC. Ce nouveau modèle a permis d'analyser les changements induits dans la production biologique primaire océanique et dans le flux de CO_2 entre l'atmosphère et l'océan, à une échelle globale et régionale. Enfin une synthèse des résultats a été réalisée en évaluant la consommation nette de CO_2 atmosphérique calculée pour les modèles terrestres, et en comparant celle-ci au dégazage de carbone estimé à long terme par le modèle océanique. L'étude prédit un dégazage océanique préindustriel de 0.23 Pg C $yr^{-1,}$ quise presente principalement à proximité de l'embouchure des rivieres. Le modele indiqueaussi un transfert inter-hémisphère de carbone, avec un apport des rivières à l'océan dans l'hémisphère nord, et un transfert de l'hémisphère nord à l'hémisphère sud où un dégazage se produit. De plus, une augmentation de la production biologique primaire causée par les apports des rivières est prédite dans l'Atlantique de l'ouest tropicale (+166 %), dans la Baie du Bengale (+377 %) et dans la mer de Chine orientale (+71 %), en comparaison avec les prédiction d'un modèle ne prenant pas en compte les apports des rivières.

Après l'inclusion des apports fluviaux dans le modèle HAMOCC, la modélisation biogéochimique de l'océan côtier a été amélioré selon deux approches, en augmentant le rapport de reminéralisation de la matière organique dans les sédiments côtiers, et en incluant de façon explicite la dégradation de la matière organique terrestre dissoute (tDOM) dans l'océan. Lors de l'analyse des flux côtiers, le modèle suggère une durée de résidence des eaux dans la zone côtière réduite (14-16 mois en moyenne) que ce qui a été assumé jusqu'à présent (>4 ans), ce qui indique un transfert efficace de matière organique de l'océan côtier à l'océan ouvert et un état autotrophe net de l'océan côtier, aussi bien pour la période préindustrielle que la période actuelle. L'océan côtier est un puit de CO_2 dans le modèle (0.06-0.08 Pg C yr^{-1}) pour la période préindustrielle, contrairement à ce qui a été rapporté dans la littérature. Le puit de carbone n'est pas seulement le résultat de l'état autotrophe de l'océan côtier, mais aussi associé à l'effet de la production primaire sur le niveau

d'alcalinité et aux caractéristiques physiques et biogéochimiques de l'apport d'eau des rivières à l'océan ouvert.

Dans le dernier chapitre, les perturbations océaniques induites par les changements de la concentration du CO_2 dans l'atmosphère, du climat physique et des apports biogéochimiques fluviaux durant le 20^{e} siècle, sont analysées à partir de simulations séquentielles. Les résultats de ces simulations indiquent que la réduction dans production primaire nette (NPP) observée dans les océans tropicaux et subtropicaux, expliqué par une stratification induite par la température, aurait pu être entièrement compensée par une augmentation de la NPP dans l'océan austral et dans les systèmes côtiers avec frontière terrestre à l'est (EBUS). Les simulations montrent aussi que l'inclusion des changements des apports fluviaux provoque une augmentation du NPP océanique à l'échelle globale (+ 4 %), la zone côtière étant la plus touchée (+15 %).

En conclusion, cette thèse a permis de démontrer l'importance d'inclure, dans les modèles globaux biogéochimiques des océans, les changements temporels et spatiaux non seulement des apports fluviaux, mais aussi de l'état biogéochimique côtier, afin de mieux représenter les changements dans le cycle du carbone océanique observé pendant la période historique. Le nouveau modèle développé dans ce travail devrait permettre d'affiner la prédiction des changements du cycle du carbone océanique dans le futur.

English abstract

River deliver vast amounts of terrestrially derived compounds to the ocean. These fluxes are of particular importance for the coastal ocean, which is recognized as a region of disproportionate contribution to global oceanic biological fluxes. Until now, the riverine carbon, nutrient and alkalinity inputs have been poorly represented or omitted in global ocean biogeochemistry models. In particular, there has yet to be a model that considers the pre-industrial riverine loads of biogeochemical compounds to the ocean, and terrestrial inputs of organic matter are greatly simplified in their composition and reactivities in the ocean. Furthermore, the coastal ocean and its contribution to the global carbon cycle have remained enigmatic, with little attention being paid to this area of high biological productivity in global model analysis of carbon fluxes. Lastly, 20th century perturbations in riverine fluxes as well as of the physical and biogeochemical states of the coastal ocean have remained unexplored in a 3-dimensional model. Thus, the main goals of this thesis are to integrate an

improved representation of riverine supplies in a global ocean model, as well as to improve the representation of the coastal ocean in the model, in order to solve open questions with respect its global contributions to carbon cycling.

In this thesis, I first aimed to close gaps of knowledge in the long-term implications of pre-industrial riverine loads for the oceanic cycling of carbon in a novel framework. I estimated pre-industrial biogeochemical riverine loads and their spatial distributions derived from Earth System Model variables while using a hierarchy of state-of-the-art weathering and organic matter land-ocean export models. I incorporated these loads into the global ocean biogeochemical model HAMOCC and investigated the induced changes in oceanic biological production and in the air-sea carbon flux, both at the global scale and in a regional shelf analysis. Finally, I summarized the results by assessing the net land sink of atmospheric carbon prescribed by the terrestrial models, and comparing it to the long-term carbon outgassing determined in the ocean model. The study reveals a pre-industrial oceanic outgassing flux of 231 Tg C yr^{-1}, which is found to a large degree in proximity to the river mouths. The model also indicates an interhemispheric transfer of carbon from the northern riverine inputs to outgassing in the southern hemisphere. Furthermore, I observe substantial riverine-induced increases in biological productivity in the tropical West Atlantic (+166 %), the Bay of Bengal (+377 %) and in the East China Sea (+71 %), in comparison to a model simulation which does not consider the riverine inputs.

In addition to considering supplies provided by riverine fluxes, the biogeochemical representation of the coastal ocean is improved in HAMOCC, by firstly increasing organic matter remineralization rates in the coastal sediment and by secondly explicitly representing the breakdown process of terrestrial dissolved organic matter (tDOM) in the ocean. In an analysis of the coastal fluxes, the model shows a much shorter residence time of coastal waters (14-16 months) than previously assumed, which leads to an efficient cross-shelf transport of organic matter and a net autotrophic state for both the pre-industrial timeframe and the present-day. The coastal ocean is also revealed as a CO_2 sink for the pre-industrial time period (0.06-0.08 Pg C yr^{-1}) in contrary to to the suggested source in published literature. The sink is however not only caused by the autotrophic state of the coastal ocean, but it is likely also strongly influenced by the effects of biological alkalinity production and both physical and biogeochemical characteristics of open ocean inflows.

In the final chapter, 20^{th} century oceanic perturbations due to changes in

atmospheric CO2 concentrations and in the physical climate, and to increases in riverine nutrient supplies were investigated by using sequential model simulations. The model results show that the decrease in the net primary production (NPP) in the tropical and subtropical oceans due to temperature-induced stratification may be completely compensated by increases in the Southern Ocean and in Eastern Boundary Upwelling Systems (EBUS). The model also reveals that including increases in riverine supplies causes a global ocean NPP increase of +4 %, with the coastal ocean being a particularly strongly affected region (+15 %).

This thesis shows a strong necessity to represent spatio-temporal changes in riverine supplies and of the coastal ocean state in spatially explicit global models in order to assess changes of the global cycling of carbon in the ocean in the past and potentially in the future.

Contents

List of Figures

List of Tables

Abbreviations

A_C	Carbonate alkalinity
Alk	Total alkalinity (also A_T)
CMIP5	Coupled model intercomparison project simulations, e.g. Giorgetta et al. (2013)
COSCAT	Ocean coastline segmentation based on work by Meybeck et al. (2006)
DFe	Dissolved iron
DIC	Dissolved inorganic carbon
DIN	Dissolved inorganic nitrogen
DIP	Dissolved inorganic phosphorus
DOM	Dissolved organic matter
DON	Dissolved organic nitrogen
DSi	Dissolved silica
ESM	Earth System Model
Fe-P	Iron-bound phosphorus
HAMOCC	HAMburg Ocean Carbon cycle model, see Ilyina et al. (2013)
HD (model)	Hydrological discharge model Hagemann and Dümenil (1997)
MARCATs	MARgins and CATchments Segmentation, see Laruelle et al. (2013)
MLD	Mixed layer depth
MPI-ESM	Max Planck Institute Earth System Model, see Mauritsen et al. (2019)
MPI-OM	Max Planck Institute Ocean Model, see Jungclaus et al. (2013)
(Global)-NEWS2	Global Nutrient Export from Watersheds (Seitzinger et al., 2010)
NEP	Net ecosystem production
NPP	Net primary production
OCGM	Ocean global circulation model
OMIP	Ocean Model Intercomparison Project, e.g Orr et al. (2017)
RH	Heterotrophic respiration
RT	Water residence time on the shelf
SeaWiFS	Sea-viewing Wide Field-of-view Sensor
SOCAT	The Surface Ocean CO_2 Atlas Pfeil et al. (2013)
tCDOM	Terrestrial chromophoric dissolved organic matter; tDOM specie which is not broken down by a solely biotic pathway, see Aarnos et al. (2018)
tDOM	Terrestrial dissolved organic matter
POC	Particulate organic carbon
POM	Particulate organic matter
PON	Particulate organic nitrogen
POP	Particulate organic phosphorus
WOA	World Ocean Atlas (observations)

Chapter 1

Introduction

1.1 Climate change, the carbon cycle and the land-ocean carbon transfer

Since the start of industrial revolution during the 19th century human-induced CO_2 emissions have drastically risen (Ciais et al., 2013). Atmospheric concentrations of CO_2, a strong historic Earth climate regulator, have risen from 19th century concentrations of around 280 ppm to over 400 ppm contemporarily and will likely continue to significantly augment in the future (Etheridge et al., 1996; Ciais et al., 2013; Le Quéré et al., 2018). This increase in atmospheric CO_2 concentrations has led to unprecedented changes in the Earth's climate system (IPCC, 2013). The consequences of the pronounced changes in atmospheric CO_2 concentrations include increases in atmospheric temperature, droughts, extreme weather events, sea level and retreat of glaciers. Climate change is also suggested to have social-economic based consequences, causing for instance conflicts due to increased scarcity in regional natural resources (Hsiang et al., 2011).

Due to these dramatic consequences, the global carbon cycle and its feedback on the climate system has become a topic of increased focus of research. While land and ocean are responsible for the absorption of slightly over 50 % of anthropogenic carbon emissions originating mostly from fossil fuel combustion for the present-day (Figure 1.1, Le Quéré et al. (2018)), both of these sinks have also been reported to be affected by changes in climate (Cox et al., 2000; Friedlingstein et al., 2006).

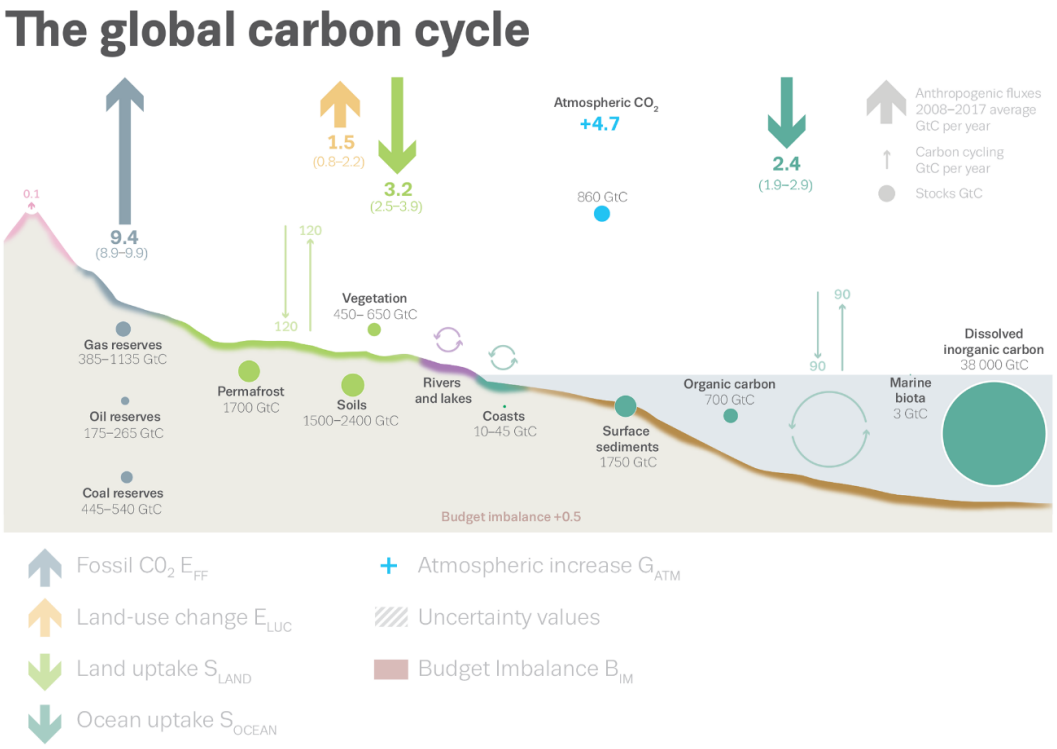

FIGURE 1.1: Perturbation of global carbon fluxes in Pg C yr^{-1} (Le Quéré et al., 2018).

The terrestrial land system is estimated to take up 3.2 ± 0.7 Pg C yr^{-1} of CO_2 for 2008-2017, a sink due to the fertilising effects of increasing atmospheric CO_2 and of increasing nitrogen availability on vegetation growth, as well as increasingly favourable conditions for plant growth in high latitude regions due to higher temperatures (Le Quéré et al., 2018).

The ocean also acts as a substantial buffer with regards to anthropogenic CO_2 concentrations, taking up 2.4 ± 0.5 Pg C yr^{-1} of anthropogenic CO_2 for 2008-2017 (Le Quéré et al., 2018). The uptake of CO_2 depends on the physical and biogeochemical state of the ocean (Sarmiento and Gruber, 2006) and is driven by the (dis-)equilibrium at the water-atmosphere interface between atmospheric CO_2 concentrations and dissolved CO_2 in the ocean. The magnitudes of the air-sea CO_2 exchange is dependent on ocean circulation, temperature, salinity and alkalinity. Furthermore, the ocean biological system is also responsible for the uptake of carbon, due to the sequestering of carbon through its ecosystem's production and export of organic carbon to ocean depths, which reduces the amount of dissolved CO_2 present in the system (Sarmiento and Gruber, 2006). While the ocean is an increasing atmospheric sink due to the sink's dependency on atmospheric CO_2 concentrations, it also

becomes less efficient with increasing CO_2 uptake, as well as with increasing temperatures (Sarmiento and Gruber, 2006).

Earth System Models (ESMs) are a vital tool to understand the land and oceanic natural and anthropogenic CO_2 uptake, as well as their feedbacks on the climate system. They aim to reproduce historical changes in climates and biogeochemical cycles as well as forecast future changes in the systems (Dunne et al., 2012; Giorgetta et al., 2013; Heinze and Ilyina, 2015; Mauritsen et al., 2019). ESMs of intermediate complexity thereby consist of 3 main components: global atmosphere, land and ocean models. These share information of model state variables with each other (such as temperature). In the case of the Max Planck Institute Earth System Model (MPI-ESM) (Figure 1.2), these three main components are ECHAM6 – the atmosphere model, the JSBACH – the land model, and MPIOM and HAMOCC – the physical and biogeochemical ocean models. Within these components, major processes which affect the climate and the carbon cycle are modelled. The components are furthermore coupled with each other through exchanges of energy, momentum, water and carbon.

While ESMs of intermediate complexity have attempted to reproduce historical changes in the Earth's climate, as well as predict future changes in climate at the centennial timescale, various important processes and feedbacks are strongly uncertain, or are not considered in the models, leading to uncertainties in the ESMs performance to closely represent the Earth's climate and carbon cycles (e.g. Stevens et al. (2013)). One large aspect omitted until now is the land-ocean transfer of terrestrial material, which most notably exports land-derived carbon to the ocean (Regnier et al., 2013). Less discussed, but potentially equally important is the transfer of nutrients and alkalinity from land to ocean (Mackenzie et al., 2002; Mackenzie et al., 2004; Seitzinger et al., 2010; Beusen et al., 2016). In the MPI-ESM, land-ocean fluxes of freshwater are accounted for but the model does not consider land-ocean transfer of important biogeochemical tracers such as carbon (C), nitrogen (N), phosphorus (P), silica (Si), iron (Fe) and alkalinity (Alk). Therefore, a wide range of processes are omitted, such as the biogeochemical release from weathering processes, the mobilization and loss of biogeochemical compounds in terrestrial systems (for instance in soils), riverine transformation processes and transport dynamics, as well as their impacts in the ocean. Another feature poorly represented or omitted until now has been the contribution of the coastal ocean, which acts as an interface between land and the ocean, to the global cycling of carbon (Bauer et al., 2013). This lacking representation has

been on one hand due to computational expenses of performing simulations with high enough spatial resolutions to represent a plausible physical state in the coastal ocean (Chen and Beardsley, 2006; Chen et al., 2007), on the other hand dominant biogeochemical processes in the coastal ocean have also been poorly constrained from observations.

In this thesis, I aim to firstly close gaps of knowledge on the origins and magnitudes of land-ocean exports of terrestrially derived compounds and represent their impacts in a global ocean biogeochemical model, with a focal point of the analysis being the coastal ocean. I thereby tackle various topics ranging from weathering release of biogeochemical tracers to discussing the dynamical multi-faceted 20th century perturbations of the global ocean. In the following brief reviews, I synthesize and discuss central topics addressed in this thesis.

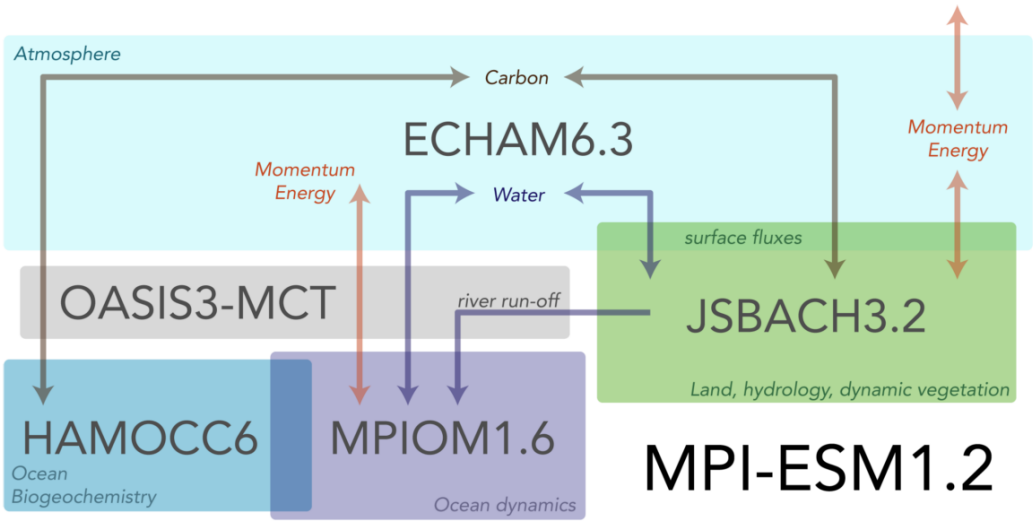

FIGURE 1.2: Max Planck Institute Earth System Model components and inter-component exchanges, from Mauritsen et al. (2019). OASIS-MCT thereby acts as a coupler between the ocean components and the land fluxes, as well as the atmospheric fluxes.

1.2 Short reviews of main topics covered in this thesis

1.2.1 Land-ocean exports: From lithology to ocean

Exports of terrestrial material supply the ocean with biogeochemical compounds through 3 major transport pathways: riverine transport, aeolian transport and groundwater transport. I thereby focus on the riverine exports of material here, since this is a major aspect of this thesis.

Rivers supply the ocean with nutrients, carbon and alkalinity (Hartmann et al., 2009; Seitzinger et al., 2010; Regnier et al., 2013; Beusen et al., 2016). The rivers are on their side supplied by weathering of the lithosphere and through the mobilization of matter from the terrestrial biosphere (Figure 1.3). While weathering processes cause the release of dissolved inorganic compounds from the chemical transformation of rock induced by its contact to water (Amiotte Suchet and Probst, 1995; Hartmann et al., 2014), the mobilization of compounds from the biosphere happens through the leaching and physical erosion of inorganic and organic matter from soils and peat-lands (Meybeck and Vörösmarty, 1999). Furthermore, vegetation also provides a direct transfer of organic matter through litter fall (e.g. Lauerwald et al. (2017)). The lithosphere and biosphere also exchange compounds through the biological uptake of weathered inorganic nutrients and sedimentation, compaction and lithification of organic matter from the biosphere to the lithosphere. Both the weathering of the lithosphere as well as the terrestrial biological primary production take up CO_2 and therefore exert a strong control on atmospheric CO_2 (Ludwig et al., 1998; Gaillardet et al., 1999; Hartmann et al., 2009). While the factors that control the weathering CO_2 uptake and release are still not fully understood, runoff, temperature, lithology, topology, soil type and vegetation have been thought to impact weathering rates (Hartmann et al. (2014) and references therein). On the other hand, the controls on land biological CO_2 uptake and carbon export are factors of light availability, water, nutrients, temperature, atmospheric CO_2 concentrations, vegetation type and topography.

Compounds exported to rivers are subject to hydrological dynamics, firstly. The dynamics of rivers, as well as catchment characteristics dictate their times of transport and transformation processes (Figure 1.3, Blair and Aller (2011)

and Beusen et al. (2016)). Secondly, they can undergo vast biogeochemical transformations, which include retention through export to freshwater sediments and outgassing (Laursen and Seitzinger, 2002; Cole et al., 2007; Battin et al., 2009; Raymond et al., 2013; Regnier et al., 2013; Beusen et al., 2016). While land-ocean exports and processes that take place along the land-ocean continuum were not considered for a long time in carbon budgets, studies such as Cole et al. (2007), Raymond et al. (2013) and Regnier et al. (2013) have assessed the quantities of carbon exported from land to ocean and the loss of carbon through outgassing during its transport to the ocean. For instance, dissolved organic carbon and particulate organic carbon exported from soils can be remineralized to dissolved CO_2, which can be outgassed. From the carbon inputs from weathering and soil exports to inland waters of around 1.6-5.1 Pg C yr^{-1} (Cole et al., 2007; Regnier et al., 2013; Drake et al., 2018), 0.75-3.1 Pg C yr^{-1} are suggested to be respired along the land-ocean-continuum (Cole et al., 2007; Tranvik et al., 2009; Raymond et al., 2013; Holgerson and Raymond, 2016; Drake et al., 2018), estimates performed by upscaling field measurements to the global scale. The large range of these estimates underline the large uncertainty in the magnitudes of the exports from land to rivers and the loss of carbon due to outgassing along the land-ocean-continuum. Alkalinity on the other hand is thought to be transported relatively passively from its weathering release to the ocean (Amiotte Suchet and Probst, 1995; Ludwig et al., 1998). Global weathering models, which rely on linear relationships between the weathering yields with runoff and and lithological composition such as the GEM-CO2 by Amiotte Suchet et al. (2003) and a model developed based on the lithologies of the Japanese Archipelago in Hartmann et al. (2009), therefore yield a good estimation of alkalinity exports provided from catchments to the ocean at the global scale. The dissolved inorganic carbon to alkalinity ratios measured at river mouths however usually deviate slightly from the 1:1 ratio deduced from weathering processes, due to dissolved CO_2 inputs from the respiration of soil organic carbon (up to 90 Tg C yr^{-1} at the river mouths globally, Meybeck and Vörösmarty (1999)). In terms of nutrients, strong gaps of knowledge exist concerning their inland water transformations and potential losses along the land-ocean-continuum, despite their importance for biological processes in the coastal ocean. Beusen et al. (2016) estimate in a global modelling approach that up to half of the nitrogen and phosphorus exports of land to rivers might be retained along the land-ocean-continuum. Furthermore, in estuaries, a substantial amount of nitrogen is thought to be outgassed due to the transformation of dissolved inorganic

nitrogen to nitrogenous gases (Laursen and Seitzinger, 2002; Seitzinger et al., 2006).

Additionally, (inorganic) rock and shale can also be eroded from rock and transported by rivers. The particulate material thereby consists of amounts vastly exceeding that of dissolved inorganic and organic exports (Compton et al., 2000; Seitzinger et al., 2010; Tréguer and De La Rocha, 2013). The biovailability of nutrients within particulate inorganic material and shale is however thought to be very low (Compton et al., 2000; Tréguer and De La Rocha, 2013). Due to its immense exports however, even a slow rate of transformation to bioavailable material might possibly impact biological systems in the coastal ocean (Tréguer and De La Rocha, 2013).

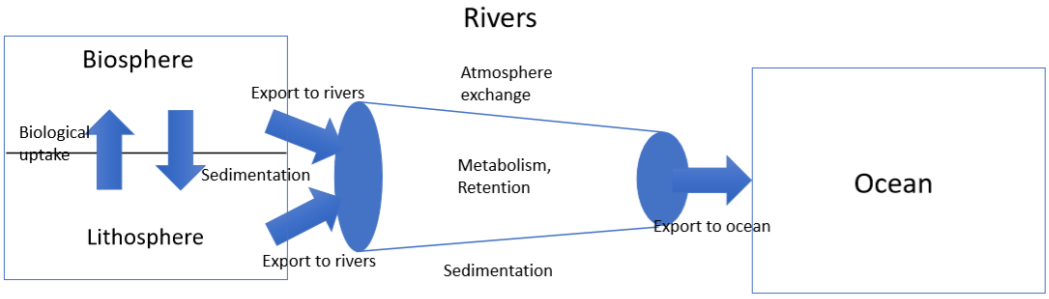

FIGURE 1.3: Simplified scheme of the transfer of material from land to ocean.

During the 20th century, anthropogenic perturbations have strongly affected riverine exports (Ittekkot et al., 2000a; Seitzinger et al., 2010; Regnier et al., 2013; Beusen et al., 2016). For one, hydrodynamical flows have been perturbed through increased retention by dams and agricultural irrigation constructions (Lehner et al., 2011). Regarding biogeochemical fluxes, nitrogen and phosphorus show the strongest perturbations, with published literature suggesting more than a doubling of global land-ocean exports with respect to their natural loads (Seitzinger et al., 2010; Beusen et al., 2016). These increased land-ocean exports are due to the increased inputs of nitrogen and phosphorus compounds to freshwater systems due to agricultural fertilizers, sewage, aquaculture, detergents. The anthropogenic implications for land-ocean carbon exports, albeit less substantial, are still estimated to be around 0.1 Pg C yr^{-1} (Regnier et al., 2013), around 10% of the pre-industrial export, which to a large part originate from increased organic carbon erosion and leaching from soils. While this increased mobilization of organic carbon is significant (circa 0.8 Pg C yr^{-1}), most of it is suggested to be remineralized

and returned to the atmosphere along the land-ocean-continuum. Studies from Maavara et al. (2014), Maavara et al. (2015), and Maavara et al. (2017) furthermore estimate substantial increased retention not only for carbon, but also for silica and phosphorus during its transport from land to ocean during the 20^{th} century.

Approaches to estimate riverine fluxes have become more and more sophisticated, using new geospatial tools with higher spatial resolution of the hydrological factors, although the estimates still mostly agree with older estimates (Bauer et al., 2013). Thereby, the river discharge remains the main driver of the supply to the ocean, although spatial distributions of lithology, soil type, slope and climate can also be significant factors. There however still exists room for substantial improvements in understanding and constraining land-ocean fluxes, with estimates for the present-day showing differences larger than 100% (Beusen et al., 2016). Most modelling approaches to estimate riverine exports report annual means (Beusen et al., 2009; Seitzinger et al., 2010) without consideration of seasonality of the exports. Extreme events, which might cause the export of 80-90 % of particulate carbon from mountainous regions, have for instance not yet been adequately modelled (Hilton et al., 2008). Processes that transform biogeochemical tracers during their transports from land to ocean are not yet constrained at the global scale (Hall et al., 2016). Furthermore, other sources of land-sea fluxes, such as groundwater discharge, remain a large area of uncertainty.

In ESMs, the transport of freshwater from land to the ocean is often represented (e.g. Mauritsen et al. (2019)). In the MPI-ESM, the hydrological model used has a higher resolution than the dynamical vegetation model (0.5 degrees) and is used to simulate the land-ocean freshwater transports (Hagemann and Dümenil, 1997). However, carbon, nutrients and alkalinity riverine transports are not included. In terms of biogeochemical tracers to the ocean, ESMs have extremely simplified river supplies (Aumont et al., 2001), often even ignoring river inputs (Weaver et al., 2001) or assuming a reflective sediment to keep the ocean biogeochemical state stable (Aumont et al., 2015). In the reflective sediment method, all or a fraction of the particulate fluxes to the sea floor, is remineralized or dissolved instantaneously and returned to ocean water column at the bottom layer, in order to keep oceanic compound inventories stable. This compensation of the sediment losses has also alternatively been performed to the surface layer (Mauritsen et al., 2019).

1.2.2 The fate of riverine exports in the ocean

Relatively little research has been conducted on the fate of land-derived material in the ocean at the global scale, in particular for nutrients and organic matter (Sharples et al., 2017). Dissolved inorganic nutrients such as dissolved inorganic nitrogen and dissolved inorganic phosphorus, which are supplied by rivers, are often limiting factors of primary production in the ocean (Tyrrell, 1999). Therefore, the supply of these compounds from rivers should enhance the primary production of the ocean relatively efficiently in the coastal ocean (e.g. Mackenzie et al. (2002). In an analysis of the fate of nitrogen and phosphorus in the coastal ocean, Sharples et al. (2017) and Izett and Fennel (2018) suggest a parametrized approach to represent the residence times and transformations of phosphorus, nitrogen and organic matter in the coastal zone, with the argument that the current state of global models are inadequate to represent complex physics of plume transports in the coastal ocean. In the study, the majority of the P (around 75%) and N (80%) provided by rivers is transported offshore to the open ocean, although it is not clear if this includes organic forms of P and N. In Izett and Fennel (2018), these estimations are strongly corrected downwards (2-45%) for P and N (3-45%), while using different parameters to quantify the residence times of the freshwater plumes, albeit with very large uncertainty ranges. Studies have also suggested substantial outgassing of nitrogenous gas due to denitrification in a widespread of coastal regions where there is strong primary production and little ventilation at deeper water layers (Seitzinger et al. (2006) and Fennel and Testa (2019) and references therein).

Despite its significant degradation during its transport from soils to the ocean and thus having been mostly transformed into a biologically non-reactive form, terrestrial organic matter is not found in substantial amounts in the open ocean and sediment pore water (Ittekkot, 1988; Hedges et al., 1997; Opsahl and Benner, 1997; Hernes and Benner, 2002; Vodacek et al., 2003a). Lignin, which is only found in terrestrial dissolved organic matter (tDOM), is measured in small fractions within organic matter in the open ocean of the Atlantic and Pacific basins, contributing no more than 3% of total dissolved organic matter (DOM) in these basins (Opsahl and Benner, 1997; Hernes and Benner, 2002). In the Arctic however, tDOM is detected in considerable amounts and accounts for up to 25% of total DOM concentrations (Benner et al., 2005). Low contributions of tDOM to the open ocean DOM pools thereby suggest that tDOM is remineralized relatively efficiently in the ocean, atleast in the lower

latitudes and thus possibly also in the coastal ocean. Recent studies have shown that the sinks of tDOM in the coastal and open ocean might be mostly abiotic (Aarnos et al., 2012; Fichot and Benner, 2014; Müller et al., 2016a; Aarnos et al., 2018). Light-induced degradation of tDOM has been reported to breakdown tDOM either directly to CO or CO_2 (Müller et al., 2016a), or transform the tDOM to a form that can be mineralized biotically (Fichot and Benner, 2014; Aarnos et al., 2018). The degradation of particulate organic matter (POM) is on the other hand less well researched. POM in the coastal ocean is usually deposited to the sediment (Blair and Aller, 2011). Here the efficiency of mineralization is dependent on a multitude of factors, including POM composition, temperature and pressure (Arndt et al., 2013). Blair and Aller (2011) propose a strong difference for the fate of terrestrial POM in the ocean between different types of catchments. High energy, high flow systems (e.g. in the Amazon delta) have high rates of POM remineralization due to oxygen exposure. Low energy, low flow environments tend to have very low remineralization efficiencies. Finally, mountainous catchments deliver strongly unreactive POM, and therefore the remineralization efficiency for coastal areas supplied by these catchments is also very low.

Ocean biogeochemical models have, if they consider riverine fluxes, not explicitly incorporated the partitioning of nutrients and carbon into inorganic and organic matter fractions, and into particulate and dissolved compounds (Aumont et al., 2001; Da Cunha et al., 2007; Bernard et al., 2011; Aumont et al., 2015; Bourgeois et al., 2016). This could have significant consequences for the distributions of these elements in the ocean. While dissolved inorganic nutrients enhance the primary production directly (Tyrrell, 1999), organic matter first needs to be remineralized, which could strongly alter the location where the available nutrients enhance the primary production. To my knowledge, the research reported in this thesis is the first to consider the fate of terrestrial organic matter and the fractionations of carbon and nutrients into distinct pools in the ocean using a three-dimensional global ocean model.

1.2.3 Global ocean biogeochemical cycling

The ocean is recognized as a central constituent in the Earth climate system that helps to regulate the climate (IPCC, 2013) due to its capacity to store heat and carbon. The ocean is estimated to have absorbed around 30% of global anthropogenic CO_2, strongly buffering the effect of increased CO_2 emissions.

Thus, the understanding of the carbon cycle in the ocean is vital to understand past and future changes in the Earth system.

The carbon cycle in the ocean consists of organic and inorganic processes (Sarmiento and Gruber, 2006). The inorganic carbon cycle is dictated by the following thermodynamic equilibrium reactions (Millero, 2007):

$$CO_2(g) \overset{H_2O}{\rightleftharpoons} CO_2(aq) \tag{1.1}$$

$$CO_2(aq) + H_2O(l) \overset{H_2O}{\rightleftharpoons} H_2CO_3(aq) \tag{1.2}$$

$$H_2CO_3 \overset{H_2O}{\rightleftharpoons} HCO_3{}^-(aq) + H^+(aq) \tag{1.3}$$

$$HCO_3{}^-(aq) \overset{H_2O}{\rightleftharpoons} CO_3{}^{2-}(aq) + H^+(aq) \tag{1.4}$$

While the difference in partial pressures between the gaseous form of CO_2, $CO_2(g)$, in the ocean and atmospheric CO_2 directly drives the ocean-atmosphere exchange of CO_2, the dissociation of CO_2 (aq) and H_2O (or also known as H_2CO_3, carbonic acid), buffers the system since the dissociation reaction decreases the dissolved CO_2 concentration. HCO_3^- can also further dissociate to CO_3^{2-}. During the addition of dissolved CO_2 to the ocean, such as during the ocean uptake of anthropogenic CO_2, the H^+ concentration is increased and thus the pH of the ocean is reduced. Furthermore, biological organisms such as coccolithophores precipitate calcium carbonate shells, which can sink to deeper ocean layers or even to the sea floor (Milliman and Droxler, 1996). The formation and export of $CaCO_3$ thereby eliminates alkalinity and carbon from the euphotic zone:

$$Ca^{2+}(aq) + 2\,HCO_3{}^-(aq) \longrightarrow CaCO_3(s) + CO_2(g) + H_2O(l) \tag{1.5}$$

Since HCO_3^- and CO_3^{2-} can take up protons and are found in relatively high concentrations in the ocean, they form the vast majority of the oceanic alkalinity (A_t), which is the proton buffer capacity of the seawater (Wolf-Gladrow et al., 2007):

$$A_t = [HCO_3^-] + 2\,[CO_3^{2-}] + [B(OH)_4^-] + [OH]^- - [H^+] + \text{minor bases} \tag{1.6}$$

The alkalinity directly affect the amount of CO_2 that can be dissolved in seawater by enhancing the dissociation reactions due to its consumption of protons. As a consequence of the fact that carbon is not stored as dissolved CO_2 in the ocean, but in ionic forms, the oceanic carbon pool accounts for 98% of carbon stored in the combined atmosphere-ocean system (Wolf-Gladrow et al., 2007). Another consequence of the CO_2 buffering is the decrease of CO_3^{2-} ion concentrations and thus the decrease in the $CaCO_3$ saturation, which can have a strong impact on the dissolution of coral reefs (Milliman and Droxler, 1996):

$$CO_2\,(aq) + CO_3^{2-}\,(aq) + H_2O\,(l) \longrightarrow 2\,HCO_3^-\,(aq) \tag{1.7}$$

The organic component of the oceanic carbon cycle, often referred to as the biological pump, is fuelled by the uptake of CO_2 in the euphotic zone, which produces organic matter (Volk and Hoffert (1985) and Honjo et al. (2014), Figure 1.4). This production of organic matter is dependent on several factors, the main ones being light, temperature and nutrient availability (Tyrrell, 1999). While most of the produced organic matter is remineralized within the euphotic zone, a small fraction escapes to the ocean interior, which eliminates carbon from a possible atmosphere-ocean interaction for longer time-scales.

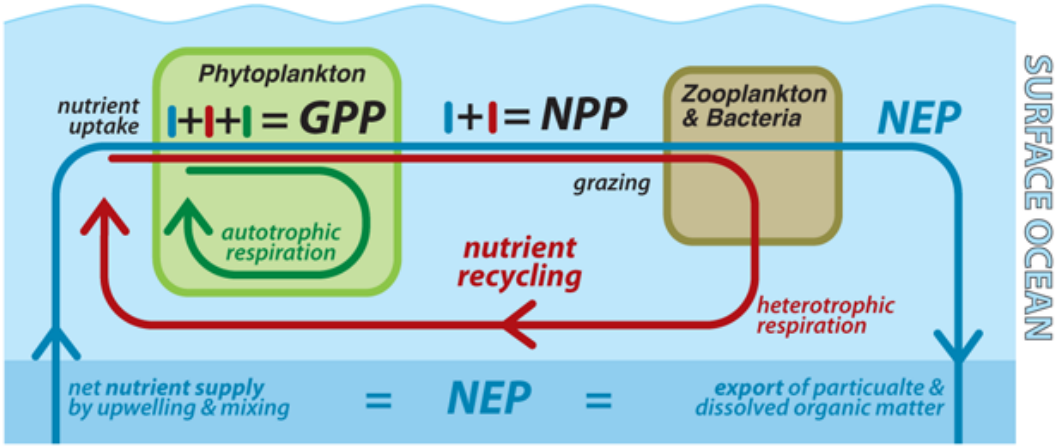

FIGURE 1.4: Scheme of oceanic biological production and nutrient cycling in the surface ocean, illustrated by Sigman and Hain (2012).

Both the inorganic and carbon cycle are subject to human-induced perturbations. On one hand, increased atmospheric CO_2 concentrations directly affect the inorganic cycle (Sarmiento and Gruber, 2006). This increased CO_2 uptake of around 2.3 Pg C yr^{-1} by the ocean has been reported to cause a widespread decrease in oceanic pH levels (Ciais et al., 2013). Although less direct, changes in ocean physics might also substantially affect inorganic and organic processes in the ocean. For instance, the ocean warming of surface layers due to the warming of the atmosphere has been reported to enhance stratification in a multitude of regions (IPCC, 2013). Increased stratification inhibits entrainment of water from deeper water layers, which are usually enriched with nutrients (Figure 1.4). Climate induced changes in atmospheric circulation patterns have also been reported (Trenberth, 1995), which also perturb biogeochemical distributions within the ocean due to changes in wind driven ocean transports.

The net biological production of organic matter (also referred to as net primary production, NPP), is estimated at around 50 Pg C yr^{-1}, which consists of around half of the global NPP (Field et al., 1998). It is unclear, how the global NPP and organic carbon exports from the euphotic layer, the well mixed near-surface layer of the ocean, have changed due to anthropogenic perturbation in the past century. While Behrenfeld et al. (2006) report a global NPP decrease of 0.57% from satellite-derived data, Saba et al. (2010) report a decadal increase of NPP of 2% at two open sites using in-situ radiotracers. In a review of drivers and uncertainties of global marine primary production, Laufkötter et al. (2015) suggested poor observational constraints of oceanic changes NPP

for the past century due to the lack of consistent long-term observations, as well as the difficulties of distinguishing between natural decadal fluctuations and the anthropogenic trends (Henson et al., 2010). Global ocean models on the other hand show varying directions and magnitudes in their trends of NPP and organic matter exports from the euphotic layer (Laufkötter et al., 2013), leaving a strong question mark on the sign and magnitude in the anthropogenic perturbation of biological cycles in the global ocean. For future projections, Bopp et al. (2013) suggest a substantially reduced NPP (circa -9 %) induced by the physical perturbation of the ocean over the 21st century, although this is without accounting for changes in nutrient supplies. Furthermore, a large uncertainty is suggested in the model comparison in the study ($\pm$ 8 %), indicating the differing responses of the different models.

In ESMs, the ocean cycling of carbon has long been represented (for instance in Sarmiento and Le Quéré (1996)) as a central component of the Earth's carbon cycle and the model results are standardly used in state-of-the-art carbon budgeting (Le Quéré et al., 2018).

1.2.4 Biogeochemical dynamics of the coastal ocean

The coastal ocean is a zone of transition between land and ocean, which is on the one hand supplied by riverine discharge (Milliman and Farnsworth, 2011) and secondly by open ocean inflows (e.g. Fennel et al. (2006)). The coastal ocean is often characterized by shallow depths and is thought to be well mixed due to turbulence caused by its bathymetry, which enhances the coupling of pelagic (surface) and benthic (deeper layer) processes (Chen and Borges, 2009). As a consequence of the availability of the nutrients provided by inflows and rivers, as well as the high efficiency of the nutrient cycling due to its shallow depths, the coastal ocean is thought to be highly biologically productive (Walsh, 1991; Mackenzie et al., 1998; Mackenzie et al., 2002; Mackenzie et al., 2004; Wollast and Chou, 1998; Liu et al., 2000; Muller-Karger et al., 2005).

In literature, the global coastal ocean has been inconsitently defined. For instance, Chen and Borges (2009) define the coastal ocean as continental shelves with depths of up to 200m, whereas Muller-Karger et al. (2005) use shelf depths of up to 1000 m. In an attempt to segment the global coastal ocean to catchment and shelf regions of similar characteristics, Laruelle et al. (2013) revealed that the shelf break occurs at varying depths globally (Figure

1.5). While certain narrow shelves have a shelf break at less than 150m depths, in the Arctic Ocean the shelf breaks can extend all the way to depths of 1000 m. From this wide range of definitions, the area of the coastal ocean also is given in a range from 22 10^6 – 35 10^6 km^2 (Andersson et al., 2005; Muller-Karger et al., 2005; Chen and Borges, 2009; Laruelle et al., 2013; Laruelle et al., 2018), which accounts for 6-15% of the global ocean area.

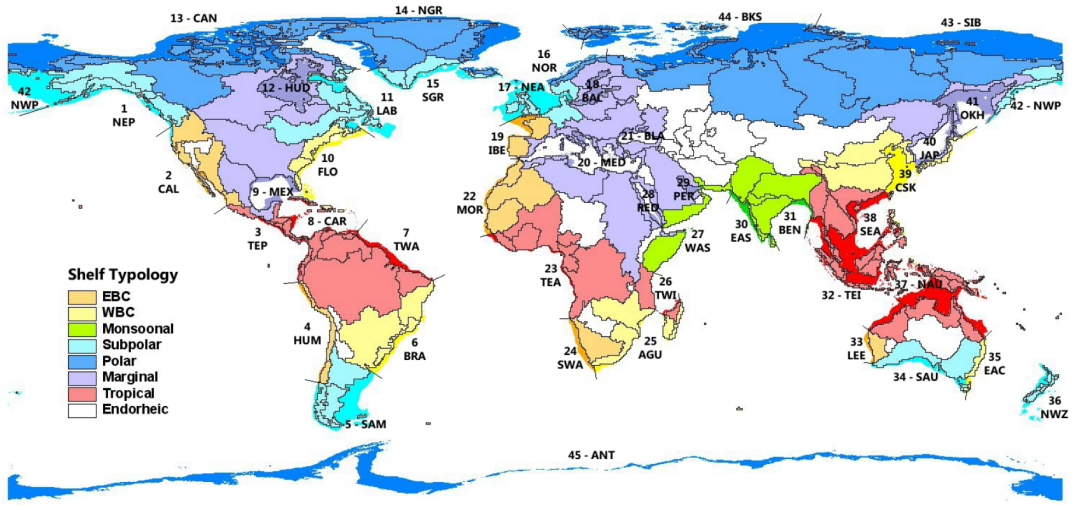

FIGURE 1.5: Global segmentation of the coastal ocean based on physical characteristics of both land catchments and shelves, as well with an outer limit constructed from strong increases in slope. From Laruelle et al. (2013).

The contribution of the coastal ocean to the global carbon cycle is an area of high uncertainty and the carbon fluxes in this heterogenous zone have been poorly quantified in the past. Despite its relatively small areal contribution to the global ocean, it is estimated to contribute 10-30 % to the global oceanic net primary production (Walsh, 1991; Longhurst, 1995; Gattuso et al., 1998; Muller-Karger et al., 2005), and to account for 30-50 % of organic carbon burial (Chen and Borges (2009) and citations therein).

It is also not clear what contribution the coastal ocean plays in the uptake of anthropogenic CO_2. In an early modelling approach, Mackenzie et al. (1998), Mackenzie et al. (2000), Mackenzie et al. (2002), and Mackenzie et al. (2004) and Andersson et al. (2005) determined with help of a box model that the coastal ocean was a pre-industrial source of CO_2 of around 0.2 Pg C yr^{-1} and just recently switched to a sink 0.2-1.2 Pg C yr^{-1} (Figure 1.6). It is also proposed in Mackenzie et al. (2004) that the coastal ocean has switched from being strongly net heterotrophic, meaning being a net DIC-producer due to

mineralization of organic material, to a substantial autotrophic state, due to the NPP enhancement through increased riverine nutrients loadings. Another consequence of the anthropogenic perturbation of riverine loads has been reported to be coastal eutrophication and hypoxia in large areas worldwide (Fennel and Testa, 2019). While oxygen depletion might have been prevalent in natural systems with poor coastal ocean water ventilation, increasing riverine nutrient loads, as well as increasing stratification of coastal waters due to increasing surface layer temperatures, has led to an increase of hypoxia zones for instance in the Baltic Sea, East China Sea and the Black Sea. From currently published literature, I conclude that the coastal ocean has been perturbed through combination of changing atmospheric CO_2 concentrations (Bauer et al., 2013), riverine supplies (Seitzinger et al., 2010; Beusen et al., 2016), physics (Mathis et al., 2019) and open ocean supplies (Fennel et al., 2006; Mathis et al., 2019). The aggregation of these effects has not been assessed in a global ocean model until now.

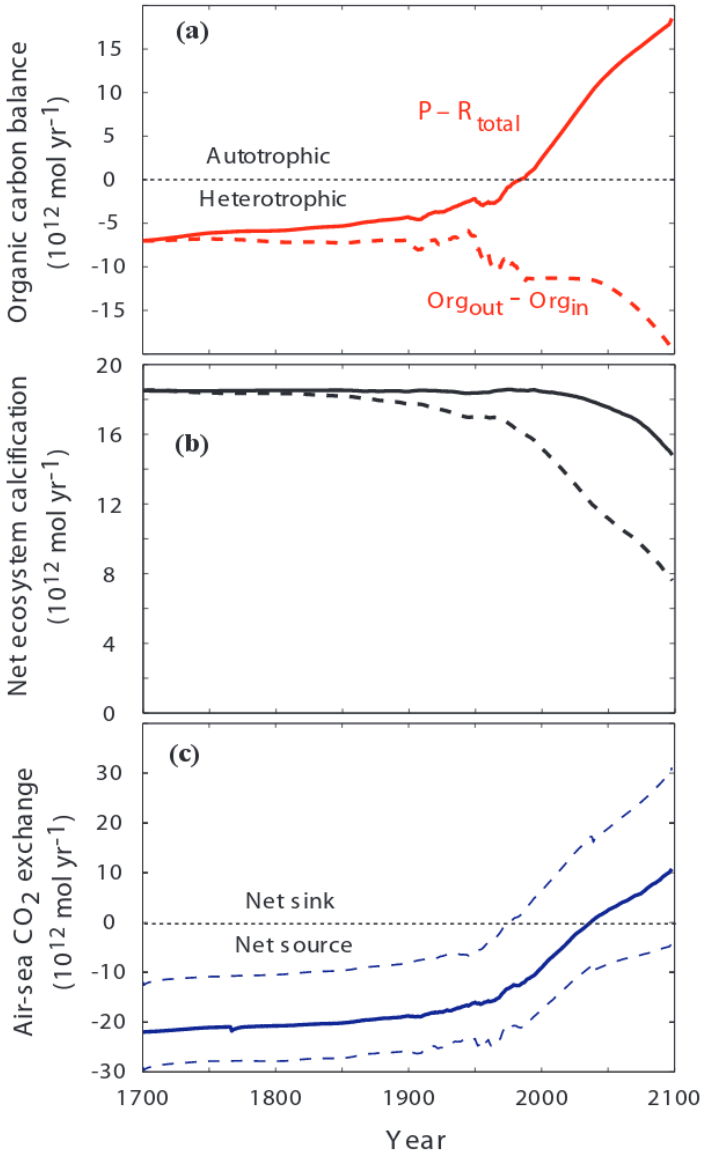

FIGURE 1.6: Evolution of the organic carbon balance, the net ecosystem calcification and the coastal CO_2 flux in a box model approach accounting for differing global residence times. From Mackenzie et al. (2004).

Until recently, a lack of data coverage along with the heterogeneity of the coastal ocean prevented an adequate assessment of the coastal ocean CO_2 flux from observations (e.g. stated in Fennel et al. (2006). The increasing coverage of coastal ocean data has however permitted the estimation of a present-day coastal ocean sink of 0.14-0.24 Pg C yr^{-1} (Wanninkhof et al., 2013; Laruelle et al., 2014), which represents a significant downward revision from the values reported previously (for instance, 0.45 Pg C yr^{-1} in Borges et al. (2005)). Furthermore, in a neural network interpolation, Laruelle et al. (2017) recently provided a pCO_2 dataset resolved globally at a 1 degree resolution, which could be used by global models for calibration and validation.

In 3-dimensional global ocean models and thus in ESMs, the coastal ocean has been poorly represented. This is on one hand due to the inadequate resolutions of global models to reproduce shallow shelves and their circulation features, as well as gaps in our understanding of coastal biogeochemical processes (e.g. Giraud et al. (2008)). While Bourgeois et al. (2016) offer an estimation for the anthropogenic CO_2 uptake of the coastal ocean within a global circulation at a relatively high resolution (0.1 Pg C yr^{-1}), land-ocean exports and processes within the coastal ocean were strongly simplified. By increasing model resolution, one could expect better constraining of the coastal ocean carbon cycle. These simulations can now be compared to an increased available amount of data, such as SOCATv4 (Bakker et al., 2016; Laruelle et al., 2017). Global models could then be used to provide a forecast of the future biogeochemical state of coastal ocean.

1.2.5 The global riverine carbon loop

As explained previously, rivers export carbon from land terrestrial systems, where carbon is drawn down from the atmosphere by weathering and biological fixation (Ludwig et al., 1998; Hartmann et al., 2009; Regnier et al., 2013), to the ocean. In the ocean, the carbon inputs have thereby been suggested to cause a natural oceanic outgassing flux of 0.2-0.8 Pg C yr^{-1} (Sarmiento and Sundquist, 1992; Aumont et al., 2001; Sabine, 2004; Da Cunha et al., 2007; Jacobson et al., 2007; Gruber et al., 2009; Resplandy et al., 2018), although the mechanisms of the carbon outgassing have yet to be fully understood. The consideration that land takes up carbon, which is exported to the ocean and is subsequently returned to the atmosphere on longer time-scales implies a carbon loop within the Earth system (Figure 1.7), as shown in Aumont et al. (2001). The long-term fate of the carbon in the ocean and its contribution to this river carbon loop has however not been assessed quantitatively. In theory, part of the riverine carbon is also exported to the ocean sediment when considering longer time scales (sedimentation flux in Figure 1.7). For instance, Sarmiento and Sundquist (1992) suggest a carbon flux to the sediment of 0.1-0.2 Pg C yr^{-1} and an outgassing flux of 0.2-0.4 Pg C yr^{-1} under natural conditions. Jacobson et al. (2007) suggest in a global model inversion approach that the outgassing was higher (0.45 Pg C yr^{-1}) and that in particular the Southern Ocean was a substantial source of carbon to the atmosphere. In a recent study, Resplandy et al. (2018) develop a new method for estimating

the pre-industrial oceanic outgassing based on ocean heat constraints. They conclude in the study that the natural outgassing of the ocean is of around 0.8 Pg C yr^{-1}, which is then also suggested to be the carbon delivered by rivers to the ocean for the pre-industrial time-frame. It is however not clear, if or how the Resplandy et al. (2018) study considers a loss of riverine carbon inputs to the sediment.

Since part of the carbon delivered by rivers is exported to the sediment, an additional long-term outgassing flux is necessary to compensate the loss of carbon to the sediment, in order to keep the atmospheric budget stable (Figure 1.7). While Sarmiento and Sundquist (1992) suggest a reconciliation of land uptake and oceanic outgassing through carbon outgassing caused by shale organic carbon oxidation, more recent studies suggest that long-term volcanic outgassing might consist of a much larger contribution to the missing outgassing term (Burton et al., 2013).

Furthermore, it was also suggested that the latitudinal distributions of riverine carbon exports might differ to latitudinal distributions in the oceanic carbon outgassing, which implies inter-latitudinal transfer of carbon within the ocean (Aumont et al., 2001; Resplandy et al., 2018). A larger northern hemispheric carbon export from land might lead to a net transfer to the southern hemispheric ocean, implying an interhemispheric transfer of carbon (Aumont et al., 2001; Resplandy et al., 2018).

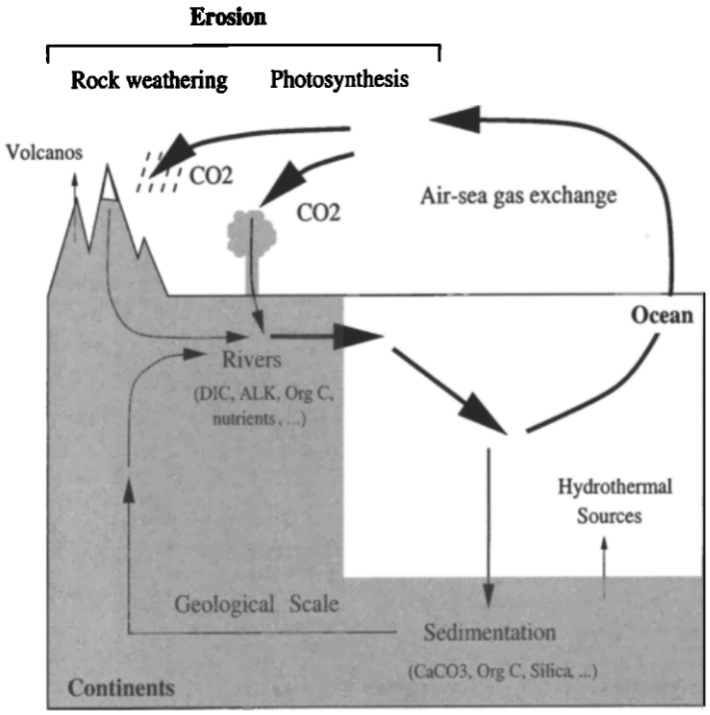

FIGURE 1.7: Scheme of the riverine carbon loop concept. From Aumont et al. (2001).

River carbon exports and the riverine carbon loop are not considered in ESMs. Until now, carbon fluxes from land to ocean have only been partly implemented in some regions, for instance Lauerwald et al. (2017) and Hastie et al. (2019) for the Amazon carbon exports and Bowring et al. (2019) for the dissolved organic carbon exports from Arctic regions. The outgassing caused by the riverine exports of carbon is however not represented in in state-of-the-art ESMs. In a global ocean model study, Aumont et al. (2001) derive carbon fluxes from the combination of a weathering and global erosion model (Ludwig et al., 1998), and spatial patterns of carbon outgassing in the ocean are assessed, although the consideration of different fractions of carbon species and the enhancement of the biological pump through riverine nutrient loads are not considered. Furthermore, this outgassing flux from the land-ocean transfer of carbon could potentially have undergone an anthropogenic-induced perturbation during the past century. Regnier et al. (2013) give a conservative estimate of the perturbation of the net land-ocean carbon flux of 0.1 Pg C yr^{-1}, which, depending on the time-scale of the outgassing in the ocean, could impact this ocean-atmosphere exchange.

1.3 Aims and research questions

As shown in the brief topical reviews (Section 1.2), previous research shows large gaps of knowledge regarding the impacts of biogeochemical riverine exports on the ocean, especially for the processes taking place at the interface between land and ocean, the coastal ocean. This includes poor constraints of the evolution of carbon, nutrient fluxes and alkalinity exports from land to ocean over the historical time period, their fate in the ocean, their impacts on the natural oceanic carbon cycle in the coastal and global ocean and their contributions to the multifarious anthropogenic perturbation of the ocean. A large degree of uncertainty is additionally associated with the coastal ocean in terms of its contribution to the global carbon cycle, in the pre-industrial as well as contemporary state. In ESMs and global ocean models, which could potentially be used to tackle these gaps of knowledge, the land-ocean transfer of biogeochemical compounds and their impacts in the ocean have not been adequately considered.

In this thesis, I provide a first benchmark for deriving land-ocean exports in a global model framework (i.e. as a function of ESM variables), for assessing their fates in the ocean, and their temporal varying impacts and contributions to the global carbon cycle in the open and coastal ocean. The coastal ocean is thereby a focal point in the thesis, due to importance the processing of the land-ocean exports, its suggested large contributions of biological fluxes and its poor representation in global models until now. To tackle these points, I build a hierarchy of weathering and land-export models, thereby considering transformations to organic matter to derive the most relevant biogeochemical land-ocean exports and their speciation for the pre-industrial time period (Chapter 2). These exports are used to extend an ocean biogeochemical model with riverine inputs, allowing a comprehensive analysis of their consequences for the global and regional ocean biogeochemistry. Furthermore, the state of coastal ocean is assessed in the global model setup, where processes affecting organic material remineralization were altered to provide a more realistic representation of this highly productive ocean area (Chapter 3). I use this setup to evaluate physical and biogeochemical indicators to subsequently assess the trophic state and sign and magnitude of the CO_2 flux of the coastal ocean for the pre-industrial time-period. Finally, the anthropogenic oceanic perturbation over the historical period is assessed in a series of different simulations, ranging from changes in the physical and biogeochemical climate

to increasing riverine nutrient supplies, both at the global scale and in a regional coastal ocean analysis (Chapter 4). As follows, I define the research questions of the three main chapters of the thesis.

Chapter 2: Oceanic CO_2 outgassing and primary production hotspots induced by pre-industrial riverine nutrient and carbon exports in a global model approach

The impacts of riverine fluxes on the global ocean's biogeochemistry have been poorly constrained conceptually as well as quantitatively. On one hand, pre-industrial exports of biogeochemical compounds from land to ocean are strongly uncertain. Secondly, the impacts of riverine fluxes of carbon, nutrients and alkalinity in the ocean have not been assessed mechanistically and quantitatively at the global scale. Thirdly, the mechanisms in the global carbon loop that cause carbon outgassing in the ocean have not been fully understood, and it is unclear how the ocean outgassing CO_2 flux compensates the land carbon uptake. In this chapter I address these points of uncertainty by attempting to constrain pre-industrial riverine fluxes and assessing their impacts on the oceanic biogeochemistry. Consequently, the following research questions were defined:

- *What is the magnitude of pre-industrial biogeochemical riverine exports derived from a hierarchy of state-of-the-art modelling approaches for weathering yields and land-ocean organic exports, and how do they compare to published estimates? Which regions show a disproportional contribution to global riverine exports?*

- *How do the riverine exports impact CO_2 outgassing and NPP fluxes in the ocean, both at the global and regional scale, and are the identified hotspots of riverine exports also reflected in disproportional regional changes to these oceanic carbon cycling indicator variables?*

- *What are the magnitudes of terrestrial sources and oceanic fates of the riverine carbon and how is the terrestrial sink of atmospheric CO_2 balanced with respect to the oceanic source of atmospheric CO_2?*

In a modelling approach, I start from deriving weathering inputs by combining spatially explicit weathering models and land-ocean export models for non-weathered compounds in a novel framework. I estimate the magnitudes of transformation of the biogeochemical compounds into inorganic and organic pools using fixed ratios of the compounds P, N and Fe in relation to organic carbon. These riverine loads are then added to a global biogeochemical ocean model, which is used for analysing the impacts of the riverine loads on the oceanic nutrient distributions, NPP and CO_2 fluxes at the global and regional scale. Lastly, I assess the potential incorporation of the riverine loads in a coupled land-atmosphere-ocean model by balancing the atmospheric sinks and sources of carbon determined by the terrestrial models and by the ocean biogeochemistry model.

Chapter 3: The efficient cross-shelf export of organic matter in the coastal ocean: Were continental shelves already a global pre-industrial CO_2 sink?

Published studies to this date leave large question marks regarding the role of coastal ocean within the global carbon cycle, both for the present-day as for the historical time-period. Previously, a combination of poorly representing the surface of continental shelves due to inadequate model resolution, and limited observational constraints of biogeochemical variables and processes taking place in the coastal ocean did not allow for a robust analysis of the coastal ocean in spatially explicit global models. Increasingly available observational data coverage of coastal regions, such as through the SOCAT project (Bakker et al., 2016) have led to better constrains of for instance the pCO_2 coastal ocean distribution and the magnitude of present-day CO_2 fluxes (Laruelle et al., 2014; Laruelle et al., 2017). Furthermore, the fate of tDOM, the dominant organic matter supply from land and important control on the coastal ocean trophic state and CO_2 flux (Cai, 2011), has been recently assessed in a series of regional observational studies (Fichot and Benner, 2014; Kaiser et al., 2017; Aarnos et al., 2018). While conceptual box model approaches such as Mackenzie et al. (1998), Mackenzie et al. (2000), Mackenzie et al. (2002), and Mackenzie et al. (2004) and Andersson et al. (2005) attempt to assess how the coastal ocean cycle has been altered in the historical time-frame and how large the contribution of the coastal ocean to the anthropogenic uptake is, they do not resolve spatial characteristics of the coastal ocean, which most certainly strongly impact the processes taking place in these regions. Furthermore,

the composition and fate oceanic tDOM have not been considered in global models.

In this chapter I use a globally explicit ocean model as a tool to estimate coastal physical variables such as residence times, as well as biogeochemical variables, such as the net ecosystem production, at the global scale. Furthermore, I use the model to tackle the temporal evolution of the coastal ocean carbon processing, by firstly assessing the pre-industrial state of the continental shelves. To tackle a number of major uncertainties in the coastal ocean carbon cycle, I define the following research questions:

- *What are the water residence times and mixed layer depths on continental shelves at a global and regional scale, and how do the global model results compare with reported regional estimates?*

- *Were continental shelves heterotrophic or autotrophic when considering a range of plausible tDOM and shelf sediment remineralization rates in the model?*

- *Was the coastal ocean a sink or a source of atmospheric CO_2 and which factors exert an important control on the global air-sea CO2 flux of the coastal ocean?*

In this chapter, I represent continental shelves using a global ocean biogeochemical model. The fluxes to continental shelves are computed dynamically within the global model, and I additionally use the pre-industrial riverine biogeochemical exports derived in Chapter 2 to drive the ocean biogeochemistry model. I perform a sensitivity analysis for rates of organic matter remineralization occurring in the shallow shelf sediment. I furthermore consider differing tDOM mineralization rates, which includes a representation of photodegradation, to analyse the fate of tDOM in the ocean and its impact on the trophic state. I then perform simulations while considering solely changes in atmospheric CO_2 over the 20^{th} century, in order to make comparisons of physical variables, as well as to evaluate the model with respect to a highly resolved present-day pCO_2 data-product (Laruelle et al., 2017), as well as global coastal CO_2 flux estimates (Wanninkhof et al., 2013; Laruelle et al., 2014). Finally, I track back in time to the pre-industrial time-period to assess the carbon fluxes taking place on the global continental shelves before its 20^{th} century perturbation.

Chapter 4: The multifaceted 20th century perturbation of the oceanic carbon cycle: Could coastal ocean and river-induced increases in NPP trump implications of increased open ocean stratification?

The ocean carbon cycle has been anthropogenically perturbed by a multitude of factors during the 20^{th} century. For one, increasing atmospheric CO_2 concentrations have caused an increased uptake of carbon in the global open ocean (Ciais et al., 2013; Le Quéré et al., 2018) and in the coastal ocean (Bauer et al., 2013). Moreover, changes in oceanic physical features, such as an increase in stratification, may have significantly perturbed oceanic carbon and nutrient cycling (Behrenfeld et al., 2006). The impacts of the physical perturbation on these cycles are however still very unclear, especially for the biological pump (Bopp et al., 2013; Laufkötter et al., 2013; Laufkötter et al., 2015). According to a model study, the global NPP has substantially decreased to increased stratification in the open ocean (Laufkötter et al., 2013). A further, albeit less discussed, biogeochemical perturbation of the ocean is the increased supply of riverine nutrients, such as N and P (Seitzinger et al., 2010; Beusen et al., 2016). While the increasing nutrient supply has been suggested to widely increase the coastal ocean NPP (Mackenzie et al., 2002; Mackenzie et al., 2004), leading to coastal eutrophication in many regions (Fennel and Testa, 2019), the magnitudes of the increase in the coastal ocean NPP and the consequent increased CO_2 sink are unknown. Furthermore, Sharples et al. (2017) suggest a very efficient cross-shelf export of nutrients, meaning that the impacts of the changing riverine supply potentially efficiently extend to the open ocean, which has not been discussed in literature nor considered in global spatially explicit model studies until now. The present-day contribution of the coastal ocean to the global ocean anthropogenic carbon uptake has also been identified as a topic of strong uncertainty. While Bourgeois et al. (2016) suggest that the coastal ocean was a less efficient sink of atmospheric CO_2 than the open ocean, Laruelle et al. (2018) report from observational data an increasing efficiency in the CO_2 uptake of various regions globally, which led to conclusions that the global coastal ocean might be becoming a more efficient CO_2 sink. I therefore attempt to explore these points using the model framework described to this point. I thereby define four research questions to tackle the multi-factor oceanic perturbation in the global and coastal ocean:

- *How strongly do the isolated and combined 20^{th} century perturbation of atmospheric CO_2 concentrations, the physical climate state and changes in riverine*

nutrient supplies affect the NPP and CO_2 fluxes in the open and coastal ocean?

- *How are coastal nutrient and carbon cycling fluxes, with the cross-shelf export as a focal point, affected by the net anthropogenic perturbation of the ocean?*

- *Which established coastal regions with similar biogeochemical attributes are most affected in their NPP and CO_2 fluxes?*

- *Is it possible to identify coastal zones of increased 20^{th} century eutrophication and hypoxia using a global model framework?*

To address the research questions, I perform sequential ocean model simulations, while driving the ocean biogeochemistry model with changing 20^{th} century atmospheric CO_2 concentrations, a changing physical climate state, and increasing riverine supplies of N and P. The model simulations are performed at a higher resolution than the configuration used in Chapters 2 and 3 in order to improve the physical representation of the coastal ocean.

Technical Note

Chapter 1 (introduction) and Chapter 5 (summary and conclusions) of this thesis are written in the first person, whereas Chapters 2, 3 and 4 are written in the third person plural to consider other contributing authors.

Throughout this thesis I use the terms coastal ocean and continental shelves to the same use, i.e. describing shallow ocean areas in proximity to land surface. The definitions are however consistent, being ocean areas with depths of less than 250 m that are in near proximity to land surface, except in Chapter 4, where I also use differing depths to define the coastal ocean.

Chapter 2

Oceanic CO_2 outgassing and biological production hotspots induced by pre-industrial river loads of nutrients and carbon in a global modelling approach

Lacroix, F., T. Ilyina & J. Hartmann (2019), *Biogeosciences Discussion*, in open discussion. https://doi.org/10.5194/bg-2019-152.

Summary Rivers are a major source of nutrients, carbon and alkalinity for the global ocean, where the delivered compounds strongly impact biogeochemical processes. In this study, we firstly estimate pre-industrial riverine fluxes of nutrients, carbon and alkalinity based on a hierarchy of weathering and land-ocean export models, while identifying regional hotspots of the land-ocean exports. Secondly, we implement the riverine loads into a global biogeochemical ocean model and describe their implications for oceanic nutrient concentrations, the net primary production (NPP) and CO_2 fluxes globally, as well as in a regional shelf analysis. Thirdly, we quantify the terrestrial origins and the long-term oceanic fate of riverine carbon in the framework, while assessing the potential implementation of riverine carbon fluxes in a fully coupled land-atmosphere-ocean model. Our approach leads to annual pre-industrial riverine exports of 3.7 Tg P, 27 Tg N, 158 Tg Si and 603 Tg C, which were derived from weathering and non-weathering sources and were fractionated into organic and inorganic compounds. We thereby identify the tropical Atlantic catchments (20 % of global C), Arctic rivers (9 % of total C)

and Southeast Asian rivers (15 % of total C) as dominant providers of carbon to the ocean. The riverine exports lead to a global oceanic source of CO_2 to the atmosphere (231 Tg C yr^{-1}), which is largely a result of a source from inorganic riverine carbon loads (183 Tg C yr^{-1}), and from organic riverine carbon inputs (128 Tg C yr^{-1}). Additionally, a sink of 80 Tg C yr^{-1} is caused by the enhancement of the biological carbon uptake by dissolved inorganic nutrient inputs, resulting alkalinity production and a slight model drift. While large outgassing fluxes are mostly found in proximity to major river mouths, substantial outgassing fluxes can also be observed further offshore, most prominently in the tropical Atlantic. Furthermore, we find evidence for the interhemispheric transfer of carbon in the model; we detect a stronger relative outgassing flux (49 % of global river induced outgassing) in the southern hemisphere in comparison to the hemisphere's relative riverine inputs (33 % of global river inputs), as well as an outgassing flux of 17 Tg C yr^{-1} in the Southern Ocean. Riverine exports lead to a strong increase in NPP in the tropical West Atlantic, Bay of Bengal and the East China Sea (166 %, 377 % and 71 % respectively). While the NPP is not strongly sensitive to riverine loads on the light limited Arctic shelves, the CO_2 flux is strongly altered due to substantial dissolved carbon supplies to the region. While our study confirms that the ocean circulation is the main driver for open ocean biogeochemical distributions, it reveals the necessity to consider riverine exports for the representation of heterogeneous features of the coastal ocean, to represent riverine-induced carbon outgassing, as well as to consider the long-term volcanic CO_2 flux to close the atmospheric carbon budget in a coupled land-ocean-atmosphere setting.

2.1 Introduction

Rivers deliver substantial amounts of land-derived biogeochemical compounds to the ocean. For the present day, they provide 4-11 Tg P yr^{-1} of phosphorus (P), 37-66 Tg N yr^{-1} of nitrogen (N), 158-200 Tg Si yr^{-1} of dissolved silica (Si) and iron (Fe, no estimate available) as dissolved and particulate inorganic and organic compounds to the ocean (Seitzinger et al., 2005; Seitzinger et al., 2010; Dürr et al., 2011; Beusen et al., 2009; Tréguer and De La Rocha, 2013; Beusen et al., 2016). They also supply carbon (C) as dissolved inorganic carbon (260-550 Tg C yr^{-1}), dissolved organic carbon (130-380 Tg C yr^{-1}), as well as particulate organic carbon (100-197 Tg yr^{-1}) to the ocean (Meybeck,

1982; Amiotte Suchet and Probst, 1995; Ludwig et al., 1996; Ludwig et al., 1998; Mackenzie et al., 1998; Meybeck and Vörösmarty, 1999; Seitzinger et al., 2005; Hartmann et al., 2009; Seitzinger et al., 2010; Regnier et al., 2013; Aarnos et al., 2018). These loads, which originate from natural and anthropogenic sources, strongly affect the biogeochemistry in the coastal ocean, where nutrients and carbon are transformed during biogeochemical processes, are exported to the sediment, or are exported offshore (Stepanauskas et al., 2002; Froelich, 1988; Dagg et al., 2004; Krumins et al., 2013; Sharples et al., 2017). In global ocean models however, biogeochemical riverine exports and their contributions to the cycling of carbon have been strongly simplified or ignored. In this study, we attempt to reduce these gaps of knowledge by estimating the magnitudes of biogeochemical riverine exports as a function of Earth System Model variables for the pre-industrial time period by using a hierarchy of weathering and land-export models. We then describe their long-term implications for oceanic biogeochemical cycles, with the NPP and CO_2 fluxes as focal points.

Natural riverine carbon and nutrients originate from the terrestrial biosphere and the weathering of the lithosphere, which both consume atmospheric CO_2 while supplying freshwaters with carbon (Ludwig et al., 1998).

Weathering directly releases nutrients (P, Si and Fe) that can be taken up by the terrestrial ecosystems, or exported directly to aquatic systems (Hartmann et al., 2014). In these ecosystems, they are reported to enhance the carbon uptake due to their limitation of the biological primary production (Elser et al., 2007; Fernández-Martínez et al., 2014). Furthermore, alkalinity and carbon are released in the weathering process, while CO_2 is drawn down from the atmosphere (Amiotte Suchet and Probst, 1995; Meybeck and Vörösmarty, 1999; Hartmann et al., 2009). Spatially explicit approaches that quantify the weathering release have a strong potential for providing fluxes of nutrients for Earth System Models (e.g. for P in Hartmann et al., 2014). They also have been used in the past to provide valuable information regarding the drawdown of atmospheric CO_2 and its transformation to surface water alkalinity (Ludwig et al., 1998; Roelandt et al., 2010). It is acknowledged that chemical weathering rates are a first-order function of hydrology, lithology, rates of physical erosion, soil properties and temperature (Amiotte Suchet and Probst, 1995; Hartmann et al., 2009; Hartmann et al., 2014). Approaches to estimate chemical weathering yields therefore depend on quantifying these controls (Hartmann et al., 2014).

The terrestrial biosphere is also a source of carbon and nutrients to freshwater

systems (Meybeck and Vörösmarty, 1999; Seitzinger et al., 2010; Regnier et al., 2013). The formation of organic matter through biological primary production consumes atmospheric CO_2 (Ludwig et al., 1998). Leaching and physical erosion can then mobilize dissolved and particulate organic matter from soils and peatlands, and export it to rivers. While the natural P and Fe within the organic matter originates from weathering, C and N mostly originate from atmospheric fixation (Meybeck and Vörösmarty, 1999; Green et al., 2004). Within rivers, autochthonous production can take place, which further transforms inorganic nutrients to organic matter while taking up CO_2. In soils and in rivers, organic matter remineralization also occurs, which transforms the organic matter back to dissolved inorganic nutrients and carbon.

Rivers therefore export P, N, Si, Fe and C as dissolved and particulate inorganic and organic compounds, as well as alkalinity to the ocean. It is known that dissolved inorganic nutrients enhance the primary production in the ocean, and thus cause an uptake of atmospheric CO_2 (Tyrrell, 1999). The riverine inputs of dissolved inorganic carbon on the other hand causes carbon outgassing in the ocean (e.g. Sarmiento and Sundquist, 1992). The fate and contributions of terrestrial organic matter to the oceanic carbon cycle have been open questions for over two decades (Ittekkot, 1988; Hedges et al., 1997; Cai, 2011; Lalonde et al., 2014). While the nutrients contained in reactive organic matter can control phytoplankton and bacterial growth in given regions (Seitzinger and Sanders, 1997; Stepanauskas et al., 2002; Björkman and Karl, 2003), the reactivity of organic matter has been strongly debated (Ittekkot, 1988; Hedges et al., 1997; Lalonde et al., 2014), since it is thought to already have undergone substantial degradation in rivers (Ittekkot, 1988; Vodacek et al., 2003b). In the case of terrestrial dissolved organic matter (tDOM), the previous riverine degradation leads to high carbon to nutrients ratios found in tDOM (i.e. C:P weight ratios of over 500, Meybeck, 1982; Seitzinger et al., 2010). The strong previous degradation of tDOM and its high carbon to nutrients ratios imply low biological reactivity in the ocean, yet tDOM is not a major constituent of organic mixtures in open ocean sea-water or sediment pore water (Ittekkot, 1988; Hedges et al., 1997; Benner et al., 2005), Recent studies have suggested that photodegradation might be responsible for partly or completely degrading tDOM to dissolved CO_2, thus possibly closing this gap of knowledge (Vodacek et al., 2003b; Fichot and Benner, 2014; Lalonde et al., 2014; Aarnos et al., 2018). The degradation of tDOM could cause substantial regional outgassing due to its large transfer of carbon (Cai, 2011; Müller et al., 2016b; Aarnos et al., 2018). In the case of terrestrial particulate organic matter

(POM), even stronger gaps in knowledge exist (Cai, 2011). POM has however been reported to affect coastal ocean biogeochemistry regionally by firstly controlling the availability of nutrients and secondly by altering the optical properties of aquatic systems (Froelich, 1988; Dagg et al., 2004; Stramski et al., 2004). Furthermore, a substantial proportion of weathered P is exported to the ocean bound to iron (Fe-P, Compton et al., 2000). Within estuaries and the coastal ocean, a fraction of P in Fe-P is thought to be desorbed, and thus converted to a bioavailable compound (dissolved inorganic phosphorus).

The cycles of P and N and their land-ocean exports have been strongly perturbed over the 20th century, leading to a doubling of P and N riverine loads at the least (Seitzinger et al., 2010; Beusen et al., 2016). In the case of C and Si, the perturbations have been reported to be far less substantial at the global scale, although regional changes could have large implications for the coastal ocean (Seitzinger et al., 2010; Regnier et al., 2013; Maavara et al., 2014; Maavara et al., 2017). It has furthermore been suggested that riverine P and N exports were already substantially perturbed prior to 1850-1900 due to increased soil erosion from land-use changes, fertilizer use in agriculture and sewage sources (Mackenzie et al., 2002; Filippelli, 2008; Beusen et al., 2016). Since global modelling studies that tackle anthropogenic perturbations of the climate are usually initialized for 1850 (Giorgetta et al., 2013) or 1900 (Bourgeois et al., 2016), these exports due to non-natural sources should also be taken into account in the initial pre-industrial model states.

Until now, riverine point sources of biogeochemical tracers have been omitted or poorly represented in global ocean biogeochemical models, despite being suggested to strongly impact the biogeochemistry of coastal regions (Stepanauskas et al., 2002; Froelich, 1988; Dagg et al., 2004; Krumins et al., 2013; Sharples et al., 2017) and to cause a natural source of atmospheric CO_2 in the ocean (Sarmiento and Sundquist, 1992; Aumont et al., 2001; Gruber et al., 2009; Resplandy et al., 2018). This CO_2 outgassing flux of 0.2 to 0.8 Gt C yr^{-1} is significant in the context of the present day oceanic carbon uptake of around 2.3 Gt C yr^{-1} (IPCC, 2013). In a modelling study tackling the interhemispheric transfer of carbon, Aumont et al. (2001) derived carbon loads from an erosion model and analyzed the oceanic outgassing caused by the riverine carbon. The impacts of nutrients and alkalinity were however not considered and carbon was only added to the ocean as dissolved inorganic carbon. Da Cunha et al. (2007) analyzed the impacts of present day river loads on the oceanic primary production in a global biogeochemical model for an

analysis period of 10 years. Bernard et al. (2011) added river loads to an ocean biogeochemistry model to focus on their implications for global opal export distributions. In a global coastal ocean study, Bourgeois et al. (2016) quantified the coastal anthropogenic CO_2 uptake, but did not analyze the impacts of riverine loads. To our knowledge, a study has yet to give a comprehensive overview of pre-industrial land-ocean river exports and their long-term global impacts on oceanic biogeochemical cycling in a 3-dimensional framework. In previously published literature, riverine loads were added according to present day estimates, despite severe perturbation of the land-ocean N and P exports having taken place during the 20th century (Beusen et al., 2016). An initial ocean state with pre-industrial riverine supplies would however be necessary to truly assess the temporal dynamical impacts associated with these perturbations. Studies until now have also not considered differing characteristics of terrestrial organic matter to those of oceanic organic matter. Furthermore, it is often unclear under which criteria the alkalinity supplies to the ocean were constrained in global models. Regional sensitivities of coastal regions to biogeochemical riverine loads have not been assessed at the global scale, largely due to the incapability of global models to represent plausible continental shelf sizes in the past (Bernard et al., 2011).

In this study, we **1.** implement a representation of pre-industrial riverine loads into a global ocean biogeochemical model, considering both weathering and non-weathering sources of nutrients, carbon and alkalinity. We compare our estimates with a wide range of published literature values, while also determining regions of strong riverine exports and their contributions to global exports. **2.** The implications of riverine fluxes for the oceanic NPP and CO_2 flux are assessed globally, as well as regionally in an analysis of shallow shelves. **3.** We evaluate the origins and fate of riverine carbon quantitatively, while assessing the balance between the land carbon uptake and the oceanic carbon outgassing. This balance of the land carbon uptake and the oceanic outgassing is then used to assess the potential implementation of riverine fluxes in a fully coupled land-atmosphere-ocean setting.

2.2 Methods

To address the objectives of this study, we derived the most relevant pre-industrial land-ocean fluxes of biogeochemical compounds dependently on

pre-industrial output of Earth System Model simulations. We used a hierarchy of models to derive biogeochemical compound sources from weathering and non-weathering to catchments, and estimated their terrestrial transformations to organic matter. This resulted in a spatially explicit quantification of global riverine loads. The derived riverine loads were then implemented into a global ocean biogeochemical model in order to assess their global and regional impacts on the ocean biogeochemistry. In order to quantify the effects of the riverine supplies on coastal regions, we also defined 10 shelves with depths of less than 250 m.

2.2.1 Deriving pre-industrial riverine loads

We first briefly describe the framework used to derive pre-industrial riverine exports here, while the individual models and assumptions are explained in detail in the next subsections. We focused on the exports of phosphorus (P), nitrogen (N), silica (Si), iron (Fe), carbon (C) and alkalinity (Alk) for global catchments. The catchments were defined by using the largest 2000 catchments from the Hydrological Discharge (HD) model (Hagemann and Dümenil, 1997; Hagemann and Gates, 2003), a component of the Max Planck Institute Earth System Model (MPI-ESM). The catchments were derived from the runoff flow directions of the model at a horizontal resolution of 0.5 degrees. The exorheic river catchments (catchments, which discharge into the ocean) were considered to be catchments with river mouths that have a distance of less than 500 km to the coastline in the HD model. Catchments with larger distances were considered to be endorheic catchments (catchments, which do not discharge into the ocean). The biogeochemical tracers released in these in the endorheic catchments in our framework were assumed to be retained permanently, whereas the riverine exports from exorheic catchments were added to the ocean.

We considered both weathering sources as well as non-weathering sources of P, N, Si, Fe, C and Alk to river catchments (Figure 2.1). These were derived, if possible, from spatially explicit models. Within the catchments, we accounted for transformations of P, N and Fe to organic matter through biological productivity on land and in rivers. These biological transformations were however not modelled dynamically in our approach. Instead, the net amounts of catchment P, N and Fe to have been transformed to organic matter on land or in rivers were derived from fixed ratios to C depending on the tDOM and

POM composition (see Figure 2.1). The composition of tDOM and POM and their its ratios of C, P, N and Fe were assumed to be identical for every catchment out of simplicity. The amounts of P, N and Fe that were transformed to organic matter were subtracted from their inorganic catchment pools, in order to avoid double counting. The organic carbon in tDOM and POM, which was derived from river mouth load estimations of the NEWS2 study (Seitzinger et al., 2010), was assumed to ultimately originate from terrestrial biological CO_2 uptake (Ludwig et al., 1998) and was therefore not subtracted from the catchment DIC pools. Additionally, a fraction P was also assumed to have been adsorbed to Fe-P. The rivers in our approach therefore deliver terrestrial organic matter (tDOM and POM), inorganic compounds (DIP, Fe-P, DIN, DSi, DFe and DIC) and alkalinity (Alk) to the ocean (Figure 2.1).

a

	Source	Model/Study		Source	Model/Study
	Weathering	Hartmann et al. (2009)	**Si**	***Weathering***	Beusen et al. (2009)
C	***Non-Weathering***				
	DOC (Atmospheric)	NEWS2		***Non-Weathering***	
	POC (Atmospheric)	NEWS2	**N**	Atmospheric	Fixed ratio to P
				Anthropogenic	
	Weathering	Hartmann et al. (2014)	**Fe**	***Weathering***	Fixed ratio to P
	Non-Weathering				
	Fertilizer (1900)	Hart et al. (2004)	**Alk**	***Weathering***	Hartmann et al. (2009)
P	Sewage (1900)	Morée et al. (2013)			Goll et al. (2014)
	Allochtonous (1900)	Beusen et al. (2016)			

b

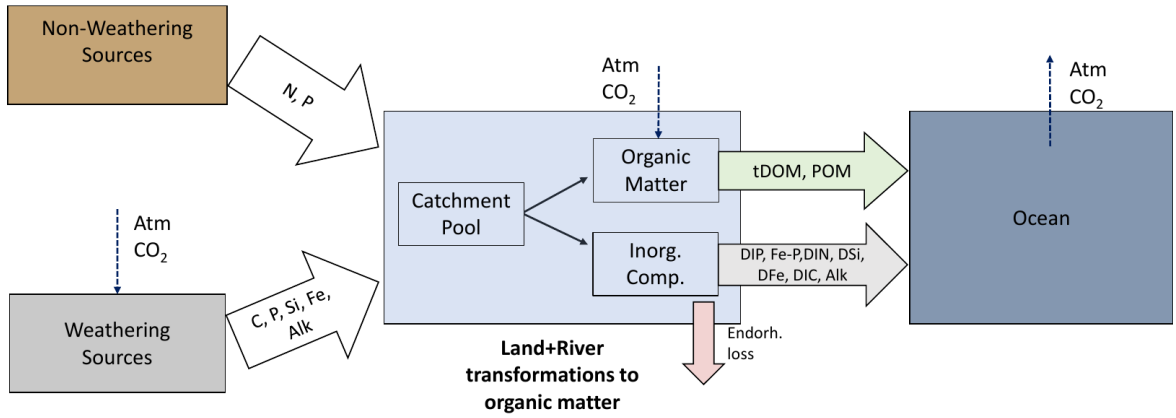

FIGURE 2.1: (a) Table of sources of nutrient, carbon and alkalinity inputs to the catchments and (b) scheme of origins and transformations of the catchment compounds The abbreviations are: Inorg. Comp.: Inorganic Compounds, tDOM: terrestrial dissolved organic matter, POM: particulate organic matter , DIP: dissolved inorganic phosphorus, Fe-P: Iron-bound phosphorus, DIN: dissolved inorganic nitrogen, DSi: dissolved silica, DFe: dissolved iron, DIC: dissolved inorganic carbon, Alk: alkalinity.

The surface runoff, surface temperature and precipitation data used to drive

the framework submodels were obtained from output of a fully coupled MPI-ESM CMIP5 pre-industrial simulation (Giorgetta et al., 2013). We thereby used the annual 100 year means of model runoff, temperature and precipitation data computed by the MPI-ESM on a 1.875 degree Gaussian grid. We scaled the runoff data to account for the runoff model bias with regards to global estimations (Fekete et al., 2002), which is discussed in Section 3.1.

Terrestrial dissolved and particulate organic matter characteristics

We assumed that the pre-industrial loads of tDOM and POM did not strongly differ to their present day loads at the global scale. In the NEWS2 study (Mayorga et al., 2010; Seitzinger et al., 2010), in which anthropogenic perturbations to riverine loads were analyzed, only small changes in POC and DOC loads to the ocean were found over the 1970 to 2000 time period. Regnier et al. (2013) suggest an anthropogenic perturbation of the total carbon flux to the ocean of around 10%, for which we did not account in this study.

The riverine loads of tDOM and POM were therefore derived from the DOC and POC river loads for the reference year 1970 (NEWS2), which were in turn determined from the models of Harrison et al. (2005) and Beusen et al. (2005). The Harrison et al. (2005) model quantifies the DOC catchment yields as a function of runoff, wetland area and consumptive water use. The Beusen et al. (2005) describes the POC catchment yields as a function of catchment suspended solids yields, which depend on grassland and wetland areas, precipitation, slope and lithology.

The riverine organic matter exported to the ocean consisted of globally constant fractions of C, P, N and Fe. The tDOM C:P consistence was based on a C:P weight ratio of 1000:1 derived from Meybeck (1982) and Compton et al. (2000). The global total N:P mole ratio was chosen to be 16:1, which is in accordance to natural and pre-industrial estimations of previous studies (Seitzinger et al., 2010; Beusen et al., 2016). For the P:Fe ratio, the same mole ratio as for the Fe biological uptake in the ocean was chosen (1:3.0 10^{-4}). The total C:N:P:Fe mole ratio of tDOM was therefore 2583:16:1:3.0 10^{-4}. The C:P ratio of riverine POM is highly uncertain, but global C:P mole ratios from observational data (56-499) (Meybeck, 1982; Ramirez and Rose, 1992; Compton et al., 2000) suggest a much closer ratio to the oceanic production and export ratios (mole C:P = 122:1, Takahashi et al. (1985)) than for tDOM. Due to this

and the gaps of knowledge on POM composition, we chose a C:N:P:Fe ratio analogous to that of oceanic POM (122:16:1:3.0 10^{-4}).

Phosphorus

P weathering yields

We derived the P weathering yields from a spatio-temporal model (Hartmann et al., 2014), which quantifies the P weathering release in relation to the SiO_2 and cation release. The model core is dependent on runoff and lithology (Hartmann and Moosdorf, 2011) and was calibrated for the extensive dataset of 381 river catchments of the Japanese Archipelago. The model was then corrected globally for temperature and soil shielding effects (Hartmann et al., 2014):

$$F_{Prelease} = \sum_{i=lith} b_{P,i} * q * F_i(T) * F_S \tag{2.1}$$

where $F_{Prelease}$ is the chemical weathering rate of P per area (t km^{-2} yr^{-1}), $b_{P,i}$ is an empirical factor representing the rate of P weathering of lithology i, q is the runoff (mm yr^{-1}), F(T) is a lithology-dependent temperature function and F_S is a parameter for soil shielding.

The lithology types consisted of 16 lithological classes from the lithological map database GliM (Hartmann and Moosdorf, 2012), which have different weathering parameters $b_{P,i}$ as well as temperature functions $F_i(T)$. The release of P was assumed to be proportional to the release of SiO_2 + cations, as in Hartmann et al. (2014). The factor $b_{P,i}$ represents the chemical weathering rate factor for SiO_2 + cations (b_{SiO_2+Cat}) multiplied with the relative P content ($b_{Prel,i}$):

$$b_{P,i} = b_{SiO_2+Cat,i} * b_{Prel,i} \tag{2.2}$$

The parameters $b_{SiO_2+Cat,i}$ and $b_{Prel,i}$ for each lithology i can be found in Hartmann et al. (2014).

Pre-industrial runoff model output of the MPI-ESM was used to force the model for q. The temperature correction function F(T) is an Arrhenius relationship for basic (rich in iron and magnesium) and acid (high silica content)

lithological classes, with activation energies normalized to the average temperature of the calibration catchments of the study (Hartmann et al., 2014). For acid rock lithologies, an activation energy of 60 kJ/mole was assumed, whereas for basic rock types 50 kJ/mole was used. Carbonate lithologies do not have a temperature correction due to the absence of a clear relationship to field data, as well as uncertainties in the mechanisms of a temperature effect on carbonate weathering (Plummer and Busenberg, 1982; Hartmann et al., 2014; Romero-Mujalli et al., 2018).

A soil shielding factor F_S was considered due to the inhibition of weathering by certain types of soils. These soils with low physical erosion rates develop a chemically depleted thick layer, which shields them from water supply, thus preventing the maximum weathering of the soil aggregates (Stallard, 1995). Wetlands and areas with a high groundwater table have also been shown to partially inhibit weathering (Edmond et al., 1995; Goudie and Viles, 2012). The average soil shielding factor was estimated for the soils Ferrasols, Acrisols, Nitisols, Lixisols, Histosols as well as Gleysols from the Harmonized World Soil Database (Hartmann et al., 2014). The factor used for these soils is 0.1, which was found to be the best global estimate for the calibration catchments in Hartmann et al. (2014), after having iteratively altered the parameter from 0 to 1.

Non-weathering P sources

Since the P cycle was already perturbed in the assumed pre-industrial state (1850) due to anthropogenic activities (Mackenzie et al., 2002; Filippelli, 2008; Beusen et al., 2016), we also accounted for P sources other than weathering ($P_{nw,catch}$). Similarly to Beusen et al. (2016), we derived the global non-weathering source of P as the sum of fertilizer ($P_{fert,global}$), sewage ($P_{sew,global}$) and allochthnonous P inputs ($P_{alloch,global}$):

$$P_{\text{nw,global}} = P_{\text{fert,global}} + P_{\text{sew,global}} + P_{\text{alloch,global}} \tag{2.3}$$

$P_{fert,global}$ was the input to the non-weathering $P_{nw,global}$ pool from the agricultural application of fertilizers, manure and organic matter (1.6 Tg P yr^{-1} globally, from Hart et al. (2004)), $P_{sew,global}$ was the P input from sewage (0.1 Tg P yr^{-1} globally, Morée et al. (2013)) and $P_{alloch,global}$ represented allochthnous organic matter P inputs (1 Tg P yr^{-1} simplified as vegetation in floodplains in Beusen et al. (2016)). The year 1900 was used as a reference, due

to previous estimates or data not being available to our knowledge. Since our framework was developed with the aim of being used in Earth System Models, we assumed soil equilibrium since this is the initial state criteria used in state-of-the-art model simulations. Therefore, P exports due to soil perturbations reported in Filippelli (2008) and Beusen et al. (2016) were not considered. The distribution of P inputs from catchment non-weathering sources was assumed to be the same as the global distribution of contemporary anthropogenic P inputs, which was derived from the NEWS2 study:

$$P_{\text{nw,catch}} = P_{\text{nw,global}} * DIP_{\text{ant,catch}} / DIP_{\text{ant,global}} \tag{2.4}$$

where $P_{nw,catch}$ is the non-weathering catchment P pool, whereas $DIP_{ant,catch}$ and $DIP_{ant,global}$ are anthropogenic inputs from the NEWS2 study for every catchment and their global sum, respectively.

P river loads

For each catchment, we estimated the total annual P inputs to the catchments ($P_{total,catch}$), as the sum of the catchment weathering yields ($P_{w,catch}$) and of non-weathering sources ($P_{nw,catch}$):

$$P_{total,catch} = P_{w,catch} + P_{nw,catch} \tag{2.5}$$

$P_{total,catch}$ was then fractionated into inorganic P and P contained in tDOM and POM, which was assumed to have been taken up on land or in rivers by the biology (Figure 2.2). After considering this net P transformation to organic matter, the remaining P was assumed to be inorganic P (IP_{catch}) for every catchment:

$$IP_{\text{catch}} = P_{total,catch} - P_{tDOM,catch} - P_{POM,catch} \tag{2.6}$$

The mole ratios of C to P in tDOM and POM were assumed to be 2583:1 (Meybeck, 1982; Compton et al., 2000) and 122:1, respectively. The IP was then fractionated into DIP and Fe-P with a ratio r_{inorg} (DIP:Fe-P = 1:2) derived from the global natural P river export estimates of Compton et al. (2000):

$$DIP_{catch} = r_{inorg} * IP_{catch} \tag{2.7}$$

and:

$$Fe - P_{catch} = (1 - r_{inorg}) * IP_{catch} \tag{2.8}$$

We did not consider shale derived particulate inorganic phosphorus in this study, since it originates from physical erosion, which does not chemically transform the shale. The resulting shale-derived material is considered to not be bioavailable in rivers or the coastal ocean (Compton et al., 2000). We also did not consider in-stream retention and sinks of P, although in-stream processes might retain nutrients within river catchments (Beusen et al., 2016).

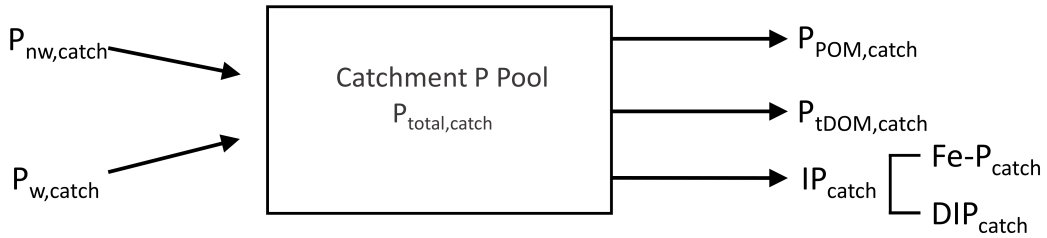

FIGURE 2.2: Scheme of catchment sources of P ($P_{w,catch}$ and $P_{nw,catch}$) and the export fractionation of catchment P ($P_{POM,catch}$,$P_{tDOM,catch}$,Fe-P_{catch} and DIP_{catch}).

Nitrogen and iron

The inputs of N to riverine catchments were derived from the total P inputs to catchments at a globally fixed mole N:P ratio of 16:1 for all species, which is the same as of their oceanic removal as organic matter (Takahashi et al., 1985). While the model study of Beusen et al. (2016) suggests a total pre-industrial N:P mole ratio of 15.5:1, a synthesis of global obervations by Turner et al. (2003) suggests a higher N:P ratio for bioavailable N and P species in most major rivers. However, processes such as denitrification in river estuaries take place that remove N primarily (Meybeck, 1982; Nixon et al., 1996; Beusen et al., 2016), which exceeds the scope of our study. For Fe, we used a Fe:P mole ratio of 3.0 10^{-4}:1 to quantify Fe inputs to the catchments for all species, which is the Fe:P export ratio of organic material in the ocean biogeochemical model.

Dissolved inorganic carbon and alkalinity

The C and Alk weathering release was derived from weathering CO_2 uptake equations that originate from the studies of Hartmann et al. (2009) and Goll et

al. (2014). Weathering reactions take up atmospheric CO_2 and release carbon in the form of HCO_3^- during carbonate weathering:

$$CaCO_3 + CO_2 + H_2O => Ca^{2+} + 2HCO_3^- \tag{2.9}$$

and silicate weathering:

$$Mg_2SiO_4 + 4CO_2 + 4H_2O => 2Mg^{2+} + 4HCO_3^- + H_4SiO_4 \tag{2.10}$$

The equations (9) and (10) dictate the release of 1 HCO_3^- (thus 1 DIC and 1 Alk) for each mole of CO_2 taken up in the weathering of silicate lithologies, and that 2 HCO_3^- (thus 2 DIC and 2 Alk) are released during the uptake of each mole of CO_2 drawn down during the weathering of carbonate lithologies.

The release equations from Hartmann et al. (2009) and Goll et al. (2014) quantify the lithology (i) dependent HCO_3^- weathering release as a function of runoff (q), temperature ($F_i(T)$), soil shielding F_S and a weathering parameter $b_{C,i}$:

$$F_{HCO_3^-} = \sum_{i=lith} b_{C,i} * q * F_i(T) * F_S \tag{2.11}$$

Modelled pre-industrial runoff from the MPI-ESM was used for q. The parameter $b_{C,i}$ is dependent on the weathering rate of the lithology and the composition of the lithology.

We derived the catchment Alk exports to the ocean as the HCO_3^- weathered annually within the catchments, assuming conservation of Alk along the land-ocean continuum. Riverine HCO_3^- is thereby considered to mainly originate from the products of silicate and carbonate weathering reactions (Amiotte Suchet and Probst, 1995; Meybeck and Vörösmarty, 1999). We did not consider additional DIC sources, for instance of CO_2 from respiration of organic matter in soil pore water, groundwater or in rivers. River observational data however show that the riverine HCO_3^- and total DIC mole exports rarely deviate by more than 10% (Araujo et al., 2014). Our assumptions lead to riverine exports of DIC and Alk at a mole ratio of 1:1.

Silica

To quantify the spatial distribution of Si export yields, we used the model of Beusen et al. (2009), which describes the dissolved silica (DSi) river export as:

$$F_{DSiO_2} = b_{prec} * ln(prec) + b_{volc} * volc + b_{bulk} * bulk + b_{slope} * slope \quad (2.12)$$

where F_{DSiO_2} is the export of DSi in Tg SiO_2 yr^{-1} km^{-2}, ln(prec) is the natural logarithm of the precipitation in mm d^{-1}, volc is the area fraction covered by volcanic lithology (no dimension), bulk is the bulk density of the soil in Mg m^{-3}, slope is the average slope based on global Agro-ecological zones (FAO, 2000) in m km^{-1}, and b_{prec}, b_{volc}, b_{bulk}, b_{slope} are the estimated regression coefficients in Beusen et al. (2009). For the precipitation, we used pre-industrial model output from the MPI-ESM, whereas the volcanic area originated from Dürr et al. (2005), the soil density from Batjes (1997) and Batjes (2002), and the average slope from the Global Agro-Ecological Zones database (FAO, 2000). The exports were aggregated for the HD model catchments, while taking into account catchment areas. The loads that were generated by the Beusen et al. (2009) model were converted to Tg DSi loads and are given accordingly in the rest of our study. We also neglected the land-ocean export of particulate silica physically eroded from land.

2.2.2 Ocean Model Setup

Ocean Biogeochemistry

The Max Planck Institute Ocean Model (MPIOM), which was used to simulate oceanic physics, is a z coordinate global circulation model that solves primitive equations under the hydrostatic and Boussineq approximation on a C-grid with a free surface (Jungclaus et al., 2013). The grid configuration used was GR15, which consists of a bipolar grid with poles over Antarctica and Greenland, and a grid resolution of about 1.5 degrees. Vertically, the configuration consists of 40 uneven spaced layers, with increasing thicknesses at greater depths. The surface boundary data, as well as river freshwater model inputs originate from the Ocean-Model-Intercomparision-Project (OMIP, Röske, 2006).

We used the Hamburg Ocean Carbon Cycle model (HAMOCC) to simulate the major biogeochemical processes that affect carbon as well as nutrients in the ocean. The standard model used was an extension of the model described in Ilyina et al. (2013), which is explained in Mauritsen et al. (2019). The changes were made to incorporate dynamical nitrogen fixation through cyanobacteria (Paulsen et al., 2017), to follow recommendations from the OMIP protocol (Orr et al., 2017) and to correct errors in the model. The model represents processes in the water column, sediment, as well as air-sea exchange fluxes. All biogeochemical tracers found in the water column are thereby fully advected, mixed and diffused by the flow fields of MPIOM. The biogeochemistry of the water column includes both organic as well as inorganic carbon cycle processes. The dynamics for the organic carbon cycle are based on a NPZD (nutrients, phytoplankton, zooplankton and detritus) model approach, which was extended to incorporate the compartments of oceanic dissolved organic material (DOM) and cyanobacteria (Six and Maier-Reimer, 1996; Ilyina et al., 2013).

A constant Redfield ratio (C:N:P = 122:16:1, Takahashi et al., 1985) and Fe:P ratio of 3.0 10^{-4}:1 dictate the composition of oceanic organic matter. The phytoplankton growth follows Michaelis-Menten kinetics as a function of temperature, light and nutrient availability. The phytoplankton produce opal when dissolved silica is available, and calcium carbonate ($CaCO_3$) when dissolved silica is depleted. The $CaCO_3$ and opal thereby sink at constant rates.

The mortality of the phytoplankton and its exudation as DOM, as well as the zooplankton grazing of phytoplankton is included. DOM can also be formed due to sloppy feeding. POM is formed from dead cells of phytoplankton and zooplankton, as well as fecal pellets from zooplankton activity. Both oceanic DOM and POM are advected according to the ocean physics, and the POM also sinks as a function of depth (Martin et al., 1987). Aerobic remineralization takes place when the oxygen concentration is above a threshold oxygen concentration, whereas at low enough oxygen concentrations, denitrification and sulfate reduction can take place.

The inorganic chemistry is based on Maier-Reimer and Hasselmann (1987), with adjustments in the calculation of chemical constants as described in the OMIP protocol (Orr et al., 2017). Total DIC and total Alk are thereby prognostic tracers from which the carbonate species are determined diagnostically.

HAMOCC also contains a 12 layer sediment module where the same remineralization and dissolution processes as in the water column take place for the solid sediment constituents (Heinze et al., 1999). The sediment consists of a fraction of pore water, which contains dissolved inorganic compounds (e.g. DIC and DIP). POM, $CaCO_3$ and opal fluxes from the water column are deposited to the top sediment layer. There is a diffusive inorganic compound flux at the water sediment-water column interface and a particulate flux from the bottom layer to a diagenetically consolidated burial layer.

The model considers the gas exchange of CO_2, O_2 and N_2 at the ocean-atmosphere interface. Since we model a pre-industrial state of equilibrium in this study, we used constant atmospheric concentrations for CO_2 of 278ppmV (Etheridge et al., 1996).

Treatment of the river loads in the ocean biogeochemistry model

The biogeochemical riverine loads were added to the ocean surface layer in HAMOCC constantly over the whole year . The locations of major river mouths were corrected manually on a case to case basis for large rivers in order to reproduce the same locations as the freshwater inputs from OMIP. The riverine freshwater discharge on the other hand varied intra-annually according to the prescribed OMIP freshwater loads (Röske, 2006).

The dissolved riverine inorganic compounds (DIC, DIP, DIN, DSi, DIC, DFe, Alk) were added to the model in their dissolved species pools in HAMOCC. We added 80% of P contained in the riverine Fe-P to the oceanic DIP pool, in order for the amount of bio-available Fe-P to be comparable with the given range in Compton et al. (2000) (1.1-1.5 Tg P yr^{-1}). The rest of the Fe-P pool was considered to be unreactive in the ocean and was eliminated. The riverine POM was added to the oceanic POM pool in the ocean model, since we assumed its consistence to be the same (P:N:C:Fe mole ratio of 1:16:122:3.0 10^{-4}).

For tDOM, we extended HAMOCC with a new tracer that was characterized with a C:N:P:Fe mole ratio of 2583:16:1:3.0 10^{-4} (Meybeck, 1982; Compton et al., 2000). tDOM was mineralized as a function of the tDOM concentration at a rate $k_{rem,tDOM}$ and also of an oxygen limitation factor (Γ_{O2}), which decreases the maximum potential remineralization rate as a function of the oxygen

concentration:

$$dtDOM/dt = k_{rem,tDOM} * tDOM * \Gamma_{O2} \quad (2.13)$$

Since a large fraction of tDOM delivered by rivers is already strongly degraded, it is to a certain extent resistent to microbial degradation (Ittekkot, 1988; Vodacek et al., 2003b). We consequently assumed a slightly slower remineralization rate of tDOM ($k_{rem,tDOM}$) compared to oceanic DOM (0.003 versus to 0.008 d^{-1} for oceanic DOM), which is within the tDOM degradation range provided in Fichot and Benner (2014) for the Louisiana shelf (0.001-0.02 d^{-1}). The oxygen limitation function used (Γ_{O2}) was analogous to that of the oceanic DOM which is described in Mauritsen et al. (2019).

Pre-industrial ocean biogeochemistry model simulations

We performed a reference simulation (REF), where the burial loss of biogeochemical tracers was compensated by a global homogeneous flux to the surface ocean, as in the standard configuration of the model. This flux served to maintain a stable ocean state. Thus in REF, the delivery of biogeochemical inputs were added directly in the open ocean while bypassing the coastal ocean, and were fully constrained by the loss of the sediment layer. Our simulation RIV however included riverine loads of inorganic compounds (DIP, Fe-P, DIN, DSi, DFe, DIC, Alk) and organic matter (tDOM, POM), which were constrained by our framework and added to their geographical river mouth locations.

REF was simulated for 5000 years to quasi-equilibrium. RIV was simulated for 4000 years first including both the water column and sediment model components, then for 10'000 years in a model version simulating only sediment processes. In these 10'000 years, the inputs to the sediment were the means of $CaCO_3$, POM and opal from the water column of the last 100 years of the standard simulation. The sediment was then coupled back to the ocean water column, with a simulation performed for 2000 more years in the full model version. For the analysis of the resulting ocean biogeochemistry, we used 100 year means of model output.

2.2.3 Definition of coastal regions for analysis

To investigate the impacts of riverine exports on coastal regions, we chose 10 coastal regions characterized by shallow continental shelves and high riverine loads that cover a variety of latitudes (Table 2.1). The shelves were defined to have depths shallower than 250m. The cutoff sections perpendicular to the coast were done according to MARgins and CATchements Segmentation (MARCATS) (Laruelle et al., 2013), except for the Beaufort Sea, Laptev Sea, North Sea and Congo shelf, where we used the COastal Segmentation and related CATchments (COSCATs) definitions (Meybeck et al., 2006) due to the vastness of their MARCATS segmentations.

TABLE 2.1: Comparison of the surface areas [10^9 m^2] of selected coastal regions with depths of under 250 m in the ocean model setup and in segmentation approaches. The comparisons were done with the MARCATS (Laruelle et al., 2013) or COSTCATs (Meybeck et al., 2006). The shelf classes were defined as in Laruelle et al. (2013).

Coastal Regions	**Major Rivers**	**Model Area**	**MARCATS /COSCAT Area**	**Shelf Class**
1. Beaufort Sea (BS)	Mackenzie	269	274	Polar
2. Laptev Sea (LS)	Lena	397	326	Polar
3. North Sea (NS)	Rhine	499	871	Marginal Sea
4. Sea of Okhotsk (OKH)	Amur	245	992	Marginal Sea
5. East China Sea (CSK)	Yangtze, Huang He	731	1299	Tropical
6. Bay of Bengal (BEN)	Ganges	245	230	Indian Margin
7. Southeast Asia (SEA)	Mekong	1795	2318	Indian Margin
8. Tropical West Atlantic (TWA)	Amazon, Orinoco	448	517	Tropical
9. Congo shelf (CG)	Congo	53	38	Tropical
10. South America (SAM)	Paraná	1553	1230	Subpolar

2.3 Global weathering

2.3.1 Runoff, precipitation and temperature patterns

The weathering yields provided in this study are dependent on the MPI-ESM pre-industrial spatial representation of surface runoff, surface temperature and precipitation (Figure 2.3a,b,c). For the modelled MPI-ESM CMIP5 100 year average, we observe high modelled precipitation and temperature in

the tropics, whereas in the subtropics and temperate zones the patterns are much more spatially variable. Above the Arctic Circle, the model shows only moderate precipitation and cold annual temperatures. Spatial patterns of high precipitation are usually also reproduced in the spatial patterns of runoff. This is however not always the case due to evapotranspiration. For instance, in northern North America, northern Europe and Siberia, a pattern of high runoff can be observed despite relatively low precipitation in these regions, which is most likely due to these regions having low vegetation densities, as well as due to the negative temperature dependency of evaporation, both of which result in lower evapotranspiration rates than in lower latitudes.

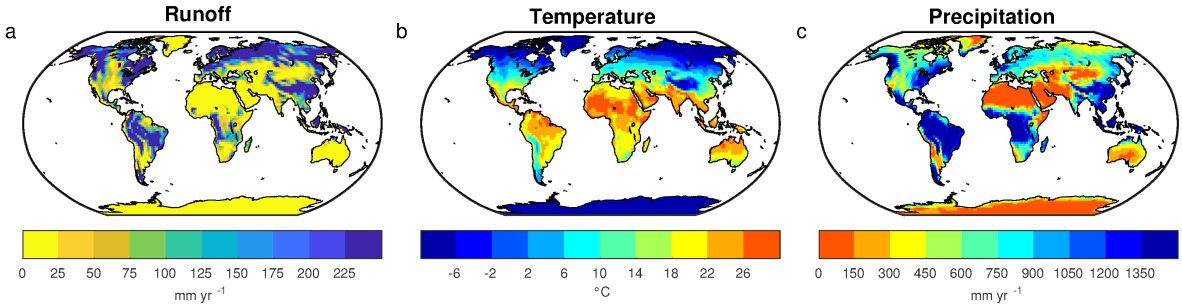

FIGURE 2.3: Modelled pre-industrial (a) surface runoff [mm a^{-1}], (b) surface temperature[] and (c) precipitation [mm a^{-1}] annual means.

Previous work by Goll et al. (2014) describes the MPI-ESM performing well when estimating surface temperatures at single grid cells with regards to observations. The global precipitation is slightly higher than is reported in the Precipitation Climatology Project (GCPC) (Adler et al., 2003), which is discussed along with spatial biases of the precipitation in Stevens et al. (2013). Most notably, the precipitation is too strong over extratropical land surface and too little over tropical land surface. Runoff on the other hand is less well reproduced globally. For the given time period of the CMIP5 simulation, the global runoff is 23,496 km^3 yr^{-1}. This is significantly lower than the global runoff estimations of 36,600-38,300 km^3 yr^{-1} (Fekete et al., 2002; Dai and Trenberth, 2002). The difficulty of representing several processes that control the runoff, such as evapotranspiration and condensation, is also reflected in the global runoff means of other Earth System Models, which range from 23,000 to 42,500 km^3 yr^{-1} (Goll et al., 2014). The spatial patterns in the CMIP5 simulation are however comparable with the mean annual runoff patterns reported in Fekete et al. (2002), with high surface runoff observed in the Amazon basin, West Africa, Indo-Pacific Islands, Southeast Asia, eastern North America, Northern Europe as well as in Siberia. Due to the strong

underestimation of the model regarding the runoff in relation to the combined runoff mean of Fekete et al. (2002) and Dai and Trenberth (2002), we conclude that a scaling factor of 1.59 is necessary to produce runoff plausibly at the global scale. The global runoff from OMIP which provides freshwater to the ocean model, is on the other hand more plausible (32,542 km^3 yr^{-1}), and was therefore not scaled.

2.3.2 Global weathering yields and their spatial distribution

The described weathering release models provide global means for weathering release rates of P, Si, DIC and Alk (Table 2.2), as well as their spatial distributions (Figure 2.4).

For P, which is derived from runoff and temperature data (Hartmann et al., 2014), the global release is 1.34 Tg P yr^{-1} when considering the runoff scaling factor of 1.59, whilst it is 0.84 Tg P yr^{-1} when omitting the scaling factor. The release calculated when compensating the model's runoff underestimation fits within the range found in published literature of 0.8 - 4 Tg P yr^{-1} (Compton et al., 2000; Wang et al., 2010; Goll et al., 2014; Hartmann et al., 2014), while it is on the lower end of this range without the scaling factor. The Hartmann et al. (2014) and Goll et al. (2014) estimates (1.1 and 0.8-1.2 Tg P yr^{-1}, respectively) originate from the same weathering model as is used here. The 1.9 Tg P yr^{-1} reported in Wang et al. (2010) was on the other hand constructed by upscaling measurement data points. In a further study, Compton et al. (2000) provide a quantification of the prehuman phosphorus cycle while distinguishing between land-ocean fluxes from shale-erosion as well as from weathering. Thereby, the total pre-human P riverine flux which originates from weathering is given by averaging P species concentrations from unpolluted rivers and multiplying them with global runoff estimates, yielding an estimate of 2.5 - 4 Tg P yr^{-1}. Both estimates originating from upscaling from river measurements are therefore higher than the P weathering flux provided in the modelling approach in this study, in Goll et al. (2014) and in Hartmann et al. (2014), which suggests further effort might be needed to better constrain the P weathering release.

Deriving the Si export from the Si model (Beusen et al., 2009) forced with MPI-ESM precipitation output amounts to a DSi global yield of 168 Tg Si yr^{-1}. This is within the range estimated by Beusen et al. (2009) (158-199 Tg Si

yr^{-1}), who used the same model while using present day observational data to drive the model for precipitation. Our estimate is also comparable with the 173 Tg Si yr^{-1} estimate provided by Dürr et al. (2011). In a synthesis of the global oceanic silica cycle, Tréguer and De La Rocha, 2013 conclude that rivers deliver around 200 Tg DSi to estuaries annually.

The modelled DIC and Alk release amounts to 374 Tg C yr^{-1}. By extrapolating from measurement data of 60 large river catchments, Meybeck (1982) suggests that the DIC export to the ocean is around 380 Tg yr^{-1} and originates directly from weathering. Further modelling studies also provide similar estimates of 260 to 300 Tg yr^{-1} (Berner et al., 1983; Amiotte Suchet and Probst, 1995). Mackenzie et al. (1998) provide an inorganic carbon flux of 720 Tg C yr^{-1} in a conceptual model that considers mass balance. Since this estimate considers both particulate and dissolved inorganic carbon fluxes, the DIC flux is however significantly lower. Accounting for a particulate inorganic carbon flux of around 170 Tg C yr^{-1} (Meybeck and Vörösmarty, 1999), the value provided by the Mackenzie et al. (1998) study would result in a global DIC load of around 550 Tg C yr^{-1}.

The atmospheric CO_2 drawdown induced by weathering is directly related to the release of HCO_3^- since silicate weathering draws down 1 mole of CO_2 per mole HCO_3^-, and carbonate weathering draws down 0.5 mol of CO_2 per mole HCO_3^- released (Eq. (2.9) and Eq. (2.10)). While we provide a modelled CO_2 drawdown of 280 Tg C yr^{-1} induced by weathering, previously estimated drawdown fluxes are suggested in the range of 220 and 440 Tg C yr^{-1} (Gaillardet et al., 1999; Amiotte Suchet et al., 2003; Hartmann et al., 2009), Goll et al., 2014). As for the DIC release, the modelled estimate is therefore comparable to what was previously suggested in published literature. The results imply that of the 374 Tg C yr^{-1} DIC released by weathering, 280 Tg C drawdown yr^{-1} originates from atmospheric drawdown, while the rest originates from the weathering of the carbonate lithology (94 Tg C yr^{-1}).

TABLE 2.2: Weathering release of P, Si, DIC and Alk, as well as CO_2 drawdown, quantified by the combination of models used in this study in comparison to published literature estimates.

Species	**Modelled weathering flux**	**Estimates**	**Source**
P release [Tg P yr^{-1}]	1.34	1.2 - 1.8	Wang et al. (2009); Hartmann et al. (2014)
Si release [Tg Si yr^{-1}]	168	158 - 200	Beusen et al. (2009); Dürr et al. (2011); Tréguer and De La Rocha (2013)
DIC release [Tg C yr^{-1}]	374	260 - 550	Berner et al. (1983); Amiotte Suchet et al. (1995); Mackenzie et al. (1998); Hartmann et al. (2009)
Alk release [10^{12} mole yr^{-1}]	18.8	-	-
CO_2 drawdown [Tg yr^{-1}]	*280*	*220 - 440*	*Gaillardet et al., 1999; Amiotte-Suchet et al., 2003 Hartmann et al., 2009, Goll et al., 2014*

The spatial distributions of the modelled weathering release of nutrients, carbon and alkalinity (Figure 2.4) show strong agreement with Hartmann et al. (2009), Hartmann et al. (2014) as well as Beusen et al. (2009), where the same models were used, but were forced with observational datasets. Generally, the patterns mostly follow the runoff and precipitation patterns, whereas the lithologies play a secondary role in explaining the spatial variability patterns. This is most likely due to runoff and precipitation having much stronger gradients of variation than the nutrient and carbon content in the different lithologies. Hartmann et al. (2014) suggest that in the case of the P release model, the temperature effect on the spatial variability is of similar magnitude as the P-content of the lithologies.

Furthermore, we observe hotspots that contribute disproportionally to the nutrients and carbon release, as is also suggested in Hartmann et al. (2009)

and Hartmann et al. (2014). The spatial distributions of the weathering release yields indicate the dominance of the Amazon, Southeast Asia as well as Northern Europe and Siberia as strong sources of weathering, despite substantial soil shielding in these regions. The Amazon and Southeast Asian regions have also been identified in other studies as regions of strong carbon yields due their the wet and warm climate, as well as due to their lithology (Amiotte Suchet and Probst, 1995). The Southeast Asian islands are also areas of weathering rates significantly higher than average, due to the combination of the warm and wet climate in the region, as well as the regional abundance of volcanic and carbonate lithologies, which (Gaillardet et al., 1999; Hartmann and Moosdorf, 2011). The northern hemispheric hotspots in eastern North America and western Europe can be explained by the carbonate lithology in these regions. While the weathering and export rates over the 6 major Arctic catchments do not appear as high as other hotspots such as in the Amazon or in Southeast Asia, the vastness of the Arctic catchments could still lead to large exports to the Arctic Ocean, and the shallowness of the Arctic shelf could result in stronger implications of the exports on the ocean carbon cycle of the Arctic Ocean (Le Fouest et al., 2013).

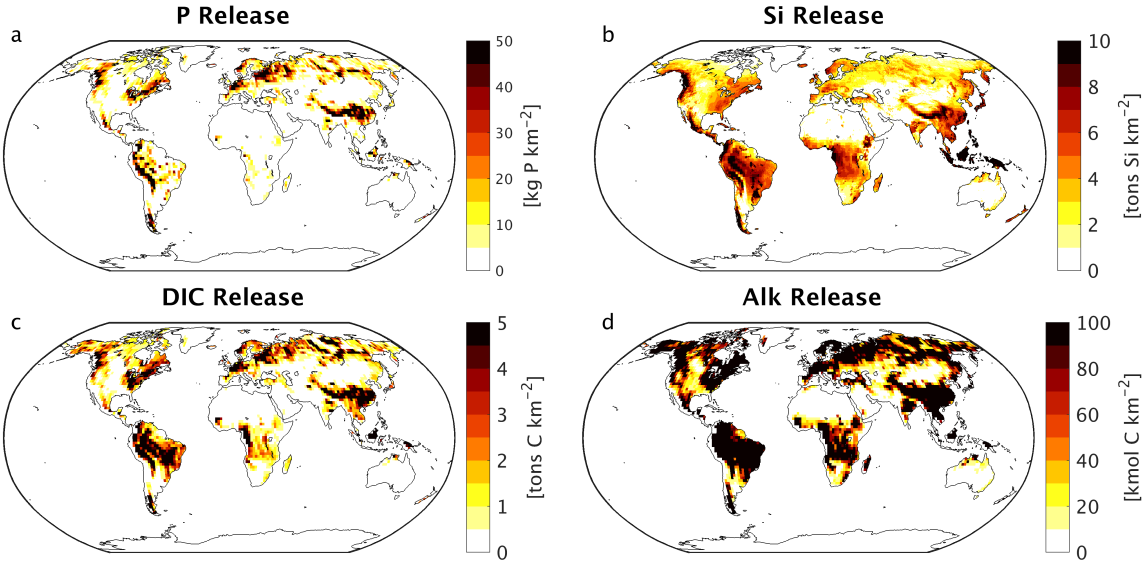

FIGURE 2.4: Weathering release rates of (a) P [kg P km^{-2}], (b) Si [tons Si km^{-2}], (c) DIC [tons C km^{-2}] and (d) Alk [kmol km^{-2}].

2.4 Pre-industrial rivers loads

In this section, we report the modelled riverine loads at the global scale, as well as their regional distributions, while comparing them to a wide range of estimates made for pre-industrial riverine loads until now. We also compare the modelled loads of P and N to contemporary estimates (NEWS2, reference year 1970), in order to grasp the magnitude of their anthropogenic perturbations. Since we focus on the implications of land-sea fluxes for the ocean carbon cycle in this study, our validation analysis revolves around the nutrient, carbon and alkalinity loads at the river mouths, omitting validation of river concentrations further upstream.

2.4.1 Global loads in context of published estimates

The cumulative pre-industrial catchment loads amount to 3.7 Tg P yr^{-1}, 27 Tg N yr^{-1}, 158 Tg Si yr^{-1} and 603 Tg C yr^{-1} delivered to the ocean globally. We thereby estimate the retention of 0.3 Tg P, 2.2 Tg N, 10 Tg Si and 19 Tg C through endorheic catchments, which do not discharge into the ocean. These values do not account for particulate inorganic compounds and in the case of P, the fraction of Fe-P assumed to not be desorbed in the ocean was also subtracted (0.2 Pg P yr^{-1}).

TABLE 2.3: Comparison of modelled global riverine loads (Model. global loads) with previous estimates [Tg yr^{-1}], except for the 1970 POP estimate, which includes all particulate P compounds from the NEWS2 study. The total loads thereby exclude particulate inorganic loads. [1] Compton et al. (2000), [2] Beusen et al. (2016), [3] NEWS2 (Seitzinger et al., 2010), [4] Beusen et al. (2009), [5] Dürr et al. (2011), [6] Tréguer and De La Rocha (2013), [7] Green et al. (2004), [8] Jacobson et al. (2007), [9] Meybeck and Vörösmarty (1999), [10] Resplandy et al. (2018), [11] Regnier et al. (2013), [12] Berner et al. (1983), [13] Amiotte Suchet and Probst (1995), [14] Mackenzie et al. (1998), [15] Cai (2011).

Species	Model. global load	Estimates and Source	Species	Model. global load	Estimates and Source
P [Tg P yr^{-1}]	3.7	4 - 4.8 (prehuman)[1] 2 (1900)[2] 7.6 (1970)[3]	N [Tg N yr^{-1}]	27	19-21 (pre-industrial)[27] 37 (1970)[3]
DIP	*0.5*	*0.3 - 0.5 (prehuman)[1]* 1.1 (1970)[3]	*DIN*	*3.4*	*2.4 (pre-industrial)[7]* *14 (1970)[3]*
DOP	*0.1*	*0.2 (prehuman)[1]* *0.6 (1970)[3]*	*DON + PON*	*24*	*19 (pre-industrial)[7]* *23 (1970)[3]*
POP	2.2	*0.9 (prehuman)[1]* *5.9 (1970)[3]*	C [Tg C yr^{-1}]	603	450 - 950 (present day)[8,9,10,11]
Fe-P	*0.8*	*1.1 - 1.5 (prehuman)[1]* -	*DIC*	*366*	*260 - 550 (present day)[12,13,14]*
			DOC	*134*	*130 - 250 (present day)[3,9,15]*
			POC	*103*	*100 - 140 (present day)[3,9]*
DSi [Tg Si yr^{-1}]	158	158 - 200 (present day)[4,5,6]			

The magnitudes of modelled land-ocean exports of P, N, Si and C, as well as their fractionations, largely agree with the wide range of estimates found in published literature (Table 2.3).

For instance, the modelled global P loads fluxes are close to the higher P export estimate range of 4 - 4.7 Tg P yr^{-1} reported in Compton et al. (2000), which was constructed by upscaling natural river catchment P concentrations to the global river freshwater discharge (thus prehuman). A recent modelling study by Beusen et al. (2016), which takes into account a more complex retention scheme within rivers than is done in our framework, suggests a lower load of 2 Tg P yr^{-1} for year 1900. The 1970 estimate (7.6 Tg P yr^{-1}) provided by the NEWS2 study, which considers substantial anthropogenic inputs, nevertheless suggests a steep 20th century increase in the global P flux to the ocean for all three cases.

The modelled DIP export to the ocean (0.5 Tg P yr^{-1}) is at the top range of prehuman estimates (0.3 - 0.5 Tg yr^{-1}) and well below 1970 estimates (1.1 Tg P yr^{-1}). A direct fractionation of the global P flux to DIP, DOP and POP is not provided in the Beusen et al. (2016) study. We estimate similar global

loads of DOP as Compton et al. (2000) (around 0.1 and 0.2 Tg P yr^{-1}). The modelled DOP value is also much lower than the 1970 value (0.6 Tg P yr^{-1}), which was also strongly anthropogenically perturbed for 1970 (Seitzinger et al., 2010). The modelled POP global load is larger than the estimate of Compton et al. (2000), which could be due to the POM C:P ratio of 122:1 chosen in our study. Strong uncertainties exist in the global C:P ratios for riverine POM, with Meybeck (1993) suggesting a weight ratio of around 57 C:P, whereas Ramirez and Rose (1992) estimate a ratio of around 500. The particulate P load given in the NEWS2 study is vastly higher than the POP load modelled in our study, but a large fraction of the estimate is likely to be directly shale-derived particulate inorganic P and thus biologically unreactive in the ocean. The modelled Fe-P (1.0 Tg P yr^{-1}) is slightly below the range estimated in Compton et al. (2000) (1.5 - 3.0 Tg P yr^{-1}). However, the assumed reactive fraction of the Fe-P loads (0.8 Tg P yr^{-1}) here is close to how much P is suggested to be desorbed in the coastal ocean in Compton et al. (2000) (1.1-1.5 Tg P yr^{-1}).

Despite our simplified assumption of N loads being coupled to P loads, the modelled global N load is also situated within the pre-human and contemporary land-ocean N loads given in the modelling study of Green et al. (2004) (21 and 40 Tg N yr^{-1} respectively). The modelled annual DIN load (3.4 Tg N) is slightly higher than the prehuman load given in the Green et al. (2004) study (2.4 Tg N yr^{-1}). In Beusen et al. (2016), the global pre-industrial N load is suggested to be lower (19 Tg N yr^{-1}) due to in-stream retention and removal.

The modelled global load of DSi is 158 Tg Si yr^{-1}, which is at the lower boundary of the range of present day estimates of 158-200 Tg Si yr^{-1}. We thereby assume that the change in the global DSi load over the 20th century is small, and therefore compare our pre-industrial estimate with present day estimates from published literature. The NEWS2 study used the same Beusen et al. (2009) silica export model forced with present day observational precipitation data, Dürr et al. (2011) and Tréguer and De La Rocha (2013) upscaled discharge weighted DSi concentrations at river mouths. Substantial amounts of particulate silica are suggested to be delivered to the ocean, yet it is not clear how much is dissolvable and biologically available (Tréguer and De La Rocha, 2013). Another point of uncertainty is the increase in river damming during the 20th century, which might have strongly increased the global silica retention in present day rivers (Ittekkot et al., 2000a; Maavara et al., 2014). The pre-industrial loads therefore might have been higher than

for the present day, but the implications of damming on the retention of biogeochemical compounds escape the scope of this study.

The modelled total C, DIC, DOC and POC fluxes are within, albeit on the lower side of the present day estimate ranges shown in Table 2.3. While the carbon retention along the land-ocean continuum might have increased, enhanced soil erosion through changes in land use might have also increased the carbon inputs to the freshwater systems, leaving question marks on the magnitude of the net anthropogenic perturbation (Regnier et al., 2013; Maavara et al., 2017). The agreement of the DOC and POC loads with estimates is not surprising, since they originate directly from the NEWS2 study, which already validated the global loads extensively.

The large spread found in the literature estimates regarding all species points towards difficulties in constraining pre-industrial river fluxes. Even for the present day, Beusen et al. (2016) note large differences between the outcomes of their study and the previous global modelling study NEWS2. Upscaling approaches, on the other hand, are often based on data collected by Meybeck (1982) for pre-1980s without taking into account more recent river measurement data. They also rely on the assumption of a linear relationship between river runoff and river specie loads. While we acknowledge a certain degree of uncertainty in the numbers provided in this study, and that possibly significant riverine processes such as in-stream retention are omitted, the modelling approach chosen nevertheless leads to pre-industrial global river loads that are in line with what was suggested previously and to a framework that could be used within state-of-the-art Earth System Models.

2.4.2 Spatial load distribution and identified hotspots

Riverine loads of the major catchments show similar spatial distributions with regards to areas of high weathering rates (Figure 2.5), with warm and wet regions yielding the largest river exports to the ocean. We observe large differences between the northern and southern hemispheres. The northern hemisphere accounts for an annual total carbon input of 404 Tg C to the ocean, vastly dominating the global loads (67% of total global C). The northern hemisphere also contributes overproportionally to the oceanic nutrient supply (69% for DIP and DIN, 60% for DSi). The dominance of northern hemispheric

riverine C land exports to the ocean is also reported in Aumont et al. (2001) and Resplandy et al. (2018).

We observe several regions of disproportionate contributions to global riverine loads. For one, rivers that drain into the tropical Atlantic consist of a major fraction of the global biogeochemical oceanic supply. This is due to major rivers of the South American continent debouching into the ocean basin, as well as considerable exports provided by the west African Volta, Congo and Niger rivers (Table 2.4). According to our framework, the seven largest rivers unloading in the region (Orinoco, Amazon, São Francisco, Paraíba do Sul, Volta, Niger and Congo) amount to a total yearly carbon flux of 123 Tg C (58 Tg DIC, 44 Tg DOC, 21 Tg POC), which consists of around 20% of the global carbon riverine exports. These regional carbon loads agree very well with estimated values derived from monthly river discharge and carbon concentrations data in Araujo et al. (2014) (53 Tg DIC, 46 Tg DOC). In terms of catchments, the pre-industrial Amazon river provides the largest inputs of biogeochemical tracers to the ocean in the region (modelled annual loads of 0.07 Tg DIP, 0.5 Tg DIN, 15.2 Tg DSi, 33.2 Tg DIC , 28.3 Tg DOC Tg, 17.1 Tg POC). Present-day data from Araujo et al. (2014) suggests annual Amazon river loads of 0.22 Tg DIP, 17.8 Tg DSi, 32.7 Tg DIC, 29.1 Tg DOC. Since DIP loads are suggested to have strongly increased due to anthropogenic inputs (NEWS2, Seitzinger et al., 2010), the pre-industrial and present day difference in the DIP loads is plausible. For the other tropical Atlantic catchments, the modelled DIC loads are close to estimated values for the Congo, Orinoco and Niger, but are overestimated for the smaller catchments of the Paraíba, Volta and São Fransisco. The DIP loads of the tropical Atlantic catchments tend to show much lower values with regards to present day data, suggesting the realistic increase in the region's DIP loads from pre-industrial exports of 81.8 10^9 g P yr^{-1} to present day loads of 276 10^9 g P yr^{-1} due to anthropogenic inputs.

Although less significant in terms of global loads, the major Arctic rivers (Yukon, Mackenzie, Ob, Lena, Yenisei) provide a large carbon supply, which consists of a dominant fraction of DIC, to the shallow basin of the Arctic Ocean. The Arctic rivers thereby provide 37.5 Tg DIC (10% of global DIC), 14.4 Tg DOC (11 % of global DOC) and 4.4 Tg POC annually to the Arctic Ocean. The total C loads of the Arctic therefore amount to 56 Tg C yr^{-1}, thus 9% of global C loads. The DIC, DOC and POC load levels are comparable to estimates of 29 Tg DIC yr^{-1} (Tank et al., 2012), 17 Tg DOC yr^{-1} (Raymond

et al., 2007) and 5 Tg POC (Dittmar and Kattner, 2003). Total Arctic DIP loads (40.8 10^9 g P yr^{-1}) derived from our modelling approach are slightly higher with regards to published literature estimates of 35.8 10^9 g P yr^{-1}. DIP inputs from anthropogenic sources are considered to be small for Arctic catchments (NEWS2), which explains why the modelled pre-industrial DIP loads are of comparable magnitudes to observed DIP loads for the present day. River loads originating from weathering models (DIC and DIP loads) thereby show a slight overestimation in the Arctic with regards to published literature estimates. Since both of these modelled exports mostly originate from weathering models due to the low anthropogenic contributions to Arctic catchment riverine loads, the runoff correction of the P and DIC weathering release models of 1.59 might be too high for this region.

Southeast Asian rivers also provide large exports of biogeochemical tracers to the ocean. The Huang He, Brahmaputra-Ganges, Yangtze, Mekong, Irrawaddy and Salween, which have catchment areas characterized by warm and humid climates, provide 92.4 Tg C yr^{-1} to the ocean (15% of global C loads). We observe vastly elevated DIP levels for the present day estimates with regards to our pre-industrial modelled levels. The NEWS2 data suggests a strong present day perturbation of the DIP loads due to anthropogenic inputs to the region's catchments, which can plausibly explain these differences.

The Indo-Pacific Islands have been identified as a region with much higher weathering yields than average Hartmann et al. (2014). Although this region only accounts for around 2% of the global land surface, it provides 7% (39 Tg) of C and in particular 10% (10 Tg C) of the global POC delivered to the ocean annually, making the region a stronger land source of POC than the entire Arctic basin. This implies that POM mobilization through soil erosion is a substantial driver of land-sea carbon exports in the region, in addition to weathering.

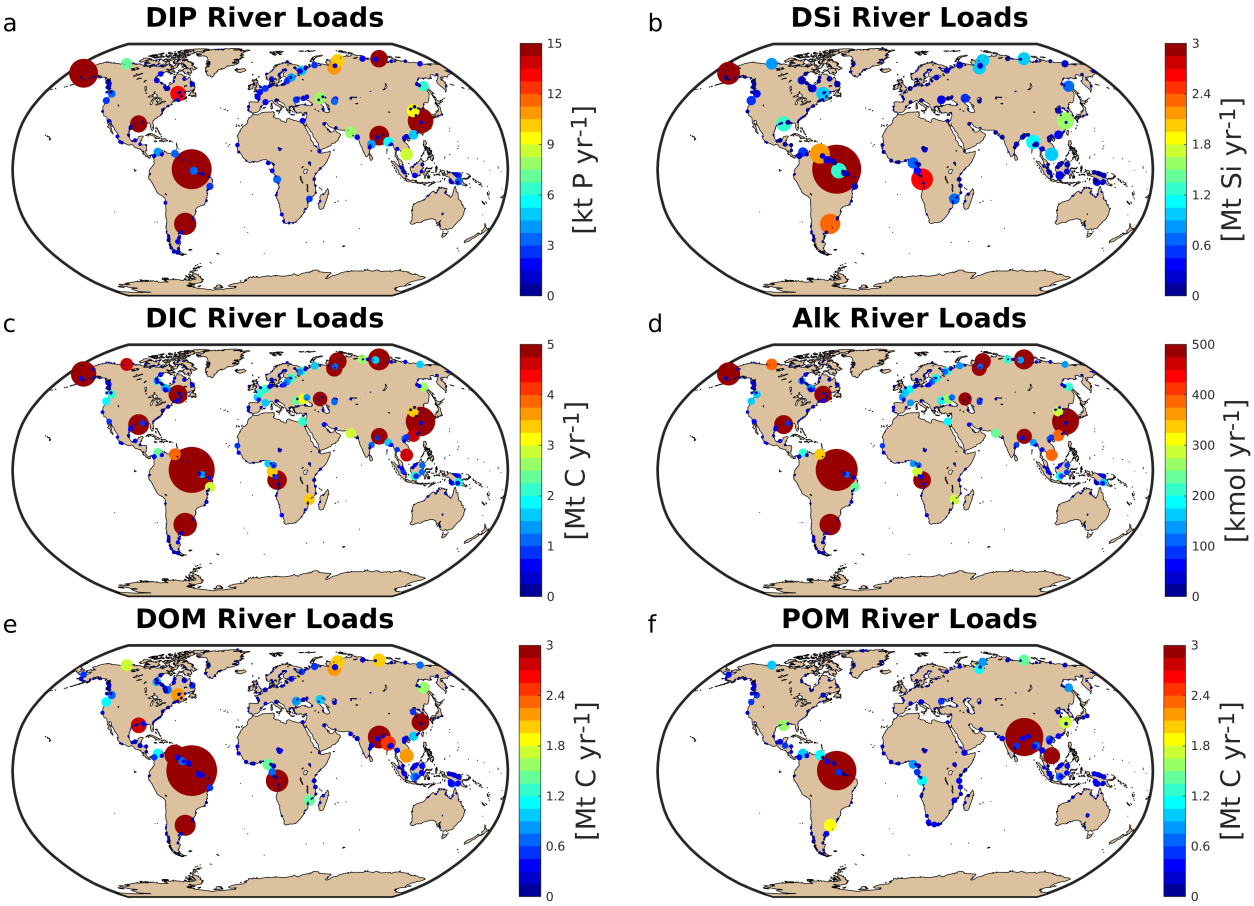

FIGURE 2.5: Modelled dissolved annual river loads of DIP (a), DSi (b), DIC (c), Alk (d), DOM (e) and POM (f).

TABLE 2.4: Regional hotspot of C loads [Tg C yr^{-1}] and DIP loads [10^9 g P yr^{-1}] compared with regional estimates: [1] Araujo et al. (2014), [2] Bird et al. (2008), [3] Tank et al. (2012), [4] Raymond et al. (2007), [5] Dittmar and Kattner (2003), [6] Le Fouest et al. (2013), [7] Li and Bush (2015), [8] Yoshimura et al. (2009), [9] Tao et al. (2010), [10] Seitzinger et al. (2010). Modelled DIP is from our approach to represent pre-industrial fluxes, whereas the DIP literature estimates are from present day data and are strongly affected by anthropogenic perturbations.

Hotspots	**Modelled**				**Estimates**			
	DIC	DOC	POC	DIP	DIC	DOC	POC	DIP
Tropical Atlantic								
Amazon	33.2	28.2	17.1	73	32.7[1]	29[1]	6.1[2]	221[1]
Congo	9	5.6	1.2	2.3	13[1]	10.58[1]	2.0[2]	18 [1]
Paraíba	2.4	0.5	0.4	<0.1	0.3[1]	0.10[1]	-	0.6[1]
Volta	3	0.5	0.5	0.1	0.1[1]	0.13[1]	-	7.0[1]
Niger	1.1	1.5	0.9	1.0	2.2[1]	0.43[1]	0.8[2]	7.5[1]
São Fransisco	6	2.9	0.2	2.4	0.5[1]	0.35[1]	-	0.5[1]
Orinoco	3.3	4.8	1.1	2.9	5.0 [1]	3.9[1]	1.7[2]	21.4[1]
Total	**58**	**44**	**21**	**81.8**	**53**	**46**	**-**	**276**
Arctic								
Mackenzie	4.5	1.7	0.4	6.0	6.29[3]	1.4[4]	-	1.5[6]
Yukon	3.1	6.1	0.9	3.8	4.45[3]	1.7[4]	-	1.9[6]
Lena	12.7	2.0	1.1	8.23	5.82[3]	5.83[4]	0.47[4]	4.4[6]
Yenisei	8.6	2.0	1.2	8.8	6.96[3]	4.69[4]	0.17[4]	7.9[6]
Ob	8.6	2.6	0.8	14.1	5.90[3]	3.05[4]	0.3-0.6[4]	20.4[6]
Total	**37.5**	**14.4**	**4.4**	**40.8**	**29.4**	**16.7**	**1.09**	**35.8**
Southeast Asia								
Ganges	7.7	5.8	15.6	21.3	4.2[7]	1.4[2]	1.7[2]	165[10]
Irrawaddy	2.5	6.1	0.9	4.6	10.8[7]	0.89[2]	3.25[2]	8.7[10]
Salween	0.7	0.3	0.7	0.8	8.4[7]	0.26[2]	2.9[2]	1.9[10]
Mekong	4.4	2.1	3.1	7.2	4.5[7]	-	-	0.9[8]
Huang He	3.6	0.5	0.3	8.3	1.3[7]	0.1[2]	6.3[2]	5.0[9]
Yangtze	23	3.5	1.7	29.9	24[7]	2.1[2]	6[2]	92[10]
Xi River	8.6	0.9	0.4	4.3	-	4.6[2]	-	25[10]
Total	**50.5**	**19.2**	**22.7**	**76.4**	**-**	**-**	**-**	**298.5**
Indo-Pacific Islands								
Total	**19.4**	**10.2**	**10.1**	**24.7**	**-**	**-**	**-**	**-**

2.4.3 Exports to chosen coastal regions

With respect to the 10 shallow shelf regions chosen for this study (Table 2.1), the catchments of the low latitude regions (5. CSK, 6.BEN, 7.SEA, 8.TWA, 9.CG) provide substantially more carbon and nutrients to the coastal ocean than the high latitude regions (Figure 2.6), although the differing size of the coastal regions and of their drainage catchments might play a strong role in explaining these differences. The tropical West Atlantic (8.TWA) has the largest input of biogeochemical tracers due to the Amazon and Orinoco rivers being a dominant source of nutrients and carbon. In the tropical regions of the Bay of Bengal (6.BEN) and Southeast Asia (7.SEA), the fraction of carbon delivered as POC is substantially higher than for the rest of the regions (Figure 2.6b). Furthermore, in the high latitude regions (1.BS, 2. LS, 3.NS, 10.SAM), the DIC loads are the major source of carbon, whereas for the other regions, organic carbon is the largest contributor to the total carbon load. The increasing contribution of DIC loads to the total carbon load at high latitudes was moreover observed for Arctic catchments in Table 2.4.

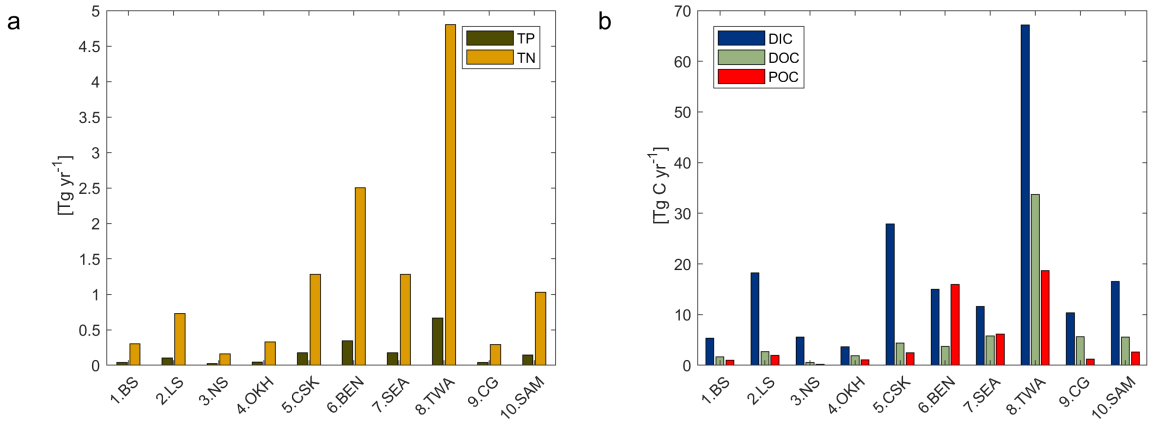

FIGURE 2.6: (a) Total P (TP) and N (TN) and (b) C (DIC, DOC and POC) exports to the chosen coastal ocean regions. TP and TN are the total P and N modelled in their dissolved inorganic species (DIP, DIN) and organic species (tDOM and POM). DOC and POC are the carbon loads from tDOM and riverine POM, respectively.

2.5 Implications for the ocean biogeochemistry

In this section, we investigate the long-term implications of considering the inputs of pre-industrial riverine loads in an ocean biogeochemical model. We thereby compare the RIV simulation, in which the described pre-industrial

riverine loads were added, to the standard model REF simulation, where biogeochemical tracers were added homogeneously to the surface ocean to compensate for particulate losses ($CaCO_3$, opal and organic matter) in the sediment and thus were necessary to maintain a stable ocean state.

2.5.1 Ocean state - An increased biogeochemical coastal sink

We observe that the total REF and RIV nutrient magnitudes of the P, N and Si inputs to the ocean are very similar (Table 2.5), implying that the differences in nutrient concentrations and NPP between RIV and REF originate from the geographic locations of inputs. Alk inputs are also added at nearly the same levels. The total carbon inputs are on the other hand increased by almost 100% in RIV in comparison to REF. These larger carbon inputs originate firstly from higher DIC to Alk ratio of the riverine loads (1:1) than is exported through the net $CaCO_3$ production (1:2). Secondly, there is a higher carbon load originating from organic matter, since the tDOM C:P ratio is higher than the oceanic DOM C:P ratio. In both cases, the model inorganic (366 Tg C yr^{-1}) and organic (237 Tg C yr^{-1}) carbon inputs in RIV show stronger agreement with the riverine inorganic (260-550 Tg C yr^{-1}) and organic carbon (270 - 350 Tg C yr^{-1}) global load estimates found in literature (Meybeck, 1982; Amiotte Suchet and Probst, 1995; Mackenzie et al., 1998; Meybeck and Vörösmarty, 1999; Hartmann et al., 2009; Seitzinger et al., 2010; Cai, 2011; Regnier et al., 2013). These higher carbon inputs result in a net long-term outgassing flux (231 Tg C yr^{-1}), which we will discuss in detail.

Despite slightly larger inputs of nutrients in RIV than in REF, lower global surface dissolved nutrient concentrations and lower global primary production rates are found in RIV. The coastal ocean therefore acts as an increased biogeochemical sink in the model, since river-delivered or newly produced particulate organic matter reaches the shelf sea floor faster than in the open ocean, allowing for less time for the organic matter to be remineralized within the water column. On shallow shelves (<250m depth), we find an increased organic matter flux of 0.25 Gt C yr^{-1} to the sediment in RIV versus a flux of 0.18 Gt C yr^{-1} for REF. Although strong uncertainties exist in literature regarding the coastal POM sediment deposition flux, the range of global values given in a review by Krumins et al. (2013) (0.19-2.20 Gt C yr^{-1}) hints that the coastal POM deposition flux is possibly improved in RIV.

TABLE 2.5: Comparison of river inputs and the ocean state for REF and RIV. Additionally, we compare the modelled mean surface DIP, DIN and DSi concentrations with World Ocean Atlas 2013 (WOA) surface layer means.

Variables	REF	RIV	WOA
(River) Inputs			
P [Tg P yr^{-1}]	3.49	3.7	
N [Tg N yr^{-1}]	25.2	27	
Si [Tg Si]	115	158	
Alk [Tg HCO_3^- yr^{-1}]	416	366	
Inorganic C [Tg C yr^{-1}]	208	366	
Organic C [Tg C yr^{-1}]	106	237	
Ocean variables			
Global net primary production [Gt C yr^{-1}]	48.87	47.09	
Net CO_2 flux [Gt C yr^{-1}]	-0.05	0.18	
Global organic material export 90m [Gt C yr^{-1}]	6.84	6.47	
Global calcium carbonate export 90m [Gt C yr^{-1}]	0.66	0.61	
Global opal production [Gt Si yr^{-1}]	1.37	1.38	
Surface Alk [mM]	2.25	2.24	
Surface DIC [mM C]	1.94	1.94	
Surface DIP [μM P]	0.439	0.413	0.48
Surface DIN [μM N]	3.90	3.76	5.04
Surface DSi [μM Si]	13.6	14.6	7.5
Oxygen minimum zones volume [km^3]	2.61	2.45	

The global mean surface concentration is lower in RIV than in the observational data of the World Ocean Atlas 2013 (WOA, Boyer et al., 2013) for DIP (0.439 and 0.480 μM P respectively) and DIN (3.90 and 5.04 μM N), and higher for DSi (13.6 and 7.5 μM Si). The WOA dataset is constructed from present day observations of an ocean state that might already be perturbed by a substantial increase in riverine P and especially N loads, whereas the model shows pre-industrial concentrations. A consideration of the substantial anthropogenic increase in DIN riverine loads (Seitzinger et al., 2010; Beusen et al., 2016) could plausibly shrink some of the disagreement with the WOA dataset in the case of DIN. A large part of the DIN underestimation is however most

likely due to notably large tropical Pacific oxygen minimum zones, which cause a large DIN sink due to denitrification and the consumption of DIN in the anaerobic breakdown of organic matter. Furthermore, the lower surface concentrations of DIP and DIN than found in the WOA dataset suggest that the coastal sink of biogeochemical tracers might be too large. Nevertheless, the surface DIN:DIP ratio in RIV is slightly improved in comparison to REF with regards to WOA, which is most likely due to the shrinking of the tropical Pacific oxygen minimum zones.

The DIP and DIN underestimation bias with respect to the WOA datasets are also reflected in the spatial distributions of the surface concentrations (Figure 2.7), where in particular the DIN concentrations are underestimated in most major basins. The spatial patterns of differences with regard to WOA data are similar for RIV and for REF, suggesting ocean physics being the dominant driver of the nutrient distributions in the open ocean (see Appendix, Figure A.3,A.4,A.5). Prominent bias of the model are lower surface DIP and DIN concentrations in the Southern Ocean, higher DSi concentrations in the Southern Ocean, and higher DIP concentrations in the tropical gyres in comparison with the WOA dataset.

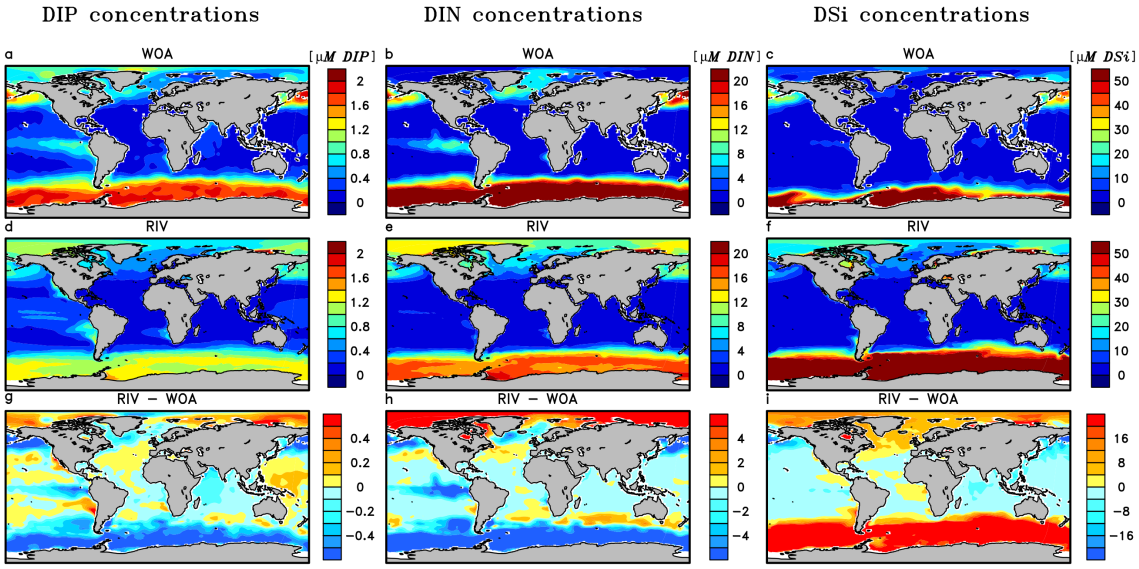

FIGURE 2.7: Surface DIP (a,d,g), DIN (b,e,h) and DSi (c,f,i) concentrations in WOA observations (a,b,c), RIV(d,e,f) and their differences RIV-OBS(g,h,i).

2.5.2 Riverine-induced NPP hotspots

The net primary production (NPP) in the most productive open ocean regions (tropical Atlantic and Pacific, north Pacific, Southern Ocean) are reduced in RIV with respect to REF, but nevertheless remain the most dominant areas of biological production (Figure 2.8a,b). However, substantial enhancements in the NPP can be found near various major river mouths. In proximity to lower latitude rivers such as the Amazon, the uptake of nutrients by phytoplankton via primary production occurs efficiently due to favorable light conditions. This freshly produced organic matter, in addition to the terrestrial supplies of organic material delivered by rivers, leads to local increases in oceanic organic material concentrations (Figure 2.8c,d).

In the tropical Atlantic, a region we identified to have major nutrient and carbon riverine supplies in section 2.4.2, the NPP is increased near the mouths of the major rivers. This is most notably the case in the Amazon plume, which mirrors the direction of the freshwater plume northwestwards (see Appendix, Figure A.1). However, in the open ocean of the equatorial Atlantic, where upwelling takes place from deeper water layers, the NPP is decreased. While considering both effects, the NPP increases by only 2% for the whole region, while there are nevertheless substantial NPP increases along the western African and eastern South American tropical shelves.

In the Equatorial Pacific, we observe a strong decrease in NPP, a feature that could be partly explained by the South American river systems, which majorly discharge into the Atlantic (Figure 2.6). Although Southeast Asian rivers deliver substantial amounts of land-derived material to the ocean, the export to the open Pacific appears to be inefficient, with model coastal salinity profiles in this region suggesting little mixing with the open ocean. Coastal parallel currents could be a key reason explaining the inefficent export (Ichikawa and Beardsley, 2002). Furthermore, the riverine loads mostly supply semi-enclosed or marginal seas (East China, South China and Yellow Seas), which have limited exchange to the open ocean and which are affected by the relatively coarse GR15 model resolution in this region (Jungclaus et al., 2013). The resulting decrease in the Equatorial Pacific NPP is responsible for most of the shrinking of oxygen minimum zones (Table 2.5). The NPP is decreased in the Benguela Current System, which is a major NPP hotspot in the model due to nutrients being entrained to the surface from deeper layers. Moreover, the NPP is increased in certain semi-enclosed seas such as the Caribbean

Sea, Baltic Sea, the Black Sea and the Yellow Sea, where satellite observation data also suggest high chlorophyll concentrations (Behrenfeld and Falkowski, 1997).

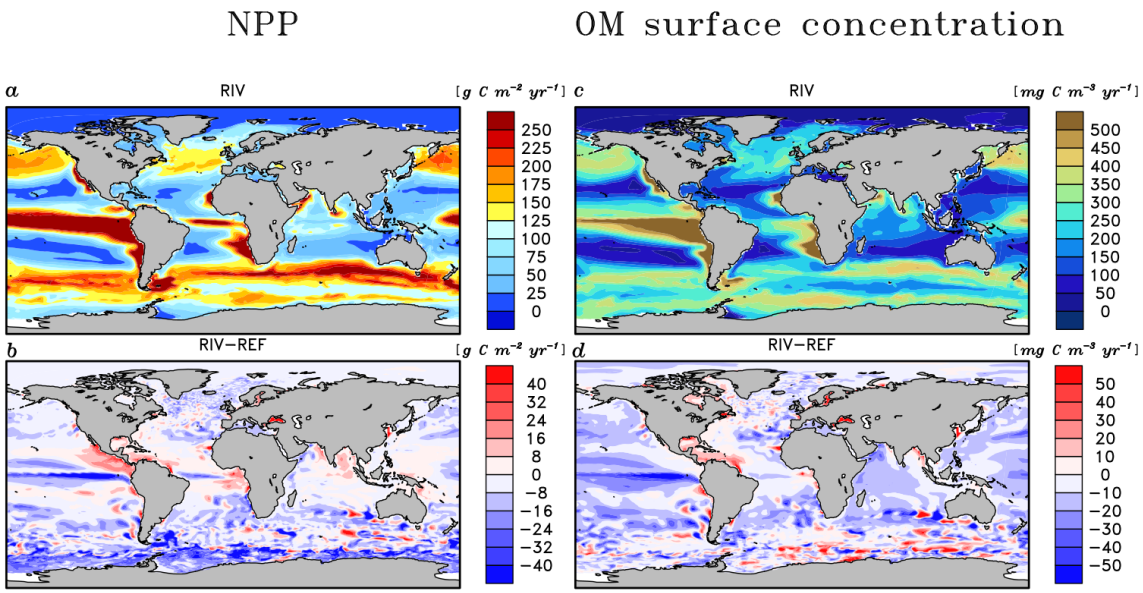

FIGURE 2.8: Depth integrated annual NPP (a,b) and total annually accumulated organic concentration (c,d) in the surface layer in the RIV simulation and RIV - REF.

The Arctic Ocean does not show a noticeable increase in NPP, despite high nutrient concentrations in the basin. This can be explained by the light limitation, as well as sea ice coverage inhibiting the primary production especially during the winter. In the entire basin, the nutrient concentrations are much higher than what is suggested in the WOA database. In Bernard et al. (2011), where nutrient inputs were added to the ocean according to the NEWS2 study, similarly high concentrations of DSi were found in the Arctic. Furthermore, Harrison and Cota (1991) suggest that nutrients limit phytoplankton growth in the late Summer in the Arctic Ocean. Although the summer primary production in the model is substantially higher than for other seasons, the NPP is never nutrient limited for the vast majority of the Arctic.

2.5.3 Riverine-induced CO_2 Outgassing

The addition of riverine carbon loads causes an oceanic CO_2 source of 231 Tg C yr^{-1} to the atmosphere (Table 2.5). The outgassing flux is thereby caused by carbon contained in tDOM, as well as considering the inputs of DIC. While the

hotspots of the riverine-induced carbon outgassing are regions in proximity to major river mouths (Figure 2.9b), a widespread, albeit weaker outgassing signal can be observed in open ocean basins. The largest outgassing fluxes are found in the Atlantic and Indo-Pacific (31% and 43% of global outgassing flux respectively), likely due to the tropical Atlantic and Southeast Asian hotspots of riverine carbon supplies (see section 2.4.2). In the Southern Ocean, we observe an increase in the outgassing flux of 17 Tg yr^{-1} when comparing RIV to REF, which is almost 10% of the total riverine-caused outgassing. The southern hemisphere shows an oceanic outgassing flux of 113 Tg yr^{-1} (49%), despite southern hemisphere land exports contributing only 227 Tg (36 %) of total riverine carbon loads to the ocean, which suggests a substantial interhemispheric transfer of carbon from the northern hemisphere to the southern hemisphere. The interhemispheric transfer of carbon in the ocean has been a topic of discussion in literature, with studies of Aumont et al. (2001) and Resplandy et al. (2018) suggesting the transport of carbon between latitudinal regions of the ocean to compensate for the heterogeneous terrestrial supplies.

The high latitude Arctic rivers (Lena, Mackenzie, Yenisei, Ob, Oder, Yukon) provide a source of carbon to their respective shelves, which causes outgassing on the Laptev shelf and in the Beaufort Sea (2.2 Tg C yr^{-1} and 2.3 Tg C yr^{-1}, respectively). The impacts of riverine carbon loads in these regions can also be observed in the present day coastal ocean pCO_2 dataset of Laruelle et al. (2017), in which these regions display very high pCO_2 values.

While all areas in proximity to the river mouths show increases in CO_2 outgassing caused by the addition of riverine inputs of carbon (Figure 2.9b), determining the net sign of the CO_2 of individual plumes in RIV is not as straightforward. A CO_2 undersaturation in many river plumes can still be observed despite the addition of riverine carbon (Figure 2.9a). Riverine nutrient, carbon, alkalinity and freshwater inputs, as well as physical and biogeochemical oceanic features all interact to affect the net CO_2 flux. The Amazon plume is a prominent example, which is a net carbon sink near the river mouth in the model despite being supplied by large amounts of carbon from the Amazon river. The near-shore Amazon plume is thereby also identified as an atmospheric carbon sink in literature (Cooley et al., 2007; Lefèvre et al., 2017).

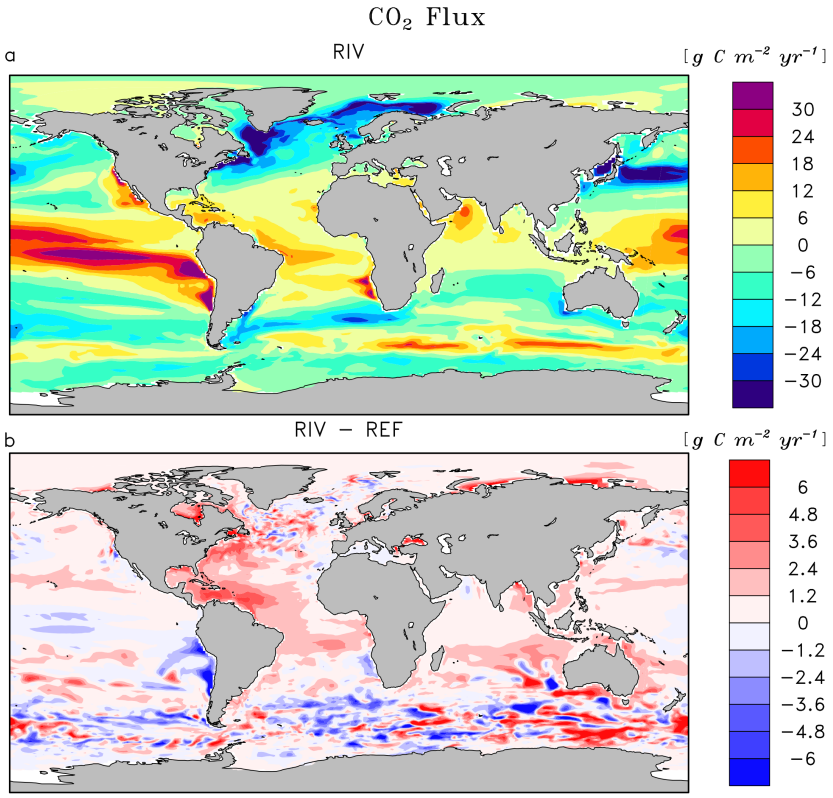

FIGURE 2.9: Annual pre-industrial air-sea CO_2 exchange flux of (a) RIV and (b) RIV-REF. A positive flux describes an outgassing flux from the ocean to the atmosphere, whereas a negative flux is from the atmosphere to the ocean.

2.5.4 Sensitivity of the NPP and CO_2 flux in chosen coastal regions

The areas of the 10 chosen coastal ocean regions (Table 2.1 in section 2.4.3) are better represented for the Atlantic shelves than eastern Asian shelves due higher resolutions of the GR15 model in the Atlantic (Jungclaus et al., 2013). We observe strong latitudinal differences in the regional riverine inputs (section 2.4.3), and analyze their implications for the coastal ocean regions here. We observe strong differences in the regional responses to the riverine loads, with a tendency of stronger relative changes in NPP on lower latitudinal shelves, and stronger relative changes in CO_2 in the higher latitudes (Figure 2.10).

For tropical and subtropical regions, we observe major NPP increases of 166%, 377% and 71% for the tropical West Atlantic (3.TWA), Bay of Bengal (5.BEN) and East China Sea (6.CSK), respectively. The availability of light, as well as

the large supplies of nutrients to these regions provide optimal conditions to enhance the biological production. Surprisingly however, the Southeast Asian shelf (6.SEA) does not show a similar substantial NPP increase as the other tropical regions despite considerable riverine fluxes to the region (Table 2.4 in Section 4.2). This is on one hand due to the large area of the defined region; the shelf is the largest that is analyzed in this study (1795 10^9 m^2), which reduces the impact of the river loads per area. Secondly, there is a larger connection area to the open ocean due to not sharing a coastal border with a continent, which implies a larger open ocean exchange, thus reducing the influence of the riverine supply with regard to open ocean supplies. The Congo shelf (9.CG) on the other hand has a very small area (53 10^9 m^2) due to a steep coastal slope. The NPP here is however already one of the highest of the chosen regions without considering rivers, suggesting that the region is already strongly supplied with nutrients from coastal upwelling.

On the temperate shelves, where there is a stronger seasonal cycle of the light limitation, the North Sea (2.NS) shows only weak enhancement in the NPP (2%) due to riverine inputs. The South American (10.SAM) and Sea of Okhotsk (4.OKH) also do not show significant NPP increases. Although the NPP is strongly enhanced in the direct proximity to the Paraná river (Figure 2.8b), the vastness of the South American shelf (1553 10^9 m^2) also makes the region less sensitive to river inputs. In published literature, the nutrient supply which drives the NPP on the Patagonian Shelf is also confirmed to be strongly controlled by the open ocean inflows (Song et al., 2016).

The Arctic shelf regions do not show a strong NPP response to the river inputs (8% and 5% increases for the Beaufort Sea, 1.BS, and Laptev Sea, 2.LS, respectively). We however do not consider seasonality of the riverine inputs. Larger inputs of nutrients in months of larger discharge (Le Fouest et al., 2013) of April to June, which are also months of better light availability, could cause a more efficient usage of the riverine nutrients, since the sea-ice coverage is strongly reduced in these months.

All regions show an increase in CO_2 outgassing due to the carbon inputs to the ocean. In the Arctic regions (Beaufort Sea and Laptev Sea), the relative change is much more pronounced, whereas the impact is generally not as strong in the lower latitude regions due to the enhancement of biological carbon uptake by the nutrient inputs. The tropical West Atlantic is an exception to this latitudinal pattern, since the large carbon riverine supplies also cause a substantial change in the CO_2 flux of the region. In the North Sea, we observe

an enhancement of carbon outgassing, but the region remains a substantial sink of atmospheric CO_2, as is still suggested for the present day by Laruelle et al. (2014).

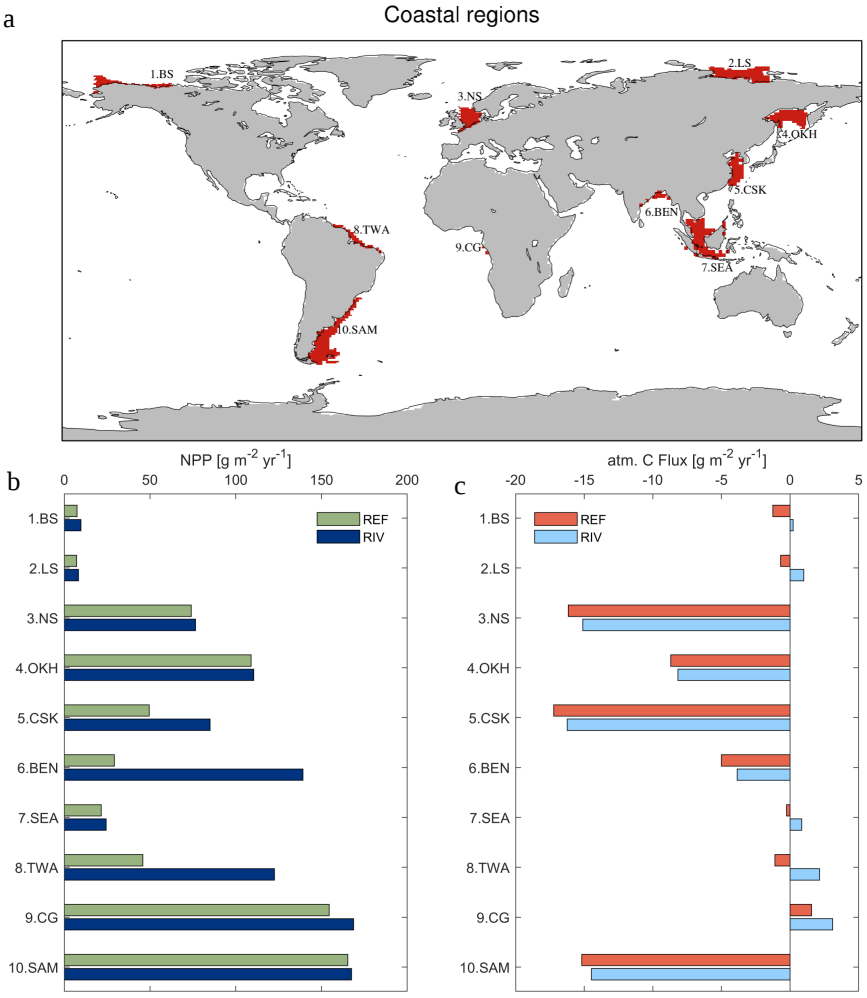

FIGURE 2.10: (a) Global map of the 10 chosen coastal regions with less than 250m depths and (b) pre-industrial annual NPP per area and CO_2 flux in the given regions [g m^2 yr^{-1}].

2.6 Origins and fate of riverine carbon

In our simplified land-ocean system (Figure 2.11), we quantify the land sources of riverine carbon (**1-3**), its riverine transfer to the ocean (**4**), and the long-term fate of the riverine carbon in the ocean (**5-10**). Here, we briefly explain the fluxes to focus on their implications. While the terrestrial fluxes are derived from the weathering and organic matter export models, the long-term oceanic fluxes are based on fluxes given by the ocean biogeochemical model. The long-term CO_2 flux is furthermore decomposed to illustrate the contributions of inorganic and organic carbon inputs to the oceanic outgassing flux in a model equilibrium analysis. The detailed derivation of the land and ocean fluxes are explained in detail in the Appendix A.3 (A.3.1 for terrestrial and A.3.2 for oceanic fluxes).

The net pre-industrial terrestrial uptake of atmospheric CO_2 and its export of rivers amounts to 529 Tg C yr^{-1} in our framework. The sink consists of 280 Tg C yr^{-1} from the CO_2 drawdown induced by weathering (**1**) and 249 Tg C yr^{-1} due to the land biological uptake (**3**). During the weathering process 94 Tg C yr^{-1} is moreover released from the lithology during carbonate weathering (**2**), which is also reported in Hartmann et al. (2009). During silicate weathering, all the carbon originates from atmospheric CO_2. The land biological uptake (**3**) is derived from the net global export of organic carbon to the ocean. It therefore implicitly takes into account the net soil carbon uptake and export to freshwaters, as well as all net sinks and sources in river systems. A total 603 Tg C yr^{-1} is transferred laterally to the ocean (**4**) while taking into consideration an endorheic catchment loss of 19 Tg C yr^{-1}.

In the ocean, riverine exports of carbon cause a long-term net annual carbon source of 231 Tg C yr^{-1}. We propose a decomposition of the long-term CO_2 flux into sources and sinks induced by the inputs of riverine species (Appendix A.3.2). Assuming model equilibrium, the oceanic outgassing flux can be decomposed into a source from inorganic carbon supplied by weathering (183 Tg C yr^{-1}, **5**), a source from terrestrial organic carbon (128 Tg C yr^{-1}), **6**), a sink caused by the enhancement of the biology due to the addition of dissolved inorganic nutrient and corresponding alkalinity production (69 Tg C yr^{-1}, **7**) and a sink due to disequilibrium at the atmosphere-water column interface in the model (11 Tg C yr^{-1}, **D1**). The production and the sinking of $CaCO_3$ and POM within the ocean lead to simulated sediment deposition fluxes of 188 Tg C yr^{-1} for $CaCO_3$ (inorg. C. flux, **8**) and 582 Tg C yr^{-1} for

POM (org. C flux, **9**). The dissolution of $CaCO_3$ and the remineralization of POM within the sediment lead to a DIC flux from the sediment to the water column of 385 Tg C yr^{-1}. The net C flux at the sediment interface (**8+9-10**) is therefore a burial flux of 385 Tg C yr^{-1}. The calculated equilibrium carbon burial flux, which is the difference between the riverine carbon inputs and the equilibrium CO_2 outgassing (**4-5-6+7**), is 361 Tg C yr^{-1}, which implies that there is a deviation of 24 Tg C yr^{-1} (**D2**) towards the sediment in the simulated model burial (385 Tg C yr^{-1}) with respect to the calculated equilibrium state burial (361 Tg C yr^{-1}). The similar deviations from the equilibrium state at the atmosphere-water column and water column-sediment interfaces suggest that the model drift in alkalinity, which most likely originates from disequilibrium in the sediment layers, translates efficiently into a perturbation of the CO_2 at the atmosphere-water column interface.

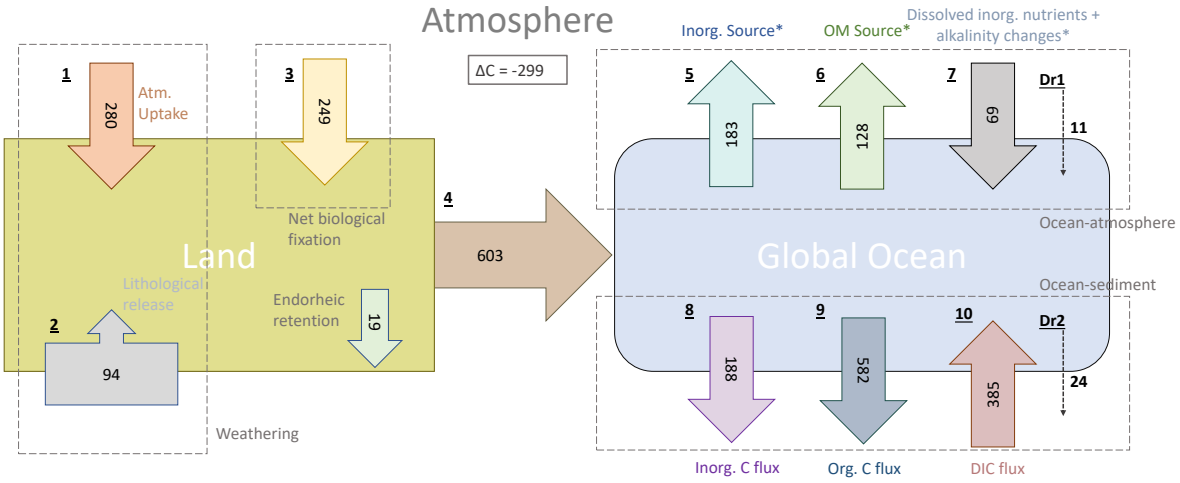

FIGURE 2.11: Origins and oceanic fate of riverine carbon in our simplified land scheme coupled to HAMOCC (RIV simulation) [Tg C yr^{-1}]. **1.** Land C uptake through weathering. **2.** Carbonate weathering lithological C flux. **3.** Net land biological C uptake (derived directly from riverine organic carbon exports). **4.** Riverine C exports. **5.** Oceanic outgassing from riverine DIC. **6.** Oceanic outgassing resulting organic material (OM) loads. **7.** Oceanic C uptake due to the enhanced primary production by dissolved inorganic nutrients and the corresponding alkalinity production. **8.** Simulated inorganic C deposition to the sediment. **9.** Simulated net organic C deposition to sediment. **10.** Diffusive DIC flux from the sediment back to the water column. * are calculated fluxes for ocean model equilibrium, whereas the other fluxes are simulated fluxes by the terrestrial and ocean models. D1 and D2 are the calculated drifts between the oceanic modelled carbon fluxes and the calculated equilibrium fluxes (derived from model equations, Appendix A.3) for the ocean-atmosphere and ocean sediment interfaces. See Appendix A.3 for the derivation of the fluxes.

The riverine induced oceanic CO_2 outgassing flux of 231 Tg C yr^{-1} is consistent with the estimate range of 200-400 Tg C yr^{-1} given in Sarmiento and

Sundquist (1992), who assume an annual riverine C flux of 300-500 Tg C, and with Jacobson et al. (2007) and Gruber et al. (2009), who suggest a slightly higher natural CO_2 outgassing flux of 450 Tg C yr^{-1}. Resplandy et al. (2018) suggest a higher land-ocean carbon (780 Tg C yr^{-1}) from the derivation of natural outgassing of carbon in the ocean. It is unclear if and how the method considers oceanic carbon removal of the riverine-delivered carbon through sediment burial.

Furthermore, we observe an imbalance in the calculated pre-industrial CO_2 land uptake from the atmosphere and the oceanic outgassing in our approach, with the land uptake outweighing the oceanic outgassing, resulting in a total net atmospheric sink of 299 Tg C yr^{-1}. Accounting for further sources of atmospheric CO_2 such as volcanic emissions and shale organic oxidation would therefore be necessary to achieve a stable atmospheric carbon budget in a fully coupled land-ocean-atmosphere setting, since Earth System Models assume constant pre-industrial atmospheric CO_2 levels. For instance, Mörner and Etiope (2002) suggest long term volcanic annual emissions in the range of 80-160 Tg C yr^{-1}, whereas Burton et al. (2013) estimate volcanic CO_2 fluxes as high as that of silicate weathering drawdown, which would reduce the disequilibrium in the pre-industrial atmospheric CO_2 budget. In our approach, the silicate weathering CO_2 drawdown is of 196 Tg C yr^{-1}. Additionally to the volcanic CO_2 emissions, the global atmospheric CO_2 land source of around 100 Tg C yr^{-1} given by Sarmiento and Sundquist (1992), due to the oxidation of organic carbon in rocks, would then approximately close the atmospheric carbon budget in our framework.

2.7 Approach advantages and limitations

2.7.1 Rivers in an Earth System Model setting

Our approach to represent riverine loads as a function of the climate variables runoff, precipitation and temperature can be used to estimate land-sea fluxes in an Earth System Model (ESM) setting. For one, this could help tackle questions of the past, since weathering rates are dependent on climate variables (Berner, 1991). For instance, strong differences in weathering for the last glacial maximum have been suggested (Brault et al., 2017). The impacts of future climate change on weathering rates and land-sea fluxes could be addressed,

as Gislason et al. (2009) and Beaulieu et al. (2012) suggest major changes in weathering due to changing climatic conditions on a decadal timescale. Furthermore, the RIV simulation can serve as a pre-industrial initial state to investigate temporal changes to the riverine loads over the 20th century, and in the future. Conclusions of Seitzinger et al. (2010) and Beusen et al. (2016) reveal strong increases DIP and DIN river loads during the 20th century, for which the oceanic impacts could be assessed.

Our approach provides a basis in order to address further questions regarding the land-ocean transfer dynamics. For one, improvements in the weathering mechanisms are possible (biological weathering enhancement and secondary mineral weathering). Ecosystem and the dynamical uptake of nutrients by the land biology, and their storage in the soil could be modelled, as well as considering hydrological flow characteristics and river biogeochemical transformation processes. The consideration of groundwater fluxes could also be included. Coastal ocean dynamics could moreover be more accurately represented by using a higher model resolution.

2.7.2 Fate and consistence of terrestrial organic matter in the ocean

The composition of terrestrial organic matter, as well as its fate in the ocean are associated with a large degree of uncertainty. Recent work shows that tDOM is mineralized efficiently by abiotic processes in the coastal zone (Fichot and Benner, 2014; Müller et al., 2016b; Fichot and Benner, 2014), despite having already been strongly degraded along the land-ocean continuum. On the other hand, few studies tackle the composition of POM, although it is thought to also be efficiently remineralized in the coastal zone sediment (Hedges et al., 1997; Cai, 2011). While the carbon loads from POM are the lowest loads of all carbon compounds considered in this study, a differing C:P ratio to the one chosen in this study would also affect the model outgassing flux estimated here.

Rates of coastal remineralization processes have been suggested to differ from those of the open ocean (e.g. Krumins et al., 2013). A higher sediment organic matter remineralization rate observed in coastal sediments (Krumins et al., 2013) could potentially reduce the coastal biogeochemical sink described in this study.

2.7.3 Arctic Ocean

The simulated nutrient concentrations in the Arctic Ocean are particularly high with regards to WOA data. Furthermore high dissolved organic material concentrations are found in observations for the Arctic (Benner et al., 2005). These characteristics suggest that this region with strong riverine inputs might be poorly represented in the ocean biogeochemistry model. Difficulties to represent the region could be due to fine circulation features, with outflows through narrow passages having been shown to be affected by model resolution (Aksenov et al., 2010). Moreover, the primary production in the region might be underestimated due to photosynthesis taking place under ice, in ice ponds and over extended daytime periods in the summer months (Deal et al., 2011; Sørensen et al., 2017), all of which are not represented in the model.

2.8 Summary and conclusions

In this study, we provide global and spatial weathering release yields for P, Si, DIC and Alk, that are derived from driving spatially explicit models with MPI-ESM output of runoff, surface temperature and precipitation. These yields show good agreement with previous assessments found in published literature. The weathering yields are of disproportionate magnitude in warm and wet regions, confirming what has been suggested until now (Amiotte Suchet and Probst, 1995; Beusen et al., 2009; Hartmann et al., 2009; Hartmann et al., 2014). Since ESMs tend to have substantial bias when quantifying the global runoff (Goll et al., 2014), runoff correction terms are needed to produce plausible weathering yields at the global scale. In the case of the MPI-ESM used in this study, which substantially underestimates the global runoff with regards to estimates of Dai and Trenberth (2002) and Fekete et al. (2002), a factor of 1.59 is necessary.

Accounting for weathering and non-weathering inputs to river catchments results in annual pre-industrial loads of 3.7 Tg P, 27 N, 168 Tg SiO_2, and 603 Tg C to the ocean. These loads are consistent with published literature estimates, although we acknowledge a certain degree of uncertainty regarding the magnitude of riverine fluxes. Even for the present day, substantial differences can be found between different approaches to derive land-ocean exports (Beusen et al., 2016). While we omit the in-stream retention of P during its riverine

transport, which reduces the global P exports to the ocean (Beusen et al., 2016), our estimate of global P export to the ocean is comparable in magnitude to an approach that determines riverine P exports by upscaling from pristine river measurements (Compton et al., 2000).

We identify the tropical Atlantic catchments, the Arctic Ocean, Southeast Asia and Indo-Pacific islands as regions of dominant contributions of riverine supplies to the ocean. These 4 regions account for over 51% of land-ocean carbon exports in total, with tropical Atlantic catchments supplying around 20% of carbon to the ocean globally. We also observe that the contributions of different carbon species differ between the regions. Most prominently, the carbon supply of the Indo-Pacific islands is dominated by particulate organic carbon loads, which have been identified to be more strongly controlled by extreme hydrological events than other C species (Hilton et al., 2008).

In the ocean, riverine inputs of carbon lead to net global oceanic outgassing of 231 Gt C yr^{-1}, a comparable value with regards to previous estimates of 200-450 Tg C yr^{-1} (Sarmiento and Sundquist, 1992; Jacobson et al., 2007; Gruber et al., 2009). This outgassing flux can be decomposed into two source terms caused by inorganic C inputs (183 Tg C yr^{-1}) and organic C inputs (128 Tg C yr^{-1}), and a net sink term (80 Tg C yr^{-1}) caused by the enhanced biological C uptake due to riverine inorganic nutrient supplies, corresponding alkalinity production and a slight model drift in alkalinity. The magnitude of the outgassing is however strongly dependent on the magnitude of riverine carbon loads, for which uncertainties still exist.

We observe evidence of a substantial interhemispheric transport of carbon from the northern to the southern hemisphere, with a larger relative carbon outgassing flux in the southern hemisphere (49% of global outgassing) than its relative riverine carbon inputs to the ocean (36% of global C loads). We also show that the Southern Ocean outgasses 17 Tg of riverine carbon, despite not having a direct riverine source of carbon, meaning that riverine carbon is transported within the ocean interior to the Southern Ocean. This interhemispheric transfer of riverine carbon in the ocean has been previously suggested to contribute to the pre-industrial Southern Ocean source of atmospheric CO_2 for the pre-industrial time-frame (Sarmiento et al., 2000; Aumont et al., 2001; Gruber et al., 2009; Resplandy et al., 2018). Here we show that riverine carbon fluxes derived from state-of-the-art land export models confirm the larger contribution of the northern hemispheric terrestrial carbon supply to the ocean. Part of the uneven hemispheric terrestrial carbon supply is then

compensated by the transport of carbon within the ocean and is outgassed remotely to the atmosphere.

Our results help identify oceanic regions that are sensitive to riverine fluxes. Riverine-induced changes in the regional NPP are mostly found in coastal regions, but significant riverine-derived CO_2 outgassing can also be observed in the open ocean of the tropical Atlantic. In general, latitudinal differences can also be observed in the sensitivity of the NPP and the CO_2 fluxes of various shallow shelves to riverine fluxes. While a high sensitivity in the NPP is found in tropical latitudes, with the tropical West Atlantic, the Bay of Bengal and the East China Sea showing large increases of 166%, 377% and 71% respectively, the relative changes in the regional CO_2 fluxes are larger at higher latitudes. For instance, the Laptev Sea and the Bay of Beaufort become a atmospheric sources of 2.2 Tg C yr^{-1} and 2.3 Tg C yr^{-1} respectively, despite previously being sinks of atmospheric CO_2 in the model. While our analysis revolves around pre-industrial riverine exports, regions that show high sensitivity might also be more strongly affected by 20th century anthropogenic perturbations of land-ocean exports.

Deriving riverine exports as a function of Earth System Model variables (precipitation, temperature and runoff) enables a representation of the riverine loop, from the terrestrial uptake of carbon, its riverine export and to its long-term outgassing in the ocean and export to the oceanic sediment. In the case of implementing the framework in a coupled land-atmosphere-ocean setting such as an ESM, the atmospheric pre-industrial budget would have to be balanced. In our study, we emphasize the need to consider a land CO_2 source originating from long-term volcanic activity and from shale organic carbon oxidation in order to close the pre-industrial atmospheric C budget.

Throughout this study, we find global heterogeneity in the spatial features of weathering fluxes, riverine loads and their implications for the ocean biogeochemistry. This, for instance, leads to the observed interhemispheric transfer of carbon in the ocean, with the dominance of northern hemispheric land-ocean carbon exports being evened out by remote oceanic carbon outgassing fluxes. Our results confirm the importance of nutrient and carbon fluxes for the biogeochemistry of various shallow shelves and for the Arctic Ocean CO_2 flux. Our study also shows the necessity to account for the riverine-induced oceanic outgassing of carbon in ocean biogeochemistry models, since our conservative estimate consists of around 10% of the magnitude of the present day ocean carbon uptake.

Chapter 3

The efficient cross-shelf export of organic matter in the coastal ocean: Were continental shelves already a global pre-industrial CO_2 sink?

Co-authors: Pierre Regnier, Tatiana Ilyina & Goulven Gildas Laruelle

Summary The contributions of continental shelves to the oceanic global carbon cycle and its anthropogenic uptake of CO_2 have been strongly debated for over two decades. While several studies have attempted to tackle the issue using conceptual box models, important physical and biogeochemical features were not taken into account, such as the 3-dimensional circulation of the ocean. Global circulation models on the other hand, have strongly simplified or ignored riverine loads and important biogeochemical processes taking place in the coastal ocean. In this study, we perform extensions to an ocean biogeochemistry model, which is coupled to a global ocean circulation model, in order to take into account the inputs of riverine biogeochemical compounds to continental shelves, as well as to represent dynamics of organic matter in the continental shelves water column and in the sediment. For this we consider a detailed representation of terrestrial dissolved organic matter (tDOM) and enhance sediment particulate organic matter (OM) remineralization in the shelf sediment. We firstly examine the physical indicators shelf water residence times (RTs) and mixed layer depths(MLDs) at the global and regional scale. We then assess the trophic state, as well as the pre-industrial state and anthropogenic perturbation of the air-sea CO_2 flux of continental shelves. Our model results show a shorter globally averaged residence

time (RT) of shelf waters (14-16 months) than was previously assumed (>4 years), and an average shelf MLD of 35 m, which does not reach the shelf sea floor (average of 92 m). While considering a continental shelf organic matter remineralization rate of over factor two of that of the deep-sea sediment, and performing experiments with plausible tDOM mineralization rates from 0.002-0.008 d^{-1}, we observe a slight autotrophic state (0.01-0.05 Pg C yr^{-1}) on the global continental shelf both for the pre-industrial and present day time periods. This autotrophic state can be explained by the enhancement of the biological production by nutrients entrained from open ocean inflows and the efficient offshore transport of organic carbon off the global shelf (0.29-0.34 Pg C yr^{-1}) caused by the short shelf RTs. Consequently, the pre-industrial continental shelves are also a slight global sink of atmospheric CO_2 (0.06-0.08 Pg C yr^{-1}) in the model, which is largely driven by regions affected by large oceanic inflows. Our representation of continental shelves is validated with good agreement in the modelled present day global shelf CO_2 uptake of 0.14-0.25 Pg C yr^{-1} with the most recent global estimates (Laruelle et al., 2014), as well as in the modelled pCO_2 distribution, which we compare to a global neural network derived spatial data-product (Laruelle et al., 2017). Our results imply that while the efficient horizontal biological pump is the main factor for the autotrophic state and the pre-industrial CO_2 sink on continental shelves, the shelves also act as an inefficient sink of anthropogenic CO_2 with respect to the open ocean when assuming a constant biological production over the historical time-period. Thus, the biological carbon uptake on continental shelves and its cross-shelf export could have a much stronger role than was thought until now.

3.1 Introduction

In spite of their relatively small global surface coverage, continental shelves host a large fraction of the global oceanic primary production, carbonate and organic carbon burial, while supplying the open ocean with large amounts of land-derived carbon and nutrients (Walsh, 1991; Milliman and Droxler, 1996; Gattuso et al., 1998; Wollast and Chou, 1998; Mackenzie et al., 2002; Chen and Borges, 2009; Sharples et al., 2017). Large uncertainties however remain associated to the quantification of these fluxes over continental shelves and the contribution of the shelves to the global carbon cycle (Borges et al., 2005; Chen and Borges, 2009; Cai, 2011; Wanninkhof et al., 2013; Gruber, 2014). In

particular, the biological trophic state of continental shelves and the sign and magnitude of their global exchange of CO_2 with the atmosphere have been topic of discussion in the literature for over two decades (Mackenzie et al., 1998; Andersson et al., 2005; Borges et al., 2005; Crossland et al., 2006; Chen and Borges, 2009; Laruelle et al., 2014). These features both are impacted by the rates of the autotrophic and heterotrophic processes, inorganic cycling processes, as well as oceanic circulation features. While several modelling approaches have been developed over the years to better understand the dynamics of carbon in continental shelf seas ranging from conceptual box models (Mackenzie et al., 1998; Mackenzie et al., 2002; Mackenzie et al., 2004; Andersson et al., 2005) and spatialized parametrizations (Sharples et al., 2017), to Oceanic Global Circulation Models (OCGMs) (Bourgeois et al., 2016), the complex hydrodynamics or important biogeochemical processes in the coastal ocean were often overly simplified. Here, we make use of mean circulation features represented in a global ocean model, while extending a biogeochemical model to improve its representation of continental shelves, in order to assess the initial and present day trophic state as well as the global CO_2 flux over continental shelves.

The Net Ecosystem Production (NEP), also referred to as net ecosystem metabolism, determines the trophic state of the oceanic environment and is defined by the balance between Gross Primary Production (GPP) and Net Ecosystem Respiration (NER) of the ecosystem (NEP=GPP-NER). While the oceanic primary production is mostly limited by light and nutrient concentrations in the ocean (e.g. Smith et al. (1987) and Tyrrell (1999), the NER is a function of the amount, composition and chemical reactivity of the organic matter ecosystem loadings, which can be terrestrially derived or autochthonously produced, and of the available oxidant, which is majorly oxygen (Smith and Hollibaugh, 1993; Cai et al., 1999; Arndt et al., 2013). The origins of the continental shelf supply of nutrients and carbon thereby strongly differs from those of the open ocean; besides the terrestrial inputs from rivers, the efficient recycling of nutrients and carbon in shelf sediments provide a direct source of these compounds to the biologically active euphotic zone (Fanning et al., 1982; Johnson et al., 1999; Giraud et al., 2008; Arndt et al., 2013). Major nutrients (N, P, Si and Fe) and carbon are therefore provided to continental shelves by three major sources: river inputs, ocean inflows and atmospheric inputs, where they are thought to be efficiently recycled.

Rivers transform, store and transport inorganic and organic land-derived

compounds along the land-ocean continuum, which are ultimately delivered to the ocean (Schlesinger, 1977; Regnier et al., 2013; Beusen et al., 2016). The exports of riverine material to the coastal ocean are reported to strongly affect the ocean biogeochemistry (Froelich, 1988; Stepanauskas et al., 2002; Dagg et al., 2004; Bernard et al., 2011; Fichot and Benner, 2014; Sharples et al., 2017). Near river mouths, the primary production is notably often controlled by the riverine nutrient supplies (Liu et al., 2000; Crossland et al., 2006; Lacroix et al., 2019). The large delivery of organic carbon and its remineralization, however, increases the heterotrophic production on continental shelves (Chen and Borges, 2009). Combined with the riverine inputs of dissolved inorganic carbon, the terrestrial organic carbon inputs cause a net global outgassing in the pre-industrial oceanic state of 0.2-0.8 Pg C yr^{-1} (Sarmiento and Sundquist, 1992; Jacobson et al., 2007; Resplandy et al., 2018; Lacroix et al., 2019).

In particular, dissolved terrestrial organic matter (tDOM) provided by rivers is thought to exert a strong control over the trophic-state of the coastal ocean, since its mineralization directly influences the CO_2 exchange between continental shelf waters and the atmosphere (Cai, 2011). However, its fate and the global extent of its mineralization has been a topic of large uncertainty (Hedges et al., 1997; Cauwet, 2002; Blair and Aller, 2011; Lalonde et al., 2014). About 20 % of tDOM delivered by rivers is estimated to be biologically reactive whereas 80 % is relatively resistant to biological breakdown and consists of very low nutrient to carbon ratios, as a consequence of strong previous degradation during its transit through rivers and inland waters (Meybeck, 1982; Søndergaard and Middelboe, 1995; Holmes et al., 2008; Fichot and Benner, 2014; Aarnos et al., 2018). Yet, tDOM is seldomly detected in oceanic seawater or oceanic sediment pore water, signifying substantial degradation within the ocean (Hedges et al., 1997). Measurements of lignin, a dominant biopolymer found only in terrigenous organic matter, have led to believe that tDOM only made a small contribution to the total dissolved organic matter (DOM) inventories in the Atlantic (0.7-2.4 %), where the lifetime of tDOM is suggested to be shorter than oceanic DOM (Opsahl and Benner, 1997), and around 1 % in the Pacific (Hernes and Benner, 2002). In the Arctic basin on the other hand, significant tDOM concentrations are found, reaching as much as 14-24 % of total DOM concentrations due to elevated tDOM concentrations of Arctic rivers and the relative shallowness of the Arctic basin (Benner et al., 2005). Furthermore, regional studies investigating the fate of tDOM suggest that a substantial amount of tDOM is processed in the coastal zone. For instance, Kaiser et al. (2017) evaluate that about half of the tDOM delivered

to the Siberian shelves is degraded on the shelf. In a regional budget of the Louisiana shelf, Fichot and Benner (2014) report that the remineralization of land-derived tDOM amounts falls in the 40-50 % range. Photodegradation might also play an essential role in understanding the fate of tDOM by removing biologically unreactive tDOM, which is mostly chromophoric dissolved organic material (tCDOM), in continental shelf waters through abiotic photodegradation (Ohta et al., 2000; Lalonde et al., 2014). This photobleaching of recalcitrant terrestrial organic matter could make it more readily bioavailable to ecosystems (Fichot and Benner, 2014; Aarnos et al., 2018). Fichot and Benner (2014) show that the dominant pathway involved in the mineralization of tDOM over the Louisiana Shelf is a combination of photooxidation and biotic breakdown. tCDOM has also been shown to absorb a substantial fraction of solar shortwave radiation, which is the main driver of primary production in the ocean (Johannessen et al., 2003; Aarnos et al., 2012; Bélanger et al., 2013).

The fate of riverine derived particulate organic material (POM) differs from that of tDOM because of the possibility of export to the sediment and subsequent burial over the continental shelf. While the fate of POM on continental shelves remains poorly understood, its mineralization is thought to be relatively efficient because the detectability of fluvial POM has been shown to be small in coastal sediments in comparison to its river loads at the global scale (Hedges et al., 1997). The reactivity of POM has been identified to be affected by intrinsic factors such as mineral composition, mineral organic associations as well as environmental factors including the duration of the transport in rivers (Blair and Aller, 2011). This study also revealed that more riverine POM is buried with a higher efficiency on passive shelves than on active shelves.

While rivers dominate the supply of nutrients and carbon in some coastal regions such as the western Tropical Atlantic, the Yellow Sea and the Black Sea (Justić et al., 1995; Fennel and Testa, 2019), continental shelves are also supplied by open ocean inflows, which mostly originate from major coastal currents, coastal upwelling and deep winter mixing (Liu et al., 2000). These inflows strongly affect the biogeochemistry of major coastal regions (Thomas et al., 2005; Qiao et al., 2006; Song et al., 2016; Holt et al., 2018) and are thought to transport large amounts of carbon and nutrient globally to the coastal zone (Wollast, 1998; Chen and Borges, 2009). In the North Sea for instance, the outer shelves are more strongly affected by anthropogenic perturbation in the open ocean than changes in river supplies (Mathis et al., 2019). In the Barents Sea, a strong nutrient supply is provided from subsurface Atlantic waters

(Pipko et al., 2017). Since these subsurface inflows are characterized by high concentrations of inorganic nutrients (and low organic concentrations), they enhance the net primary production, which in turn decreases the pCO_2.

Atmospheric depositions of nitrogen, iron and phosphorus significantly affect the oceanic biogeochemistry at the global scale by supplying substantial amounts of these compounds (Mahowald et al., 2006; Doney et al., 2007; Mahowald et al., 2008). While desert dust from the Sahara and East Asia supplies iron to the ocean (Mahowald et al., 2006), atmospheric nitrogen and phosphorus are deposited in inorganic and organic forms (Doney et al., 2007; Mahowald et al., 2008). Cyanobacteria also fix nitrogen from the atmosphere through metabolic processes, therefore creating a significant source of nitrogen to the ocean (Karl et al., 1997; Großkopf et al., 2012). This global nitrogen source of 70-150 Tg N yr^{-1} thereby exceeds the present day source from riverine supplies (Beusen et al., 2016). While atmospheric sources are provided to the seawater to a large degree in the open ocean, the coastal regions can also be strongly affected, especially at the regional scale (Luo et al., 2014).

Regarding the present day trophic state of the continental shelves, recent studies suggest net global autotrophy (Bauer et al., 2013), although net heterotrophy has been reported in several large regions globally (Chen and Wang, 1999; Thomas et al., 2005). Using conceptual box model approaches, Mackenzie et al. (2004) and Andersson et al. (2005) suggest that the pre-industrial global coastal zone ocean was net heterotroph, meaning that more DIC was produced in the coastal ocean than was consumed as a result of the input of terrestrial carbon and that the trophic state switched at the end of the 20^{th} century. These assessments however did not resolve spatial features and therefore, the complex heterogeneity in hydrodynamics of the continental shelves was not considered. It is also acknowledged by Andersson et al. (2005), that the global coastal water residence times of 4-11 years assumed in the study are strongly uncertain, which could strongly affect the results. Residence times of coastal waters, which strongly differ from a region to the next, have been shown to act as an important control over biogeochemical processes (Borges et al., 2005; Izett and Fennel, 2018; Fennel and Testa, 2019), exports of nutrients (Sharples et al., 2017) and the fate of terrestrial organic matter (Painter et al., 2018).

Until recently, global estimates of the air-water CO_2 flux over continental shelves were derived from limited collections of local flux estimates (Borges et al., 2005; Chen and Borges, 2009; Laruelle et al., 2010; Cai, 2011). However, the

growing community effort to gather and organize observational databases of oceanic pCO_2 measurements (Bakker et al., 2016) have led to better estimates in recent years (Laruelle et al., 2014) and the development of interpolated high resolution pCO_2 maps for continental shelves (Laruelle et al., 2017). The most recent estimates of the global CO_2 uptake by continental shelves report a range of 0.14-0.25 Pg C yr^{-1} globally (Wanninkhof et al., 2013; Laruelle et al., 2014). These studies offer a basis of global and spatial validation for model results. The pre-industrial sign and magnitude of the CO_2 flux and its anthropogenic perturbation is on the other hand much more difficult to assess due to the lack of long-term observational data. The coastal zone was revealed to be a pre-industrial source of atmospheric CO_2 in a conceptual box model study in Mackenzie et al. (2004) and Andersson et al. (2005). The study also suggested that the continental shelf was a large anthropogenic carbon sink of around 0.5 Pg C yr^{-1}. The perturbation of the 20^{th} century coastal CO_2 flux was also recently assessed using a global spatially explicit ocean biogeochemistry model in Bourgeois et al. (2016), although implications of coastal specific processes and river supplies were not assessed. This study nonetheless evaluated the global anthropogenic coastal ocean CO_2 uptake to 0.12 Pg C yr^{-1}, thus also suggesting that continental shelves are inefficient in their uptake of anthropogenic CO_2 compared to the open ocean. Laruelle et al. (2018) on the other hand, reported an increasing efficiency of the coastal CO_2 sink over the last few decades from the extrapolation of observational time-series of several large regions.

Up until now, biogeochemical cycling and the role of continental shelves regarding the perturbation of global carbon fluxes have been assessed in three types of approaches. Mass balancing (e.g. Gattuso et al. (1998) and Chen and Borges (2009)) from global estimates can give an indication of the magnitude of unknown fluxes at the global or regional scale but do not provide means for a temporal analysis, or offer mechanistic explanations. The conceptual box model approach used in Mackenzie et al. (1998), Mackenzie et al. (2002), Mackenzie et al. (2004), and Andersson et al. (2005), enables a comprehensive estimation of global carbon fluxes in the on the global continental shelf, as well as an assessment of the anthropogenic perturbations of the fluxes. The model however relies on estimates of flux rates at the box boundaries, such as the coastal water inflows and residence times, which are often difficult to determine. The model also does not consider the heterogeneity of spatial features in the horizontal or in the vertical. Global ocean general circulation models (OCGMs) coupled to ocean biogeochemistry models could potentially

provide global spatially resolved carbon fluxes for continental shelves, while also enabling a mechanistic and temporal analysis of the features. Until now, continental shelves have however mostly been represented in OCGM-based analysis of carbon fluxes due to their inadequate spatial representation of the shelf's bathymetries and areas (Liu et al., 2000; Muller-Karger et al., 2005; Bourgeois et al., 2016). Moreover, biogeochemical riverine fluxes have largely been ignored or poorly represented. Furthermore, specific coastal characteristics, such as the higher efficiency of the recycling of organic matter in continental shelf sediment than for the global ocean, have also not been considered. Recent improvements in the spatial resolutions of OCGMs and in the understanding of the biogeochemical processes controlling the carbon cycle over continental shelves now enables us an to analyse the impacts of land derived material and, in particular, for the fate of tDOM (Fichot and Benner, 2014; Kaiser et al., 2017; Aarnos et al., 2018). In Lacroix et al. (2019), a representation of biogeochemical riverine fluxes including tDOM has been introduced in order to assess their contributions to global oceanic biogeochemical cycling, as well as for specific coastal regions.

In this study, we use an extended biogeochemical model coupled to an OCGM, in order to assess the pre-industrial and present day trophic states and the air-sea CO_2 exchange of continental shelves. Although we do not tackle the implications of processes at the mesoscale here, the model represents the mean oceanic circulation features, and therefore open ocean inflows to the continental shelves and their biogeochemical characteristics. Atmospheric inputs and the most important biogeochemical processes taking place on continental shelves are also represented in the biogeochemical model, which was extended to consider an explicit description of the riverine fluxes to continental shelves and the efficient benthic cyling of nutrients and carbon. We perform model simulations to equilibrium for the pre-industrial state, while considering plausible ranges of organic matter remineralization on the continental shelves. We then perform a transient model simulation over the 1850-2015 period with increasing atmospheric CO_2. We validate the representation of continental shelves in the model with present day observational datasets and estimates. In our analysis, we first assess and discuss two physical features in the model, the continental shelf residence times (RTs) and mixed layer depths (MLDs), in the context of previous global and regional estimates given in published literature. We discuss the organic carbon cycle under current and pre-industrial conditions, in order to assess the net trophic state of the continental shelves. An emphasis is therefore placed on the extent to which

tDOM mineralization controls the organic carbon dynamics in continental day global datasets and air-sea CO_2 flux estimates. Finally, we use the simulations to provide insight on the pre-industrial state of the DIC budget, tackling the question of whether continental shelves were a global sink or a source of CO_2 to the atmosphere for the pre-industrial time period, and what these results imply for the anthropogenic CO_2 flux.

3.2 Methods

To represent the physical as well as the biogeochemical characteristics of the continental shelves, we used a global circulation ocean model coupled to an ocean biogeochemical model, which was modified and extended to incorporate a better representation of continental shelf biogeochemical cycling (Figure 3.1). The biogeochemical model in particular was extended to consider inputs of riverine carbon, nutrients and alkalinity exports (Lacroix et al., 2019). Furthermore, the sediment component of the model was modified to consider the efficient biogeochemical processing of organic matter on continental shelves. We performed a number of simulations to consider uncertainties in sediment organic matter mineralization and the tDOM breakdown rates for pre-industrial conditions. Additionally, a historical (1850-2015) transient simulation was performed, in order to assess the performance of the model with respect to contemporary data-sets. In our analysis, continental shelves were defined as areas with less than 250 m depths to quantify indicators of the physical and biogeochemical states of the shelves.

3.2.1 Standard ocean model description

The physical fields which advect, mix and diffuse biogeochemical tracers were computed by the global ocean model Max Planck Institute Ocean Model (MPI-OM). MPI-OM is a z coordinate global circulation model which solves primitive equations under the hydrostatic and Boussineq approximation on a C-grid and a free surface. The grid configuration used in this study is the GR15 grid, which has a pole over Antarctica and one over Greenland, and resolution of around 1.5 degrees. Vertically, the model configuration has 40 uneven layers that increase in thickness with depth. The model was

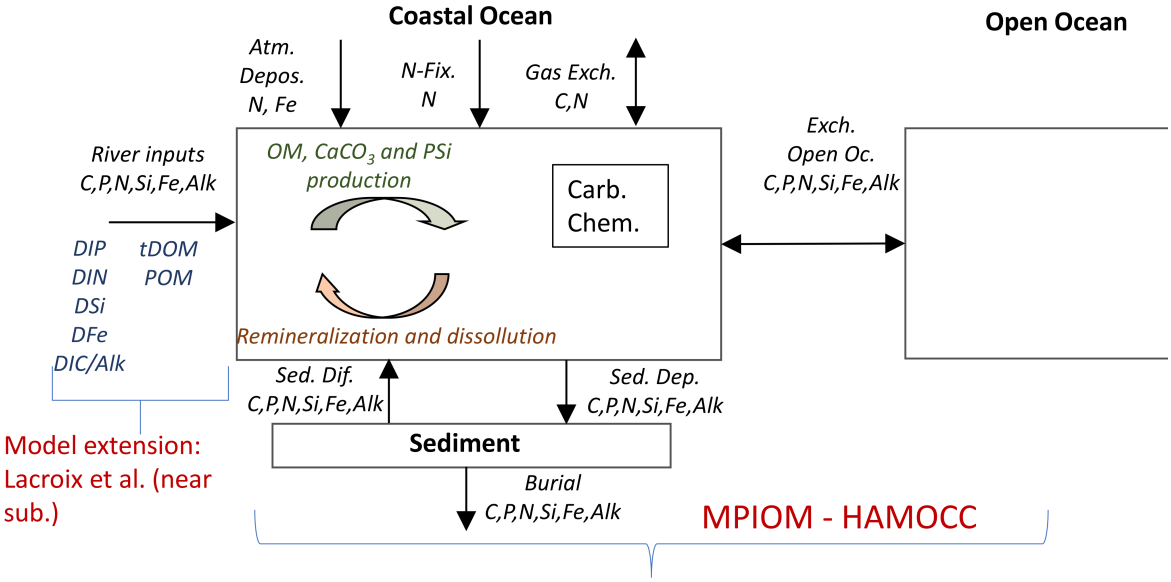

FIGURE 3.1: Representation of the coastal ocean in the framework of the OCGM Max Planck Institute Ocean Model (MPIOM) coupled to the ocean biogeochemical model HAMOCC, which simulates biogeochemical processes in the water column, the dynamical exchanges of nutrients, carbon and alkalinity at the water column-atmosphere and water-column sediment interface. Within the water column, organic matter (OM), $CaCO_3$ and particulate silica (PSi) are produced biologically, and are mineralized/dissolved within the water-column and sediment. A carbonate chemistry model (Carb. Chem.) simulates the inorganic carbon cycling in the model. At the water column-atmosphere in interface, fluxes of C, N and Fe are represented through atmospheric deposition (Atm. Depos.), N-fixation (N-Fix.) and gas exchange (C, N). At the water-column sediment interface, sediment deposition (Sed. Dep.) and diffusive inorganic fluxes (Sed. Dif.) take place. The model was extended to consider riverine inputs (C, P, N, Si, Fe and Alk, Lacroix et al. (2019)) in their speciation compounds. The exchange of the continental shelves with the open ocean (Exch. Open Oc.) takes place dynamically within the model.

forced with Ocean-Model-Intercomparison-Project (OMIP) data for the surface boundaries and the freshwater inputs (Röske, 2006).

The HAMburg Ocean Carbon Cycle model (HAMOCC) simulates the most important biogeochemical processes in the ocean by representing the organic and inorganic carbon cycle (Six and Maier-Reimer, 1996; Ilyina et al., 2013; Mauritsen et al., 2019). The organic cycle is based on a NPZD (nutrients, phytoplankton, zooplankton and detritus) model, with the addition of a dissolved organic material pool (Six and Maier-Reimer, 1996) and of cyanobacteria (Paulsen et al., 2017). Phytoplankton takes up inorganic nutrients and carbon following the modified Redfield ratio of C:N:P = 122:16:1 (Takahashi et al., 1985) and is limited by light and nutrient availability (nitrate, phosphate, dissolved silicate and iron). The phytoplankton growth follows Michaelis-Mentis kinetics, with its growth limited by light, nutrients and temperature. Furthermore, cyanobacteria also contribute to the production of organic material while fixing nitrogen dynamically (Paulsen et al., 2017). Dissolved organic matter (DOM) and particulate organic matter (POM) are exuded during the lifetime and death of the phytoplankton. Grazers transform organic material to nutrients and dissolved inorganic carbon (DIC) by feeding on phytoplankton or other grazers. Furthermore, POM and DOM is mineralized by bacteria in the presence of enough oxygen. POM can also undergo anaerobic remineralization by denitrification and sulfate reduction. The sinking speed of POM is dependent on depth (Martin et al., 1987). Phytoplankton produce particulate silica (PSi) and $CaCO_3$, with fixed ratios with respect to their net primary production. The production $CaCO_3$ is limited by the dissolved silicate concentration, since silica shells are preferred to $CaCO_3$ shells. Atmospheric dust inputs, which contain iron, are also included using the flux field of Mahowald et al. (2006).

The inorganic chemistry is represented in the model based on Maier-Reimer and Hasselmann (1987) with adjustments in the chemical constants according to the Ocean Model Intercomparison (OMIP) project, as is described in Mauritsen et al. (2019). The model furthermore considers the ocean-atmosphere gas-exchange fluxes of CO_2, O_2, and N_2.

The sediment consists of 12 layers where aerobic and anaerobic remineralization processes, $CaCO_3$ and PSi are represented. Particulate fluxes of POM, PSi, $CaCO_3$ and dust from the water column add matter to the top layer by sedimentation. Mineralization and dissolution within the sediment creates a source of dissolved carbon and nutrients that can be exchanged from the

sediment pore water between the different layers or to the water column. In the deepest sediment layer, there is a flux to a diagenetically consolidated burial layer.

3.2.2 Model modifications and extensions

Consideration of POM mineralization in the coastal sediment

The remineralization of POM in the sediment of continental shelves has been suggested to be more efficient than in the deep ocean sediment due to, for instance, the freshness of coastal POM, which leads to a more efficient recycling of nutrients and carbon (Johnson et al., 1999; Giraud et al., 2008; Arndt et al., 2013). While the rate of mineralization of POM is set at 0.001 d^{-1} for the deep-sea sediment in the standard HAMOCC setup (e.g. Mauritsen et al. (2019), we tested several remineralization rates for POM (namely, 0.0013 d^{-1}, 0.0026 d^{-1} and 0.0068 d^{-1}) for sediment depths shallower than 250 m. In deep ocean sediment, the remineralization rate was maintained at 0.001 d^{-1}, as in previous model configurations. We retained the rate of 0.0026 d^{-1} for the main simulations of the study based on comparisons of coastal NPP and OM burial with published estimates (Gattuso et al., 1998; Chen and Borges, 2009; Krumins et al., 2013), which is discussed later in this chapter.

Representation of riverine loads

We represented a spatial distribution of pre-industrial riverine loads that were added to the ocean model at river mouths constantly across the year (Lacroix et al., 2019). HAMOCC was extended with riverine inputs from this representation for alkalinity (A_c), dissolved organic carbon (DIC), dissolved inorganic phosphorus (DIP), dissolved inorganic nitrogen (DIN), dissolved silica (DSi), dissolved iron (DFe), terrestrial dissolved organic matter (tDOM), particulate organic matter (POM) and iron-bound phosphorus (Fe-P) (Chapter 2, Figure 2.1), which is briefly explained in this section.

We considered both weathering and non-weathering sources of nutrients and carbon, which were added to the catchment pools (and assumed as inorganic compounds). From these pools, a part of the (inorganic) compounds were assumed to be transformed into organic matter (tDOM and POM) for P, N, Fe. The carbon in organic matter on the other hand was assumed to originate from

atmospheric CO_2 uptake by the terrestrial and riverine biology. The organic matter, which was derived from organic carbon loads from the NEWS2 study (Seitzinger et al., 2010), was thereby assumed to consist of organic P, N , C and Fe in globally fixed ratios (in relation to organic C loads from NEWS2). The global loads of carbon and nutrients were assessed to be within the ranges of upscaled estimates (Lacroix et al., 2019), for which a brief summary is given in the next subsections. In the regions of major riverine supply of the tropical Atlantic, South East China and the Arctic, which were analysed in more detail, the riverine carbon loads were well reproduced with regards to regional estimates.

Alkalinity and DIC Catchment yields of DIC and A_c were derived from driving the spatial weathering release model of Hartmann et al. (2009), modified as described in described in Goll et al. (2014), with pre-industrial runoff and temperature data from the Max Planck Institute Earth System Model (MPI-ESM CMIP5, Giorgetta et al. (2013)). As described, the yields were calculated as a function of runoff, temperature, lithology and soil properties. Weathering of silicate and carbonate lithologies reactions produce HCO_3^- ions, thus DIC to A_c in a ratio of 1:1. The alkalinity is assumed to be transported by rivers passively (Ludwig et al., 1998). We neglect the DIC source from soil dissolved CO_2, which we assumed to be returned to the atmosphere to a large degree during its transport in rivers. Therefore, we also assumed an A_c to DIC ratio of 1:1 at river mouths, which reflects field observations in the vast majority of rivers (e.g. in Araujo et al. (2014) for tropical Atlantic catchments). In catchments highly affected by organic soil exports, the DIC might deviate from the HCO_3^- concentrations, but rarely by more than 10 % (Meybeck and Vörösmarty, 1999). We performed modifications with respect to Lacroix et al. (2019) based off comparisons with observations (Tank et al., 2012) for major Arctic catchments. The global DIC load of 0.33 Pg yr^{-1} provided by the approach is within the estimate range of 0.26-0.55 Pg yr^{-1} (Lacroix et al. (2019) and citations therein).

Organic Matter: tDOM and POM We derived tDOM catchment exports from the DOC exports provided by the Global Nutrient Export from WaterSheds 2 (NEWS2) study (Mayorga et al., 2010; Seitzinger et al., 2010). The NEWS2 terrestrial model performs multiple regressions with environmental

drivers to calculate nutrients and carbon export from watersheds at a 0.5 degree resolution (Harrison et al., 2005). The tDOM exports were thereby scaled to represent the more recently acknowledged estimate of around 0.24 tg C yr^{-1} (Hedges et al., 1997; Cai, 2011; Bauer et al., 2013; Aarnos et al., 2018), which represented a significant increase with respect to the range simulated by the NEWS model (0.14-0.17 Pg C yr^{-1}) used in Lacroix et al. (2019). The tDOM C:P weight ratio of 1000 was derived from Meybeck (1982), where global measurements of DOP and DOC were extrapolated globally and confirmed in Compton et al. (2000). In the model study NEWS2, a natural C:P weight ratio of 425 of tDOM is suggested. We also assumed a tDOM N:P mole ratio of 16:1 out of simplicity, although we found very close estimates to this in literature for global loads (Meybeck, 1982; Seitzinger et al., 2005; Seitzinger et al., 2010).

The exports of riverine POM were derived from the POC exports of the Beusen et al. (2005) model output generated by NEWS2 (Seitzinger et al., 2010). We added riverine POM to the oceanic POM pool, with the reasoning that riverine POM C:N:P ratios found in literature are closer to oceanic POM than for tDOM. The POM mole C:P ratio thereby was reported to range from 57:1 to 315:1 according to Meybeck (1982) and Ramirez and Rose (1992). The global POM C:N:P:Fe ratio were chosen to be 122:16:1:3.0 10^{-4}. The processing of POM in the coastal ocean is also suggested to be relatively efficient, although this depends on the POM composition, as well shelf characteristics (Blair and Aller, 2011).

Phosphorus The phosphorus inputs to river catchments were assumed to consist of weathering and non-weathering exports to the catchments (see Chapter 2, Figure 2.1). The weathering release was calculated as in the study of Hartmann et al. (2014), where the yields are also described as a function of runoff, temperature, lithology and soil properties, with the runoff and temperature extracted from the MPI-ESM CMIP5 pre-industrial output. The non-weathering sources of phosphorus included fertilizer (Hart et al., 2004), sewage (Morée et al., 2013) and allochthonous (Beusen et al., 2016) input estimations for the year 1900, as done in (Beusen et al., 2016). These non-weathering inputs were distributed globally according to the spatial distribution of present day anthropogenic DIP exports (NEWS2). Part of the P inputs to the catchments was assumed to be transformed to organic matter during its residence on land and in rivers. To determine how much of the riverine P load was contained within organic matter and eliminated from the

inorganic catchment pool, we used the stoichiometry of the organic matter (P:C = 1:122 for riverine POM and P:C = 1:2584 for tDOM). The remaining P was assumed to be inorganic P:

$$IP_{\text{catch}} = P_{total,catch} - P_{tDOM,catch} - P_{POM,catch} \tag{3.1}$$

with IP_{catch} being the inorganic catchment load of inorganic phosphorus, $P_{total,catch}$ the sum of weathering and non-weathering catchment inputs, $P_{POM,catch}$ the fraction of catchment inputs of P transformed into POM and $P_{DOM,catch}$ the fraction of catchment inputs of P transformed into tDOM.

Silica, nitrogen and iron The DSi export to the ocean was obtained by driving the Beusen et al. (2009) model with MPI-ESM CMIP5 precipitation output. The global load of 168 Tg Si yr^{-1} is comparable to recent estimates of 158 – 200 Tg SiO_2 yr^{-1} (Lacroix et al., 2019). We did not consider the biological availability of particulate silica, although this might be considerable (Tréguer and De La Rocha, 2013).

DIN and DFe riverine loads were quantified by using fixed ratios of DIP:DIN = 1:16 and DIP:DFe = 1:3.0 10^{-4}. Both N and Fe were also contained in organic matter at the same ratios in relation to phosphorus. The calculated global export of N of 27 Tg N yr^{-1} is between the purely natural flux estimate of 21 Tg N yr^{-1} (Green et al., 2004) and 1970 exports of 38 Tg N yr^{-1} (NEWS2).

Treatment of the inorganic riverine inputs in HAMOCC The dissolved inorganic riverine loads were added to their respective pools in HAMOCC: DIN, DIP, DSi, DFe, DIC and A

tDOM dynamics in the ocean

The tDOM was represented separately to oceanic DOM since it is assumed to be strongly degraded upon its arrival in the ocean (Ittekkot, 1988; Vodacek et al., 2003a), to have very high C:P and C:N ratios (Meybeck, 1982; Seitzinger et al., 2010) and that a large fraction of the tDOM might be transformed abiotically in the ocean (Fichot and Benner, 2014; Kaiser et al., 2017; Aarnos et al., 2018). Assuming the C:N:P ratios described in the previous section and a typical organic matter composition (C:H:O = 1:2:1) (for instance in Krumins et

al. (2013)), we derived the following tDOM mineralization equation (omitting Fe in the equation here out of simplicity):

$$(CH_2O)_{2583}(NH_3)_{16}(H_3PO_4) + 2615O_2 = 2583CO_2 + 16NO_3^- + H_2PO_4^- + 17H^+ + 2599H_2O \quad (3.2)$$

Because of the large uncertainties associated with the breakdown of tDOM in the ocean, we performed simulations to test a range of tDOM degradation rates in the ocean. We thereby represented 5 different scenarios of tDOM degradation in the ocean with the following approximated lifetimes:

$T_{tDOM,inst}$ = 0 years

$T_{tDOM,labile}$ = 0.3 year

$T_{tDOM,photoox}$ = light-dependent

$T_{tDOM,semi\text{-}labile}$ = 1.5 years

$T_{tDOM,semi\text{-}ref}$ = 20 years

These account for two different types of tDOM degradation pathways in the ocean. The first pathway ($T_{tDOM,labile}$, $T_{tDOM,labile}$, $T_{DOM,semi\text{-}labile}$, $T_{DOM,semi\text{-}ref}$) assumes that that the degradation of tDOM is solely a function of tDOM and oxygen concentrations (therefore representing purely biotic breakdown). The lifetimes were chosen to represent the tDOM lifetime in the case of instantaneous mineralization at the river mouth, e.g. assumed in Bernard et al. (2011) and Bourgeois et al. (2016), the lifetime of labile tDOM mineralization suggested in Fichot and Benner (2014), as well as the lifetimes of semi-labile and semi-refractory oceanic DOM suggested in Hansell et al. (2012). We did not consider a fully refractory rate (Hansell et al., 2012), due to its lifetime of over 20'000 years exceeding sensible model simulation lengths, and the lack of observation of considerable amounts of tDOM in the open ocean. The second pathway ($T_{tDOM,photoox}$) represents the photodegradation breakdown effect that is caused by the exposure of abiotic tCDOM to shortwave radiation.

Under the first breakdown pathway, tDOM is mineralized as a function of the tDOM concentrations and a oxygen limitation function Γ_{O_2}, which only allows degradation when oxygen concentrations are higher than the threshold concentration ($thres_{aerob}$=5 10^{-2} μ M O_2):

$$\frac{dtDOM}{dt} = k_{rem,tDOM} * tDOM * \Gamma_{O_2} \tag{3.3}$$

With $k_{rem,tDOM}$ being the remineralization rate (d^{-1}) and tDOM the tDOM concentration (kmol C m^{-3}). The $k_{rem,tDOM}$ rates were derived solving the Eq. 3.3 with ($T_{tDOM,labile}$, $T_{tDOM,labile}$, $T_{DOM,semi\text{-}labile}$ and $T_{DOM,semi\text{-}ref}$). The approximation given by the equation is only valid if oxygen limitation does not play a large major role in the limitation of the tDOM degradation (Eq. 3.4). This assumption is verified in section 3.3.1.

$$k_{rem,tDOM} = \frac{1}{T_{tDOM,rate}}$$

(3.4)

The second breakdown pathway included the breakdown of biologically unreactive chromophoric dissolved organic material (tCDOM). We assumed that 20 % of the tDOM loads consisted of biologically reactive tDOM that was mineralized according to Equation 3.3 with $T_{tDOM,labile}$, whereas 80 % of the tDOM consisted of biologically unreactive tCDOM, which was partly photooxidized. To derive the photooxidation parametrization, we used the averaged tDOM breakdown rates measured on the Louisiana Shelf given in Fichot and Benner (2014) for all 4 seasons, and fitted a linear relationship between these values and the averaged modelled regional surface shortwave radiation in these regions. We also set a minimum rate of degradation, corresponding to a tCDOM lifetime of 20 years (semi-refractory rate as described in Hansell et al. (2012)). The breakdown process was suggested to be due to combined biotic and abiotic breakdown, as suggested in Fichot and Benner (2014):

$$\frac{dtDOM}{dt} = \frac{dk_{rem,shwav}}{dr_{shwav}} * tCDOM * \Gamma_{O_2} \tag{3.5}$$

with $k_{rem,shwav}$ being the averaged regional tCDOM breakdown rates in the Fichot and Benner (2014) study and r_{shwav} the averaged regional surface shortwave radiation in the model for the given seasons. The oxygen threshold used was also $thres_{aerob}$=5 10^{-2} μ M O_2.

The validation of the tDOM breakdown rate via photodegradation was done by comparing the contribution of tDOM to the total oceanic DOM for different open ocean basins (Opsahl and Benner, 1997; Hernes and Benner, 2002; Benner et al., 2005), regional tDOM budget studies (Fichot and Benner, 2014; Kaiser et al., 2017), as well as in a comparison with regional tCDOM photodegradation rates measured in Aarnos et al. (2018) for the photodegradation pathway.

The quantification of the shortwave radiation in the water column, which depends on the radiation, the light spectrum and the absorption by water and phytoplankton, is described in Paulsen et al. (2018).

Little is known on the oceanic fate of riverine POM. Riverine POM was therefore added to the pool of oceanic POM, since riverine POM C:N:P ratios found in literature are closer to oceanic POM (riverine POM mole C:P ratio ranging from 57:1 to 315:1 (Meybeck, 1982; Ramirez and Rose, 1992; Lacroix et al., 2019)) than for tDOM. The processing of POM in the coastal ocean is also suggested to be relatively efficient, although this depends on the POM composition as well local shelf hydrodynamical characteristics (Blair and Aller, 2011).

3.2.3 Physical and biogeochemical indicators of continental shelves

Continental shelf definition

For the analysis of our simulations, continental shelves were defined as the ocean cells located in proximity to land and with depths of less than 250 m. The model bathymetry, which is based on the ETOPO 2 bathymetry (Commerce and Atmospheric Administration, 2006), was used to mask areas with depths greater than 250 m. The 250 m threshold chosen here is slightly more inclusive than the 200 m cut-off depth suggested as an adequate representation of the global continental shelf in Chen and Borges (2009), Laruelle et al. (2010) and Bourgeois et al. (2016), but still only accounts for shallow shelf regions. We also did not consider the Antarctic shelves in our coastal ocean analysis due to its strong differences in their characteristics with other shelves (very deep shelves, ice coverage and lack of terrigenous loads).

Physical indicator: Shelf residence times (RTs)

We implemented an inert tracer in the ocean model to estimate residence times (RTs) of total continental shelf waters as well as of the shelf surface waters. The surface water RTs were thereby quantified in order to give an estimation of the RTs of freshwater inputs, since they are also added to the oceanic surface layer in the model.

To perform the global and regional RT estimation, we assumed that the outflows, which determine the turnover rate of shelf waters, were approximately consistent over time. This is an approximation, since there is a degree of seasonal as well as interannual variability in the shelf outflow rates, and also water exchange between the model grid cells within the continental shelf definition. In the idealized state, the export of the inert tracer M, which is only added at the time of initialisation (t=0), is a function of the outflow rate Q_{out} and of the shelf volume V_c (Figure 3.2). The rate of change of M is therefore:

$$\frac{dM}{dt} = \frac{Q_{out}}{V_C} * M(t) \tag{3.6}$$

The exponential decay constant k_{exp} of the water mass over the shelf is therefore $\frac{Q_{out}}{V_C}$. Due to the observed near-exponential loss of water from the global shelves, we derived a decay constant k_{exp} obtained by applying the MATLAB curve fitting tool *cftool*. The RTs were derived by estimating the mean lifetime of the exponential decay:

$$RT = \frac{1}{k_{exp}} \tag{3.7}$$

The estimations of the RTs were done as described at the regional and global scale. Since Q_{out} is also the sum of the oceanic inflows Q_{in} and freshwater inflows Q_{FW}, the oceanic inflows can also be estimated though:

$$Q_{in} = \frac{V}{RT} - Q_{FW} \tag{3.8}$$

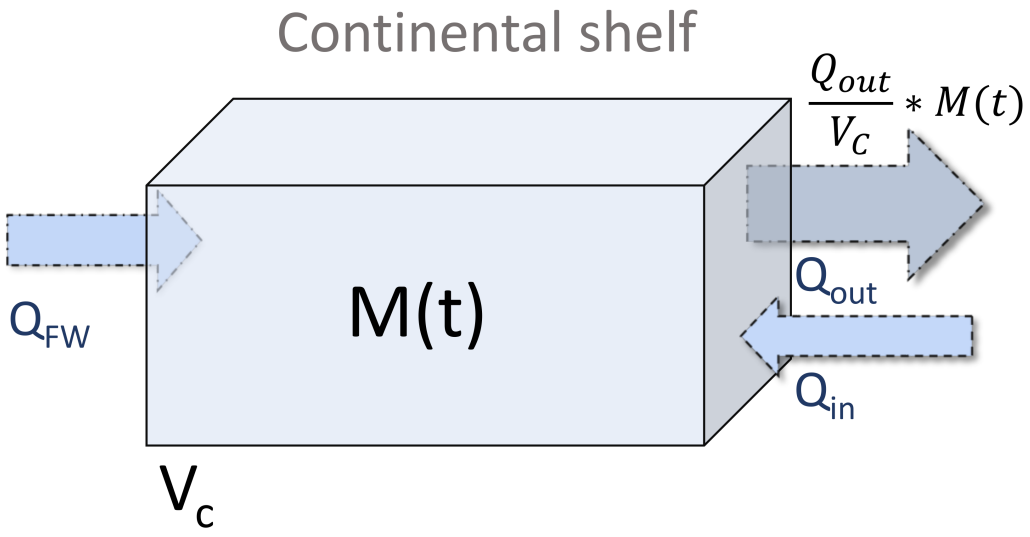

FIGURE 3.2: Idealized representation of water inflows and outflows on continental shelves. Q_{out} is the outflow rate, Q_{in} is the freshwater input rate and Q_{in} is the inflow from open ocean waters. V_c is the shelf volume, while M represents the inert tracer mass, which was added in the experiment.

3.2.4 Biogeochemical Indicators: NPP, NPP_c, R_H, NEP and cross-shelf exports

DIC and dissolved CO_2 inventories in the model are affected by biological processes on continental shelves which transform inorganic and organic compounds. For one, the net ecosystem production (NEP) is defined as the GPP minus the NER, and results in a net change to the DIC pool by producing or eliminating organic matter. In HAMOCC, the net ecosystem production (NPP) is directly simulated in the model, which already accounts for the GPP and the organism respiration of the phytoplankton. The NEP is therefore the NPP of all phytoplankton types and cyanobacteria (NPP) minus the total heterotrophic respiration of organic matter (RH).

$$NEP = NPP - RH \tag{3.9}$$

RH consists of the mineralization of tDOM, riverine POM, remineralization of oceanic POM and DOM through aerobic and anaerobic pathways, as well as the respiration caused by the metabolism of zooplankton, in the water column and in the sediment.

Calcium carbonate production consumes DIC but thereafter increases the oceanic pCO_2 by consuming twice as much alkalinity than DIC:

$$2HCO_3^- (aq) + Ca^{2+} (aq) \rightarrow CaCO_3 (s) + CO_2 (aq) + H_2O(l) \tag{3.10}$$

We therefore also consider the offset in dissolved CO_2 caused by the net production calcium carbonate $CaCO_3$ (NIC), which includes $CaCO_3$ dissolution, in NEP_c:

$$NEP_c = NPP - RH - NIC \tag{3.11}$$

While the NEP quantifies the balance of DIC within the system, NEP_c provides a more direct indication of the biologically driven CO_2 balance on the continental shelves.

The cross-shelf net export was furthermore calculated by closing the continental shelf budget, considering all sinks and sources of the tracers as well as changes in inventories within the continental shelf.

3.2.5 Pre-industrial and present day simulations

The pre-industrial state was achieved by forcing the ocean model with OMIP forcing and using a constant atmospheric CO_2 concentration of 278 ppm (Etheridge et al., 1996). We first performed simulations for different sediment POM remineralization rates (0.0013 d^{-1}, 0.0026 d^{-1}, 0.0069 d^{-1}) for 200 years, of which we retained the 0.0026 d^{-1} for further simulations. We performed simulations over 2'000 years for the 5 tDOM mineralization scenarios ($T_{tDOM,labile,}$ $T_{tDOM,labile}$, $T_{DOM,photoox}$, $T_{DOM,semi\text{-}labile}$, $T_{DOM,semi\text{-}ref}$), starting from a spin-up of the sediment module of 5'000 years for the new shelf sediment POM remineralization rate.

We also performed a transient model simulation over the 1850 - 2015 period using the $T_{DOM,photoox}$ tDOM mineralization rate. The simulations were driven by increasing atmospheric CO_2 concentrations (from 278 to 399 ppm according to Etheridge et al. (1996)). We did not consider changes in ocean circulation or changes in riverine nutrient loads in the simulation.

To compare the implications of the model extensions on the global biogeochemical state in the model, we used the pre-industrial reference simulation (REF), which does not account for riverine inputs, and a simulation RIV, which accounts for riverine fluxes, but not for the upscaling of the tDOM loads and also not for the enhancement in the POM remineralization in continental shelf sediments. Both of the simulations originate from the Lacroix et al. (2019) study (Chapter 2).

3.3 Results and Discussion

3.3.1 Implications of the model extensions for oceanic carbon cycling

In this section, we discuss the implications of the model modifications and extensions on global ocean biogeochemical variables, such as NPP, nutrients concentrations and the CO_2 flux.

Global shelf area

Since the alterations made to the model affect the contribution of continental shelves to the global carbon cycle, we start by evaluating the physical representation of the global continental shelf in our set-up. Our definition of the continental shelves yields a total surface area of 20.3 10^6 km^2 for continental shelves, which amounts to $\sim$ 5 % of the global ocean surface. This estimate is slightly lower than evaluations of the global continental shelf area, which ranges from 22 to 45 km^2 (Chen and Borges, 2009; Cai, 2011; Laruelle et al., 2010; Laruelle et al., 2013; Laruelle et al., 2018). The referred studies however used strongly inconsistent definitions of the outer limit of the continental shelf, often surpassing the 250 m depth limit chosen here. In our model, over 50 % of continental shelves are characterized by depths of 80 m and less, as is suggested in Laruelle et al. (2013). In Lacroix et al. (2019), major wide passive shelves such as the tropical West Atlantic and Patagonia were shown to be well represented, whereas narrow active shelves such the West African shelves or the Benguela Current System were less well reproduced in comparison to shelf surface area assessments by Meybeck et al. (2006) and Laruelle et al. (2013). While shelves in Southeast Asia are comparable in size

with the regions defined in Laruelle et al. (2013), the shelves located along the mid- and north-western Pacific are underestimated. While omitting the Antarctic shelves, which we exclude in this study due to its strongly differing characteristics to the the other shelves, we derive a total surface area of 19.7 km^2 for continental shelves.

Shelf sediment remineralization of POM

The altered continental shelf sediment POM remineralization rates of 0.0026 d^{-1} and 0.0068 d^{-1} produce a substantial increase of the continental shelves NPP in the model as a result of the enhanced recycling of nutrients and their subsequent mixing back into the shallow water column, while at the 0.0013 d^{-1} rate the NPP we do not observe a substantial change to the standard deep ocean rate of 0.001 d^{-1} that is used in the standard model. The global distributions for the open ocean of the NPP remain almost identical however (i.e. for the 0.0026 d^{-1} rate shown in Figure 3.3).

The simulations produce POM shelf deposition to shelf burial efficiency rates of 67 %, 15 % and 7 % and shelf POM contributions to the global burial of 80 %, 74 % and 49 % for POM remineralization rates of 0.0013 d^{-1}, 0.0026 d^{-1} and 0.0068 d^{-1} respectively. The burial of POM on the shelves is thus almost null when using a remineralization rate of 0.0068 d^{-1} and was not significant at the global scale, contradicting substantial shelf burial rates of POM reported in literature. On the other hand, the 0.0013 d^{-1} rate recycled only a small part of the POM deposited in the sediment. In reviews of literature estimates, Krumins et al. (2013) report a shelf burial to shelf deposition range of 8-23 %, and Chen and Borges (2009) report a burial contribution to the global burial of around 50-80 % for POM. The agreement organic matter burial rates on the global shelf is therefore best reflected at the rate of 0.0026 d^{-1}. The results presented in the rest of this study therefore reflect the simulations at this rate.

Despite similar open ocean NPP distributions, we observe an increase in the shelf NPP contribution, with the most pronounced increases in the East China Sea, the North Sea, on the tropic West Atlantic shelf, the eastern North American shelf and the Louisiana Shelf at the rate of 0.0026 d^{-1} (Figure 3.3). At the standard model remineralization rate of 0.001 d^{-1}, these regions show very low biological productivity. A high NPP on shallow continental shelves has been reported by Muller-Karger et al. (2005) an analysis of a satellite-based

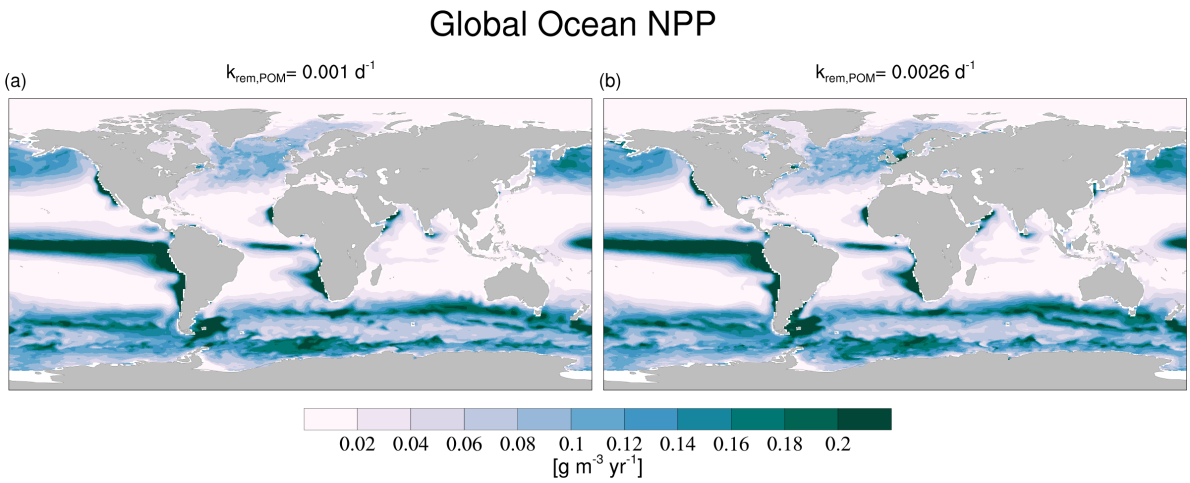

FIGURE 3.3: Annual mean oceanic NPP rates [g C m^{-3} yr^{-1}] the upper 12 m of the oceanic water column.

NPP data-product, as well as in the Sea-viewing Wide Field-of-view Sensor (SeaWiFS) data-product.

The oceanic fate of tDOM

Simulations performed with each of the five time-constants for tDOM degradation generate strongly differing inventory estimates ranging from 96 to 1487 Tg C (Table 3.1). In addition, the simulation using the semi-refractory tDOM reactivity did not reach steady state after 2000 years of simulation and the resulting tDOM inventory would thus be even higher at equilibrium. We observe that the estimated residence times (estimated as in Eq. 3.4) of tDOM in the ocean ($T_{tDOM,labile}$=125 d and $T_{tDOM,semi\text{-}labile}$=547 d) are nearly the same as the residence times computed in the model (131 d and 529 d, derived by dividing computed model inventories and computed model breakdown rates). This indicates that for these rates, the oxygen limitation does not play a significant role. This is most likely due to tDOM being added to the model surface layer along with freshwater, which causes a certain degree of stratification, and a large part of the tDOM river inputs therefore does not reach ocean depths where oxygen is limiting.

The rate of tDOM mineralization strongly affects its distribution within continental shelves and the open ocean (Figure 3.4). While a background signal of tDOM is detected by lignin measurements in large portions of the open ocean (Hedges et al., 1997), its contribution to total DOM (marine + terrestrial) in the ocean rarely exceeds a few percent in the Atlantic and Pacific basins (Opsahl

TABLE 3.1: tDOM inventories and removal rates. The lighter values in the (c) row represent the values for the photooxidation of tDOM (tCDOM). A steady state for tDOM in (e) was not reached.

tDOM reactivity scenarios	*tDOM river loads* [Tg C yr^{-1}]	$k_{rem,tDOM}$ [d^{-1}]	*Theoretical tDOM residence time* $k_{rem,tDOM}^{-1}$ [d]	*Global oceanic tDOM inventory* [Tg C]	*Model residence time* d	*Average modelled surface removal rate* [Mg C d^{-1}]
(a) $T_{tDOM,inst}$	230	-	-	-	-	-
(b) $T_{tDOM,labile}$	230	0.008	125	95.6	131	2.9
(c) $T_{tDOM,photoox}$	230(180)	-	-	461(262)	731(145)	3.4(3.2)
(d) $T_{tDOM,semi\text{-}labile}$	230	0.002	547	333	529	1.3
(e) $T_{tDOM,semi\text{-}ref}$	230	0.0001	7300	>1487*	>2349*	0.4*

and Benner, 1997; Hernes and Benner, 2002). The Arctic is an exception in this respect, with tDOM concentrations being 7 to 16-time larger than at low and mid latitudes (Benner et al., 2005). Based on these observations, we therefore consider that both the instantaneous and semi-refractory tDOM rate constants are not realistic and, in what follows, we only retain the (b) $T_{tDOM,labile}$ labile, (c) $T_{tDOM,photoox}$ and (d) $T_{tDOM,semi\text{-}labile}$ as plausible tDOM remineralization rates for further scrutiny in the rest of the study.

The tDOM distributions range from being almost completely mineralized near the river mouths for $T_{tDOM,labile}$ to a distribution where a major part of the DOM in the Arctic, Atlantic and Indian Oceans consists of tDOM for $T_{tDOM,semi\text{-}labile}$. Our simulation accounting for photooxidation (Table 3.1 (c)) leads to a tDOM distribution in the global ocean roughly comprised between those obtained with the semi-labile and semi-refractory rates. A stronger latitudinal gradient in tDOM inventories is nonetheless observable when considering the photooxidation case $T_{tDOM,photoox}$. Furthermore, this simulation leads to a larger global inventory than at the $T_{tDOM,semi\text{-}labile}$ mineralization rate (Table 3.1 (d)), but the surface layer tDOM concentrations are higher on average when photooxidation is accounted for, showing that tDOM degradation rates are very high at the surface due to abundant shortwave radiation exposure (3.4 Mg C d^{-1}), whereas they are less than for $T_{tDOM,semi\text{-}labile}$ in the deeper water layers.

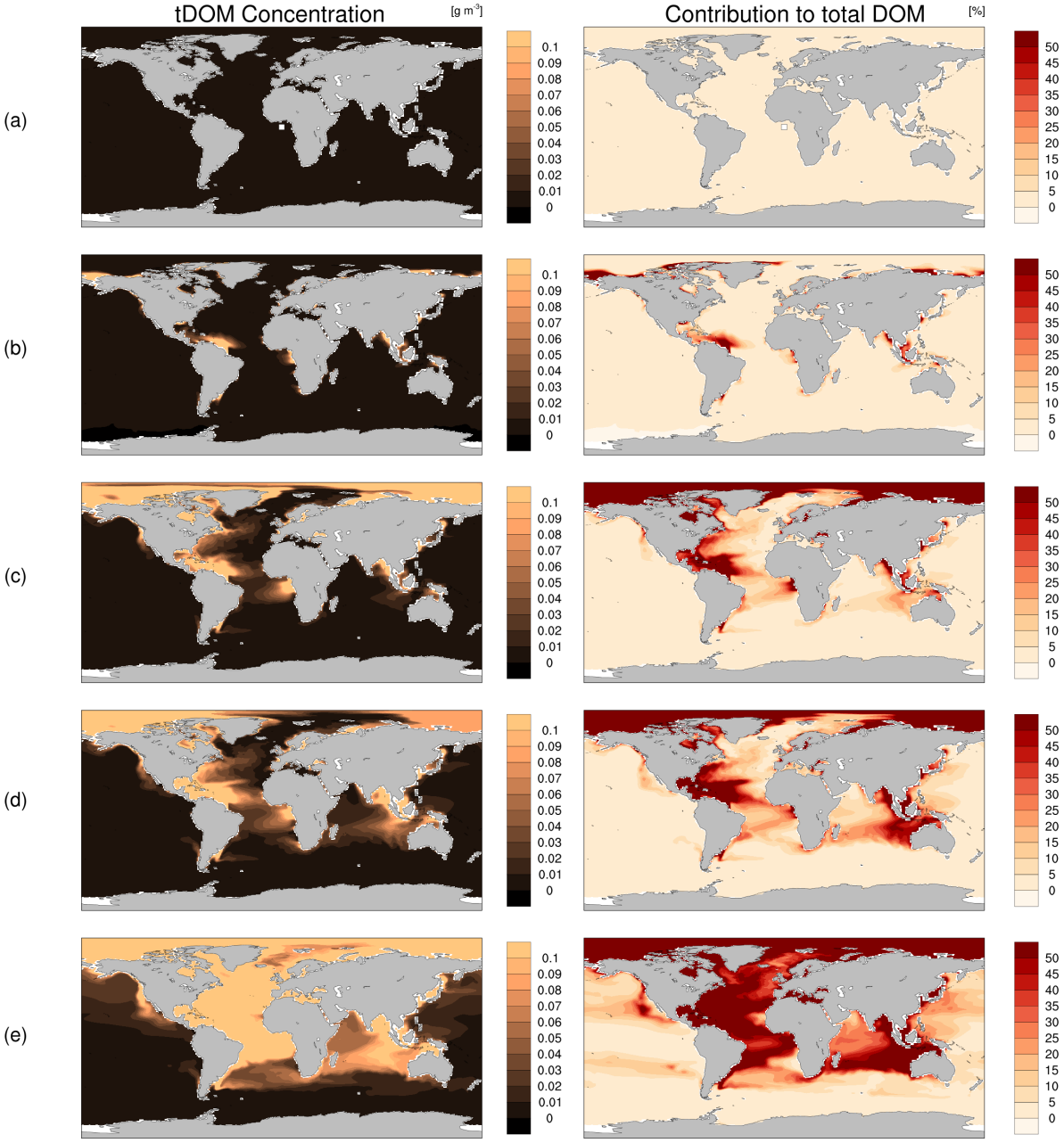

FIGURE 3.4: Left panels are the tDOM surface concentrations (reported in g C m^{-3} yr^{-1}) and right panels are the fractions of tDOM to total surface layer DOM concentrations [%] for (a) $T_{tDOM,inst}$, (b) $T_{tDOM,labile}$, (c) $T_{tDOM,photoox}$, (d) $T_{tDOM,semi\text{-}labile}$ and (e) $T_{tDOM,semi\text{-}ref}$ tDOM degradation scenarios.

For the three given tDOM degradation cases that we retained, the degradation on the global continental shelf ranges from 0.11 Pg C yr^{-1} for $T_{tDOM,labile}$ (48 % of riverine tDOM loads) to 0.06 Pg C yr^{-1} for $T_{tDOM,semi-labile}$ (26 % of riverine tDOM loads). In the simulation with $T_{tDOM,photoox}$, 0.07 Pg C yr^{-1} is mineralized on the shelf (30 % of total loads). The total riverine loads of tDOM comprise of 0.18 Pg C yr^{-1} of biologically unreactive tDOM (tCDOM, determined as 80 % of tDOM loads). Of these tCDOM loadings, 0.05 Pg C yr^{-1} is mineralized. Therefore, the fraction of tCDOM mineralized on continental shelves (28 %) is between the fractions of total tDOM mineralized on shelves using the labile and semi-labile rates (48 % and 26 %, respectively).

To further evaluate the tDOM breakdown in different regions, we compare our simulations to the few regional studies available: the regional budgets for the Louisiana Shelf Fichot and Benner (2014), the Baltic Sea (Seidel et al., 2017) and the Siberian Shelf (Kaiser et al., 2017), as well as estimates of plume photodegradation in 11 river plumes (Aarnos et al., 2018).

TABLE 3.2: Regional budgets of tDOM degradation in Tg C yr^{-1} and its fraction in the context of tDOM river loads to the given region. The river loads from the regional budgets differ from the river loads modelled in this study. Louisiana shelf: Fichot and Benner (2014), Baltic: Seidel et al. (2017) and Arctic, East Siberian Shelf: Kaiser et al. (2017)

tDOM degradation

	Observed	**Modelled**		
		$T_{tDOM,labile}$	$T_{tDOM,photoox}$	$T_{tDOM,semi-labile}$
Louisiana Shelf				
Annual mean	0.68 (44%)	1.75 (35%)	1.22 (25%)	0.39 (8%)
Summer	0.341	0.55	0,47	0,04
Winter	0.07	0.51	0,21	0,03
Baltic (Year mean)	1.75 (40%)	2.32 (82%)	2.29 (81%)	2.09 (74%)
Arctic (Year mean)	12.2 (54%)	16.9 (69%)	9.5 (39%)	1.29 (5%)

The magnitudes of the regionally integrated tDOM mineralization simulated by our model compare well with those reported in the literature (Table 3.2). The best agreement is found on the Louisiana shelf and Arctic Ocean when the labile and photooxidation rate constants are used, while in the Baltic Sea, the semi-labile run provides the best estimate. These results can be explained by the fact that the reactivity of tDOM and tCDOM is likely heterogeneous

regionally across continental shelves. Moreover, the relative mineralization in the Baltic Sea is much higher than what is calculated by Seidel et al. (2017). This mismatch may be the consequence of the difficulties to simulate the narrow outflow of the semi-enclosed Baltic Sea in the model resolution used here.

We are only aware of a single study that reports the seasonal variation of tDOM mineralization on a regional tDOM budget (Fichot and Benner, 2014). Nevertheless, we observe substantial improvement in the representation of the seasonality in tDOM breakdown on the Louisiana shelf when considering light-induced degradation (Table 3.2). While the simulation with semi-labile rate constant better reproduces tDOM shelf mineralization in winter, summer tDOM mineralization is better captured with the labile and photooxidation constants. Although the seasonal variability might also be caused by temperature effects, as well as seasonally varying riverine tDOM loads, Fichot and Benner (2014) suggest that a large part of the tDOM degradation is either directly induced by light (photooxidation) or indirectly (photo-enhanced biomineralization).

Our results also show reasonable agreement between modelled and observed tDOM photo-degradation rates (Table 3.3). Our simplified approach to model the breakdown of tCDOM through shortwave radiation allows us to reproduce the order of magnitude of the photo-mineralization rate observed in the field. The match between simulated and observed tDOM photo-mineralization rates is particularly good in the plumes of the Amazon and the Yangtze rivers. However, while the tDOM mineralized within the plumes is strongly dependent on the riverine supply of tDOM, which likely explains most of the good agreement in regions of large rivers, we emphasize on the representation of the net release of DIC from the tDOM photo-mineralization in the coastal zone in this study, and not on the detailed photo-mineralization process.

TABLE 3.3: Comparison of modelled photo-mineralization rates with rates measured in plumes from Aarnos et al. (2018).

River	*Observed tDOM photo-mineralization* [Tg C yr^{-1}]	*Modelled tDOM photo-mineralization* [Tg C yr^{-1}]
Amazon	6.98	5.58
Congo	3.04	1.43
Danube	0.08	0.36
Ganges-Brahmaputra	0.13	0.32
Lena	1.36	0.44
Mekong	0.13	0.04
Mississippi	0.24	0.74
Parana	0.23	0.11
St Lawrence	0.07	0.43
Yangtze	0.23	0.28

Implications for global oceanic carbon cycle variables

In our simulations, the total global NPP ranges from 49.1 to 49.2 Pg C yr^{-1}, which is similar to the NPP calculated by the model simulation RIV (47.4 Pg C yr^{-1}) and by the standard model version REF (48.5 Pg C yr^{-1}) (Table 3.4). The higher NPP simulated in this study is a consequence of the more efficient recycling of nutrients in the coastal zone due to the enhanced sediment POM remineralization rate. The surface concentrations of DIN and DIP simulated here are also slightly higher due to the increased recycling of the nutrients in the coastal zone. With the model modifications, the contribution of the continental shelves to the global NPP is higher with respect to RIV and REF. Considering only pre-industrial riverine loads and increased sediment recycling of nutrients on continental shelves, the global shelf NPP is enhanced to 1.99-2.02 Pg C yr^{-1} (around 5 % of global NPP), whereas in the standard model run (omitting rivers and enhanced coastal POM sediment remineralization), the coastal NPP only amounts to 1.34 Pg C yr^{-1}, 2 % of the global NPP for the same surface area. The contribution of the continental shelves in the context of the global carbon cycle and anthropogenic CO_2 currently is strongly debated in literature (Borges et al., 2005; Chen and Borges, 2009; Cai, 2011; Wanninkhof et al., 2013; Gruber, 2014). Estimates from 10 % to as a high as 30 % reported

in the literature (Walsh, 1991; Gattuso et al., 1998; Muller-Karger et al., 2005; Chen and Borges, 2009) indicate a strong underrepresentation of the coastal zone in OCGMs until now. These estimates should however be interpreted with caution because of the lack of universally admitted definition of the coastal ocean and continental shelves (Laruelle et al., 2013). For instance, for the 30 % value given in Muller-Karger et al. (2005), the study considers areas with up to 2000 m depth, and should not be directly compared to shallow shelf studies such as ours. Furthermore, satellite-based based observational estimates might also have large methodological uncertainties in the coastal ocean (Saba et al., 2010; Saba et al., 2011). While the model modifications substantially increase the contribution of the global continental shelf to the global NPP, it is still only equal to around the global oceanic average. It is however plausible that increases of riverine nutrient supplies throughout the 20^{th} century (Seitzinger et al., 2010; Beusen et al., 2016) might have elevated the continental shelf NPP to higher than its areal contribution, while we here consider a representation of pre-industrial river supplies. Furthermore, the coarse resolution might underestimate nutrient supplies through open ocean inflows.

TABLE 3.4: Overview of global values that impact the organic carbon cycle from the model simulations in this study, simulation RIV, which includes riverine fluxes as described in (Lacroix et al., 2019) but omits enhanced remineralization in the coastal sediment, and a simulation in the standard HAMOCC setup (REF), as described for instance in (Mauritsen et al., 2019). The range given in this study is for the simulations with tDOM lifetimes $T_{tDOM,labile}$, $T_{tDOM,photoox}$ and $T_{tDOM,semi\text{-}labile}$

Global variables	This study	RIV	REF
Organic carbon cycling variables			
NPP [Pg C yr^{-1}]	***49.08-49.20***	***47.44***	***48.49***
Bulk phytoplankton	46.92-47.02	45.53	46.15
Cyanobacteria	2.16-2.18	1.91	2.34
Coastal	1.99-2.02	1.45	1.34
Organic Matter Dep. [Pg C yr^{-1}]	0.70-0.71	0.65	0.68
Surface DIP [μM P]	0.434-0.437	0.413	0.439
Surface DIN [μM N]	4.01-4.03	3.76	3.90

Global values that impact inorganic carbon fluxes in the pre-industrial ocean state are also strongly comparable with those simulated using previous model

TABLE 3.5: Overview of global values that impact inorganic cycling of carbon from the model simulations in this study, for the present day (p-d) using tDOM lifetime $T_{tDOM,photoox}$, for the pre-industrial (p-i) simulations with tDOM lifetimes $T_{tDOM,labile}$, $T_{tDOM,photoox}$ and $T_{tDOM,semi\text{-}labile}$, for simulation RIV (p-i), and REF.

	This study			
Global variables	p-d	pi	RIV (p-i)	REF (p-i)
		Inorganic cycling variables		
CO_2 Flux[Pg C yr^{-1}]	***-2.05***	***0.31-0.34***	***0.18***	***-0.04***
Open ocean	-1.90	0.37 - 0.42	0.28	
Coastal ocean	-0.15	-0.06 - -0.08	-0.10	0.14
Surf. DIC Conc. [mM C]	0.20	0.194	1.94	1.94
Surf. Alk. Conc. [mM]	2.23	2.22	0.18	0.21
$CaCO_3$ dep. [Pg C yr^{-1}]	0.23	0.22	0.18	0.21
Opal deposition [Pg Si yr^{-1}]	1.38	1.41	1.38	1.37

configurations (Table 3.5), except for the air-water CO_2 flux. This is a consequence of the latter being dependent on the riverine carbon inputs. For the pre-industrial state, the CO_2 outgassing flux in this study (0.31-0.34 Pg C yr^{-1}) is larger than in RIV (0.18 Pg C yr^{-1}). This originates from the increased carbon inputs to the ocean by scaling of tDOM from 0.14 to 0.24 Pg C yr^{-1} in this study. REF on the other hand does not consider riverine carbon inputs and therefore does not simulate pre-industrial carbon outgassing. The global calcium carbonate flux to the sediment (0.23 Pg C yr^{-1}), which exports carbon and alkalinity from the water column, is similar to the global estimate (0.30 Pg C yr^{-1}) by Milliman and Droxler (1996) based on upscaling from regional observations. The opal production rates are also comparable between the simulations, which is important due to the inhibiting effect of the opal production on the calcium carbonate production in the model. The present day simulation, which was performed using $T_{tDOM,photoox}$ parametrization approach for tDOM degradation, predicts an oceanic uptake of CO_2 of 2.05 Pg C yr^{-1} due to the increase in atmospheric CO_2 concentrations. The anthropogenic uptake, is therefore 2.38 Pg C yr^{-1}, the difference between the pre-industrial and present day CO_2 fluxes. These values are in line with the acknowledged contemporary uptake range of 2-2.9 Pg C yr^{-1} (Ciais et al., 2013; Le Quéré et al., 2018). This uptake results in the oceanic increase in surface DIC concentrations and a slight enhancement of the $CaCO_3$ export to the sediment due to larger oceanic

carbonate ion concentrations.

3.3.2 Carbon cycling on continental shelves

In this section, we discuss the role of continental shelves in the context of the carbon cycle while focussing especially on the trophic state and CO_2 flux of the global shelf. We start with an assessment of physical indicators, which have strong controls on the cycling of carbon on continental shelves: residence times (RTs) and mixed layer depths (MLDs). We then perform global budgets for the organic cycling of carbon on the shelves and determine their net global trophic state. We use a historical simulation (using the $T_{tDOM,photoox}$ reactivity for the tDOM degradation) performed for 1850-2015 altering only the atmospheric pCO_2 in order to assess the model performance with respect to recent observation-based estimates of the coastal CO_2 sink. We then rewind in time and construct global coastal carbon budgets for pre-industrial conditions (atmospheric pCO_2 = 278 ppm) for the different tDOM reactivities.

Physical variables: RT and MLD

The RT of shelf waters is an important metric for continental shelves as it provides a timescale for transformation processes (e.g. organic matter production and remineralization) to happen, before compounds are transported offshore. The inert tracer simulation reveals that 50 % of the water is transported offshore within 9 months for all shelf water and 8 months when accounting for only the surface water (Figure 3.5-a and 3.5-b). The assumption of a global exponential decay of the inert tracer mass on the global shelf holds relatively well, although we observe a faster initial decay and a slower decay than the exponential function at around 15 months. With the derived exponential decays (0.064 yr^{-1}), we estimate a RT of around 16 months for all continental shelf water (Figure 3.5-a). The surface water (0.071 yr^{-1}) on the other hand has a significantly lower residence time on the shelves for 14 months on average only. The shorter shelf residence of the surface can be explained by a combination of two factors, which are also discussed in Kang et al. (2013) and Sharples et al. (2017). The flow of the freshwater plumes generated by major rivers usually carries freshwater perpendicularly to the coastal, causing a faster export off the shelf than water masses affected by currents parallel to the shoreline. Moreover, the low-salinity of the freshwater induces stratification, keeping

river-derived waters at the surface, where it is more susceptible to wind stress and offshore export. On river dominated shelves, Sharples et al. (2017) also suggest weak vertical mixing and significant river plumes. This leads to a very fast decay of the tracer signal for instance in the Amazon (Figure 3.5-c), where a majority of the water is transported offshore within one month. In the Laptev Sea on the other hand, the assumption of the exponential decay does not hold as well (Figure 3.5-d), most likely due to the high seasonality of currents and freshwater inflows in the region.

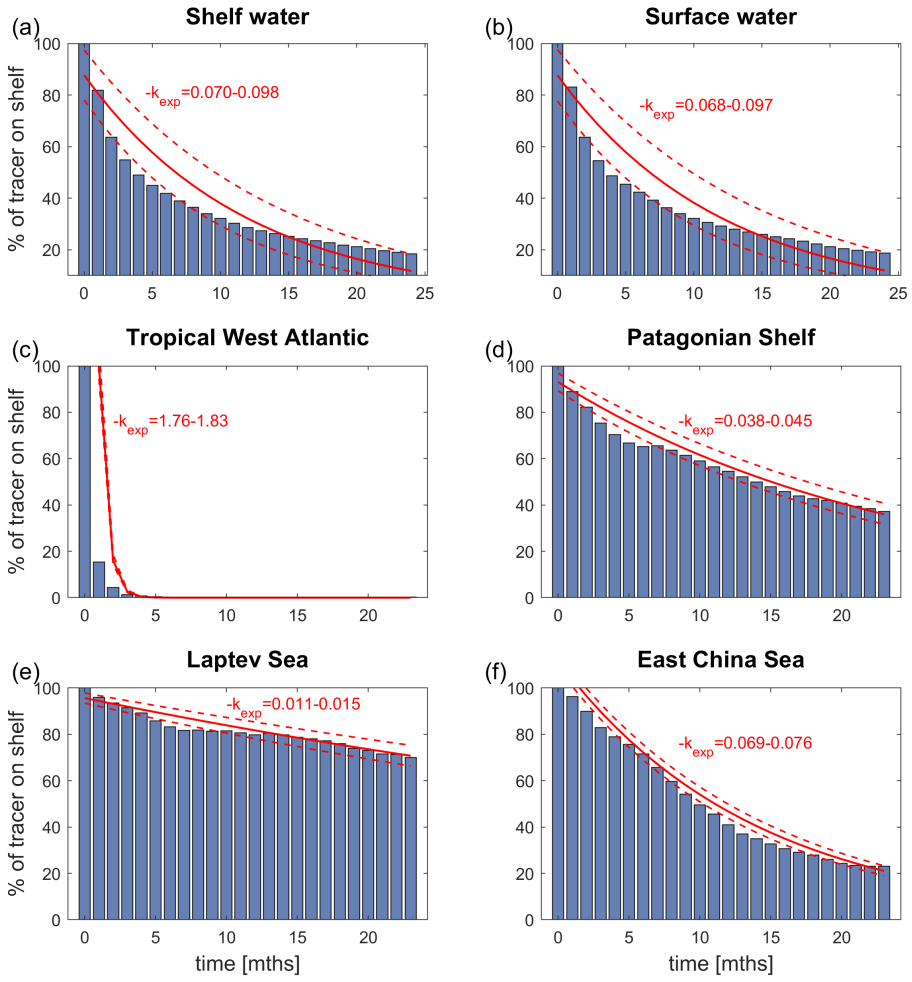

FIGURE 3.5: Fraction of inert tracer mass [%] remaining on the shelves after given times [mths] for experiments where the tracer was initially added in (a) all continental shelf waters, (b) all continental shelf surface waters, (c) near the Amazon river mouth (-50.3 E 2.2 N) and (d) in the Laptev Sea (126 E 79 N). The estimated exponential decay coefficient k_{exp} is given in [yr^{-1}].

The large spatial variability in continental shelf water RTs (Figure 3.6) strongly

agree with the spatial distribution of freshwater RTs reported in the parameterized approach of Sharples et al. (2017). Overall, high latitude continental shelves show much longer shelf RTs than temperate and tropical regions. This can be explained partly by the much larger average width of high latitude continental shelves. Water remains on the Arctic shelves for over two years, whereas tropical shelves often have RTs of half a year on average. Indeed, these continental shelves are much narrower on average, and often strongly affected by river flows (e.g. Amazon, Congo). Lower RTs in tropical systems could also be explained due to the weaker Coriolis force at such latitudes (Sharples et al., 2017). The RTs simulated by the model can reproduce the observed high RTs observed for Arctic Shelves, the East China Seas and the North Sea (Table 3.6). For narrow tropical shelves, our model-based estimates are also the very low, agreeing with regional estimates. As can be observed in Figure 3.6 and Table 3.6, the RTs simulated by the model are much lower for river-dominated shelves such as the tropical West Atlantic RT (supplied by the Amazon river) and at the Mississippi river mouth, where the RTs are of less than one month.

Previous conceptual box model studies had assumed much larger global RTs (from 4 years upwards) than shown here when constraining the shelf circulation assumptions of the models (Rabouille et al., 2001; Mackenzie et al., 2004; Andersson et al., 2005). These models thereby had a stronger emphasis on freshwater inflows. Our results show, through the low modelled RT values, that oceanic inflows across the shelf break play a prominent role for the continental shelf water supply. This is emphasized by contrasting our global RT estimate with a quantification of RTs considering only freshwater fluxes and a fully mixed coastal ocean. Dividing the global continental shelf volume (1.78 10^{15} m^3) by global riverine freshwater loads (0.032 10^{15} m^3 yr^{-1}) of the model leads to an estimated water RT of 55 years, which differs strongly from the RTs determined by the inert tracer experiment. As a comparison, Laruelle et al. (2013) estimate the global shelf volume to 1.79 10^{15} m^3 for depths of <200 m and Fekete et al. (2002) estimate the global discharge at 0.038 10^{15} m^3 yr^{-1}, which would lead to an RT of 47 years, thus a vastly higher value than given in our model. Using the model-derived shelf RT of 16 months, we can estimate the total oceanic inflows as 1.25 10^{15} m^3 yr^{-1} from the relationship between RT and water through-flow (Eq. 3.8). The oceanic inflows are thus 40 times larger than the freshwater inputs in our approximation. Such large oceanic inflows do not only have important implications for continental shelves biogeochemistry because of their RTs but also because the biogeochemical characteristics

of these waters likely strongly differ from those of the land-derived riverine inputs.

The mixed layer depth (MLD) is a further important controlling factor of the biogeochemistry of continental shelves, since it is an indicator of stratification within the water column. The MLD is often smaller than the sea floor depth on continental shelves (Figure 3.7), suggesting that the shelves are not fully mixed. Globally, we simulate an average shelf MLD of 37 m, and an average shelf seafloor depth of 92 m. MLDs compare relatively well with regional MLDs reported in published literature. For one, Álvarez et al. (2016) report that the (Northern) Patagonian shelf MLD is estimated between 30 and 60 m, while it is 20-60 m in the model. The MLD is however strongly seasonal in reported observations as well as in the model. Similarly, the East China Sea MLD is estimated to range between 14 and 50 m (Delcroix and Murtugudde, 2002) and varies from 10 m on the inner shelf to 80 m on the outer shelf in the model. However, in the Laptev Sea, the MLD can be as deep as 25 m (Stranne et al., 2018) whereas it is mostly less than 10 m due to freshwater-induced stratification in the model. Finally, the Amazon River is reported to induce a strong pycnocline of 3 to 30 m in the tropical West Atlantic (Pailler et al., 1999), which is also represented in the model (MLD < 10 m). While these comparisons show a plausible representation of the average annual shelf MLDs, we nonetheless acknowledge large spatial and temporal variability of this physical characteristic, which might not be appropriately represented in the coarse resolution of the model. Although full mixing to the ocean floor occurs in very shallow continental shelves such as the inner shelf of the North Sea, in deeper areas such as the Patagonian shelf, the MLD does not reach the sea floor. Furthermore, in regions characterized by strong riverine freshwater inputs (e.g. the Bay of Bengal and the west Tropical Atlantic), the low salinity plumes create a very shallow MLD due to the lower density of the freshwater compared to saline waters. As a result, major plumes having much shorter RTs on the shelves than average (Figure 3.6) due to efficient outward stratified plume flow is also confirmed here.

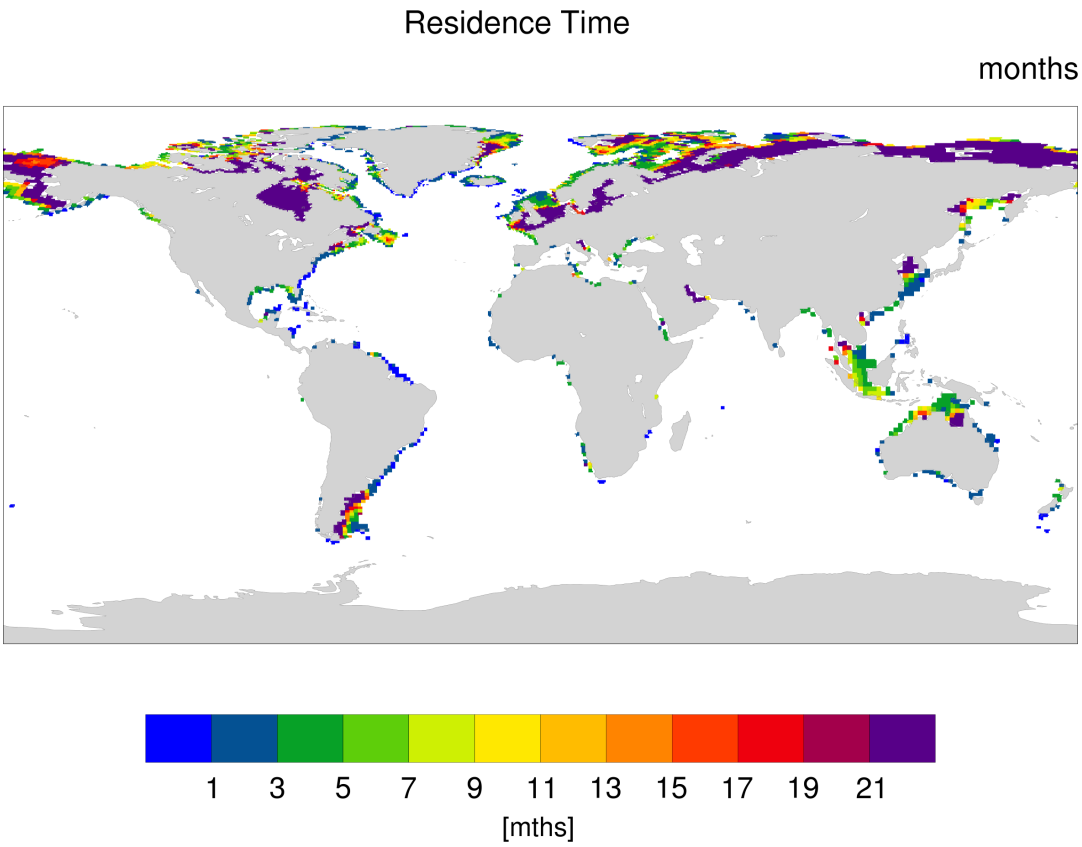

FIGURE 3.6: Continental shelf water RTs [mths] derived from the near-exponential decay of the inert tracer mass on shelves.

TABLE 3.6: Global continental shelf RTs [mths] derived from the near-exponential decay of the inert tracer mass on shelves (Model shelf water RT), compared to regional estimates from a combination of in-situ tracer experiments and high-resolution regional models (Regional Studies shelf water RT), and to a global parametrization approach to estimate river plume residence times (Sharples et al. (2017) freshwater RT).

Coastal regions	*Model shelf water RT*	*Regional Studies shelf water RT*	*Source*	*Sharples et al. (2017) freshwater RT*
North Sea	0.3-6 yr	0.4-4 yr	Huthnance (1997), Blaas et al. (2001)	1 yr
Great Barrier Reef	1-3 mth	2-6 weeks	Hancock et al. (2006)	2 weeks
South Atlantic Blight	2-12 weeks	1 mth	Gong et al. (2010)	1-2 mth
Tropical West Atlantic	<1 mth	2-4 wks	Moore and Oliveira (2008)	1-2 weeks
Laptev Sea	>4 yr	1-6 yr	Schlosser et al. (1994), Eicken et al. (2005)	>1yr
East China Sea	1-17 mth	0.5-4 yr	Nozaki et al. (1989), Ren et al. (2006), Men and Liu (2015)	1 yr
Sunda Shelf (South East Asia)	3-13 mth	1-12 mth	Mayer et al. (2015)	1-12 mth
Sea of Beaufort	5-15 mth	3-6 mth	Schlosser et al. (1994)	< 1mth
Bay of Bengal	3-5 mth	3 mth	Sarin et al. (1994)	1-3 mth
Sea of Okhotsk	1-5 yr	1.5-3 yr	Yasuda et al. (2002)	< 1 yr

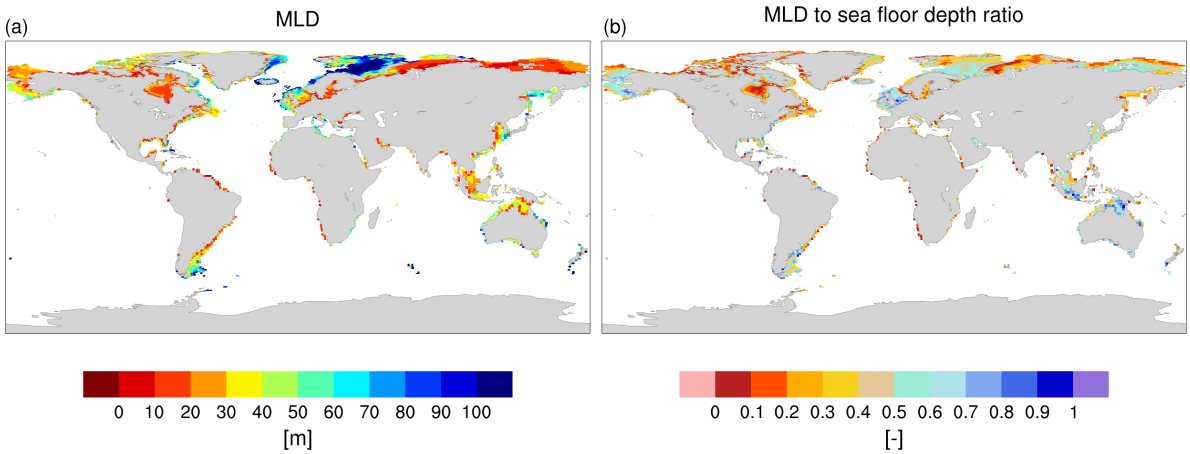

FIGURE 3.7: Annually averaged mixed layer depth [m] and ratio of the mixed layer depth and the sea floor depth of continental shelves.

Continental shelves organic carbon cycling (pre-industrial)

In addition to the net production of organic matter of 1.99-2.02 Pg C yr^{-1} on continental shelves (NPP), 1.94-2.01 Pg C yr^{-1} of the organic material is mineralized (RH, Figure 3.8) for the pre-industrial time period. This includes riverine POM, autochthonous POM and tDOM mineralization in the water column as well as in the sediment. The resulting NEP, the difference between NPP and RH, is thus slightly positive in all simulations (0.01-0.05 Pg C yr^{-1}), which suggests the shelves are therefore in an autotrophic state in all simulations with plausible tDOM mineralization rates. We also observe an efficient export organic matter on the shelves globally (0.29-0.34 Pg C yr^{-1}).

The shelf particulate organic carbon sediment deposition flux of 0.37-0.38 Pg C yr^{-1} accounts for over half of the global particulate organic flux to the global oceanic sediment (0.71 Pg C yr^{-1}). This is in line with suggestions that half of the oceanic organic carbon deposition takes place on continental shelves (Gattuso et al., 1998; Chen and Borges, 2009). Of the organic carbon exported to the sediment, 0.32 Pg C yr^{-1} is (re)mineralized and returned to the water column, whereas 0.07-0.08 Pg C yr^{-1} is buried diagenetically. The burial efficiency of around 15% compares well with efficiencies reported by a review of 8 studies addressing coastal organic deposition and mineralization (Krumins et al., 2013). In the study, the range of particulate organic C flux to the sediment was given from 0.19 to 2.2 Pg C yr^{-1} with a net burial flux ranging from 0.06 to 0.67 Pg C yr^{-1} and a burial ratio comprised between 8 and 23% in the individual estimates.

The substantial offshore transport of organic matter and the positive NEP reported here is consistent with our results with respect to RTs. First, our study reveals short RTs for continental shelf waters (around 16 months), and even shorter residence times for surface waters on the shelves (14 months). Shorter shelf residence times imply a more efficient export of organic matter before it is mineralized. Moreover, the physical and biogeochemical characteristics of the waters carried by the large oceanic inflows are likely different to those of the riverine inputs. Since oceanic inflows are often brought from subsurface oceanic layers to compensate surface divergence, they are generally characterized by low organic matter content and high nutrients concentrations (Yasuda et al., 2002; Pipko et al., 2017; Combes and Matano, 2018). While these entrained nutrients enhance NPP, the low organic matter supplies from the oceanic inflows do not considerably affect the RH (Chen and Borges, 2009). As a consequence, oceanic inflows have a positive effect on the NEP. Rivers on the other hand, carry large amounts of organic matter, which was produced by the terrestrial biosphere. When this organic material is mineralized in the ocean, the subsequent release of DIC leads to a reduction of the NEP.

The vertical stratification of the continental shelf waters also could play a significant role in explaining the efficient offshore transport of organic material and positive NEP. Since rivers with high runoff also carry high loads of land-derived organic material (Bauer et al., 2013), the export of the riverine derived organic material beyond the shelf break is faster for surface waters (14 months). Low MLD to sea floor depth ratios can be found in regions with strong freshwater influence such as, for instance, on the tropical West Atlantic shelf (Pailler et al., 1999) or on the East China Sea (Delcroix and Murtugudde, 2002). A larger cross-shelf export of organic matter prior to its mineralization thus leads to a higher NEP in the coastal zone. Therefore, resolving the coastal ocean in the vertical is of substantial importance for grasping the sign and magnitude of the NEP.

In previous studies, the RTs of the continental shelves were at times estimated by solely considering the flushing of continental shelves by freshwater inputs as calculated by Rabouille et al. (2001), Meybeck et al. (2006) and Laruelle et al. (2013), leading to much longer shelf residence times, since open ocean inflows are potentially forty times larger than the freshwater inputs (Broecker and Peng, 1982). While the conceptual box models found in Mackenzie et al. (2002), Mackenzie et al. (2004), and Andersson et al. (2005) considered an inflow flux from the open ocean, the residence times assumed in these studies

(>4 years) might indicate a strong underestimation of the oceanic inflows. The negative NEPs resulting in the conceptual box model studies (-0.1 to -0.3 Pg C yr^{-1}) could therefore be a consequence of the underrepresentation of oceanic inflows. In previous OCGM studies in which riverine loads are considered (e.g. Dunne et al. (2012) and Bourgeois et al. (2016)), organic matter is assumed to be rapidly degraded in the coastal ocean and therefore an instantaneous release of DIC from the organic matter is assumed. However, in literature, terrigenous material is reported to already be highly degraded upon arrival to the ocean (Aarnos et al., 2018). It is thus highly unlikely that the entirety of terrigenous organic material is mineralized on continental shelves. For instance, tDOM cross-shelf export fractions of 50-70 % are suggested in regional budgets of shelves with major river inputs (Fichot and Benner, 2014; Kaiser et al., 2017; Aarnos et al., 2018). The range of tDOM export (60-83 %) in our simulations is consistent with this range. A slower OM degradation rate implies larger cross-shelf export, which in its turn also explains the more positive NEP reported here.

Although we report and discuss global values here, spatial heterogeneity of the NEP can also be found regionally (Figure 3.9-a) and in the vertical (Figure 3.9-b). In general, shelves with favourable conditions for biological production (high insolation and temperature) are areas of positive NEP, whereas the high latitude regions are often net heterotroph. The Patagonian shelf is a strong exception here, as the regional NEP is strongly positive. Furthermore, since the primary production takes place exclusively at ocean depths where there is substantial shortwave radiation, whereas remineralization processes are present at greater depths, there is a strong vertical gradient in the continental shelf NEP, with a positive NEP near the surface and a negative NEP at greater depths (Figure 3.9-b).

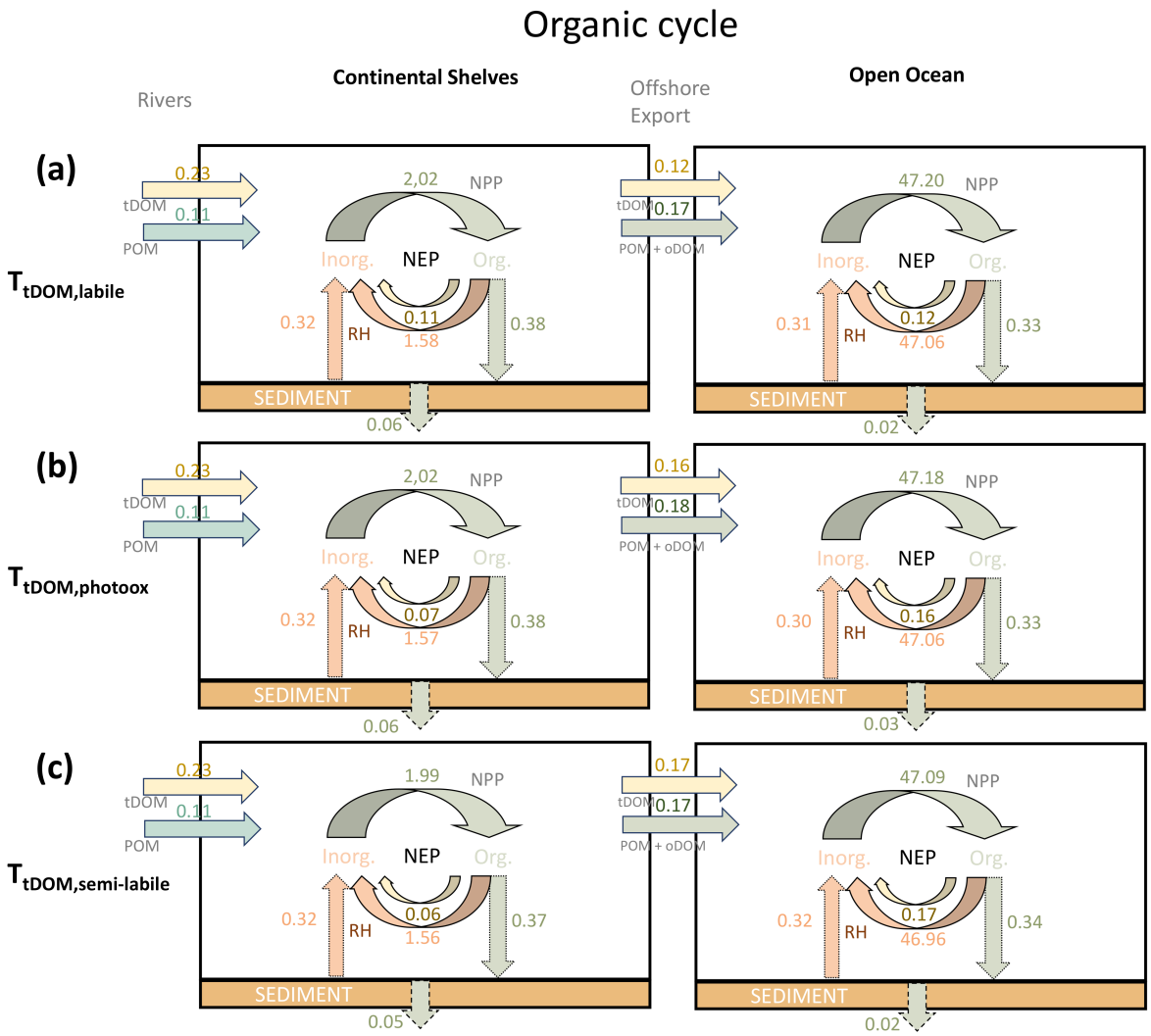

FIGURE 3.8: Organic cycling of carbon for simulations (a) $T_{tDOM,labile}$, (b) $T_{tDOM,photoox}$ and (c) $T_{tDOM,semi-labile}$ tDOM degradation cases. yellow arrows thereby indicate the transport and mineralization of tDOM, green arrows are processes that produce or transport organic carbon [Pg C yr^{-1}]. The NPP considers the organic production by all phytoplankton species. The RH consists of all remineralization processes of POM (red arrows) and of tDOM (yellow arrows). RH also considers remineralization in the sediment (red arrow from the sediment. POM is deposited to the sediment (green arrow to the sediment).

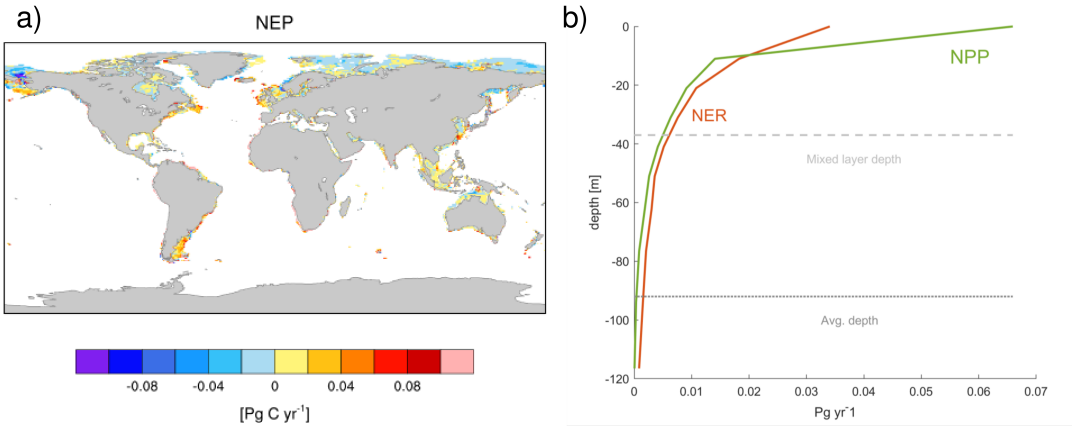

FIGURE 3.9: Spatial distribution of annual NEP (a) and depth integrated NPP and NER of the global continental shelf (b) for the scenario $T_{tDOM,photoox}$.

Modelled present day CO_2 flux in the context of present day estimates

The organic carbon cycle directly affects continental shelf DIC budgets and therefore the air-sea CO_2 flux. Due to our assumption of constant riverine inputs of carbon and nutrients, the organic carbon cycle remains nearly identical under pre-industrial conditions (NEP=0.05 Pg C yr^{-1}) to the present day (as seen in the NEP in Figure 3.10). This is due to using a constant physical atmospheric forcing for the simulation, leaving the increase of atmospheric CO_2 as the only driver of change for the CO_2 flux between the pre-industrial and present day state. The increase of atmospheric CO_2 concentrations is also believed to be the dominant driver of anthropogenic perturbation on the global coastal carbon cycle (Bauer et al., 2013).

For the present day, for which we average model output of the historical simulation from 1998-2015, the model shows a global continental shelf CO_2 uptake of 0.15 Pg C yr^{-1}, which amounts to 5% of the global oceanic CO_2 uptake (Figure 3.10). The net cross-shelf export of DIC (0.25 Pg C yr^{-1}) is slightly lower than the riverine inputs (0.32 Pg C yr^{-1}). The offshore transport of DIC still however implies that the coastal ocean acts as a source of DIC to the open ocean. The magnitude of DIC storage within the coastal ocean is also significant (0.05 Pg C yr^{-1}), being as large as the modelled NEP (0.05 Pg C yr^{-1}) and larger than $CaCO_3$ production (0.03 Pg C yr^{-1}) in the model. The shelf NEP_C, which accounts for the dissolved CO_2 increase through $CaCO_3$ production, is 0.02 Pg C yr^{-1}, meaning that the continental shelf biology is both a very slight net consumer of DIC (NEP <0) and of dissolved CO_2 (NEP_c<0) in the model.

The CO_2 flux simulated here is comprised within the present day estimate range of 0.14-0.25 Pg C yr^{-1} (Wanninkhof et al., 2013; Laruelle et al., 2014), albeit at the lower end. The modelled shelf CO_2 flux is strongly spatially heterogeneous globally, with a strong sink of CO_2 being found in the temperate latitudes (0.78 Pg C yr^{-1} and 1.11 Pg C yr^{-1} for northern and southern hemispheres, respectively), a small sink found in the Arctic (0.10 Pg C yr^{-1}) and a moderate source found in subtropical and tropical shelves (0.16 Pg C yr^{-1} and 0.15 Pg C yr^{-1} for northern and southern hemispheres). The spatial variability of the pCO_2 simulated by our model for continental shelves is thereby in good agreement with the interpolated dataset of Laruelle et al. (2017) (Figure 3.11). Tropical shelves are generally regions characterized by high pCO_2 values, whereas temperate and high latitudinal regions are characterized by low pCO_2. In previous budgets based on the compilation of regional air-water CO_2 flux estimates (Laruelle et al., 2010; Chen and Borges, 2009; Cai, 2011), tropical shelves are also reported as sources of CO_2 to the atmosphere. However, a strong variability in the pCO_2 levels can be observed within latitudinal bands in our simulation as well as in the dataset of Laruelle et al. (2017). For instance, the Barents Sea is characterized by very low pCO_2 levels (locally bellow 300μ atm) and by a corresponding intense CO_2 sink in the model, while the Laptev shelf, which is under the strong NEP control of large riverine carbon loads through the Lena river, shows some of the highest pCO_2 values globally (exceeding 500 μatm locally) and provides a source of CO_2 to the atmosphere. Much higher than atmospheric pCO_2 partial pressures are also reported in measurements in the southern Laptev Sea near the Lena delta (Semiletov et al., 2013; Anderson et al., 2009), as well as on the outer Siberian shelf (Pipko et al., 2017) in observational studies. In the Barents Sea, however, the pCO_2 is considerably lower due to high productivity induced by the supply of nutrients from the Atlantic (Lauvset et al., 2013; Pipko et al., 2017), which results in one of the strongest global sinks of atmospheric CO_2. When budgeting over the entire Arctic Ocean, as is done in (Laruelle et al., 2014), areas of these very different regional air-sea CO_2 fluxes are not considered.

The riverine inputs of DIC (0.33 Pg C yr^{-1}) used in our simulations are situated well within present day constraints of 260-550 Pg C yr^{-1} (Berner et al., 1983; Amiotte Suchet and Probst, 1995; Meybeck and Vörösmarty, 1999; Lacroix et al., 2019). The modelled DIC export off the shelves (0.25 Pg C yr^{-1}) is on the other hand more difficult to assess, with the sign and the magnitude of the net exchange with the open ocean strongly disagreeing in literature. While

Bauer et al. (2013) suggest an cross-shelf export of DIC of 0.5-0.7 Pg C yr^{-1}, Mackenzie et al. (2004) only suggest a very small DIC cross-shelf export of 0.04 Pg C yr^{-1}, and Chen and Borges (2009) finally even suggests a net global influx from the open ocean of 0.32 Pg C yr^{-1}. The results from Chen and Borges (2009) were thereby derived from a mass balancing approach, in which it is concluded that a DIC flux from the open ocean is needed to sustain the high rate of transformation of DIC to organic carbon on continental shelves. In carbon budgets for large regions however, a slight net DIC export is suggested for the North Sea (Thomas et al., 2005) and the East China Sea (Chen and Wang, 1999).

While our simulations show carbonate production rates of 0.03 Pg C yr^{-1} for continental shelves (Figure 3.10), this only takes into account pelagic carbonate production and omits benthic and coral reefs calcium carbonate production. Milliman and Droxler (1996) evaluated the global carbonate production for continental shelves to 0.3 Pg C yr^{-1} when taking into account shallow water production, although the uncertainties for almost all of the production fractions exceed 100% in the study. Depending on the sensitivity of the continental shelf CO_2 flux to the pCO_2 increase caused by this subsurface production of calcium carbonate, an underestimation of the production might affect the results proposed in our study.

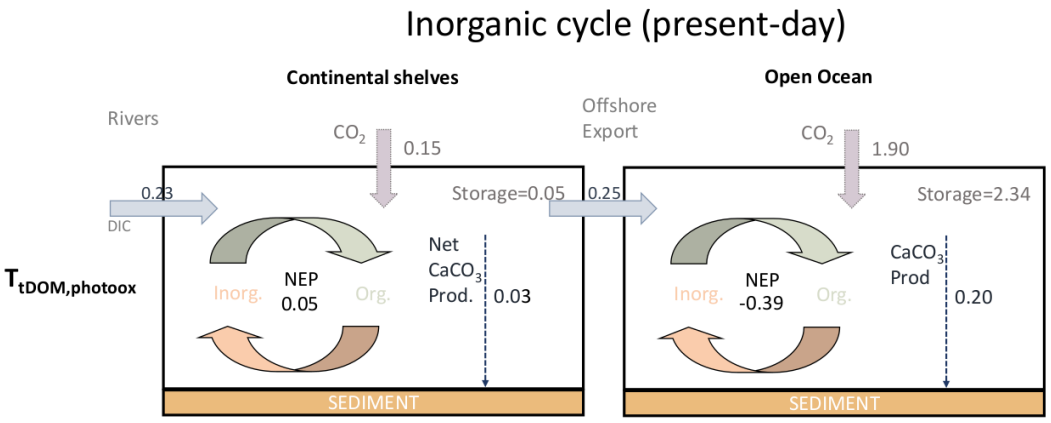

FIGURE 3.10: DIC budgets of the continental shelves and the open ocean for the present day (1998-2015) at the $T_{tDOM,photoox}$ tDOM degradation rate [Pg C yr^{-1}]. The purple arrows from the top of the boxes imply a flux from the atmosphere to the ocean. Net $CaCO_3$ Prod. is the net calcium carbonate production (including dissolution of calcium carbonate), which eliminates DIC from the ocean pool. The NEP accounts for NPP in the water column, as well as the remineralization (RH) of organic matter in the water column and in the sediment. The NEP consumes DIC, therefore it should be subtracted from the DIC pool when budgeting.

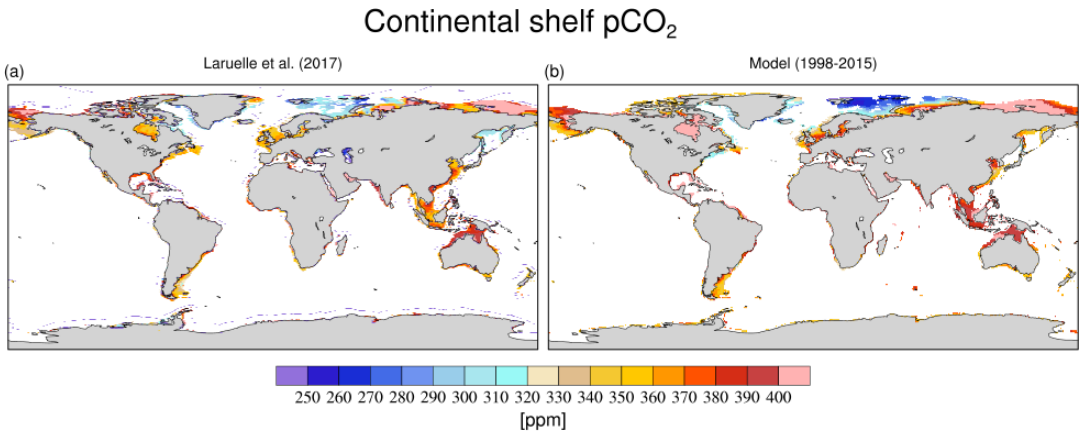

FIGURE 3.11: Continental shelf pCO_2 derived from a neural network interpolation observational data-product Laruelle et al. (2017) and the modelled continental shelf pCO_2 for an average of 1998-2015 using the $T_{tDOM,photoox}$ tDOM degradation case (Modelled). We only show the Laruelle et al. (2017) data points for depths of less than 250 m, since the study used a more inclusive definition for the coastal ocean based on slope gradients.

Implications for the pre-industrial CO_2 flux

The pre-industrial autotrophic state causes a slight DIC sink (NEP=0.01-0.05 Pg C yr^{-1}) on the global continental shelf. The simulations show, on the other hand, a slightly larger pre-industrial continental shelf sink of atmospheric CO_2 (0.06-0.08 Pg C yr^{-1}, Figure 3.12).

The pre-industrial CO_2 sink is thereby mostly caused by seven major regions: the Alaskan Shelf, the Barents Sea, eastern North America, the North Sea, the East China Sea and the Patagonian shelf (Figure 3.13). At least four of these regions (Barents Sea, East China Sea, North Sea and Patagonian Shelf) have been shown to be strongly affected by oceanic inflows (Chen and Wang, 1999; Thomas et al., 2005; Qiao et al., 2006; Pipko et al., 2017; Combes and Matano, 2018). This underlines the importance of using modelling tools that are able to capture such oceanic circulation features and their physical (i.e. temperature, salinity) and biogeochemical (e.g. alkalinity, CO_2 saturation, nutrient concentrations) characteristics in global continental shelf studies.

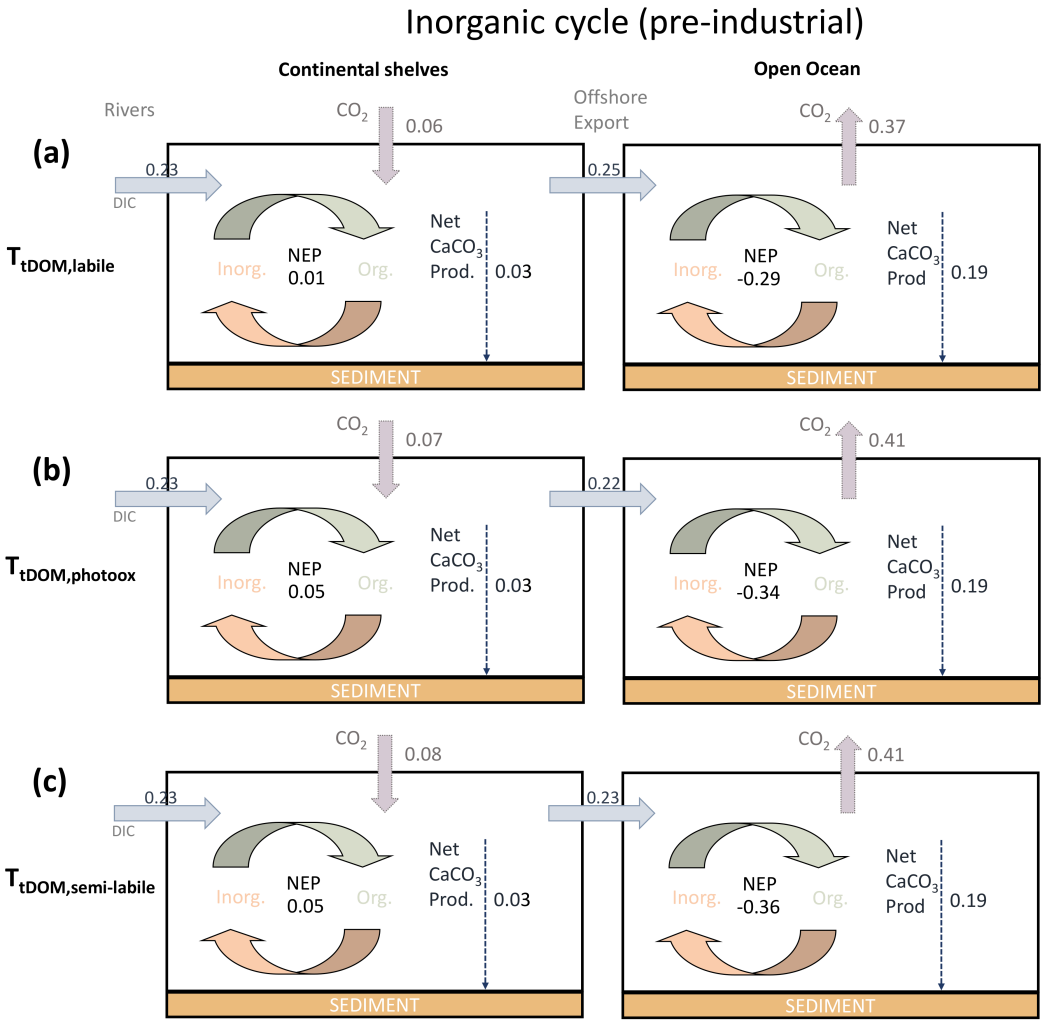

FIGURE 3.12: Pre-industrial global carbon cycle of the coastal and open ocean at the (a) $T_{tDOM,labile}$ (b) $T_{tDOM,photoox}$ and (c) $T_{tDOM,semi-labile}$ tDOM degradation rate. The purple arrows from the top of the boxes imply a flux from the atmosphere to the ocean. The NEP accounts for NPP in the water column, as well as remineralization of organic matter in the water column and in the sediment. The NEP consumes DIC, therefore it should be subtracted from the pool when budgeting.

That the CO_2 flux deviates to what would be expected from only considering the NEP on continental shelves, originates from the CO_2 flux not only being driven by the DIC producing/eliminating organic biological processes, but also being dependent on the $CaCO_3$ production, changes in alkalinity, temperature and salinity of oceanic inflows, and of riverine riverine supplies to the continental shelves, as well as the previous CO_2 saturation state of the inflows. This is also observable in a comparison between the spatial patterns of the NEP (Figure 3.9-a) and of the pre-industrial CO_2 flux (Figure 3.13). In regions such as the Patagonian shelf, the east coast of North America and the East China Sea, the CO_2 sink appears to be governed by the positive NEP. This

could be due to the strong supply from open ocean inflows in these regions which strongly enhance the NPP, but do not provide substantial amounts of organic matter loading that would immediately decrease the NEP (Chen and Wang, 1999; Chen and Borges, 2009; Song et al., 2016). The Siberian shelves are also a source of CO_2 to the atmosphere, likely to a large degree due to their heterotrophic states, caused by large terrestrial organic matter loadings to the shelves. However, on other shelves, the sign of the CO_2 flux differs from that of the NEP. For instance, the Sunda shelf has a strongly positive NEP, most likely due to very favourable conditions for biological production and nutrient supplies from the open Pacific, it is however a strong pre-industrial source of CO_2 in the model, likely due to the warming of the shallow shelf waters, which decreases the CO_2 solubility in the ocean. The cooling of Atlantic water supplies to the Barents Seas could also lead to the low pCO_2 in the region, since the NEP is only positive in some of the region.

Furthermore, the stratification of continental shelf waters (as seen in the MLDs of Figure 3.7-a), which can be very strong regionally due to major freshwater inputs, is partly responsible for the vertical gradient in the NEP (Figure 3.9-b). Since the autotrophic processes are more dominant in near-surface layers, the net effect of the organic production processes on the CO_2 flux might be stronger than is suggested by the total shelf NEP, whereas the DIC produced by mineralization of organic matter in subsurface water layers translates less efficiently to outgassing. This is also reflected when comparing our simulations of different tDOM mineralization rates: the effect of the change of NEP due to lower mineralization rates (a 0.04 Pg C yr^{-1} difference between $T_{tDOM,labile}$ and $T_{tDOM,semi\text{-}labile}$) only has an effect of half of this magnitude on the CO_2 flux (0.02 Pg C yr^{-1}).

A further explanation of the CO_2 flux exceeding the NEP is that alkalinity is produced in autotrophic processes (Wolf-Gladrow et al., 2007), which is not considered by our indicators NEP and NEP_c. In the surface continental shelf ocean layer (upper 12 m in the model), which has a direct exchange with the atmosphere, the NEP is strongly positive (0.77 Pg C yr^{-1}). The positive NEP also leads to alkalinity production in a mole fixed ratio to C (A_c:C=17/122), derived for the model stoichiometry as in Wolf-Gladrow et al. (2007). The resulting alkalinity production in the surface layer caused by the net biological organic matter production (8.6 Tmol yr^{-1}) is likely a major factor for the higher CO_2 uptake than would be expected by our continental shelf biological indicators NEP and NEP_c. Furthermore, the cooling or heating,

as well as increases or decreases in salinity of oceanic inflows can affect the magnitude of the CO_2 flux, although these effects are regionally variable.

While there still exist uncertainties regarding the magnitude of the CO_2 flux for the present day, it is largely acknowledged that shelves are a contemporary sink of atmospheric CO_2 (Wanninkhof et al., 2013; Laruelle et al., 2014). These most recent data-based estimates report a sink of 0.14-0.25 Pg C yr^{-1}. However, due to uncertainty regarding of the initial pre-industrial state, it has until now not been possible to fully assess the magnitude of the anthropogenic perturbation of the CO_2 exchange between continental shelves and the atmosphere. Most studies investigating the perturbation suggest that shelves were a strong pre-industrial source of CO_2 (Smith and Hollibaugh, 1993; Ver et al., 1999; Mackenzie et al., 2000; Mackenzie et al., 2002; Mackenzie et al., 2004; Andersson et al., 2005), all using conceptual box model approaches. Our model simulations however suggest that pre-industrial continental shelves might have been a weak CO_2 sink. A major argument for this sink is that we find a much lower global RT than is assumed to constrain the box model studies, which lead to a much more efficient coastal export of organic matter than assumed until now. The modelled mean shelf MLDs, which are less than half of the mean global sea floor depth, also suggest a certain degree of stratification on continental shelves, which can only be fully be taken into account using a global circulation model. The pre-industrial sink suggested in our study is consistent with the combined conclusions from Laruelle et al. (2014) (present day CO_2 sink of around 0.19 Pg C yr^{-1}) and Bourgeois et al. (2016) (anthropogenic perturbation of the CO_2 flux of 0.12 Pg C yr^{-1}), the latter estimating the anthropogenic perturbation of the coastal CO_2 sink by using a spatially explicit model.

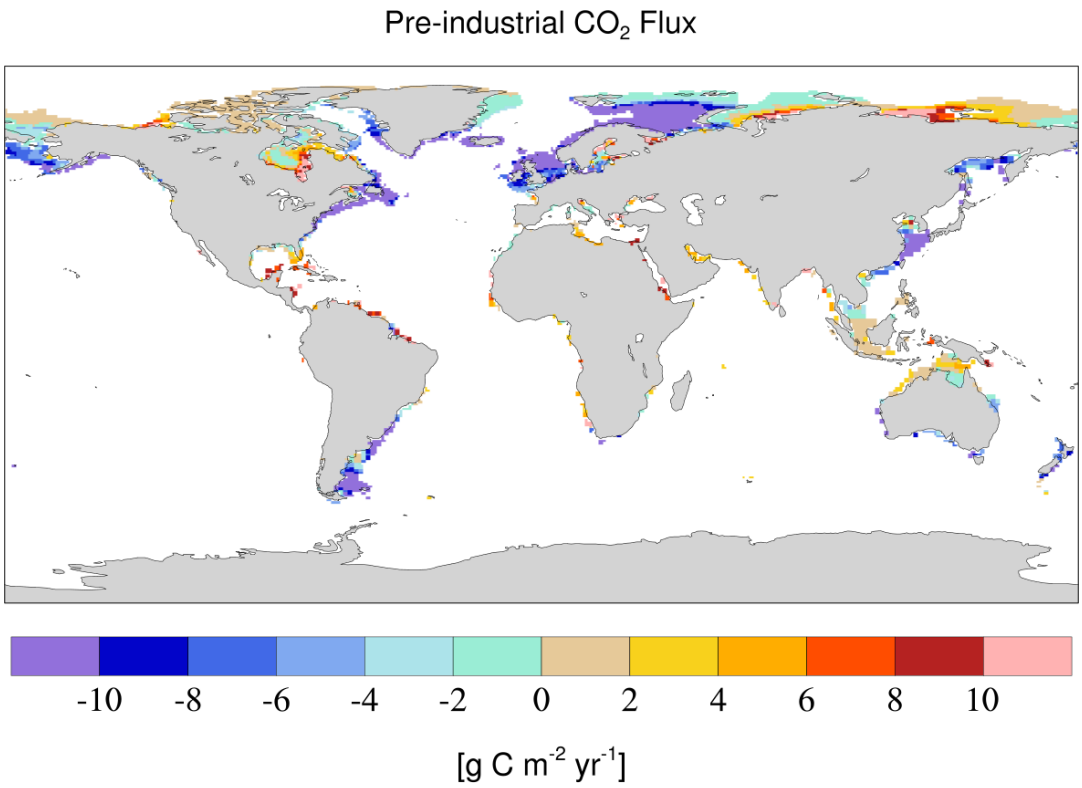

FIGURE 3.13: Pre-industrial continental shelf CO_2 flux [g C m^{-2} yr^{-1}] for the tDOM degradation case $T_{tDOM,photoox}$.

Spatial heterogeneity of the CO_2 flux on the Arctic shelves

Combining the modelled data and conclusions from observational data perspectives can help give a potential mechanistic explanation of the strongly differing CO_2 fluxes in the Arctic, where the Barents Sea and the Laptev Sea reside on opposing sides of the CO_2 flux spectrum as most prominent examples. For one, the Laptev Sea is supplied by the Lena River, which exports large amounts of carbon to the region (Ludwig et al., 1998; Seitzinger et al., 2010). Since we also determine long coastal water residence times in the region (Figure 3.5 and Table 3.6), this carbon is not transported offshore efficiently, which allows a longer time-frame for remineralization processes and subsequent outgassing of the terrestrial carbon, whereas the limited light supply inhibits the primary production processes for most of the year. Furthermore, the Laptev Sea is covered in sea-ice for most of the year (91-94 % yearly mean of sea-ice coverage). Ice coverage largely inhibits the supply of light to the marine biology, and in the case of the model the primary production does not take place at all under ice. It also inhibits the heat exchange between the atmosphere and the water column. Thus, the Laptev Sea temperature does

not decrease as substantially in the winter as for other regions such as the Barents Sea (Pipko et al., 2017), which would increase the CO_2 solubility. The ice barrier also implies that in the months of the coldest Arctic temperatures, and therefore of largest potential CO_2 uptake, the CO_2 exchange of the Laptev Sea does not take place. In the Barents Sea on the other hand, the large influx of nutrients causes an enhancement of the biological carbon uptake, whereas the DIC supply also brought by the open ocean inflows does not translate in carbon outgassing to the atmosphere due to the cooling of the waters. Since the Barents Sea is ice-free for all of the winter, the CO_2 exchange also takes place during the cold winter temperatures, explaining why it is one of the largest CO_2 sinks globally in the model.

Implications for the anthropogenic CO_2 sink

We can derive an anthropogenic carbon sink of 0.08 Pg C yr^{-1} from the difference of modelled present day and pre-industrial state for the tDOM breakdown scenario $T_{tDOM,photoox}$. This strongly disagrees conclusions with conceptual box model approaches, which suggest a large anthropogenic perturbation of the CO_2 flux of up to 0.5 Pg C yr^{-1} (Mackenzie et al., 2004; Andersson et al., 2005), thus consisting of a large part of the global ocean sink for the present day (around 2.3 Pg C yr^{-1} in Ciais et al. (2013)). On the other hand, it is more consistent with the conclusions from Bourgeois et al. (2016), which suggest an inefficient anthropogenic coastal uptake of 0.12 Pg C yr^{-1}. We suggest three possible mechanisms explaining the inefficient sink of anthropogenic carbon on continental shelves. For one, the volume of the continental shelves is small due to shallow depths by definition (92 m on average), which does not allow for large storage of anthropogenic carbon within the shelves. Secondly, the stratification caused not only by freshwater fluxes, but also stronger warming of coastal surface layers, inhibits the exchange of the surface layers with deeper subsurface layers. The strongest carbon sinks in the open ocean are caused in regions of convergence and formation of the deep water, such as in the North Atlantic (e.g. Gruber et al. (2002)). Such formations of deep water do not take place on continental shelves. Thirdly, the Arctic shelves consist of a contribution of 25 % to the defined total shelf area, part of which are covered in ice for large periods of the year. The ice coverage results in a barrier to the atmospheric anthropogenic carbon uptake in the months of highest solubility (cold winter months).

3.4 Model limitations

Since the biogeochemistry of the ocean is strongly affected by physical transport and mixing, an adequate representation of ocean currents and mixing is necessary in order to adequately represent the biogeochemistry on continental shelves. While the spatial resolution of the model used to perform our simulations is a significant improvement over most similar studies in the past and a much more realistic representation than box models because it enables a representation of the main hydrodynamical features of continental shelves, the model is not capable of reproducing circulation at the mesoscale, such as smaller coastal currents and eddies. For instance, the importance of eddies has been shown in eastern boundary upwelling systems (Gruber et al., 2011; Turi et al., 2016), but their contributions to wider passive shelves remains unclear.

Continental shelves, or the coastal ocean, have been inconsistently defined in published literature Laruelle et al. (2013), which could strongly impact their estimated global contributions to the global NPP and CO_2 flux. For instance, Muller-Karger et al. (2005) use a coastal ocean definition of up to 2000 m to derive a coastal contribution of around 30 % to the global NPP, whereas other less inclusive definitions are far closer to 10 % (for instance Gattuso et al. (1998)). The global shelf defined in our study accounts solely for shallow continental shelves (<250 m). As a consequence of this, the global shelf area is situated at the lower end of area estimates of other studies, and the volume of the shelves is smaller, which might explain some of the inefficiency of the continental shelves to take up anthropogenic CO_2 in the simulations. We however also emphasize that it is on shallow shelves that the efficient pelagic-benthic coupling takes place. At deeper depths, the distance to the euphotic zone, where the primary production takes place, is increased, and the remineralized nutrients need to be mixed further upward in order to enhance the primary production.

Shallow water carbonate production is regarded as an important contributor to the global carbonate production, due to particularly productive species such as corals, molluscs, foraminifera and red algae (Milliman and Droxler, 1996; Woodroffe et al., 2017). The benthic carbonate production is therefore thought to be very efficient despite a lower area coverage than the pelagic production. In this study, we however do not consider benthic carbonate production, and therefore underestimate the continental shelf $CaCO_3$ production in the

model. This is of consequence for the CO_2 flux because the $CaCO_3$ production would cause a source of dissolved CO_2 within the coastal ocean, albeit in subsurface waters. Due to the production taking place in subsurface waters, it is unclear if produced dissolved CO_2 would be exchanged efficiently with the atmosphere. We therefore are unable to assess the quantitative consequences of not considering shallow water benthic production and recommend further research on this topic.

Finally, the global present day CO_2 flux and pCO_2 distribution given in this study, which we use to compare to the estimates of Laruelle et al. (2014) and the data product of Laruelle et al. (2017), could also be affected by the doubling of riverine supplies of bio-available nutrients suggested during the 20^{th} century as a consequence of agricultural fertilizer usage and other anthropogenic perturbations of nutrient cycles (Seitzinger et al., 2010; Beusen et al., 2016). Such enhancement of the coastal biological carbon uptake would likely decrease pCO_2 over many continental shelves. The human-caused increase in riverine nutrients supplies also strongly varies regionally and might help explain the discrepancy between our modelled pCO_2 and that of Laruelle et al. (2018) in near-shore areas of the North Sea, Louisiana Shelf and Southeast Asia (Figure 3.11), where river exports increased substantially since the mid-to-late-1950s (Rabalais et al., 2002; Radach and Pätsch, 2007; Wang et al., 2015; Fennel and Testa, 2019).

3.5 Summary and conclusions

To date, many aspects of the carbon cycle remain poorly understood and quantified on continental shelves. In this study, we present a comprehensive analysis of carbon fluxes on continental shelves with the help of a global 3-dimensional OCGM, which accounts for land-ocean fluxes of inorganic and organic compounds, supplies from atmospheric exchange and open ocean-coastal ocean exchanges. The model was thereby extended in order to better represent the efficient benthic-pelagic coupling on continental shelves and the oceanic fate of tDOM.

The enhanced sediment remineralization rate in sediments of continental shelves enhance the NPP on the shelves, which increases its contribution to the total oceanic NPP. This helps improve the model in the respect that high NPP rates are suggested on continental shelves (Walsh, 1991; Gattuso et al.,

1998; Muller-Karger et al., 2005). Nevertheless, the continental shelves only still contribute to the NPP in the same fraction as their global contribution to the ocean surface area (around 5%), which could be caused by oceanic inflow underestimations in our model setup. Our simulations also reveal that for tDOM, breakdown rates between a labile ($\sim$ 0.3 yr) and semi-labile ($\sim$ 1.5 yr), and our parametrized representation of photooxidation yield realistic tDOM concentrations in the open ocean with respect to observational studies in the Arctic, Pacific and Atlantic (Opsahl and Benner, 1997; Hernes and Benner, 2002; Benner et al., 2005).

Despite the relatively coarse spatial resolution of the model, the global continental shelf represented in this study is comparable to the actual surface area of shallow shelves worldwide (around 21 10^6 km^2 for a depth threshold of around 250 m), and also realistically represents the annual mean physical features of coastal residence times and mixed layer depths with respect to regional studies, despite not considering oceanic mesoscale circulation features. We thereby observe shorter residence times (14-16 months for global shelf waters) than were assumed in conceptual box model studies. The model also suggests a certain degree of stratification on continental shelves, in particular for areas with large freshwater inputs (e.g. the tropical West Atlantic, Louisiana Shelf).

The low residence times, along with the stratification caused by riverine freshwater, are also reflected in the efficient offshore transport of organic matter off the continental shelves, causing a slight pre-industrial and present day autotrophic state (NEP=0.01-0.05 Pg C yr^{-1}) for the global continental shelf. In previous studies, continental shelves were thought to be strongly heterotrophic for the pre-industrial time period (Mackenzie et al., 2004; Andersson et al., 2005). The simulations however also reveal that spatial heterogeneity can be found between different regions globally, and that there is also a vertical gradient in the NEP, with a very positive NEPs being found near surface layers and increasingly negative NEPs with depth.

By performing a transient simulation until present day conditions, we generate a global pCO_2 distribution in strong agreement with a state-of-the-art data-derived climatology (Laruelle et al., 2017) and calculate a net CO_2 uptake of 0.15 Pg C yr^{-1} for continental shelves, which is in line with recent constrained estimates (Wanninkhof et al., 2013; Laruelle et al., 2014; Laruelle et al., 2017). Backtracking the time-line of our simulation to the pre-industrial time-frame reveals that the pre-industrial continental shelves might have also have been

a slight sink of 0.06-0.08 Pg C yr^{-1}, and that regions of strong CO_2 sinks are regions where the carbon cycling is suggested to be controlled by open water inflows in published literature.

The results from our simulations imply that continental shelves were a slight pre-industrial sink, which was driven by the biological carbon uptake and its offshore transport, thus an efficient horizontal biological pump. Meanwhile, in the historical simulation, where the atmospheric CO_2 is increased, but the biological state is unchanged, the continental shelves are an inefficient anthropogenic sink for this time-period, likely since the continental shelf anthropogenic CO_2 uptake is not transfered to deeper subsurface oceanic layers. These results strongly disagree with the assumptions made until now, which suggested that continental shelves were a pre-industrial source of CO_2 but a very efficient sink of anthropogenic sink of CO_2. Thus, we here stress the understanding of the dynamics and the evolution of the 3-dimensional continental shelf biological pump, in order to assess changes in carbon cycling on continental shelves for the past and future.

Chapter 4

The multifaceted 20th century perturbation of the oceanic carbon cycle: Could coastal ocean and river-induced NPP increases trump implications of increased open ocean stratification?

Co-authors: Pierre Regnier, Tatiana Ilyina & Goulven Gildas Laruelle

Summary

The implications of human-caused perturbations on the oceanic biological cycling of carbon, and how these biological changes affect the CO_2 flux, are strongly uncertain. While it has been impossible to definitely determine the sign and magnitude of the change in oceanic net primary production (NPP) on an observational basis, models have shown a stratification-induced decrease of the global NPP over the past 60 years. These models however did not consider nutrient supply increases through increased riverine loads and nitrogen deposition. Furthermore, the coastal ocean in these models was poorly represented in terms of the physical circulation (i.e. due to very coarse model resolutions) and of the biogeochemical processes (e.g. omitting riverine biogeochemical inputs). In this study, we quantify changes in the NPP and in the CO_2 flux induced by increases in the atmospheric CO_2 concentrations, perturbations in the physical climate, as well as increasing riverine and nitrogen

deposition supplies. Our model results suggest that the global oceanic NPP increased (+2.13 Pg C yr^{-1}) when considering increases in riverine supplies are larger than the unsubstantial changes due to changes in the modelled physical state of the ocean (-0.02 Pg C yr^{-1}). The increase is thereby of relative importance for the global ocean (+ 4 %), and in particular for the coastal ocean (+15 %), where most of the enhancement of the NPP takes place. The simulations also show an increase in the NPP of Eastern Boundary Upwelling Systems (EBUS), an effect that has been suggested to be due to the strengthening in the regional upwelling in published literature. We observe an increased P limitation in many coastal regions the model due to increasing N:P ratios of river loads. We also show, in the first global P and N budgets for the coastal ocean based on a spatially explicit model, that the increased nutrient riverine loads are transferred relatively efficiently to the open ocean as organic matter (33 % for P and 73 % for N). In a regional coastal segmentation analysis, we show that mid-to-high latitude shelves are in general a very efficient anthropogenic CO_2 sink, but that this sink might be counterbalanced by tropical and Siberian shelves, which are much less efficient anthropogenic CO_2 sinks than the global oceanic average. Finally, we attempt to identify regions established in literature as hotspots for increased eutrophication and hypoxia by examining the proxy variables NPP, mixed layer depths and minimum oxygen concentrations on a regional basis.

4.1 Introduction

The global biogeochemical cycles of N and P, essential nutrients for terrestrial and aquatic ecosystems (Elser et al., 2007; Fernández-Martínez et al., 2014), have been strongly perturbed by activities to supply an increasing population with food and energy (Stumm, 1973; Galloway, 1995; Gruber and Galloway, 2008), causing an alteration to riverine transports of these elements to the ocean during the 20th century (Beusen et al., 2016). These increased riverine exports have been reported to have caused changes in element ratios, increased eutrophication and ecosystem changes in coastal ocean regions (Ittekkot et al., 2000a; Seitzinger et al., 2005; Diaz and Rosenberg, 2008; Fennel and Testa, 2019). The coastal ocean is thereby thought to be a substantial contributor to the oceanic biological production (Walsh, 1991; Gattuso et al., 1998; Muller-Karger et al., 2005) and an area of the global ocean of high economic and societal importance (Hall, 2001; Bowen and Riley, 2003; Lange and Jiddawi,

2009). At the same time, it has been suggested that large-scale physical and biogeochemical features of the ocean dynamics have also been perturbed by changes in the Earth's climate and atmospheric circulation during the same time period (Behrenfeld et al., 2006; Church et al., 2011; Kuhlbrodt and Gregory, 2012; Laufkötter et al., 2013). The implications of the combined changes in atmospheric state and in nutrient supply to the ocean for the coastal and open ocean biological production as well as for the oceanic anthropogenic carbon sink remain largely uncertain (Henson et al., 2010; Beaulieu et al., 2013; St-Laurent et al., 2017). In this study, we address this gap of knowledge by using a model resolution, which offers a better representation of the physical features of the coastal ocean, and consider temporal changes in riverine nutrient supplies over the 20th century.

The ocean's biological productivity is controlled by light availability and nutrient concentrations, which are in their turn dependent on physical features such as ocean circulation, stratification and temperature (Tyrrell, 1999; Behrenfeld et al., 2006). Increased atmospheric temperatures due to anthropogenic emissions of greenhouse gases have caused widespread regional increases in oceanic surface layer temperatures, thereby leading to a stronger thermal stratification of the ocean and a decrease in mixed layer depths (e.g., Rhein et al. (2013). This increased stratification inhibits the vertical transport of dissolved inorganic nutrients from the deeper subsurface ocean layers to the surface, which in turn likely affects the biological pump by decreasing the net primary production (NPP) and organic matter exports from the euphotic layer (e.g. Behrenfeld et al. (2006)). Observation-based approaches have however shown contradicting results with respect to the sign and magnitude of the global oceanic NPP change over the last decades. For instance, using satellite-derived data Behrenfeld et al. (2006) reported an annual global decrease in the oceanic NPP of 0.57% since 1998. These findings contrast with the results of Saba et al. (2011), which revealed an oceanic NPP increase of 2% per year at two low-latitude open ocean stations monitored during the 1988-2007 period. Model results have shown however that these opposing trends might be explained by the natural decadal variability in the oceanic NPP (Henson et al., 2010; Beaulieu et al., 2013). Furthermore, Laufkötter et al. (2015) suggested that the length of the observational time-series is in any case too short to make definitive conclusions regarding the long-term trend in the oceanic NPP during the 20th century. In a single-model simulation, Laufkötter et al. (2013) reported a decrease in marine production of 6.5% from 1960 until 2006, with the tropical and subtropical open ocean as the dominant contributor to

this negative trend. It should however be noted, that the potential effects of increased land-derived nutrient supply through rivers and atmospheric deposition were not considered in the study.

Furthermore, due to the coarse resolution of the model applied in the Laufkötter et al. (2013) paper, the effects of physical changes in the coastal NPP could not be adequately assessed. Previously published literature has however identified the coastal zone as a particularly sensitive region to changes in the climate state. Regional increases in thermal stratification have been observed in a multitude of coastal regions globally (Fennel and Testa (2019) and citations therein), thereby possibly inhibiting nutrient supply. Regional changes in the coastal ocean circulation induced by changes in atmospheric circulation have also been reported, but the implications of these changes for the global oceanic NPP remain uncertain. For instance, an increase in wind stress parallel to the coast has been suggested to enhance nutrient availability for photosynthesis in upwelling regions such as the Benguela Current System (Bakun, 1990).

The delivery of N and P to the ocean has been shown to have drastically increased over the past century (Seitzinger et al., 2010; Beusen et al., 2016; Yang and Gruber, 2016; St-Laurent et al., 2017). Since the 1960s, the mobilization of nutrients to freshwater systems has been strongly enhanced due to activities such as fertilizer use, human discharge and animal waste (Ricker-Gilbert and Jayne, 2017). In addition, the carbon fluxes from land-to-ocean have also been affected by anthropogenic activities, although the increased C supplies to the ocean are suggested to be less substantial in magnitude than for N and P (Regnier et al., 2013; Maavara et al., 2017). The analysis is complex, since while there is an overall consensus of augmented terrestrial-derived matter fluxes to freshwater systems during the 20th century, global retention of land-derived material has also increased along the land-ocean continuum (Regnier et al., 2013; Beusen et al., 2016). The perturbation of Si riverine exports due to the increase attributed to enhanced weathering (e.g. Goll et al. (2014)) is thought to be globally smaller than the increased retention along the land-ocean-continuum (Ittekkot et al., 2000b; Maavara et al., 2014). In particular, dams built for agricultural or energy production purposes act as efficient filter, retaining and transforming C, N, P and Si within the reservoirs (Ittekkot et al., 2000a; Maavara et al., 2014; Maavara et al., 2017; Maavara et al., 2019). Other significant hydrological impacts are caused by extracting water for irrigation purposes or for the construction of canals (Ferguson and Maxwell, 2011).

Due to increased riverine loads and higher atmospheric N deposition, strong alterations of the NPP have been reported for extensive oceanic regions (Kim et al., 2011; Fennel and Testa, 2019). In addition to the significant magnitude of the perturbations, the N:P ratios of the riverine exports have also changed, with the supply of N having increased faster than P in relative terms (Seitzinger et al., 2010; Beusen et al., 2016). This unequal increase in N and P has also been reported to cause changes in N:P ratios in some coastal regions (Seitzinger et al., 2002). Increased nutrient inputs have been shown to cause mesotrophic to eutrophic conditions in the coastal ocean, thus favouring the development of "dead zones", as already observed in various coastal regions (Diaz and Rosenberg, 2008). The increased availability of nutrients stimulates the production of organic matter in the surface layers of the coastal ocean, which in turn favours the heterotrophic decomposition of the produced organic material in the subsurface layers (Vollenweider et al., 1992), thereby depleting the oxygen levels and forming areas of hypoxia (Breitburg et al., 2018; Fennel and Testa, 2019). Coastal eutrophication has also been demonstrated to favour the growth harmful algae blooms and the onset of fish poisoning (Diaz and Rosenberg, 2008). The stratification of coastal waters is another driving factor of eutrophication and decreasing oxygen concentrations, since it directly impacts the supply of oxygen through vertical mixing and ventilation (Fennel and Testa, 2019). For instance, temperatures in the Baltic Sea and the East China Sea have risen by 2 and 3 degrees, respectively, during the past century. The resulting enhanced stratification, in conjunction with the enhanced riverine nutrient supply, has contributed to increasing coastal eutrophication and hypoxia (Yan et al., 2003; Ludwig et al., 2009; Wang et al., 2015). The formation of such dead zones is therefore a result of high productivity and poor ventilation.

An increase in NPP could also favour an increase in the uptake of atmospheric CO_2 through stimulation of the biological pump (Bristow et al., 2017). The magnitude of the enhanced carbon uptake through the biological production enhancement in relation to changes in the perturbation of atmospheric CO_2 and physical oceanic changes is unexplored. While it is largely acknowledged that the pre-industrial ocean was a source of carbon to the atmosphere (Sarmiento and Sundquist, 1992; Aumont et al., 2001; Jacobson et al., 2007; Gruber et al., 2009; Resplandy et al., 2018) and that the ocean is currently an important sink of anthropogenic CO_2 (Ciais et al., 2013), it is not clear when the switch from a CO_2 source to sink took place. Furthermore, the contribution of the coastal ocean to the global oceanic carbon uptake is uncertain. Using

several million pCO_2 measurements gathered in the SOCATv2 database (Pfeil et al., 2013; Bakker et al., 2016; Laruelle et al., 2014) suggested that the coastal ocean is a present-day sink of CO_2 of 0.14-0.24 Pg C yr^{-1}. The decomposition of this flux into a pre-industrial flux and an anthropogenic perturbation can however not be achieved from observations. In a model simulation, we showed that the coastal ocean might have already been a sink in pre-industrial times (Chapter 3) and that the anthropogenic coastal CO_2 sink might not exceed 0.1 Pg C yr^{-1} for the present day. This result is in close agreement with the only other estimate reported by (Bourgeois et al., 2016) in a spatially explicit global model, which however also excludes riverine flux perturbations and physical changes to the ocean circulation. Therefore, estimates until now suggest that the coastal ocean could contribute less to the anthropogenic sink per area than the open ocean. In an analysis of observational data by Laruelle et al. (2018), a stronger increasing CO_2 sink in the coastal ocean in comparison to the open ocean was reported for several broad coastal regions, although the analysis also revealed a strong heterogeneity in the regional CO_2 flux.

In a conceptual box model, Mackenzie et al. (2004) show a significant perturbation of the NPP in the coastal ocean. The global magnitude of the oceanic NPP enhancement due to increased riverine exports of nutrients has however not been quantified until now in a spatially resolved model (such as OCGM). Therefore, the effects that these increases might have on the global 20th century NPP trend were not considered in model studies such as Laufkötter et al. (2013). Similarly, quantitative estimates of changes in nutrient and carbon fluxes for the coastal ocean and their exports to the open ocean have not been made in a 3-dimensional setup. In a recent paper focusing which parametrizes river plume dynamics, Sharples et al. (2017) nevertheless shows that the offshore export of river-derived N and P is very efficient, implying that changes in the riverine supply of the coastal ocean might extend much further to the open ocean.

The aim of our study is thus to investigate the combined implications of increasing atmospheric CO_2 concentrations, changes in ocean physics and enhanced N-P riverine supplies for the global oceanic cycling of carbon for the first time in an OCGM.

We tackle the 20th century perturbation of the oceanic carbon cycle with the following specific objectives in mind:

- Firstly, changes in NPP are quantified for the global and coastal ocean,

using sequential model simulations to isolate the effects of increasing CO_2 concentrations, altered ocean physics and riverine load perturbations.

- Secondly, we focus on the coastal ocean changes in biogeochemical cycling and establish carbon and nutrient budgets for the start of the century and present-day, thereby assessing the magnitude of their anthropogenic perturbations and underlying drivers.
- Thirdly, by segmenting the coastal ocean into 45 regions globally, we assess spatial changes in the coastal NPP and air-sea CO_2 fluxes at the global scale and assess areas of disproportionate contributions to the global changes in the NPP and in the air-sea CO_2 exchange. The uptake of anthropogenic CO_2 by the coastal ocean is specifically targeted.
- Fourthly, coastal zones showing signs of increased eutrophication for the simulation timeframe are identified at the global scale.

4.2 Methods

In this study, we perform transient simulations to assess the implications of changes in atmospheric $CO_{2,}$ ocean physics and riverine fluxes on oceanic carbon cycles. We thereby use the framework previously described in Chapters 2 and 3 to represent riverine fluxes and the coastal ocean within the biogeochemical model HAMOCC. As a major modification to solely assessing the impacts of changing atmospheric CO_2 concentrations, we here consider the physical perturbation of the ocean through changes in the physical climate state by driving the ocean model forced with a 20^{th} century reanalysis of the atmospheric state. Furthermore, we analyse the induced changes from anthropogenic perturbations of riverine loads of P and N for the 20^{th} century, which were derived from the Global Nutrient Exports from WaterSheds (NEWS2) study (Mayorga et al., 2010; Seitzinger et al., 2010). The model simulations are also performed at a higher spatial resolution of 0.4°, enabling a better representation of the physical features of the coastal ocean than in Chapters 2 and 3.

4.2.1 Overview of the model configuration

The physical and biogeochemical processes in the ocean were simulated by the ocean circulation model Max Planck Institute Ocean Model (MPI-OM) and by the ocean biogeochemical model HAMOCC, respectively. Both models are also more extensively described in Chapters 2 & 3.

The MPI-OM simulates ocean physics and circulation, which dictate the transport of biogeochemical tracers through advection and diffusion. In this study, we used an eddy-permitting horizontal resolution of around 0.4 ° (MPI-OM TP04 configuration), which allows for a better representation of the ocean bathymetry and physics than the GR15 configuration (roughly 1.5 °) used in the previous chapters. In particular, the higher resolution setup is reported to improve the representation of ocean currents in the North Pacific, eastern Tropical Pacific, Indian Ocean and South Atlantic (Jungclaus et al., 2013). Furthermore, the atmospheric state used to force the ocean physics was obtained from the ERA-20C 20th century reanalysis (Poli et al., 2016). In the ERA20C reanalysis, a coupled atmosphere-land surface-ocean waves model was forced with observational data for sea ice cover, surface temperature, solar forcing and atmospheric composition changes to assimilate surface pressure and marine wind observations at a resolution of 125 km. In contrast to the Ocean Model Intercomparison Project (OMIP; Röske (2006)) used in Chapters 2 & 3, the ERA-20C considers changes in the atmospheric state during the 20th century, provides a finer spatial resolution of 125 km horizontal resolution and 91 vertical levels and an improved valuation of observational datasets.

The standard version of HAMOCC represents the major processes that affect the organic and inorganic carbon cycle in the water column and in the sediment, as well as the gas exchange through the air-sea interface (Ilyina et al., 2013). The organic biogeochemistry module is based on a classical NPZD formulation (Nutrients, Phytoplankton, Zooplankton, Detritus) with the addition of dissolved organic matter (DOM) and cyanobacteria pools (Six and Maier-Reimer, 1996; Paulsen et al., 2017). The inorganic pools in HAMOCC include phosphate, nitrate, silicate, iron, inorganic carbon, alkalinity, and oxygen as dissolved variables as well as opal and calcium carbonate as particulate constituents.

In this thesis, HAMOCC was extended to include riverine loads of nutrients, carbon and alkalinity (see previous chapters). In the pre-industrial state, we consider the land-derived fluxes of dissolved inorganic phosphorus (DIP),

dissolved inorganic nitrogen (DIN), dissolved silica (DSi), dissolved iron DFe and iron bound phosphorus (Fe-P), dissolved inorganic carbon (DIC), terrestrial dissolved organic matter (tDOM) and riverine particulate organic matter (POM). All inputs, except for tDOM, were directly added to their corresponding pools at the oceanic geographic location of their river mouths. HAMOCC was extended with an additional pool for tDOM, characterized by differing C:N:P:Fe ratios and differing mineralization rates than those applied to the dissolved oceanic organic matter (see Chapter 2 & Chapter 3). Here, we used a C:N:P:Fe ratio for tDOM of 2584:16:1:3.0 10^{-4} and a mineralization rate of 0.008 d^{-1}, which is in the range of 0.001-0.02 d^{-1} given for the breakdown of tDOM on the Louisiana shelf (Fichot and Benner, 2014). Additional inputs of nitrogen to the ocean originate from atmospheric deposition as given by the flux field of Doney et al. (2007) and the dynamical fixation of N by cyanobacteria of (Paulsen et al., 2017). Iron is also supplied through dust deposition (Mahowald et al., 2006).

In HAMOCC, organic matter is decomposed through aerobic and anaerobic mineralization pathways. Oxygen is consumed at a O_2:P ratio of 172:1 (Takahashi et al., 1985) and 2615:1 (Eq. 3.2 in Chapter 3) during POM and tDOM oxidation, respectively. At low oxygen levels, mineralization of organic matter occurs through denitrification and sulphate reduction, the former pathway leading to a depletion of the DIN pool. Furthermore, sedimentary POM mineralization originating from land inputs and export production was increased in coastal sediments (depth <250 m) to 0.0026 d^{-1} as in Chapter 3, in order to capture the generally higher rates of organic matter remineralization reported for shallow marine environments (e.g. Thullner et al. (2009), Arndt et al. (2013) and Krumins et al. (2013). The value of the rate constant was chosen in order to achieve a plausible POM deposition to burial ratio of 15 % for the global coastal ocean, which falls within the range of 8-23 % reported by Krumins et al. (2013) in a review of previously published literature.

4.2.2 Pre-industrial and anthropogenic perturbation of the land-sea fluxes

Pre-industrial riverine loads from weathering and non-weathering sources were derived at catchment scales for P, N, C, Fe, Si and Alk as reported in Chapter 2. We accounted for their speciation into their dissolved inorganic species DIP, DIN, DSi, DFe, DIC, tDOM, POM and Fe-P. The new tDOM pool

follows the C:N:P ratio 2584:16:1 reported in Chapters 2 & 3 , which leads to simulated tDOM ocean basin concentrations in line with observational studies by Benner et al. (2005), Opsahl and Benner (1997) and Hernes and Benner (2002) and regional mineralization rates of the same magnitude as those reported by Fichot and Benner (2014) and Kaiser et al. (2017).

The 20th century changes in nutrient (N and P) fluxes to the ocean were derived from the Global-NEWS2 study (Mayorga et al., 2010; Seitzinger et al., 2010), which is a global spatially explicit, multi-element, multi-form model that was developed to produce hindcast (1970), present-day (2000) and future (2030 and 2050) scenarios of global riverine nutrient exports to the ocean. The model consists of multiple independent sub-models for element forms, which were designed to have the consistent global model inputs of catchment loads, hydrological characteristics and basin definition. The model thereby considers both anthropogenic as well as natural diffuse and point sources inputs of P and N to the global river network. The anthropogenic sources of P and N were derived from diffusive sources of fertilizer use and animal manure, as well as point sources of human excreta and detergents, which were all were quantified explicitly based on Bouwman et al. (2009). We extracted these anthropogenic fractions of the NEWS2 N and P river fluxes to derive their anthropogenic perturbations.

The evolution of riverine loads to the ocean, including the spatial distribution of these changes, were based on the global distribution of the exports at two points in time: a "pre-industrial" time slice (year 1900) and the contemporary period (year 2000). For the pre-industrial state, riverine loads and their distributions were constrained as presented in Chapter 2. The increase in P and N between the two time points were derived from the present-day anthropogenic riverine loads of DIP, DOP, DIN and DON from the run5_c00 NEWS2 model output for the reference year 2000 (Mayorga et al., 2010; Seitzinger et al., 2010). To estimate the temporal evolution of the P and N increase, we approximated the global temporal evolution of the P and N according to simulations of (Beusen et al., 2016). In the study, the global riverine P trend is shown to be weak and nearly linear for 1900-1930, followed by a much steeper (about four-fold faster) nearly linear increase for 1930-2000 (Figure 4.1). For N, the global increase patterns are similar, although the increase is shown to become even steeper from 1975 onwards (Beusen et al., 2016), a non-linear increase which we do not consider here. These time-varying anthropogenic inputs were then added to the background pre-industrial catchment inputs

calculated following the methodology of Chapter 2.

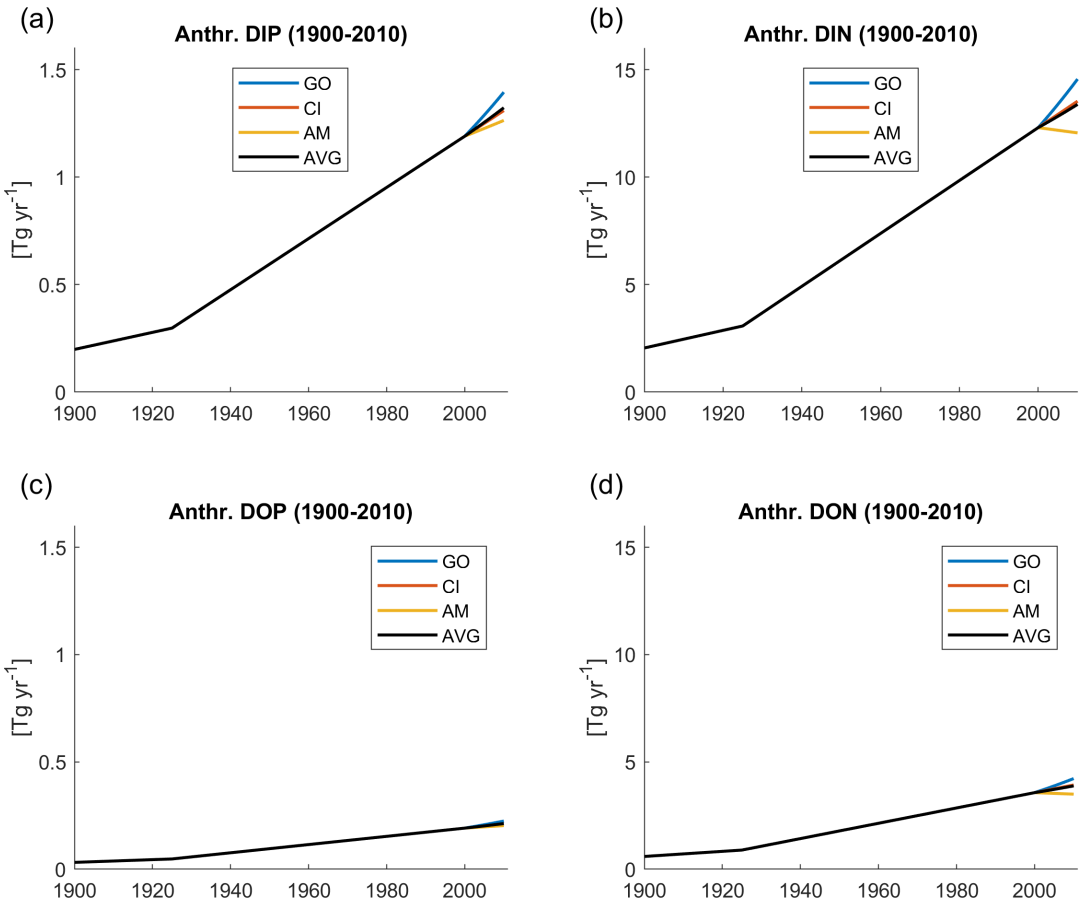

FIGURE 4.1: Trajectories of global anthropogenic riverine (a) DIP, (b) DIN, (c) DOP and (d) DON loads [Tg yr^{-1}] as derived from NEWS2 (Seitzinger et al., 2010). The 1900-1930 increases are 4.0, 41, 0.6 and 12 103 Mg yr^{-1} and the 1930-2000 increases are 15.9, 164, 2.6 and 48 Mg yr^{-1} for DIP, DIN, DOP and DON respectively.

For the changes in riverine loads from 2000 to 2010, we averaged over two different scenarios from the Global-NEWS2 study that consider distinct agricultural policy and water management strategies, and a "business-as-usual" scenario. We thereby averaged two extreme NEWS2 scenarios (the Global Orchestration (GO) and Adapting Mosaic (AM) trajectories) and our "business-as-usual" scenario, which follows the same rate of increase as the one applied for the 1930-2000 increase (CI) (Figure 4.1). While the GO scenario, which is based on the assumption of a more globalized future world, shows a strong increase in DIP, DOP, DIN and DON river loads due to a high global agricultural productivity combined with low fertilizer efficiency, the AM scenario shows a decrease in global DIN loads for 2000-2010 due to the high fertilizer efficiency and removal of DIN and DIP in wastewater (Table 4.1).

The anthropogenic fluxes of DIP and DIN were added to the corresponding DIP and DIN pools in HAMOCC at the corresponding location of the river mouths. It was assumed that these inputs are homogeneously distributed during the course of a given year. We furthermore assumed that anthropogenic DOP and DON within organic matter is highly reactive in the coastal ocean, and therefore, the riverine exports of these species were also added to the DIP and DIN pools in HAMOCC instead of adding them to the tDOM pool. In this study, we focus on the land-ocean P and N exports, which have undergone the strongest changes over the 20th century (Seitzinger et al., 2010). The other species are kept constant, although perturbations of carbon and silica exports have also been reported at the global and regional scale (Ittekkot et al., 2000a; Regnier et al., 2013; Maavara et al., 2014; Maavara et al., 2017). For one, organic carbon inputs to catchments are reported to be increased due to land-use changes, which in turn caused increased mobilization. On the other hand, retention may substantially retain carbon and silica along the land-ocean-continuum.

4.2.3 Model initialization and transient simulations

To speed up the initialization of the ocean biogeochemical state, the model was firstly spun up for 1000 years in its full configuration (Figure 4.2-a). Then, an average of the particulate fluxes from the last 10 years of this simulation was extracted to force the sediment module in an isolated mode for 10'000 years (Figure 4.2-b). The sediment was then coupled back to the water-column and the full configuration was run again for another 1000 years (Figure 4.2-c). The atmospheric CO_2 was set to 1800 levels of around 278 ppm. The ocean physics were forced by the ERA20C dataset repeatedly over the timeframe 1905-1930, since this is the furthest back in time that this dataset is complete.

Once the initialization was completed, we performed the transient simulations for the timeframe 1800-2010 (Figure 4.2-d), in order to also include the "smooth" changes in atmospheric CO_2 concentrations during the 19th century. The physical atmospheric state, which drives the ocean model's physics, and riverine loads were only altered from 1905 and 2000, respectively. We thus focus on the 1900-2010 timeframe in the analysis, as we are unaware of historical reconstructions consistent with the ERA-20C reanalysis previously to 1900. We performed four sequential simulations to isolate effects of changing atmospheric CO_2, changes in the physical climate state and the

perturbation of riverine fluxes (Table 4.1). The pi-control simulation, where none of the riverine loads, atmospheric CO_2, or atmospheric state are altered, was performed to check for substantial model drifts over the historical time period. In the CO_2-only simulation, only the atmospheric CO_2 concentration was altered from 278 to 389 ppm as given by Etheridge et al. (1996), whereas for the climate-only simulation, the atmospheric CO_2 Etheridge et al. (1996) and physical climate state (ERA-20C datasets) were perturbed. In the ant-riv simulation, we considered changes in atmospheric CO_2 and physical drivers as in climate-only, while also adding changes in anthropogenic riverine loads for 1900-2010, which were calculated as an average of the 3 scenarios GO, CI and AM. To assess the differences between the start of the 20^{th} century and the contemporary time period, we averaged ocean biogeochemistry model output over 1900-1910 and 2000-2010, respectively.

The isolated effects due to increasing atmospheric CO_2, to changes in the physical ocean drivers and to river perturbations were calculated from the differences between the 4 sequential simulations. The riverine-induced changes are obtained from subtracting clim-only from riv-ant results, while changes in the physical state of the ocean can be assessed by subtracting co2-only from the clim-only output. The effects of rising atmospheric CO_2 are extracted from the difference between co2-only from pi-control simulations.

TABLE 4.1: Simulation scenarios

Simulation scenario		**Description**	**DIP 2000-2010 increase [% yr^{-1}]**	**DIN 2000-2010 increase [% yr^{-1}]**
pi_control		No river load increase	-	-
CO_2_only		CO_2 alterations from 1800-2010	-	-
climate_only		CO_2 alterations and atmospheric alteration as prescribed by ERA20C forcing.	-	-
ant_riv		CO_2 alterations, atmospheric alteration as prescribed by ERA20C forcing and riverine perturbations from an average of 3 scenarios.		
	GO	High agricultural productivity with low increase in fertilizer efficiency. Increase in P and N removal in wastewater.	1.6	0.58
	CI	Continuation of 2000 status quo, with the same relative increase from 1970-2000 assumed for 2000-2011.	0.98	1.17
	AM	Medium agricultural productivity with high increase in fertilizer efficiency. Increase in P and N removal in wastewater.	-0.21	0.64

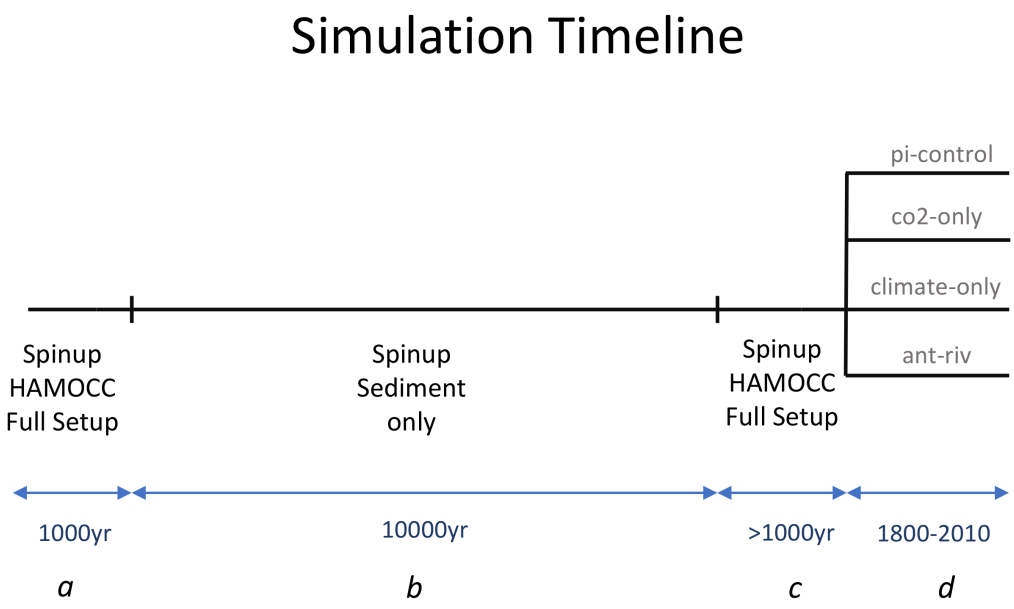

FIGURE 4.2: Simulation timeline.

4.2.4 Definition of the coastal ocean in the TP04 configuration

The definitions of the global coastal ocean vary strongly in literature, from considering only the shallow shelf (Chen and Borges, 2009; Laruelle et al., 2018), to limiting the shelves as a function of the slope of the bathymetry (Laruelle et al., 2013; Laruelle et al., 2014; Bourgeois et al., 2016), to also including anarea with a minimum distance from the coast (Laruelle et al., 2017). These different delineations of the coastal ocean impact the results of individual studies, especially regarding the contribution of the coastal ocean to the global carbon cycle and air-sea CO_2 fluxes. In our analysis, we considered two coastal ocean definitions. The first follows the more classic definition, considering global shallow water shelfs with an outer limit corresponding to a water depth of less than 250 m in the model. This definition was used for most of our analysis. It is slightly more inclusive than the 200 m outer limit of Chen and Borges (2009), allowing to include numerous shelves that extend significantly further than 200 m (Laruelle et al., 2013). The model bathymetry, and therefore the ocean depths, originates from an interpolation of the ETOPO 2 bathymetry and modification (Commerce and Atmospheric Administration, 2006) to the TP04 model grid (see for instance Jungclaus et al. (2013)).

The second definition was used primarily for the regional analysis performed in this study. Since it relies on the MARgins and CATchments Segmentation (MARCATS) proposed by Laruelle et al. (2013), we follow their delineations, which were determined from abrupt increases in the shelf slope. For each MARCATS section, we identified which depth level (20 m, 50 m, 80 m, 120m, 180 m, 200 m, 250 m, 350 m, 500 m or 1000 m) was closest to the average outer limit computed by the Laruelle et al. (2013) methodology. The delineation parallel to the coast was then done manually to approximate their MARCATS limits.

4.3 Results and discussion

4.3.1 Perturbations of riverine loads and of the physical ocean

During the 20th century, riverine DIP exports to the ocean increased due to detergent, fertilizer, manure and sewage inputs (Seitzinger et al., 2010; Beusen et al., 2016). In our framework, the global DIP load increases from 0.5 to 1.6 Tg P yr^{-1} from 1900 to 2010 period, with the 1900 load already including an anthropogenic perturbation of circa 0.2 Tg P yr^{-1}. The global DIN load increases from 3.6 Tg N yr^{-1} to 17.1 Tg N yr^{-1} over the same period as a result of sewage, manure and fertilizer inputs to freshwaters (Seitzinger et al., 2010), with the anthropogenic fraction of the 1900 DIN load already contributing a load of 2.1 Tg N yr^{-1}. Changes in organic nutrients loads are however less pronounced. We estimate increases in global DOP and DON loads from 0.1 to 0.4 Tg P yr^{-1} and from 1.5 to 5.4 N yr^{-1}, respectively.

The POP, Fe-P and PON loads remain the same as was derived for pre-industrial fluxes (Chapter 2). Accounting for the total loads when considering both natural and anthropogenic loads of all species of P and of N amounts to total global loads of 5.3 Tg P yr^{-1} and 46 Tg N yr^{-1} for the year 2010, with an anthropogenic contribution of 1.4 Tg P yr^{-1} and 17 Tg N yr^{-1}. Thus, the total P and N loads increase from 3.7 to 5.3 Tg P yr^{-1} (41 % increase) and 27 to 46 Tg N yr^{-1} (70 % increase) during this period. The P and N loads, which are however readily available for primary production in our framework (DIP, DOP, DIN and DON) show a much stronger increase of +133 % and +241 % . The N:P ratio of the anthropogenic increase is 19:1, which is therefore higher than the Redfield ratio of organic matter formation in the ocean (16:1). The

global N load is thereby higher by 7 Tg yr^{-1} N than would be expected using a global 16:1 N:P ratio with respect to P.

A review of estimates of global P and N loads reveals that large uncertainties still exist for the present-day land-ocean exports. Existing estimates lead to ranges comprised between 4-21 Tg yr^{-1} for P and 36.5-60 Tg yr^{-1} for N (Meybeck, 1982; Green et al., 2004; Bouwman et al., 2005; Van Drecht et al., 2005; Seitzinger et al., 2010; Beusen et al., 2016). Our value falls within this range, although it is also not completely independent of the Seitzinger et al. (2010) estimate due to our use to the anthropogenic load components of that study. Regarding the loads for 1900, our estimates of 3.7 Tg P yr^{-1} and 27 Tg N yr^{-1} also are comparable with previous assesments of 2 – 4.5 Tg P yr^{-1} (Compton et al., 2000; Beusen et al., 2016) and 14-21 Tg N yr^{-1} (Green et al., 2004; Beusen et al., 2016).

The distribution of the anthropogenic P and N riverine load perturbation differs to a degree from the pre-industrial distribution, although the larger rivers also tend to undergo the largest magnitudes of perturbations (e.g. the Amazon, Ganges and the Yangtze, Figure 4.3). The oceanic basins with the largest global P and N relative increase are the Pacific (+39 % P and +44 % N) and the Atlantic (+28 % P and +29 % N). The loads from Arctic rivers only change marginally, with the large basins such as the Lena or the Mackenzie being suggested to be nearly pristine for present-day in the NEWS2 study (Seitzinger et al., 2010). The Pacific Ocean experiences a very steep increase in nutrient loads from the middle of the 20^{th} Century, which is mainly attributed to fast population growth of many Southeast Asian countries (Beusen et al., 2016). As a result, Southeast Asian catchments are more strongly affected by anthropogenic perturbations than the global average, although the tropical Atlantic and European rivers are also strongly affected by changing loads. While the Amazon river remains the largest supplier of DIP and DIN to the ocean due to large natural fluxes (see Chapter 2), the anthropogenic increases are moderate (0.03 Tg P yr^{-1} and 0.36 Tg N yr^{-1}) and larger or similar human-induced perturbations of P and N take place for the Ganges (0.11 Tg P yr^{-1}, 1.46 Tg N yr^{-1}), the Yangtze (0.049 Tg P yr^{-1} and 0.86 Tg N yr^{-1}) and the Mississippi (0.024 Tg P yr^{-1} and 0.53 Tg N yr^{-1}) rivers.

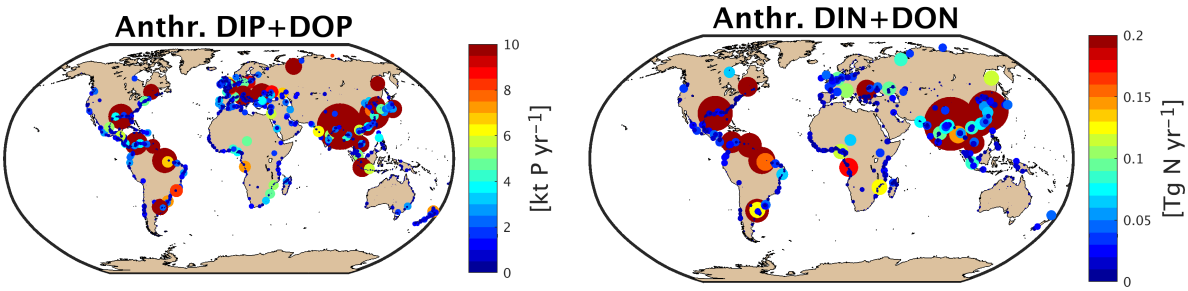

FIGURE 4.3: Increase in (a) P (DIP+DOP) and (b) N (DIN+DON) loads to the ocean, estimated from the difference between the mean of 1900-1910 and the mean of 2000-2010 periods.

The ERA-20C reanalysis, which is used as the atmospheric forcing to drive the oceanic physical circulation of the MPI-OM model, shows an average increase in global atmospheric surface temperature of around 1 K between 1900-1910 and 2000-2010. This increase leads to a widespread increase of surface layer (<50 m) temperatures in the ocean of circa 0.5 K globally, although regionally it can even exceed 1 K (Figure 4.4-a). This warming of the surface ocean is in line with that previously reported in previous literature (e.g. 0.2-0.5 K for the upper 100 m in Levitus et al. (2005). The warming of the ocean's surface layers leads to increased stratification. As a result, the mixed layer depth tends to decrease in the open ocean (Figure 4.4-b), which can be seen in the model by the mean global mixed layer depth decreasing from 111 m for 1900-1910 to 94 m for 2000-2010 on average. Despite this global decline in the mean mixed layer depth, increases can however be observed in the southern North Atlantic, the Southern Ocean and the Arctic. For the latter, our results are in line with those reported by Lind et al. (2018). In the coastal ocean, we also observe a strong increase in surface layer temperatures of 0.5 K on average, which is similar to the global ocean average temperature increase. The change in the mixed layer depths is however strongly variable, and the global mean remains almost constant at 36 m on average over the global coastal oceandespite the strong increase in temperatures. This result could be explained by changes in the atmospheric circulation patterns, although these are strongly spatially heterogenous (e.g. Turney et al. (2017)) and, while taking account the very differing spatial features of the coastal ocean, their impacts are difficult to assess at the global scale.

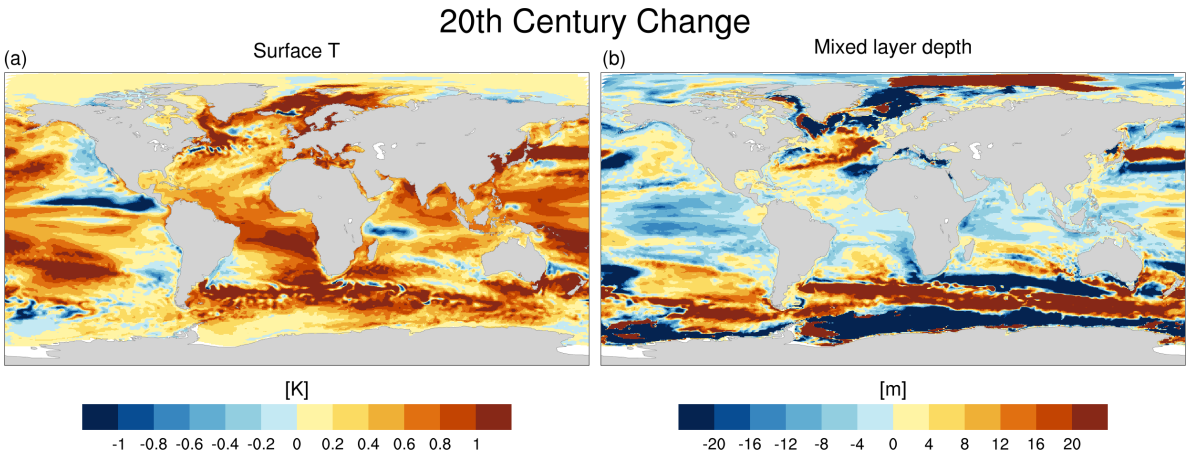

FIGURE 4.4: Changes in (a) surface layer oceanic temperatures (<50 m) and (b) mixed layer depths during the 20th century.

4.3.2 20th century changes in coastal and open ocean nutrient limitation, NPP and CO_2 fluxes

When considering all perturbations (both physical ocean and riverine perturbations), the global average DIN and DIP concentrations in the surface layers of the ocean increase from 3.1 to 3.4 μ M N^{-1} and from 0.28 to 0.29 μM P over the 20th century. The relative increase in DIN concentration is thereby larger than for DIP, which reflects the changes in land-derived supplies of both elements. In turn, the global NPP rises from 54.4 to 56.5 Pg C yr^{-1}. The relatively similar increase in the global NPP (4 %) in comparison to the DIN (9 %) and DIP (3 %) concentration increase suggests an efficient enhancement of the NPP by the additional river-borne nutrients, but that an equal part of increased riverine supply is also stored in the ocean. For DIN, the increased storage is stronger than for DIP due to the higher than Redfield N:P ratio of the riverine supplies. Figure 4.5 shows that the spatial patterns of nutrient stock changes are complex, with both regions of increased and decreased concentrations of DIN and DIP. We also observe a strong increase in DIN and DIP concentrations over most of the Southern Ocean. Here, the present-day mixed layer is deeper in the areas of higher DIP and DIN concentrations than for 1900-1910 (Figure 4.4-a), which results in the entrainment of nutrient-rich water masses from deeper oceanic layers. The North Pacific is also a region where a substantial increase of DIN and DIP can be observed. Concentrations of DIN particularly increase in eastern Asian seas and in the Bay of Bengal, which are regions with strong enhancement of nutrients delivery to the ocean,

especially for DIN. Arctic coastal regions show an increase in DIP and DIN, which is likely not river-induced.

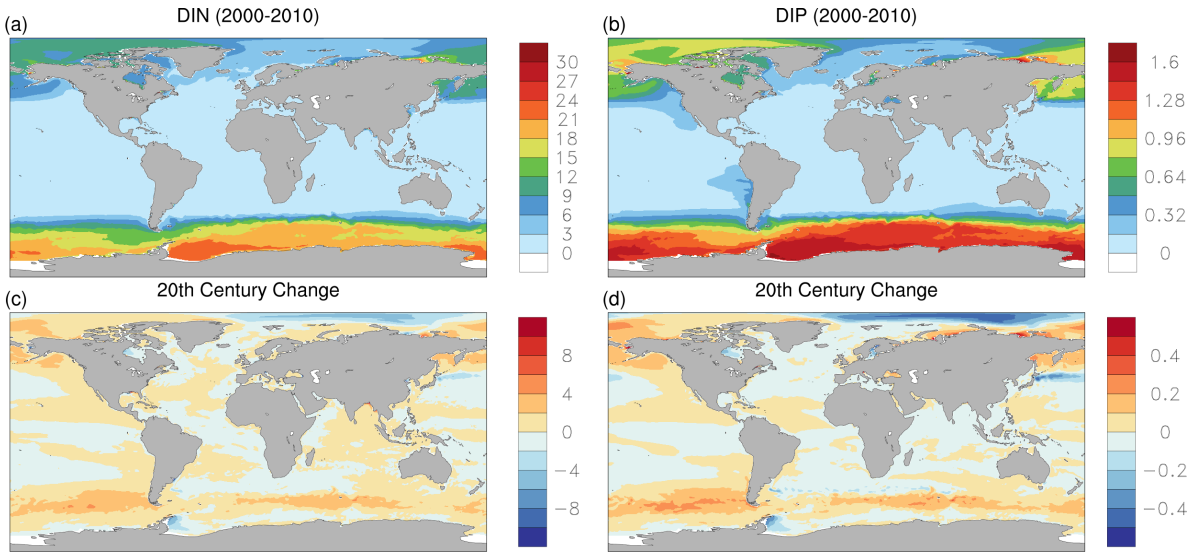

FIGURE 4.5: 2000-2010 average concentrations of (a) DIP and (b) DIN, and changes over the 20th century considering all perturbations. The changes are calculated as the difference between the mean 2000-2010 and the 1900-1910 for (c) DIN and (d) DIP respectively.

Due to the increase in the riverine N:P ratio (19:1) which exceeds that of Redfield, we simulate a substantial global increase in P limitation in coastal regions of the eastern North America into the open Atlantic, Sea of Japan and the Bay of Bengal for the 20th century (Figure 4.6). The Amazon outer plume however, which was previously P limited, switches to being N limited. The Red Sea also shows a decrease in P limitation. The decrease in P limitation could be due to lower N:P river load ratios for these regions. The increase in the riverine N:P ratio could however be compensated by enhanced coastal denitrification induced by the increased production of organic matter or by a decrease in N fixation. These effects could be significant in the Amazon plume, as the present-day nearshore biological production is limited by P in the model, whereas in the outer plume the limitation switches to an N-limited ecosystem.

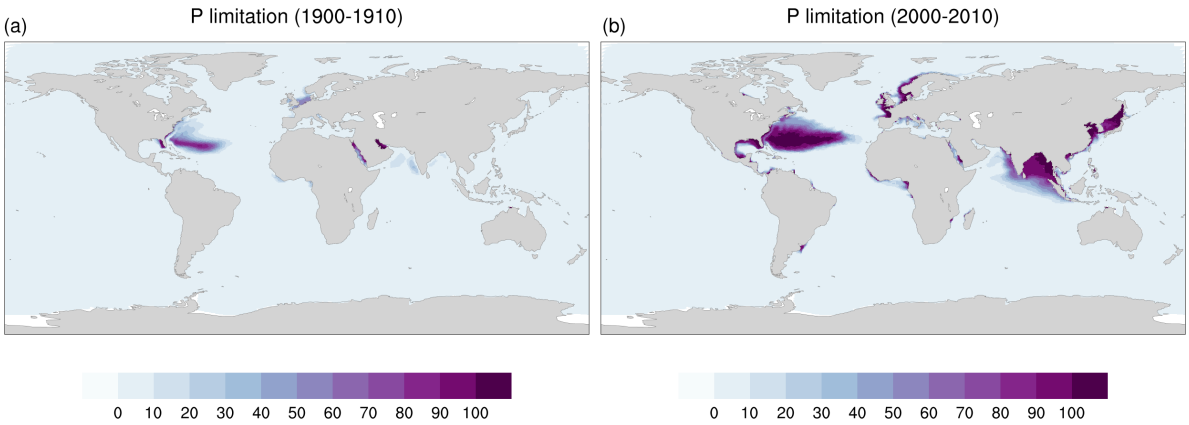

FIGURE 4.6: Annual mean of P limitation for 1900-1910 and 2000-2010 [%] considering all perturbations.

Considering all perturbations leads to a substantial present-day oceanic sink of CO_2 (1.71 Pg C yr^{-1}), which nearly directly follows the perturbation of atmospheric CO_2 concentration (Figure 4.7-a,-b). In the model spin-up, which was done at an assumed 1800 atmospheric CO_2 concentration levels of 278 ppm, we observe an average oceanic source of 0.33 Pg C yr^{-1} to the atmosphere in the model spin-up, which is caused by riverine loadings of carbon (Sarmiento and Sundquist, 1992; Jacobson et al., 2007; Resplandy et al., 2018; Lacroix et al., 2019). For 2000 to 2010, the oceanic uptake of anthropogenic carbon is therefore 2.06 Pg C yr^{-1}, which is in the lower range of the anthropogenic sink that the Intergovernmental Panel on Climate Change 2013 (IPCC, 2013) and Le Quéré et al. (2018) report for the present-day (2.3 $\pm$ 4 Pg C yr^{-1}). During the 20^{th} century, the global CO_2 flux evolves from a very slight 1900-1910 averaged source of 0.01 Pg C yr^{-1} to the present-day value, implying a 20^{th} century increase in the anthropogenic carbon sink of 1.72 Pg C yr^{-1}. Although the ocean switches from a carbon source to a sink previously to 1900 for given years, the exact time of the switch is difficult to determine through one simulation, since decadal variability is an important driver of the short-term signal of the global CO_2 flux (Li and Ilyina, 2018).

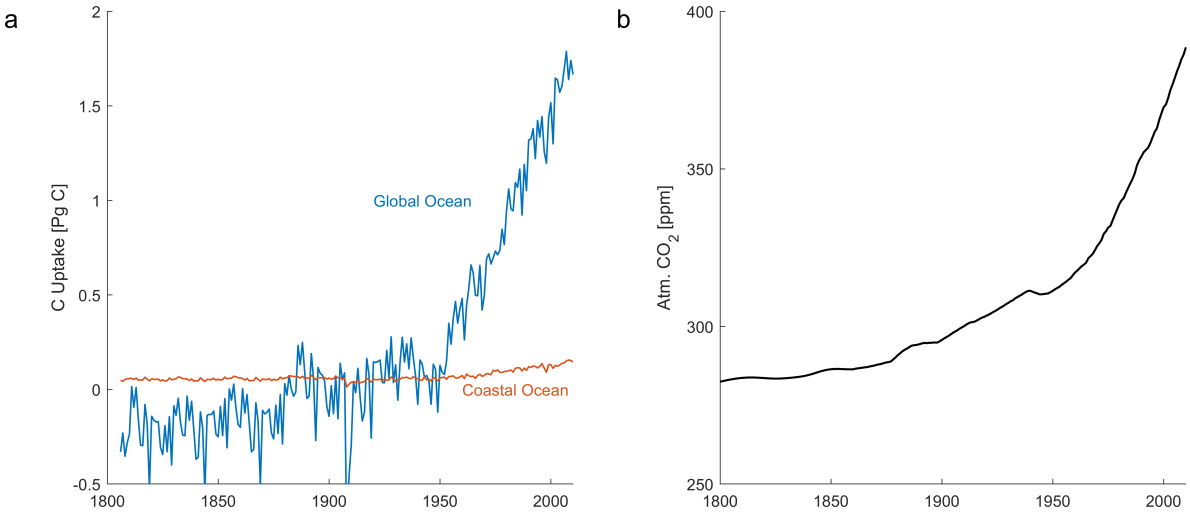

FIGURE 4.7: (a) Oceanic carbon uptake considering all perturbations in comparison to (b) the atmospheric CO_2 concentrations.

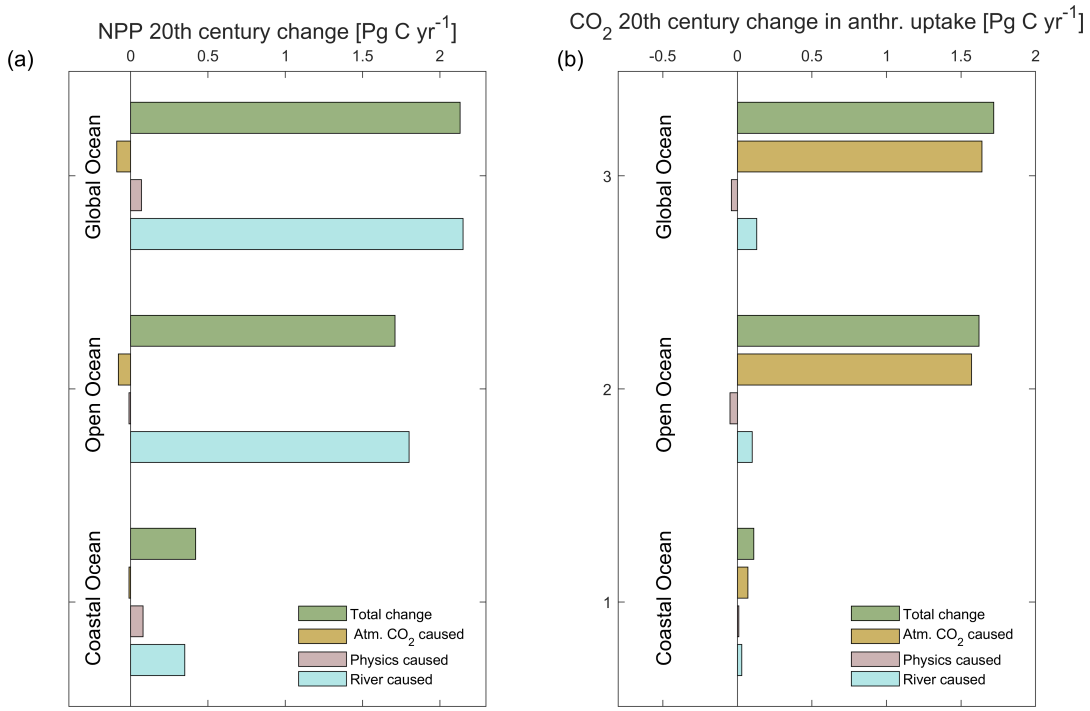

FIGURE 4.8: Total differences between the (a) NPP and (b) CO_2 means of 1900-1910 and 2000-2010 (Total change), as well as differences induced by only changing atmospheric CO_2 (Atm. CO_2 caused), only atmospheric changes (Physics caused) and riverine changes (River caused).

Through our successive simulations we can attribute the total 20th century change in ocean NPP and air-sea CO_2 flux and the spatial patterns of the changes to perturbations of rising atmospheric CO_2, in the ocean physics and in riverine supplies (Figure 4.8 and Figure 4.9). Unsurprisingly, the increase in atmospheric CO_2 has virtually no effect on the oceanic NPP (-0.03 Pg C yr^{-1}),

the change being either caused by a slight model drift or decadal variability. The physical perturbation of the ocean on the other hand unexpectedly has only a very minor effect on the global NPP (+0.01 Pg C yr^{-1}), whereas the enhanced riverine fluxes cause a substantial global NPP increase of 2.15 Pg C yr^{-1}. Spatially, the NPP is increased in the coastal ocean in the model (+0.42 Pg C yr^{-1}, considering all perturbations), as well as in the open ocean (1.71 Pg C yr^{-1}). The sign and magnitude of the NPP change is however strongly variable in the global ocean (Figure 4.9-a)). While we observe a decrease in the eastern Equatorial Pacific and Pacific subtropical gyres, coastal upwelling regions (e.g. the Benguela Current System), the Southern Ocean, the western Equatorial Pacific and the North Pacific show increases in NPP. The coastal ocean shows strong increases of over 10 g C m^{-2} yr^{-1} taking place in many regions globally.

The mixed layer depth decreases globally due to the 20^{th} century heating of the oceanic surface layers, which inhibits the entrainment of nutrients from deeper oceanic layers and thus decreases the NPP in the open ocean (-0.07 Pg C yr^{-1} caused by physical changes only). This is especially the case for the tropical and subtropical open oceans, where there are significant decreases in NPP (circa -0.2 Pg C yr^{-1} and -0.1 Pg C yr^{-1} for the tropical and subtropical oceans, respectively), which agrees with conclusions from Laufkötter et al. (2013) in their model study. The change in the mixed layer depth is however spatially very heterogenous, with some regions even showing an increase in the mixed layer depth. For instance, an increase in the mixed layer depth takes place in parts of the Southern Ocean and which enhances the primary production in total for the region (+0.3 Pg C yr^{-1}). The increase of the Southern Ocean NPP over the 20^{th} century also agrees with what is reported by Laufkötter et al. (2013). The physical perturbation of the ocean however does not significantly decrease the global coastal ocean mixed layer depth and the coastal NPP even slightly increases as a result of 20^{th} century changes in ocean physics (0.08 Pg C yr^{-1}), which could be mostly strongly driven by the increases in the Eastern Boundary Upwelling Systems (EBUS). Regional changes in coastal ocean circulation due to changes in the wind stress could explain this NPP enhancement. For instance, more favourable coastal upwelling conditions induced by larger wind-stress in some regions could exceed the increased stratification effects in other regions (Bakun, 1990). Furthermore, the heating of the coastal ocean could also cause more favourable conditions for primary production by phytoplankton, since the photosynthesis in the model is also temperature dependent.

The coastal NPP enhancement observed in Figure 4.9-a can be largely attributed to the increased riverine loads (Figure 4.9-c), which causes an increase in the coastal NPP of 0.35 Pg C yr^{-1}, but the imprint of land-derived nutrient inputs is also recorded in the open ocean, with a riverine-induced increase of 1.8 Pg C yr^{-1} of the open ocean NPP. These increases are widespread over the Atlantic, Pacific and Indian Oceans, albeit they are mostly significant in the Indian and Atlantic Oceans. While the Equatorial Pacific shows a strong signal of higher NPP, which could possibly be explained by the enhanced nutrient supplies from the East Asian and Southeast Asian regions observed in Figure 4.3. This increase in the Equatorial Pacific is largely not significant, likely due to the large natural variability in the NPP in this region, for which trends in the NPP have been strongly debated in literature.

Up to this day, there exists strong disagreement regarding the magnitude and sign of the NPP trend over the 20th century. For one, the lack of sufficiently long data series makes an observational constraint very difficult (Henson et al., 2010; Laufkötter et al., 2013; Laufkötter et al., 2015). It is thus not surprising that observation-based approaches to constrain NPP trends have resulted in contradicting conclusions (Behrenfeld et al., 2006; Chavez et al., 2010; Saba et al., 2011). While Laufkötter et al. (2013) suggest an average decrease of 6% for the past 50 years, the differing results to ours could be explained by two main reasons, which were omitted or not adequately represented in the model simulations used in the Laufkötter et al. (2013) study: physical changes in the coastal ocean and the increase in riverine supplies. Firstly, we observe an slight increase in the coastal ocean NPP due to physical changes, which is largely due to increases in upwelling regions. These regions of fine-scale physical processes, where water from deeper layers are entrained to the surface, are poorly represented in models of coarse resolution and have been shown to be improved by increasing the ocean model resolution (Milinski et al., 2016). Our model results here could confirm the conclusions by (Bakun, 1990), that an strengthening of coastal parallel winds could have increased the NPP in EBUS regions in the past century. Secondly, models of the generation of the Laufkötter et al. (2013) study often did not consider riverine supplies to the ocean, and none of them considered the temporal increase of these supplies for the 20th century. Furthermore, the effect of increased anthropogenic nutrient supplies leads to enhanced global oceanic NPP of (4 %), which is larger than the physically-induced open ocean decrease in our model, which is notably relevant for the coastal ocean (+14 %). A further thought on the matter is the decrease in non-upwelling open ocean regions, whereas an increase in most

regions where substantial upwelling takes place, for both the open ocean (e.g. North Pacific) and in the coastal ocean (e.g. Benguela Current System). We therefore suggest that the increased stratification in the open ocean, where upweeling does not take place, causes less transports of nutrients from deeper layers to the surface ocean layers, and that the nutrients accumulate here until they are brought back to the surface in upwelling regions, which undergo substantial increases in NPP.

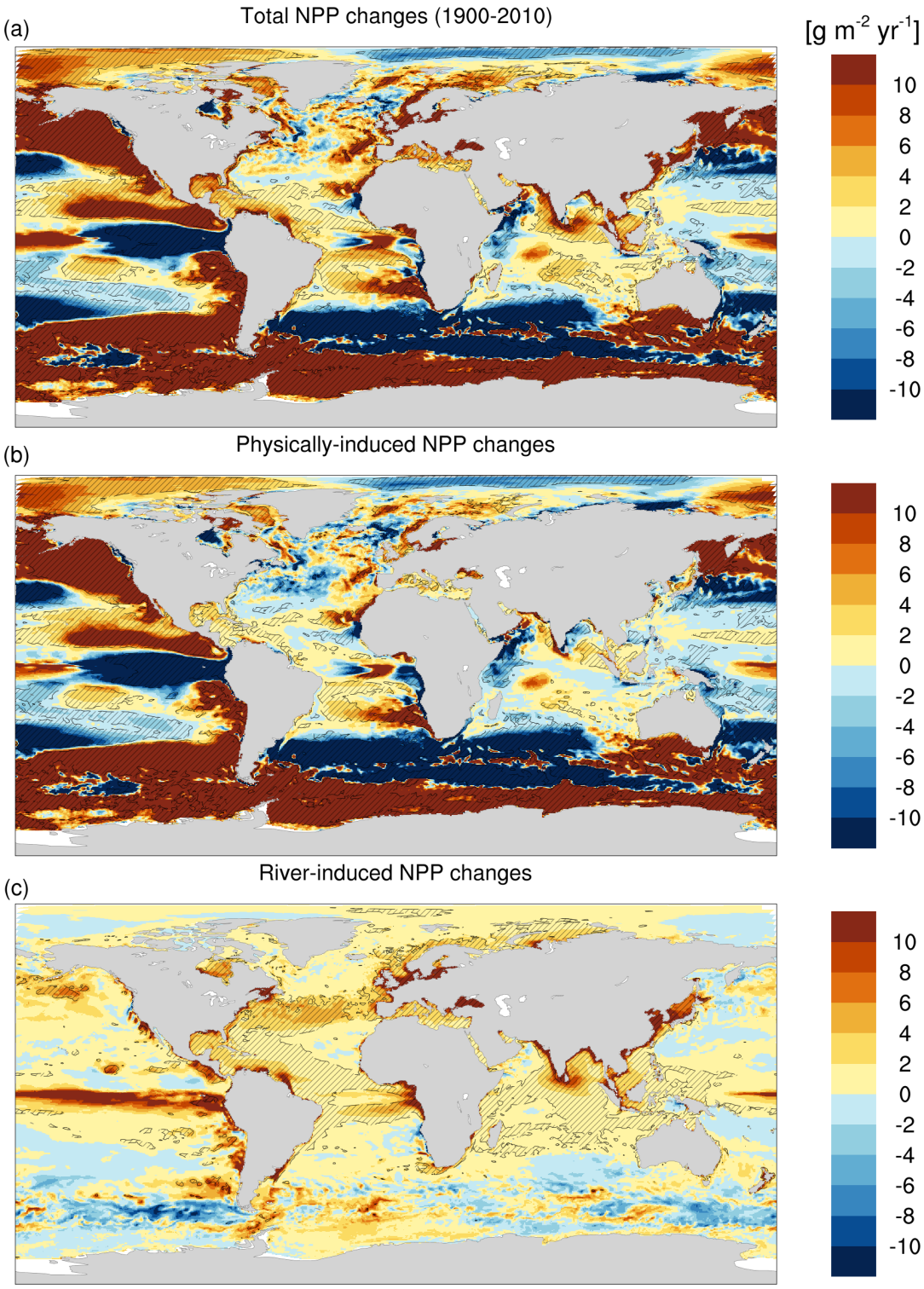

FIGURE 4.9: Changes in NPP for the 20th century for (a) all perturbations, (b) physical induced changes and (c) increases in riverine supplies. The significance (dashed areas meaning a significance of $p < 0.05$) was tested through an Independent Samples t-test.

The net oceanic uptake of CO_2 is on average 1.72 Pg C yr^{-1} higher for the present-day (2000-2010 average) compared to the 1900-1910 period (Figure 4.8-b). Taken that the pre-industrial outgassing flux calculated in the model

spin-up (with year 1800 atmospheric CO_2 concentrations) is equal to 0.33 Pg C yr^{-1}, the present-day global ocean anthropogenic CO_2 uptake is on average 2.12 Pg C yr^{-1}, which is in line with the estimate reported by the IPCC of around 2.3 Pg C yr^{-1} (Ciais et al., 2013) and 1.9-2.4 by the Global Carbon Budget 2018 (Le Quéré et al., 2018).

The effect of increasing atmospheric CO_2 is expectedly the dominant driver of the oceanic uptake, thereby causing an uptake of 1.64 Pg C yr^{-1} (4.8-b). Part of the uptake is alleviated by the 20th century changes in ocean physics (decreased uptake of 0.04 Pg C yr^{-1}). In contrast, riverine perturbations stimulate the uptake of atmospheric CO_2 by 0.13 Pg C yr^{-1} globally. The trends are very similar for the open ocean only, with an overall enhanced CO_2 uptake of 1.62 Pg C yr^{-1}, resulting from the balance between increases induced by atmospheric CO_2 (1.57 Pg C yr^{-1}) and rivers (0.1 Pg C yr^{-1}) and a decrease resulting from the ocean physics (0.05 Pg C yr^{-1}). In the coastal ocean, all three drivers stimulate atmospheric CO_2 uptake (0.11 Pg C yr^{-1}), with about 0.07 Pg C yr^{-1}, 0.01 Pg C yr^{-1} and 0.03 Pg C yr^{-1} being attributed to atmospheric CO_2, oceanic physics and river supplies respectively.

The increase in the ocean CO_2 sink only due to rising atmospheric CO_2 is well established and is caused by the disequilibrium maintained between the ocean dissolved CO_2 concentrations and the increasing atmospheric CO_2 concentrations (Ciais et al., 2013). The decrease in the CO_2 uptake attributed to physical ocean changes is caused by multiple factors. For one, we simulate a decrease in the open ocean mixed layer depth, where the physically-induced global decrease in the CO_2 uptake takes place. A shallower mixed layer depth inhibits the exchange of surface oceanic layers with deeper layers, which in turn decreases the efficiency with which CO_2 dissolved in the surface layers is transferred to the deep ocean. In the coastal ocean however, where firstly the mixed layer is unaffected at the global scale and secondly the storage capacity is much smaller than for the open ocean, no clear signal in the CO_2 flux can be observed. Furthermore, the ocean surface layers show a substantial increase in temperature (Figure 4.4-a), which causes a reduction in oceanic CO_2 uptake efficiency due to a temperature-induced decrease in CO_2 solubility and a shift in the carbonate system. In the coastal ocean, the temperature-induced decline of the uptake efficiency is likely compensated by the increase in the biological uptake observed in Figure 4.9-a. The total river enhancement of the atmospheric carbon sink is relatively small, but still contributes to 8 % of the global increase in 20th century ocean carbon uptake.

4.3.3 Perturbations of nutrient exports from the coastal zone

The model simulations reveal that the oceanic NPP is not only affected in the coastal zone, but also in the open ocean. This suggests that part of the enhanced nutrient supply is transported offshore. In this section we assess the changes in riverine nutrient supplies on the budgets of P and N in the coastal zone while considering all perturbations, and how these changes translate into changes to the open ocean supply from the coastal ocean. We first analyse the 1900-1910 mean fluxes (Figure 4.10 and Figure 4.11) and then the anthropogenic perturbations of these fluxes for 2000-2010 (Figure 4.10 and Figure 4.11), while assessing the model results in context of previously made mass balance estimates (Wollast (1998), Figure 4.11).

The coastal ocean is supplied with a total of 3.7 Tg P yr^{-1} and 27 Tg N yr^{-1} from rivers at the beginning of the century (1900-1910). For P, this riverine supply consists of 1.4 Tg P yr^{-1} as inorganic P and 2.3 Tg P yr^{-1} as organic matter (both in tDOM and riverine POM). In the coastal zone, 62.4 Tg P yr^{-1} are taken up during the biological production of organic matter, with 10.1 Tg P yr^{-1} deposited to the sediment as organic matter. The remineralization of the organic matter in the water column and in the sediment (both from terrestrial supplies and autochthonous) release 47.9 Tg P yr^{-1} and 6.8 Tg P yr^{-1} back to the water column as DIP respectively. A minor flux of P is buried in the sediment (3.3 Tg P yr^{-1}), whereas 7.1 Tg P yr^{-1} is exported offshore as organic matter. At the coastal ocean-open ocean interface, there is a net flux of inorganic P from the open ocean to the coastal zone (6.4 Tg P yr^{-1}) and an offshore export of organic P (6.9 Tg P yr^{-1}). Budgeting the organic P export and inorganic open ocean supplies results in a net offshore export of 0.5 Tg P yr^{-1}. In terms of the coastal N budget, rivers supply 9.1 Tg N yr^{-1} and 18.8 Tg N yr^{-1} to the ocean as inorganic N and organic N, respectively. 451 Tg N yr^{-1} are taken up by the biology. Additionally, 347 Tg N yr^{-1} and 49 Tg N yr^{-1} are remineralized in the water column and within the sediment. There is a combined net deposition flux and cyanobacteria N fixation from the atmosphere of 6 Tg N yr^{-1}, which is fully compensated by a denitrification flux of 6 Tg N yr^{-1}. While the net burial flux is of 34 Tg N yr^{-1}, consisting of a deposition flux of 73 Tg C yr^{-1} organic N and a resuspension flux of 49 Tg N yr^{-1}. Meanwhile, 53 Tg N yr^{-1} are exported offshore, whereas the DIN influx consists of 49 Tg N yr^{-1}. This results in a small net offshore export flux of 4 Tg N yr^{-1}.

The anthropogenic perturbation increases riverine loads of DIP by 1.2 Tg P yr^{-1}. The enhancement of riverine supplies lead to a multi-fold increase in the uptake through primary production (+8.9 Tg P yr^{-1}), and increase in the organic deposition flux (1 Tg P yr^{-1}) and regeneration through remineralization (+6.8 Tg P yr^{-1} and +0.3 Tg P yr^{-1} in the water column and sediment, respectively). We thus observe a multi-fold cycling of the nutrients within the coastal zone; before the increased P is exported offshore or to the sediment, it is on average taken up during primary production and subsequently released through mineralization processes several times. There is a slight increase in the organic offshore export (+1.1 Tg P yr^{-1}). The net inorganic flux to the coastal zone is increased by 0.7 Tg P yr^{-1}, which could originate from two reasons. First the higher than Redfield ratio of the anthropogenic perturbation of riverine supplies, inorganic P is efficiently and exported to a greater degree as organic P than in its inorganic form. Thus, less inorganic P is exported off the shelf. Secondly, the supply of DIP from the open ocean could be increased through inflows (for instance in the EBUS regions). Nevertheless, the offshore transport of total P increases by 0.4 Tg P yr^{-1}. The DIN riverine input is increased by 15 Tg N yr^{-1} due to the anthropogenic perturbation of the riverine loads. This enhances the DIN uptake through biological production by 65 Tg N yr^{-1}. We observe a slight decrease in the cyanobacteria nitrogen fixation, and an increase of denitrification of both 1 Tg N yr^{-1}. This can be explained that at increased DIN concentrations, which are due to the higher than Redfield ratio N:P ratio for the anthropogenic perturbation of riverine loads, cyanobacteria take up oceanic DIN instead of fixing N_2 from the atmosphere. The offshore export of organic nitrogen is increased by 9 Tg N yr^{-1} and a decrease in the net inorganic nitrogen inflow flux can be observed (+2 Tg N yr^{-1}), meaning more N is likely exported offshore as DIN. The resulting anthropogenic perturbation of the total N offshore transport is +11 Tg N yr^{-1}, which is higher in relation to the increased inputs (41%) than for P (33%).

The anthropogenic perturbation induces an increase in the ratio of net offshore export to burial of the nutrients (Figure 4.12). While the offshore export to burial ratio is 0.15 and 0.17 for P and N respectively for 1900-1910, the anthropogenic perturbation offshore export to burial ratio is around 0.6 and 2.2 for P and N respectively, signalling also a much stronger relative increase in relative N exports of the perturbed riverine loads. This higher export for N than for P is due to the increase in riverine N:P load ratios. The ratio of the increased exports and the total riverine induced perturbation is thereby 33% and 73% .

Few studies have addressed the coastal budgets of P and N in the coastal ocean. While the N fluxes suggested by Wollast (1998) in a mass balance approach are in general much larger than the ones simulated by the model, the fluxes magnitudes in relation to another are similar. We observe both in our model results and in Wollast (1998) that the DIP and DIN supplies from riverine fluxes, denitrification, cyanobacteria fixation and remineralization are unable to maintain the organic matter production in the coastal zone (for instance in the 1900-1910 period), implying that open ocean inflows play a large role in supplying nutrients for the coastal biological production. In Chapter 3 we suggest inflows from the open ocean to the coastal zone to have a very large global contributors to ocean flushing and that the inflows could be substantial sources of nutrients in the large shelf areas of the North Sea, the Patagonian Shelf, the Barents Sea and the Sea of Okhotsk, where literature suggests that the nutrients are entrained from deeper open ocean layers to drive the primary production in these regions (Thomas et al., 2005; Pipko et al., 2017; Combes and Matano, 2018). Both our model results for the pre-industrial and present day time periods and the budget from Wollast (1998) results show that the coastal ocean is a source of N to the open ocean, which is in agreement with what is observed in regional studies (e.g. Fennel et al. (2006) and Noriega and Araujo (2011).

Sharples et al. (2017) address the fate of riverine-delivered P and N in a globally parametrization of plume residence times in the coastal ocean and of biological transformations. Since the study only represents the fate of riverine P and N, disregarding open ocean P and N supplies, it is not directly comparable to the absolute 1900-1910 and 2000-2010 budgets. However, since the perturbations of the coastal nutrient concentrations and of the coastal NPP was determined to be mostly induced by the riverine loads (Figure 4.5 and 4.8), these riverine perturbations of P and N can be compared to the Sharples et al. (2017) results. The study Sharples et al. (2017) study estimates a high efficiency in the criss-shelf export of riverine P (75 %) and N (80 %), but these values were corrected downwards by Izett and Fennel (2018) while revisiting the parametrized approach, leading exports of 2.8–44.3 % for DIP and 7.3–44.3 % for DIN riverine inputs. Our model also suggests values in this range for the anthropogenic P perturbation (33 %) and although it is higher for N (73 %). In our dynamical model simulation, we however take into account for 3-dimensional circulation features in the coastal ocean and dynamical changes in biological processes, which are not possible in such a parametrized approach. For instance, a much stronger N supply to the coastal zone causes

an increase in P limitation in our model, meaning P is taken up more efficiently, and therefore less efficiently exported (Figure 4.6). Furthermore, we account for the complex interplay of seasonal variations of the physical coastal ocean circulation and of the biological production. For instance, a high regional organic production and in a period of low mean transport would lead to a lower offshore transport for N and P, than when accounting solely for yearly means of coastal residence time and organic transformations.

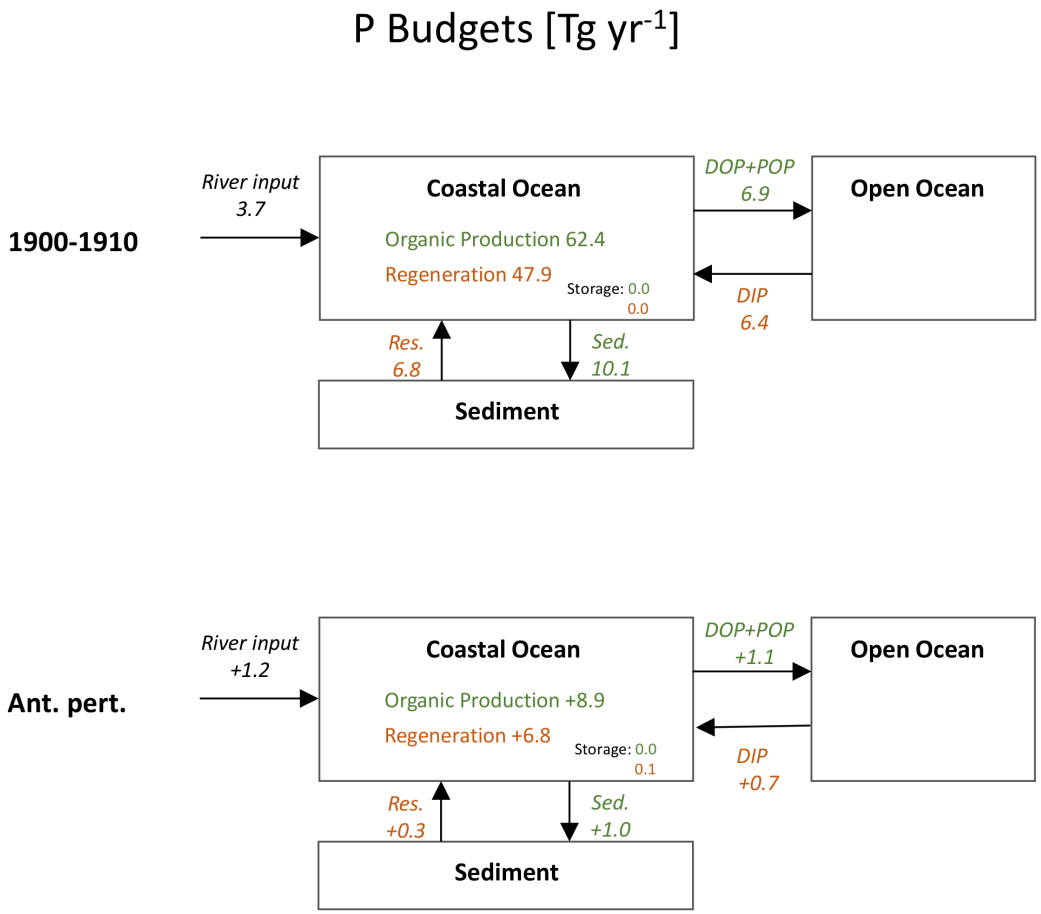

FIGURE 4.10: P budget for the coastal ocean at the beginning of the century (1900-1910) and for the 20th century perturbation of the fluxes (Ant. Pert.). The fluxes in green are generation or transport fluxes of organic P, whereas fluxes in orange are generation of DIP. Organic production considers the primary production through both bulk phytoplankton as well as cyanobacteria. Regeneration is the total of all water column remineralization processes (including zooplankton respiration). Sed. is the sediment deposition flux and and Res. the flux of DIP back to the water column.

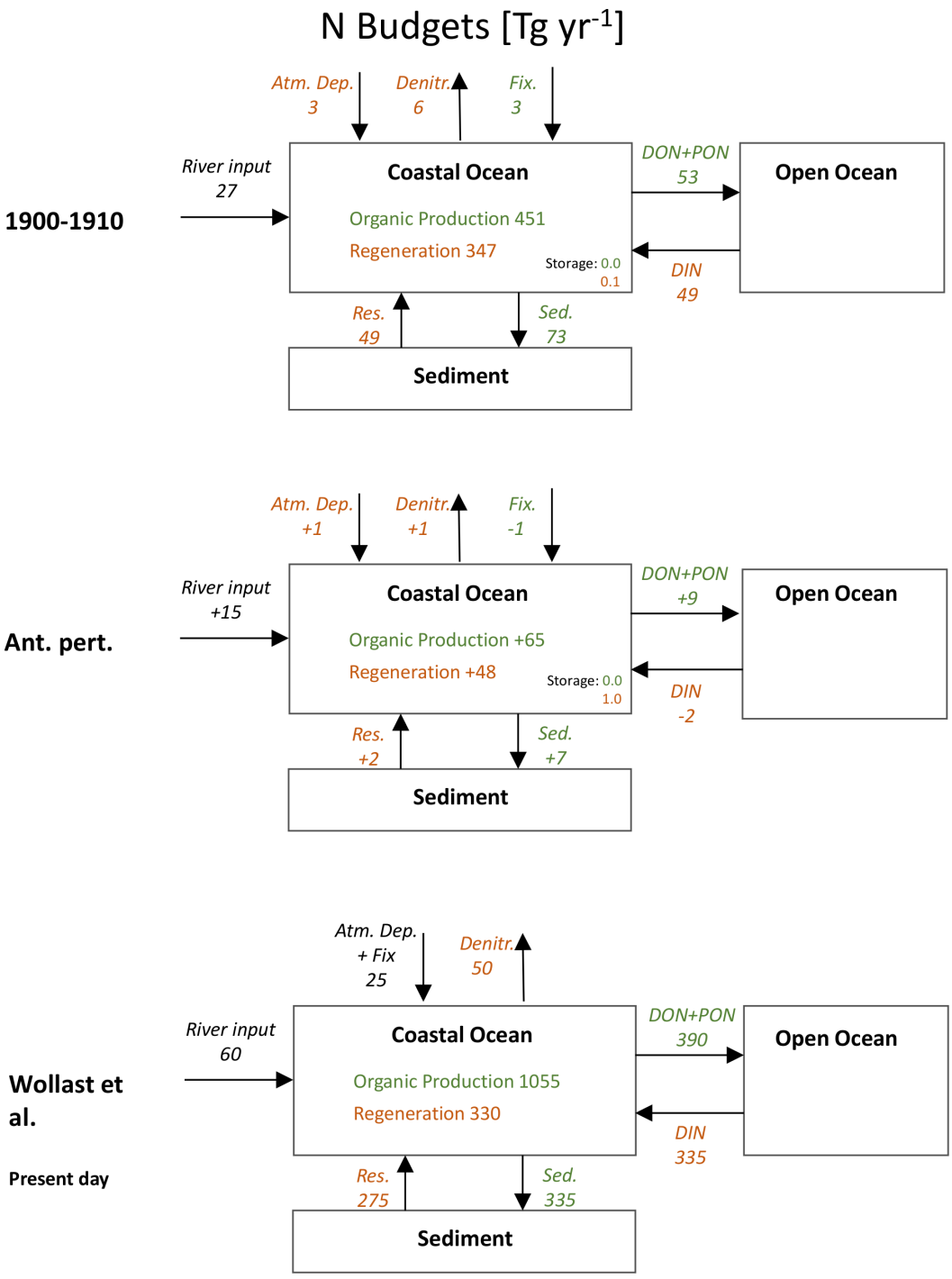

FIGURE 4.11: N budget for the coastal ocean at the beginning of the century (1900-1910) and for the 20th century perturbation of the fluxes (Ant. Pert.). The fluxes in green are generation or transport fluxes of organic N, whereas fluxes in orange are generation of DIN. Organic production considers the primary production or organic matter both through bulk phytoplankton as well as cyanobacteria. Regeneration is the total of all water column remineralization processes (including zooplankton respiration). Atm Dep. is the atmospheric deposition of DIN, Denitr. is the loss of DIN due to denitrification, and Fix. Is the N fixation through cyanobacteria. Sed. is the sediment deposition flux and and Res. the flux of DIN back to the water column.

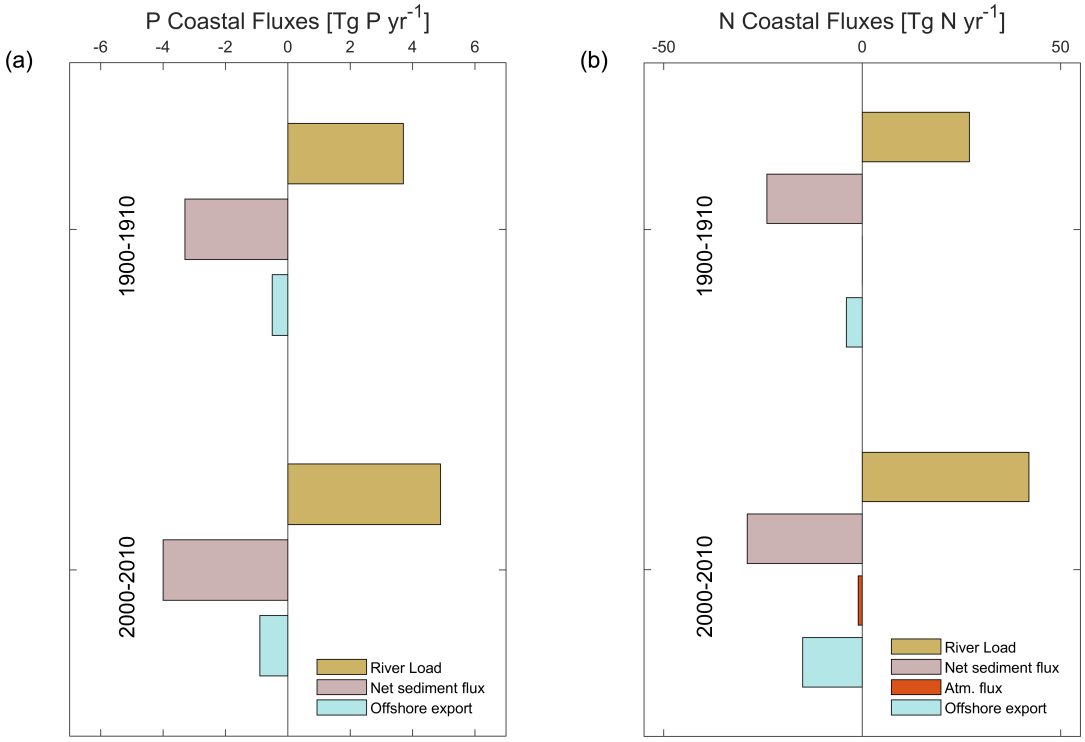

FIGURE 4.12: Net mean annual (a) P and (b) N fluxes to and from the coastal ocean for 1900-1910 and 2000-2010: riverine loads (River load), net sediment burial flux (Net sediment flux) and the offshore exports. Positive values are a flux to the coastal ocean, whereas negative values are a flux from the coastal ocean.

4.3.4 Perturbation of global inorganic and organic carbon cycling in the coastal ocean

At the start of the century (1900-1910), the supply of organic carbon from the rivers in the model is 0.34 Pg C yr^{-1} and the produced organic matter within the coastal zone is 2.95 Pg C yr^{-1}, of which 2.36 Pg C yr^{-1} is mineralized within the coastal zone (including sediment mineralization), 0.16 Pg C yr^{-1} is buried in the sediments, and 0.45 Pg C $yr^{-1}$is exported offshore (Figure 4.13). The open ocean NPP is 51.47 Pg C yr^{-1}, while the remineralization reaches 51.65 Pg C yr^{-1} and the burial is only 0.04 Pg C yr^{-1}.

Due to all perturbations, we observe a 0.42 Pg C yr^{-1} (15 %) increase in the coastal ocean NPP from 2.95 to 3.37 Pg C yr^{-1} during the 20^{th} century in the simulations (accounting for all perturbations). About one quarter of this extra produced organic matter is then transported offshore (0.10 Pg C yr^{-1}), a vast majority of the remainder (0.32 Pg C yr^{-1}) being remineralized within the coastal zone, leaving only 0.03 Pg C yr^{-1} of enhanced burial in shelf sediments.

In comparison to the results reported in Chapter 3, we observe an even more efficient cross-shelf export of organic matter, which can be explained by the increase in resolution. The surface coverage of the coastal ocean is improved with respect to Chapter 3, and narrow shelves have a more important areal contribution to the global shelf, which also usually have very short residence times of under one month (Figure 4.14, Sharples et al. (2017)). An increase in model resolution on one hand likely also leads to shorter water residence times due to the better representation of open ocean inflows at the cross-shelf boundary, as well as wind shear stress at the surface layer. The efficient cross-shelf transport of organic carbon causes a more positive coastal NEP (0.25 Pg C yr^{-1}) for the 1900-1910 timeframe, confirming our suggestions that the coastal ocean might have been autotrophic in its pre-industrial state (Chapter 3), albeit even more autotrophic in this case.

The increase in nutrients provided by rivers due to anthropogenic activities has long been suggested to cause a direct increase in coastal NPP (e.g. in Mackenzie et al. (2002)), which we also observe in our study. The magnitude of this riverine-induced increase in coastal NPP and newly produced organic matter has, however, not been quantified until now. Our results suggest that the increased riverine nutrient supply (233 % for biologically available N and 175 % for biologically available P) is however relatively inefficient at increasing coastal NPP (only by about 15 %), once again indicating the large influence of open ocean supplies for the "background" coastal ocean NPP.

The extra produced organic matter as a result of the perturbation of riverine fluxes is also efficiently exported to the open ocean, thus increasing the NEP by +0.09 Pg C yr^{-1} with regard to the 1900-1910 state. This can be explained by the biogeochemical and physical dynamics of the NPP enhancement by riverine fluxes. Since the anthropogenic perturbation of the NPP arises mostly from the riverine nutrient supplies for the coastal zone (Figure 4.8), the enhancement of the organic matter production takes place in the stratified river plumes. We also suggest in Chapter 3 that the residence times of riverine freshwater is shorter than for the average coastal ocean waters, due to increased stratification and a plume flow perpendicular to the coast, a mechanism which is also discussed in Sharples et al. (2017). In Sharples et al. (2017), very short water residence times (<7 days) are calculated for major low latitude river plumes. Therefore, organic material produced within such river plumes should be exported rapidly, thus causing the observed increase in the NEP. A substantial increase in coastal NEP has also been suggested previously in literature, such

as in Andersson et al. (2005), but we suggest here, as in Chapter 3, that the initial pre-industrial state of the coastal ocean was already clearly autotrophic due to the efficient cross-shelf transport of carbon.

The DIC export to the ocean (0.33 Pg C yr^{-1}) is constant over the entire simulation time-period. For 1900-1910, the coastal global NEP and net calcium carbonate production consume 0.25 Pg C yr^{-1} and 0.04 Pg C yr^{-1} DIC, respectively. While the DIC removal from $CaCO_3$ 0.04 Pg C yr^{-1} in the coastal ocean, it is 0.27 Pg C yr^{-1} in the global ocean, respectively, which is slightly more than we suggested in Chapter 3 in both cases. The higher DIC removal by the organic matter production and $CaCO_3$ in the coastal zone leads to a significantly lower DIC export than reported in Chapter 3. While the DIC cross-shelf exports were around the same as the riverine inputs in Chapter 3, the cross-shelf DIC exports shown here are clearly smaller (0.09 Pg C yr^{-1}). During the 20^{th} century the coastal NEP is enhanced by 0.09 Pg C yr^{-1} (taking into account all anthropogenic perturbations), while the $CaCO_3$ is not substantially increased (+0.01 Pg C yr^{-1}). While the simulation shows a present-day global open ocean uptake of carbon of 1.62 Pg C yr^{-1} higher than the 1900-1910, only 0.11 Pg C yr^{-1} of the increase in air-sea uptake can be attributed to the coastal ocean. This corresponds to about of 7 % of the global perturbation flux, a fraction that is similar to the contribution of the coastal ocean area to the global ocean area (also around 7%).

Our model suggests that, while the coastal ocean is a source of DIC to the open ocean in the pre-industrial state due to its offshore transport both for the pre-industrial time-frame and the present-day, although less so for the latter. In literature, contradicting suggestions exist with respect to the sign of the DIC exchange with the open ocean. While long-standing box model studies suggested that the coastal ocean was a substantial source of DIC to the open ocean (e.g. Mackenzie et al. (2002)), Chen and Borges (2009) report in a mass balance calculation that a net DIC flux from the open ocean to the coastal ocean is needed to sustain the coastal organic matter production. In the first study, to our knowledge, to consider a global 3-dimensional circulation and perturbation of riverine exports, we suggest the ocean was a net DIC supplier to the open ocean. The shelf behaviour regarding its input and output of DIC is however most likely strongly regionally dependent. For instance, published literature reveals that the North Sea is a net source of DIC to the open ocean (Thomas et al., 2005), whereas upwelling systems such as the California Current System provide a large sink of open ocean DIC

(Frischknecht et al., 2018).

In comparison to Chapter 3, we observe here an even stronger lateral biological pump, with substantial amounts of organic matter being exported offshore. This biological production of organic carbon and its removal of DIC contributes to the pre-industrial coastal sink of 0.05 Pg C yr^{-1} also observed here. Furthermore, the alkalinity increases in near-surface waters also likely contribute to this sink, as discussed in Chapter 3. Here again, physical characteristics of the open also likely strongly control the CO_2 flux. For instance, the inputs from open ocean subsurface inflows dictate the primary production on the Patagonian shelf (Song et al., 2016). Furthermore, the cooling of water masses during the winter likely causes sinks in regions such as the Barents Sea, causing a shift in the carbonate system and higher solubility of atmospheric CO_2, thus taking up more carbon (Pipko et al., 2017).

The effect of anthropogenic perturbations on the coastal ocean air-sea CO_2 flux is inconclusive in literature. The model study by Bourgeois et al. (2016) suggest that the coastal ocean is an inefficient sink of atmospheric carbon in a global ocean model, whereas Laruelle et al. (2018) show regional evidences for an increasing sink through regional observational data. Despite considering two additional factors compared to the model work of Bourgeois et al. (2016) (changes in atmospheric ocean physics drivers and perturbations of the riverine fluxes), the anthropogenic perturbation of around 0.11 Pg C yr^{-1} simulated here for the 20th century is roughly the same in both studies. A likely explanation could be that the decreasing coastal ocean uptake due to increasing temperatures compensate the increasing sink attributed to the enhancement of biological uptake by the riverine nutrient supply.

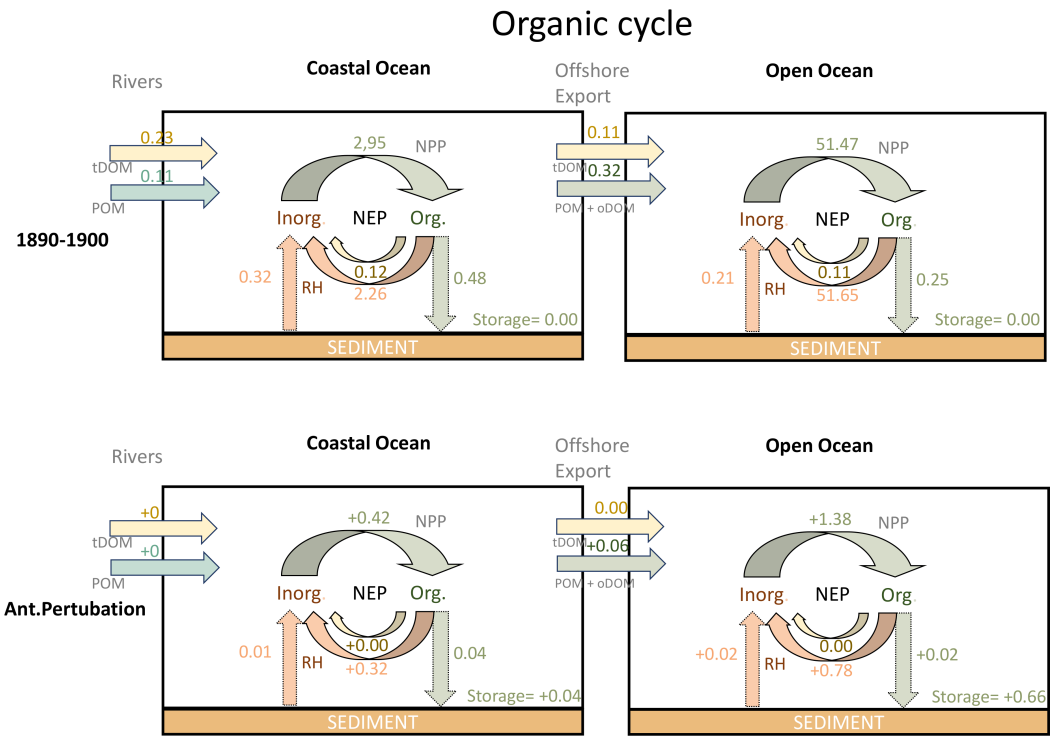

FIGURE 4.13: Carbon budgets for the organic carbon cycling in the coastal and open ocean [Pg C yr^{-1}]. Green arrows signal the transformation to organic matter or transport of organic matter. The red arrows are the transformation to inorganic species. Yellow arrows are the transports and remineralization of tDOM.

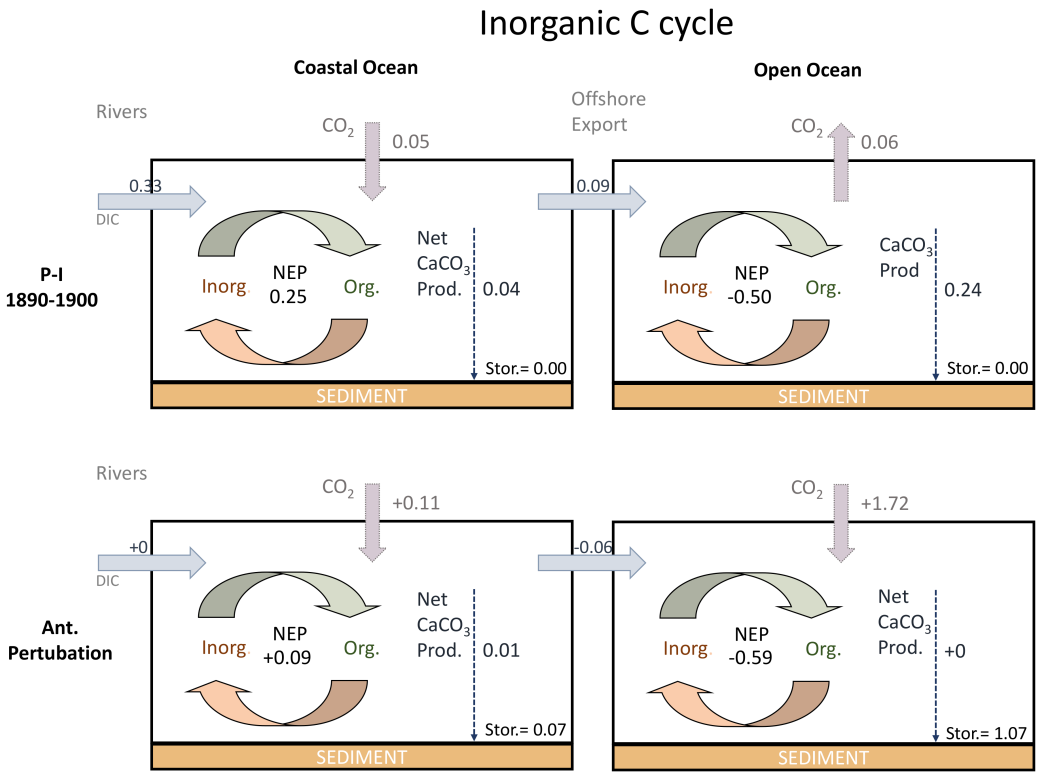

FIGURE 4.14: Carbon budgets for the inorganic carbon cycling in the coastal and open ocean [Pg C yr^{-1}]. The purple arrows from the top of the boxes are the air-sea carbon exchange. The NEP accounts for NPP in the water column, as well as the remineralization (RH) of organic matter in the water column and in the sediment.

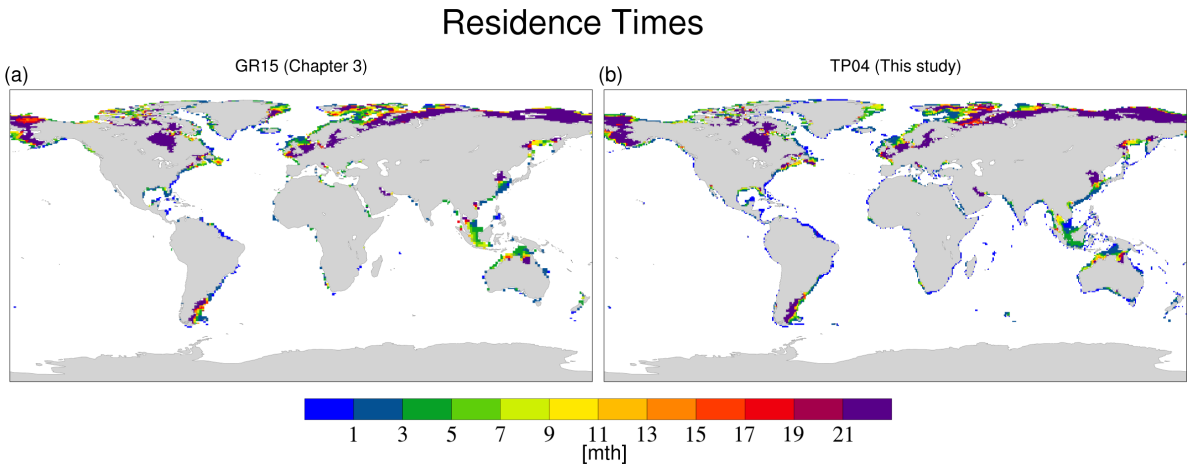

FIGURE 4.15: Residence times of the model simulations (a) in the GR15 model configuration (Chapter 3) and (b) in the TP04 configuration used in this study [mth].

4.3.5 Regional assessment of 20th century changes in NPP and CO_2 flux

We note that the present-day air-sea CO_2 flux of 0.16 Pg yr^{-1} reported in the previous sections falls within the range reported by Laruelle et al. (2014) based on observations (0.15-0.25 Pg C yr^{-1}). Furthermore, our model-derived regionalized pCO_2 estimates show good agreement with the global observation-based pCO_2 reported by Laruelle et al. (2017) (Figure 4.16). In what follows, we pursue our in identifying dominant coastal regions with respect to global changes in the NPP and the CO_2 air-sea exchange, while attempting to reconcile what appears to be contradicting trends in the global coastal CO_2 flux reported by Bourgeois et al. (2016) and Laruelle et al. (2018).

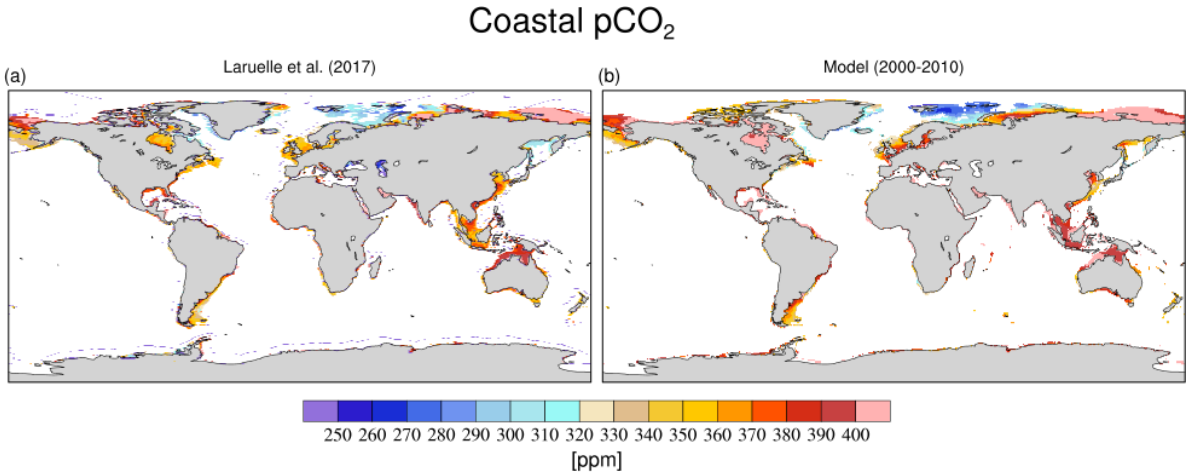

FIGURE 4.16: 4. Comparison of modelled pCO_2 distribution for (a) the present-day (2000-2010) with (b) neural network interpolation approach of Laruelle et al. (2017) [ppm].

The anthropogenic changes in the regional riverine inputs (for instance, 0 to 2128 10^3 Mg N yr^{-1}), NPP (-13 g C m^{-2} yr^{-1} to 115 g m^{-2} yr^{-1}) and CO_2 flux (+1.3 to -13.2 g m^{-2} yr^{-1}) vary strongly spatially for the MARCATS (see Table 4.2). In general, MARCATS which undergo a strong increase in riverine inputs, and also have semi-enclosed boundaries or trenches inhibiting potential cross-shelf exports show the high increases in NPP. For instance, the semi-enclosed Black Sea (21-NLA), East China Sea (39-CSK) and Sea of Okhotsk (41 -OKH) show some of the highest NPP increases per area in the model (115, 41 and 43 Pg C m^2 yr^{-1} respectively). These regions have also been identified as hotspots for coastal eutrophication in published literature (Moncheva et al. (2002) and Fennel and Testa (2019) and references therein). Furthermore, we also identify

the Californian Coast (2-CAL), the Persian Sea (29-PER), the Eastern Arabian Sea (30-EAS), the Bay of Bengal (31-BEN) and South Australia (34-SAU) as regions experiencing major changes in NPP per area. For the Californian Coast, the observed NPP increase in the model is most likely not only due to increases in riverine loads, but also possibly due to an intensification of the coastal upwelling in this EBUS, which consists of the primary supply of nutrients in the region (Kahru et al., 2009). The Bay of Bengal, which is supplied by the Ganges river, shows the largest N river load increase (2.13 Tg N yr^{-1}), enhancing the areal NPP by 88 g C m^{-2} yr^{-1}. For the North East Atlantic (17-NEA), where the supplies are strongly increased during the 20th Century due to nutrient fluxes from European agriculture and sewage Seitzinger et al. (2010), we simulate an NPP increase of 28 g C m^{-2} yr^{-1}. The largest increases in relation to their 1900-1910 mean states take place in the Baltic Sea (+58 %), Mediterranean Sea (20-MED) (+50 %) and Persian Sea (+38 %), which are all semi-enclosed seas.

In addition to large variability in the CO_2 flux change between the different MARCATs segmentations, we also observe strong heterogeneity even within MARCATs segmentation (Figure 4.17). For instance, the North Eastern Atlantic shelf (17-NEA), which receives large nutrient inputs from European rivers and which consists of a large present-day sink in agreement with literature (Thomas et al., 2005), we observe a less efficient than average increase in the CO_2 sink in most of the North Sea, while the nearshore regions and the outer shelf show a stronger than average increase in the CO_2 sink. Although the implications of climate change on the North Sea are highly uncertain, Gröger et al. (2013) also suggest a decreasing efficiency for most of the North Sea carbon uptake in a regional model study due to stronger stratification.

Our model simulations provide useful elements to reconcile the conclusions from Bourgeois et al. (2016) and Laruelle et al. (2018), which disagree whether the coastal ocean is becoming an increasingly more efficient sink of CO_2 than the average global ocean. Our model results show regional agreement with the Laruelle et al. (2018) analysis, which suggest that the CO_2 sink is increasing more strongly than average on the Mexico (9-MEX), Florida (10-FLO) and Southern Greenland (14-SGR), Japan (41-JAP) and Barents Sea shelves (43-BKS). The mid and high latitude shelves thereby (excluding Arctic shelves) tend to consist of a stronger increasing sink than average (Figure 4.17). The model however shows that tropical shelves, as well as Arctic shelves do not the same tendencies. For Arctic shelves, which consist of

over 20 % of the global shelf, the substantial ice-coverage could inhibit the thermal transfer between atmosphere and the ocean during the winter, while also causing a barrier for the CO_2 exchange flux in the months of the largest potential uptake. Furthermore, a riverine enhancement of the biological carbon uptake also does not take place due to the limited anthropogenic riverine inputs in the region according to NEWS2. In tropical regions, the temperature increases shown in these regions (Figure 4.4-a), which could cause a shift in the carbonate system, could help explain these increases, although other regions also undergo strong temperature increases. In the Laruelle et al. (2018) study, stronger weight is given to mid-to-high latitude shelves (excluding the Arctic shelves) when extrapolating to the global scale due to the availability of observational data in these regions. The Arctic and tropical shelves are on the other hand dramatically under sampled which prevents a robustly supported trend analysis. Our model agrees with Laruelle et al. (2018) that large shelf regions have experienced a much larger than global ocean average increase in their CO_2 uptake, especially in the mid latitudes. However, they also suggest that overall, the global shelf CO_2 uptake might not be substantially higher than average, mostly due to differing trends on tropical and Arctic shelves. Such dynamics urgently calls for more intense surveys of pCO_2 changes in the low latitudes and in the Arctic Ocean. Furthermore, the differing conclusions from Bourgeois et al. (2016) and this study with the Laruelle et al. (2017) could also originate from inconsistencies in the temporal analysis period. Laruelle et al. (2018) report strong increases in the efficiency of the CO_2 uptake on a shorter time scale, starting from the 1980s, than is done here and in Bourgeois et al. (2016), where solely the entirety of the 20^{th} century is taken into account. A more rapid increase in the coastal ocean CO_2 uptake towards the end of the 20^{th} century is plausible due to stronger increases in riverine nutrient inputs and stronger changes in atmospheric circulation at the back-end of the 20^{th} century. In the analysis in this study, the short-term trends were however not considered.

4.3.6 Implications for 20^{th} century changes in subsurface oxygen levels

The model results show a widespread 20^{th} century coastal increase in NPP due to increases in nutrient land-ocean exports, whereas the impacts of 20^{th} century climate change on mixed layers are strongly regional (Figure 4.18-a,-b).

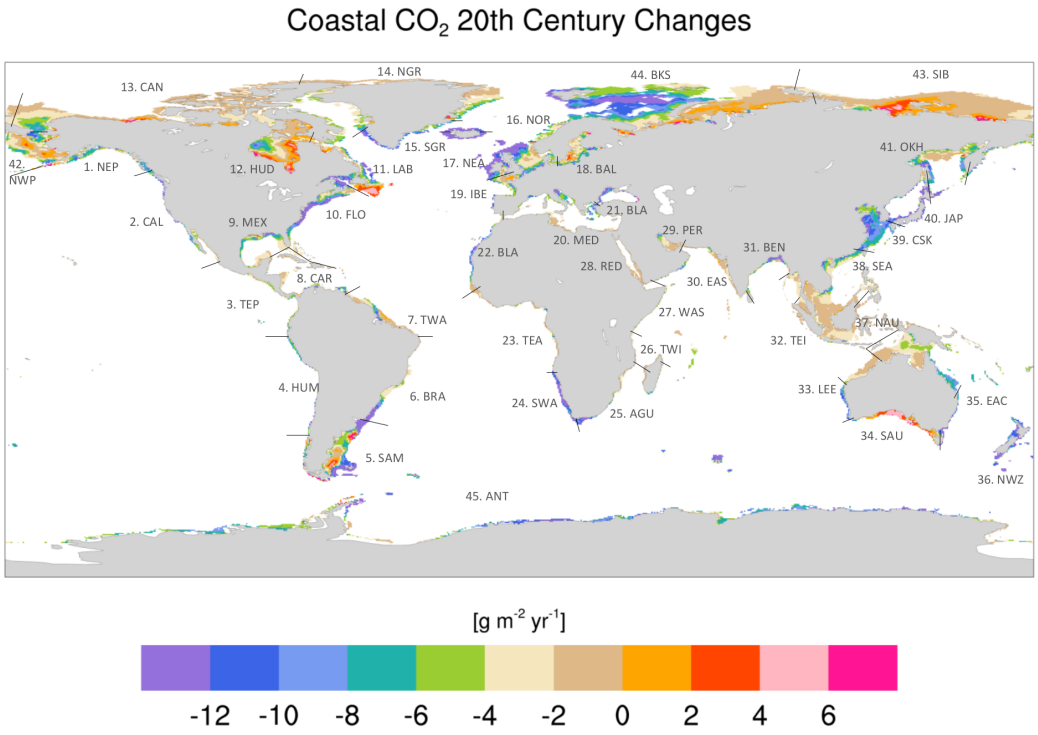

FIGURE 4.17: Coastal flux change for the 20th century. A negative flux is defined as a flux from the atmosphere to the ocean (oceanic CO_2 uptake). The colour scale is centred around the coastal ocean average change in CO_2 uptake of around 4.2 g C m^{-2} yr^{-1}. Colours towards red/pink correspond to a lower than average coastal ocean CO_2 uptake change, whereas colours towards blue/purple correspond to a more efficient uptake than the average coastal ocean.

TABLE 4.2: MARCATS and their outer shelf depths in the model, shelf areas and 20th changes in riverine N inputs, nutrient ratio, CO2 flux and NPP. The changes are derived from the difference between 2000-2010 means and 1900-1910 means.

MARCATS	Depth	Model Area (10^9 m)	Area Laruelle et al. (2013)	River N increase [10^3 Mg]	River P increase [10^3 Mg]	Mole N:P river load increase [-]	Change in CO_2 uptake per area [g m^{-2} yr^{-1}]	NPP change per area [g m^{-2} yr^{-1}]	NPP relative change
1-NEP	500	378	461	46	5	21	-5.8	+14	+7.%
2-CAL	250	183	214	100	10	22	-5.9	+59	+20.%
3-TEP	250	110	198	208	17	27	-4.4	+1	+2.%
4-HUM	250	91	143	64	8	17	-8.7	+19	+2.%
5-SAM	350	905	1230	21	1	45	-5.3	+23	+8.%
6-BRA	350	172	521	736	68	24	-11.8	+7	+5.%
7-TWA	180	441	517	898	52	38	-3.9	+19	+13.%
8-CAR	180	239	344	409	43	21	-4.3	+34	+35.%
9-MEX	180	510	544	261	21	27	-4.5	+24	+30.%
10-FLO	180	510	854	213	34	14	-6.7	+12	+12.%
11-LAB	350	750	395	219	13	36	-1.2	+14	+9.%
12-HUD	250	823	1064	64	2	77	-1.4	+4	6.%
13-CAN	250	1103	1177	1	0	71	-2	+5	+13.%
14.NGR	500	625	614	8	0	38	-7.7	+4	+6.%
15-SGR	500	117	270	8	0	38	-8.2	+4	+5.%
16-NOR	180	310	219	35	3	23	-4.3	+11	+9.%
17-NEA	250	771	1112	605	58	23	-9.1	+28	+24.%
18-BAL	250	374	383	134	21	14	-3.6	+33	+24.%
19-IBE	350	315	283	266	31	19	-4.9	+26	+20.%
20-MED	250	485	580	381	65	13	-5.5	+29	+50.%
21-BLA	350	71	172	446	47	21	-12.7	+115	+58.%
22-MOR	180	227	225	125	8	33	-5.7	+20	+8.%
23-TEA	250	125	284	535	24	50	-3.1	+36	+11.%
TOTAL/AVG	**327 (avg)**	**23 10^3**	**30 10^3**	**15'126**	**1303**	**29 (avg)**	**-4.2 (avg)**	**+23 (avg)**	**+17%(avg)**

MARCATS	Depth	Model Area (10^9 m)	Area Laruelle et al. (2013)	River N increase [10^3 Mg]	River P increase [10^3 Mg]	Mole N:P river load increase [-]	Change in CO_2 uptake per area [g m^{-2} yr^{-1}]	NPP change per area [g m^{-2} yr^{-1}]	NPP relative change
24-SWA	1000	384	308	64	4	36	-12.8	+13	+2.%
25-AGU	250	144	254	206	14	32	-3.8	+10	+10.%
26-TWI	350	21	72	44	2	46	-2.3	+10	+16.%
27-WIB	180	95	102	188	9	47	-3.1	+36	+25.%
28-RED	180	127	190	5	1	10	-1.5	+3	+4.%
29-PER	250	200	233	42	9	10	-2.8	+11	+38.%
30-EAS	180	278	342	23	1	37	-2.5	4+4	+27.%
31-BEN	250	378	230	2128	147	32	-7.5	+84	+77.%
32-TEI	180	108	809	89	4	56	-2.2	+37	+35.%
33-LEE	350	107	118	149	11	30	-1.8	+4	+6.%
34-SAU	350	155	452	19	4	11	1.3	+57	+47.%
35-EAC	350	313	139	10	1	17	-6.6	-13	-16.%
36-NWZ	350	237	283	279	33	19	-12.6	-4	-1.%
37-NAU	250	2251	2463	195	12	35	-3	-2	-2.%
38-SEA	250	2491	2318	1906	98	43	-2.5	+21	+29.%
39-CSK	350	699	1299	220	32	15	-8.8	+41	+25.%
40-JAP	5	399	277	245	60	9	-13.2	+39	+25.%
41-OKH	500	277	992	115	11	23	-7.6	+43	+25.%
42-NWP	350	29	1082	0	0	-	-5.9	+26	+18.%
43-SIP	350	1701	1082	1	1	4	-1	0	+1.%
44-BKS	350	2453	1918	129	16	18	-5.6	+2	+3.%
45-ANT	1000	2714	1727	0	0	-	-6.5	+19	+31.%
TOTAL/AVG	**327 (avg)**	**23 10^3**	**30 10^3**	**15'126**	**1303**	**29 (avg)**	**-4.2 (avg)**	**+23 (avg)**	**+17%(avg)**

Regional changes in NPP can reach values as high as 50 % for some large shelves (Table 4.2), and at concomitant, decreases in mixed layer depths can be observed, which implies a decrease in the ventilation of subsurface coastal water layers. In this section, we discuss the implications of these changes for the oxygen concentrations in the subsurface coastal water column.

Although the average global oxygen concentration under the average coastal ocean mixed layer depth (36 m) only drops from 0.242 mg l^{-1} to 0.240 mg l^{-1}, we observe a widespread regional decrease in the minimum oxygen concentrations (Figure 4.18-c). These decreases are particularly strong in the Black Sea, the Patagonian Shelf, the Barents Sea and the East China Sea. In the model, we observe considerable NPP increases in the Black Sea and East China Sea due to increased riverine inputs, but no decrease in the mixed layer depth is predicted for these regions. The steep increases in riverine nutrient inputs for these two regional seas are consistent with regional studies (Yan et al., 2003; Ludwig et al., 2009; Wang et al., 2015; Fennel and Testa, 2019). For the Barents Sea, which is remote from large rivers having experienced increases in nutrient inputs, the mixed layer depth is strongly reduced, a result which might explain the lack of ventilation and decreased oxygen minimum concentration. On the Namibian shelf, which is also reported to be an area of increased hypoxia in Fennel and Testa (2019), we also observe an increase in NPP, a strengthening of the stratification and a decrease in the oxygen minimum along the coast.

As a result of the increased production and sinking of organic matter in the coastal zone, we observe an increase in the coastal removal of nitrogen through water column and sedimentary denitrification from 6.51 Tg N yr^{-1} to 7.27 Tg N yr^{-1}. This increase signals that the oxygen levels are not sufficient to sustain the enhanced remineralization of the organic matter everywhere. The relative increase in denitrification (12 %) is around the same as the increase in the coastal NPP (15 %), which implies that the enhancement of denitrification through increased supplies of organic matter is near linear. The relative increase in denitrification is particularly strong in the water column (from 0.46 Tg N yr^{-1} to 0.61 Tg N yr^{-1}), which suggests an increase in zones of low oxygen concentrations, where denitrification becomes a major respiration pathway.

The model therefore shows that an increase in coastal NPP translates into a widespread drop of oxygen minimum concentrations. Regions with a concomitant decrease of the mixed layer depth could be more strongly affected, since the subsurface waters are not supplied with sufficient oxygen, as is

discussed in Fennel and Testa (2019). Furthermore, denitrification increases as a result of the decreasing oxygen concentrations in the subsurface layers of the coastal ocean. Although model resolution might not yet fully resolve the physical processes that control coastal ventilation and prevent a full quantitative analysis of coastal deoxygenation, the identification of changes in NPP and MLD as two key control factors of oxygen levels could be used to further interpret regional observations of increased oxygen deficiency and carry future projections.

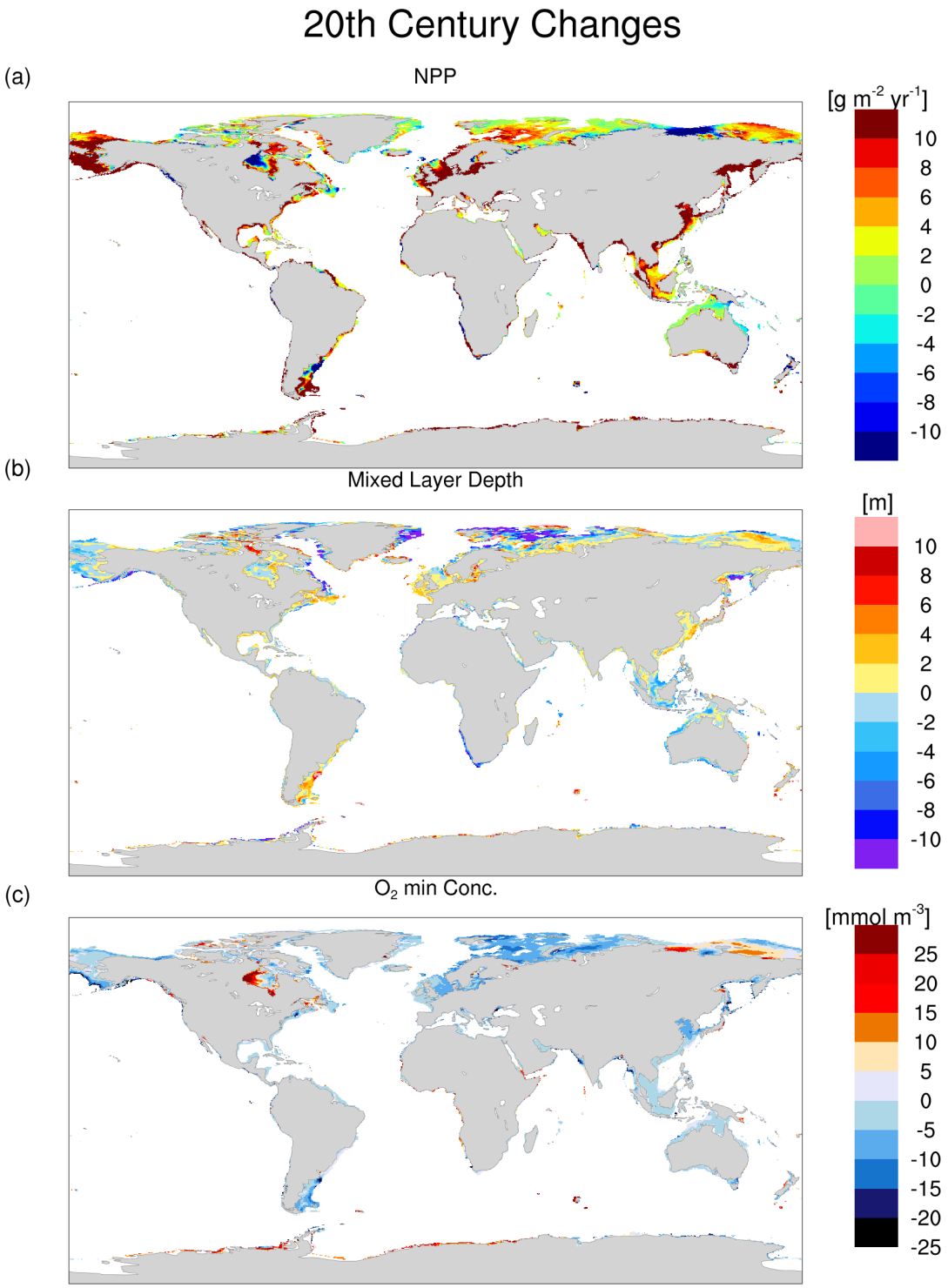

FIGURE 4.18: Changes in coastal (a) NPP, (b) mixed layer depth and (c) oxygen minimum concentrations during the 20th century

4.4 Limitations of our model study

While the model resolution used in this study is improved compared to earlier ones (for instance in the previous chapters), circulation features at the meso- and sub-mesoscales are still not represented, although they might be important for the coastal zone, especially regionally. For instance, Gruber et al. (2009) suggest that meso-scale eddies play a large role in the offshore transport of organic carbon in EBUS, acting as a supressing factor for the primary production in these regions. While the spatial resolution of the model is eddy permitting, the eddies are nevertheless not yet explicitly resolved (Jungclaus et al., 2013). An even higher resolution could potentially be used, but our study requires a long model spin-up in order to achieve a close to equilibrium model state. Since oceanic inflows from deeper layers play an important role in the biogeochemistry of the coastal ocean (Chapter 3), it is vital to represent them and this can only be achieved if a stable state in the global ocean biogeochemistry is achieved. Due to CPU requirements, we thus needed to make a trade-off between the highest possible model resolution while still being able to run a spin-up time of several thousands of years leading to a state of quasi-equilibrium for the global ocean.

Regarding the changes in riverine inputs, we assumed a simple temporal evolution in catchment P and N loads. In particular, the relative temporal changes are assumed identical for every catchment, although they have been reported to vary regionally by Seitzinger et al. (2010) and Beusen et al. (2016). For instance, nutrient fluxes discharging into the Atlantic Ocean and Mediterranean Sea have increased strongly at the beginning of the 20th century followed by a decrease from 1980 to 2000, while fluxes to the Pacific show a sharp increase from 1980 to 2000 after a slow increase at the beginning of the century. These distinct temporal evolutions might to some degree cause spatial variations in the trends simulated here. However, since we compare averages for present day (2000-2010) and the beginning of the century (1900-1910), the results should be largely unaffected by the actual trends between these time periods. This conclusion might not hold when assessing trends on a shorter time-scale, such as for the comparison with the recent decadal trends of Laruelle et al. (2018), where the temporal regional differences to the simplified approach to quantify changes in nutrient loadings could play an important role.

While our model study accounts for changes in P and N riverine inputs, we have assumed constant global C and Si loads. This choice was guided by the

results of the NEWS2 model study, which do not show important changes in land-derived C and Si fluxes at the global scale for the 20th century. Furthermore, there is yet to be catchment estimates with a spatially resolved model, which dictates anthropogenic changes in C fluxes globally that we could use in this study. While the NEWS2 study offers two different scenarios for 1970 and 2000, the submodels used in the study have relatively rigid structures regarding their model inputs. On one hand, a fully dynamic vegetation could play a role in impacting the anthropogenic carbon fluxes from the terrestrial biosystem to catchments. Furthermore, more frequent extreme climate events could cause larger exports of particulate organic carbon (Hilton et al., 2008), which is not considered in approaches such as NEWS2 that only account for the yearly means in its input variables and output. It has however been suggested in literature that C fluxes to the ocean might have increased by about 10-30 % during the 20th century (Mackenzie et al., 2002; Regnier et al., 2013), although a study by Maavara et al. (2017) also reveals a retention of 13 % caused by increased retention along the land-ocean-continuum through damming. A change of this C load to the ocean would have little effect on the coastal NPP, but might affect the NEP and the CO_2 flux, especially regionally. An increase in the coastal CO_2 flux could reach a value of up to 0.1 Pg C yr^{-1}, in the extreme case that all of the anthropogenic increase in the land-ocean C export estimated by Regnier et al. (2013) (0.1 Pg C yr^{-1}) is mineralized and outgassed in the coastal ocean. Our results in this study however suggest that a considerable fraction of river-delivered organic carbon is transported offshore.

Furthermore, we do not consider changes in freshwater inputs to the ocean through increased retention along the land-ocean-continuum, for instance by increased damming. These changes most likely do not play a large role in the ocean at the global scale, since the volume of only the coastal ocean (around 1.78 10^{15} m^3) is much larger (by around a factor 55) than the freshwater inputs discharge (0.032 10^{15} m^3 yr^{-1}). At a regional scale, the alteration of freshwater inputs might however play a larger role.

4.5 Summary and conclusions

Our study relied on multiple model simulations of ocean physics and biogeochemistry to quantify changes in the cycling of carbon and nutrients due to

increasing atmospheric CO_2, ocean physical changes, and perturbations of riverine nutrient fluxes. While the effects of changes in oceanic physics on the ocean biogeochemistry have been previously tackled for the historical time period (e.g. Laufkötter et al. (2013), these model did not address the impacts on the coastal ocean due to coarse model resolutions (up to 3.6 degrees) nor did it investigate the ocean's response to increased nutrient supplies from riverine nutrient inputs and nitrogen deposition.

Our model results reveal widespread increases in surface ocean temperature (0.5 K on average), which lead to an increased stratification and a decrease in the globally averaged mixed layer depth from 111 m to 92 m. The stratification is most affected in the tropical and subtropical open ocean, where the decreased mixed layer depth inhibits nutrient supply from the deeper layers and thereby decreases the open ocean NPP in these regions by 0.2 Pg C yr^{-1} and 0.1 Pg C yr^{-1}, respectively. Increases in the mixed layer however also take place due to enhanced mixing in some regions, leading for instance to an NPP increase in the Southern Ocean (0.3 Pg C yr^{-1}), for which other modelling studies have reported changes of varying magnitudes and signs (Laufkötter et al., 2013; Laufkötter et al., 2015)). We also observe a physically induced increase in the NPP in upwelling regions of the open (e.g North Pacific) and coastal (e.g. Benguela Current System) oceans. This result is in agreement with the suggestion that upwelling in EBUS regions might have been enhanced due to the strengthening of coastal parallel winds in such regions (Bakun, 1990). It could however also imply that nutrients accumulate in the deeper subsurface oceanic layers due to the weakening of the vertical exchange observed in the open ocean, and are only made available to biology again in these upwelling regions where they would strongly enhance NPP. In the coastal ocean outside of EBUS, physical changes are difficult to disentangle; we do not observe a clear tendency towards increases or decreases in the mixed layer depth. The changes in coastal NPP are also variable in sign and in magnitude, which we suggest might be caused by complex evolutions in regional atmospheric circulation patterns.

In terms of the impacts of riverine inputs, their change during the 20th century leads to an increase in the global oceanic NPP (+2.13 Pg C yr^{-1}, for all perturbations), which largely dominates the effects of the physical changes at the global scale. This 4% increase in the global NPP is even stronger in relative terms for the coastal ocean, with a 15 % increase in NPP corresponding to an absolute flux of 0.42 Pg C yr^{-1}. The signal of river-induced increase in

biological productivity however also largely spreads to the open ocean (+1.71 Pg C yr^{-1}).

In the simulations, the 20th century increase in anthropogenic CO_2 uptake by the global ocean is 1.72 Pg C yr^{-1}, with an 0.11 Pg C yr^{-1} increase in the coastal ocean and 1.61 Pg C yr^{-1} in the open ocean. The increase in the anthropogenic sink is largely caused by the atmospheric CO_2 perturbation (1.64 Pg C yr^{-1}), with only a small decrease caused by ocean physical changes (0.04 Pg C yr^{-1}) and a slight riverine-induced increase (0.13 Pg C yr^{-1}). The riverine-induced sink, which is caused by the enhancement of the biological production, thus contributes 8% to the global ocean CO_2 sink.

Our study is the first to address the P and N budgets in the global coastal ocean using a spatially resolved approach. The model results suggest an efficient export of riverine nutrients associated to organic matter, which explains why the riverine-induced NPP enhancement is also substantial in the open ocean. In quantitative terms, we simulate that 33% and 73% of the increasing anthropogenic riverine supplies of P and N are respectively transported offshore. These offshore transports are within the vast bounds reported in the recent studies by Sharples et al. (2017) and Izett and Fennel (2018), with export fractions comprised between 2.8–80 % for P and 7.3–90 % for N. The parametrized approaches of Sharples et al. (2017) and Izett and Fennel (2018) were partly motivated by the assumption that state-of-the-art global circulation models were not capable of representing offshore exports of freshwater and nutrients. We however show that our model provides reasonable estimates of coastal residence times (Chapter 3) while taking into account the 3-dimensional structure of the coastal ocean dynamically. The circulation state of the coastal ocean should furthermore be improved in the TP04 resolution used here.

While the combination of NPP and increased coastal stratification potentially causes an increase in coastal hypoxia, the extent of these changes is difficult to quantify. In the model, we observe a substantial decrease in minimum oxygen concentrations in the East China Sea and Black Sea, most likely due to enhanced riverine inputs. In the Barents Sea, the stratification is increased, which leads to less ventilation and to a lower oxygen minimum. Regions of strong decrease in oxygen minimum are in part comparable with regions identified in the recent review study of Fennel and Testa (2019). Regions, which are characterized by both NPP increases and mixed layer depth decreases in our

global study, could therefore be identified as regions of strong vulnerability to hypoxia under present-day conditions and in the future.

Finally, we confirm our findings from Chapter 3 that the pre-industrial coastal ocean was net autotrophic, although even more strongly in this case (NEP=0.25 Pg C yr^{-1}), due to the efficient transport of organic matter from the coastal ocean across the shelf (0.42 Pg C yr^{-1}). This horizontal biologic pump contributes to a coastal CO_2 sink under pre-industrial conditions of 0.05 Pg C yr^{-1}, which is roughly similar to the value suggested in Chapter 3 for the same tDOM degradation rate (coastal sink of 0.06-0.08 Pg C yr^{-1}).

The perturbation in the coastal NPP and CO_2 flux is spatially highly variable. While previous studies partly disagreed in the efficiency of the coastal ocean anthropogenic CO_2 uptake (Bourgeois et al., 2016; Laruelle et al., 2018), our study permits a global analysis supported by a relatively detailed representation of the coastal ocean. Our results show that the increase in the CO_2 sink during the 20th century is much larger than average in mid to high latitude regions and in EBUS, while tropical coastal zones and most Arctic regions partly counterbalance this increased CO_2 sink. The Arctic shelves, which contribute to over 20% of the global shelf in our definition, could be regions of inefficient CO_2 uptake due to substantial ice coverage over the whole year, which on one hand inhibits the thermal exchange during winter months, while also inhibiting the air-sea gas exchange during the coldest months of high carbon uptake potential. Taken that the Laruelle et al. (2018) study might put more emphasis on regions acting as disproportionate sinks (mid to high latitudes, excluding the Arctic Ocean, due to the availability of data in these regions, part of the discrepancy between their results and the present study could be explained by this spatial bias. The disagreements could also be due to the different time-periods analysed. While we use the start and the end of the 20th century to diagnose the perturbation, Laruelle et al. (2018) evaluate the coastal CO_2 sink on a much shorter time-scale.

Observational data and models have been unable to agree on the magnitude and sign of past changes in global ocean NPP. Nevertheless, global models have the tendency to project substantial decreases in NPP for the 21st century, although these are strongly variable between different models (Bopp et al., 2013). It is however important to recognize that these models fail to realistically represent coastal ocean physics and biogeochemistry despite their often-stated importance for the oceanic carbon cycle. Furthermore, the increases in oceanic nutrient supplies have not yet been considered in model

studies. While our results are based on a single model study, we show that physical changes in EBUS systems and riverine nutrient perturbations both have significant impacts on the NPP that may counteract the suggested decrease due to enhanced stratification. The stimulation of nutrient inputs via the upwelling and riverine routes could further be strengthened in the future due to climate and land-use changes. Therefore, our study reveals that improved representations of land-derived nutrient supplies, as well as of physical and biogeochemical processes in the coastal ocean are important to fully grasp the effects of anthropogenic perturbations on the global ocean carbon cycle over the historical period and in the future.

Chapter 5

Summary and conclusions

In this thesis, several topics relevant to the influence of riverine carbon and nutrient exports on the ocean's biogeochemistry were addressed, from the estimation of pre-industrial riverine fluxes using weathering and land export models to the complex perturbation of the ocean carbon cycle during the 20^{th} century. A synthesis of carbon fluxes can be found in Figure 5, where terrestrial and oceanic pre-industrial fluxes are derived from all chapters and the anthropogenic perturbations for the oceanic fluxes are taken from Chapter 4. In Chapter 2, I first presented a framework pre-industrial land-ocean riverine exports dependently on Earth System Model (ESM) variables. As a novelty here, we used state-of-the-art models to quantify weathering yields of biogeochemical compounds, as well as estimates for other sources (anthropogenic and atmospheric), and also accounted for their transformations to organic matter. The implications of these exports for oceanic NPP and CO_2 fluxes were assessed at the global and regional scales in a spatially resolved global ocean biogeochemistry model. In Chapter 3, I focused my research on the enigmatic land-ocean transition zone, the coastal ocean, by firstly assessing the state of physical indicators such as the mixed layer depth and coastal water residence times in the MPI-OM, and secondly deriving coastal carbon fluxes for the present-day and the pre-industrial time periods. For this I considered a range of plausible organic matter mineralization rates for terrestrial dissolved organic matter (tDOM), as well as for organic matter remineralization in coastal sediments. In Chapter 4, I analysed the contributions of anthropogenic perturbations related to atmospheric CO_2 concentration, physical climate and riverine nutrient supplies, to changes in oceanic NPP and air-sea CO_2 fluxes at the global as well as on the regional scale. To conclude this thesis, I now revisit the research questions stated in the introduction in the light of my own results, and discuss their implications for future research.

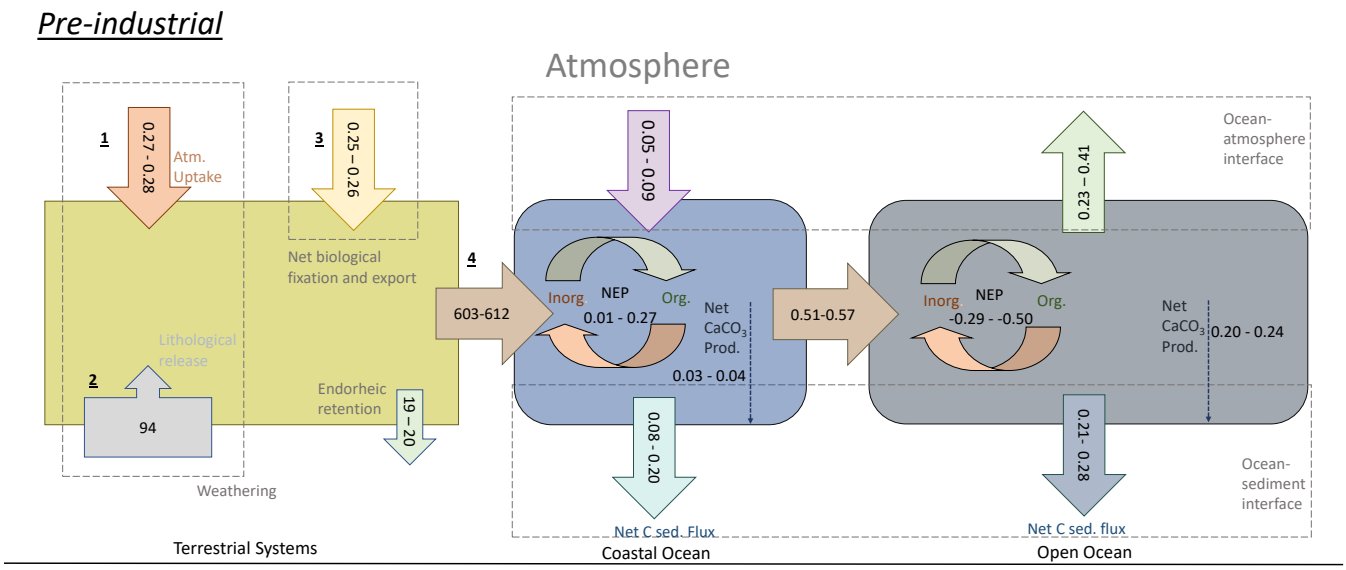

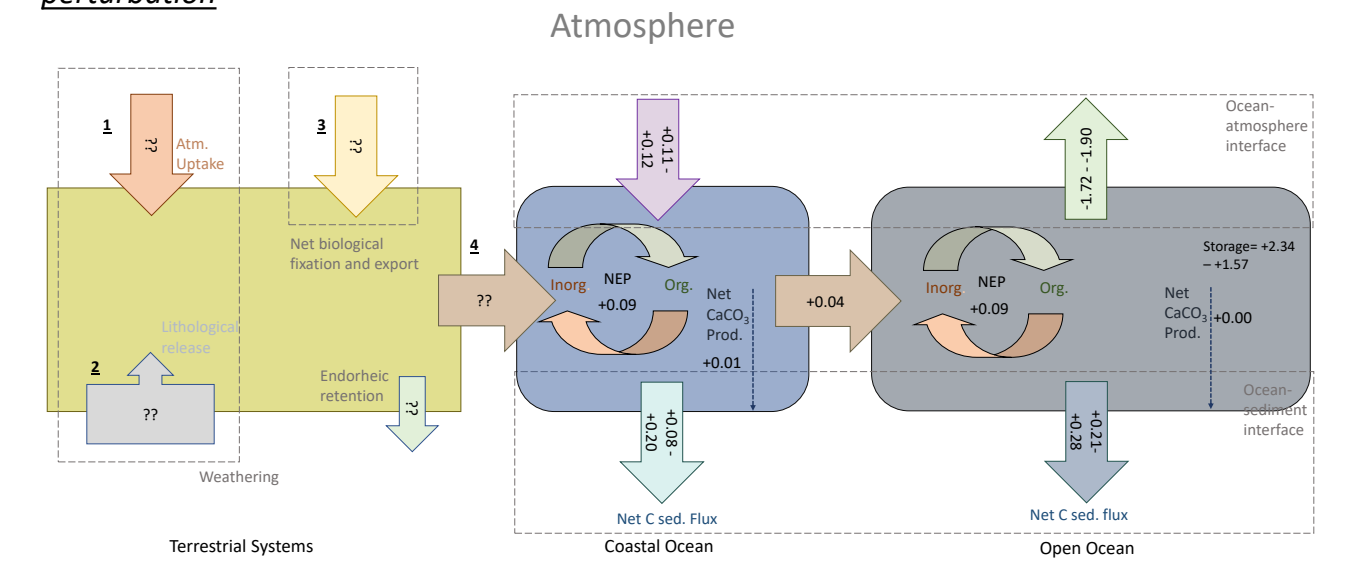

Chapter 2: Oceanic CO_2 outgassing and primary production hotspots induced by pre-industrial riverine nutrient and carbon exports in a global model approach

- What are the magnitudes of pre-industrial biogeochemical riverine exports derived from a hierarchy of state-of-the-art modelling approaches for weathering yields and land-ocean organic exports, and how do they compare to published estimates? Which regions show a disproportional contribution to global riverine exports?

I derived riverine exports based on inputs to catchments from weathering and non-weathering (atmospheric, anthropogenic) sources. In this specific approach, which is developed with the aim of being used in state-of-the-art Earth System Models (ESM), I constrained the inputs for the year 1850, for which anthropogenic inputs to river systems were already contributing to the total fluxes (Filippelli, 2008; Beusen et al., 2016). I furthermore estimated the transformation of inorganic compounds to organic matter based on global ratios of organic matter consistence assumed to the best of my knowledge (i.e. C:N:P:Fe ratios) . The approach leads to pre-industrial exports of 3.7 Tg P yr^{-1}, 27 Tg N yr^{-1}, 168 Tg Si yr^{-1} and 603 Tg C yr^{-1}, which are entailed with a degree of uncertainty, taken that data to validate them are essentially missing. The estimates are however consistent with values reported in previous approaches (P: 2-4.5 Tg P yr^{-1}, N: 19-21 Tg N yr^{-1}, Si: 158-200 Tg Si yr^{-1}, 450-950 Tg C yr^{-1}), although it is important to recognize that modelled land-ocean exports remain poorly constrained even for the present-day (Beusen et al., 2016).

The tropical Atlantic region in the approach is identified as a major source of carbon loads to the ocean, supplying 20% of global carbon loads, mostly due to the large exports from the Amazon River. Further tropical regions such as South East Asia and the Indo-Pacific islands are also hotspots of carbon export. The Arctic catchments, due to their vast surface area and large runoff, also deliver a considerable amount of carbon (12 % of global carbon loads) to the Arctic Ocean. The nutrient supplies largely follow the same distributions, which confirms that runoff is the main control factor of the export of biogeochemical compounds in state-of-the-art catchment models (Bauer et al., 2013). While we observe from the models used that riverine carbon fluxes are dominated by dissolved inorganic carbon (DIC) inputs (and therefore higher alkalinity) in the Arctic, the tropical regions deliver organic carbon dominantly. In particular, the Southeast Asian and Indo-Pacific catchments are strong sources of particulate organic carbon (POC), which dominate the total land-ocean carbon exports in these regions. The erosion of POC is strongly driven by extreme events such as storms (Hilton et al., 2008), which are not modelled explicitly in global river models (Bauer et al., 2013). For the Southeast Asia and Indo-Pacific islands regions, the representation of such extreme events, which release large amounts of particulate matter to the ocean, might significantly contribute to the yearly carbon exports. A better consideration of these short timescale events, which are not incorporated in approaches such as Global-NEWS2 (Seitzinger et al., 2010), is an important future challenge to predict present and future riverine loads in these regions.

A significant caveat in the approach developed in this chapter is the omission of in-stream retention. For nitrogen, substantial in-stream retention is plausible, since denitrification causes an N loss through outgassing of nitrogenous gases (Laursen and Seitzinger, 2002). For phosphorus in-stream retention takes mostly place through deposition in freshwater sediment (Kronvang et al., 2007), for which little observational constraints exist at the global scale. Filippelli (2008), for instance, synthesized the global phosphorus cycle from terrestrial transformations to its fate in the ocean, but in-stream retention is even not mentioned. Using a spatially resolved modelling approach, Maavara et al. (2015) proposed significant retention of phosphorus of up to 12 % of the global input flux to catchments mostly attributed to river damming. The modelling study by Beusen et al. (2016) however suggests even higher retention efficiency, with around half of the phosphorus retained during transit under pre-industrial conditions when river damming was not thought to be a significant retention factor. For present-day, the Beusen et al. (2016) study also estimates a global land-ocean export of around 4 Tg P yr^{-1}, which is significantly lower than the 11 Tg P yr^{-1} computed using the NEWS2 model. It remains however unclear which precise mechanisms could contribute to this substantial decrease and whether catchment exports were largely overestimated in the past, partly because there is no thorough validation regarding the magnitude of retention in the modelling studies.

- *How do the riverine exports impact CO_2 outgassing and NPP fluxes in the ocean, both at the global and regional scale, and are the identified hotspots of riverine exports also reflected in disproportionate regional changes to the oceanic indicator variables?*

To investigate the effects of riverine fluxes globally and regionally, I performed model simulation to equilibrium using an extended version of HAMOCC, where the pre-industrial riverine supplies are added to the model at the catchment's river mouths. This simulation was compared to the standard HAMOCC version, where nutrients, carbon and alkalinity are added homogeneously throughout the ocean to compensate for sediment burial losses of these compounds. Despite increased riverine inputs in comparison to the reference simulation, global variables related to ocean production (e.g. NPP, nutrient surface concentrations, calcium production, silicate production) are almost all reduced, which indicates that the coastal ocean acts as an increased biogeochemical sink in the model. This is due to the new location of the model inputs; in the coastal ocean, the freshly produced organic material sinks to the

sea floor faster, whereas in the open ocean, the produced organic matter has a longer residence time within the water column, thus being remineralized to a greater extent before potentially reaching the sediment. This result agrees with literature to a certain extent, a large part of the organic burial and calcium carbon exports to the sediment being reported to occur within the coastal zone (Milliman and Droxler, 1996; Gattuso et al., 1998; Muller-Karger et al., 2005; Chen and Borges, 2009). However, the modelled burial rates of organic matter in proportion to the deposition flux from the ocean, which are later analysed in Chapter 3, are higher in comparison to the range suggested by Krumins et al. (2013) in a review of literature estimates. Arndt et al. (2013) also suggested higher remineralization rates in coastal sediments compared to those in the open ocean. For these reasons, I increased the coastal sediment organic matter remineralization rates in Chapter 3, an adjustment that could have some impacts on the results shown in Chapter 2. As a result of a tighter benthic-pelagic coupling, I would expect a slightly higher global and regional NPP and higher nutrient concentrations than those reported in Chapter 2.

The addition of river nutrients at their correct geographical location in my experiment not only slightly decreases the global NPP and nutrient concentrations, but also affects their regional distributions. When considering riverine fluxes in HAMOCC, coastal NPP and surface nutrient concentrations are especially increased near river mouths, although most hotspots of NPP remain very similar to those identified in the reference simulation. This result confirms that the oceanic physical circulation is a dominant driver of the distributions of biogeochemical processes in comparison to changes in the spatial distribution of the ocean biogeochemical inputs (i.e. of the riverine inputs).

Regarding CO_2 dynamics, the increased terrestrial carbon inputs with respect to the standard model inputs, which are in essence "CO_2 neutral", lead to a long-term outgassing flux at model equilibrium of 231 Tg C yr^{-1}, which is caused by inorganic and organic carbon inputs. In the case of the inorganic inputs, the riverine C:Alk inputs ratio of 1:1 is higher than the 1:2 export ratio to the sediment (as $CaCO_3$). Therefore over the whole lifecycle of alkalinity in the ocean, from its input to its export to its export to the sediment, the DIC and thus the pCO_2 in the ocean is increased. For the organic matter, the C to nutrient ratio of tDOM is much larger than the one associated to the organic matter export flux to the sediment, which also increases the ocean's pCO_2, thus causing a long-term net outgassing flux. The outgassing is found mostly

in proximity to river mouths, but it can be observed further offshore such as in the open tropical Atlantic. In Aumont et al. (2001) and Resplandy et al. (2018), the interhemispheric transport of carbon is suggested to carry significant amounts of riverine carbon between latitudes and to cause outgassing in regions differing from those where riverine inputs occur. My simulation results are consistent with this hypothesis, and I observe a much stronger CO_2 outgassing in the southern hemisphere compared to the riverine carbon inputs received by this hemisphere. Furthermore, the Southern Ocean also shows an outgassing flux sustained by riverine C inputs, which could originate from the transport of river borne carbon via the deep ocean route.

- *What are the magnitudes of terrestrial sources and oceanic fate of the riverine carbon and how is the long-term terrestrial sink of atmospheric CO_2 balanced with respect to the oceanic source of atmospheric CO_2?*

By combining the results from the weathering, land export and ocean biogeochemistry models used in my thesis, I have provided a quantitative assessment of the origin and sources of carbon within the land-ocean system. Details are provided in Chapter 2, but here, I revisit my quantitative assessments in the light of published literature. First, the net CO_2 uptake caused by weathering (0.2 Pg C yr^{-1}) is comparable to the value reported in the synthesis study by Regnier et al. (2013) (0.3 Pg C yr^{-1}). A total land biological uptake (including terra-firm and inland aquatic system fluxes) can be approximated from Regnier et al. (2013) by balancing all fluxes from and to the atmosphere, while omitting the weathering uptake component. The net biological uptake and export to river systems in our approach (0.3 Pg C yr^{-1}) is significantly smaller than the 0.7 Pg C yr^{-1} calculated from Regnier et al. (2013). This is mostly likely due to the relatively low DOC and POC land-ocean exports modelled in the NEWS2 study (Seitzinger et al., 2010), from which the net land biological uptake used in my framework is derived. In the ocean, a fractionation of the long-term fate of the carbon was done based on the fundamental inorganic and organic carbon process equations of the ocean biogeochemistry model. From model equations, I derived the contribution of inorganic carbon riverine loads (0.18 Pg C yr^{-1}) and organic carbon riverine loads (0.13 Pg C yr^{-1}) to the total CO_2 outgassing flux. I was also able to constrain the CO_2 long-term sink (0.06 Pg C yr^{-1}) caused by the terrestrial inputs of dissolved inorganic nutrients and corresponding shifts in alkalinity, which enhance the biological uptake of carbon. The uptake of nutrients furthermore creates a carbon sink (0.02 Pg C yr^{-1}) due to alkalinity increases caused by primary production

(Wolf-Gladrow et al., 2007). In Regnier et al. (2013), the outgassing flux in the ocean is estimated at 0.5 Pg C yr^{-1}, with all of the flux occurring in the open ocean. This higher value is not surprising, since the outgassing flux is strongly dependent of the riverine carbon loads, for which the Regnier et al. (2013) study estimates at a significantly larger magnitude (1 Pg C yr^{-1} for carbon excluding physically eroded particulate inorganic carbon), whereas I estimate 0.6 Pg C yr^{-1} in my framework. The simulations in Chapter 2 also estimates a slightly lower sediment burial flux (0.4 Pg C yr^{-1} in Chapter 2 vs 0.6 Pg C yr^{-1} in Chapter 3).

The performed quantification of the sources and fate of terrestrial carbon neglects feedbacks to the atmospheric Earth system component, since the atmospheric state is completely fixed and only used to drive the terrestrial and oceanic models in my simulations. Coupling the land models, the ocean model and the atmospheric component would however be possible within an ESM framework. In order to close the riverine loop in the ocean model and balance the land carbon uptake and the oceanic carbon outgassing for the pre-industrial state would require the addition of a long-term flux from volcanic carbon emissions (e.g. from Burton et al. (2013)), as well as from organic carbon oxidation in shale (e.g. as estimated by Sarmiento and Sundquist (1992)).

Chapter 3: The efficient cross-shelf export of organic matter in the coastal ocean: Were continental shelves already a global pre-industrial CO_2 sink?

- *What are the water residence times and mixed layer depths on continental shelves at a global and regional scale, and how do the global model results compare with reported regional estimates?*

  By performing simulations with an inert dye tracer that was added at river mouths for the whole coastal ocean, I determined the coastal water residence time on shelves, and the residence time of freshwater globally as well as regionally. Overall, the spatial patterns of water residence times on the shelves compared relatively well with published global (e.g. Sharples et al. (2017)) and regional estimates. For instance, coastal water residence times on narrow, plume dominated shelves such as the tropical West Atlantic shelf are under one month, as reported by the model results of Sharples et al. (2017) or in a field experiment using

natural Ra isotopes by Moore and Oliveira (2008). For Arctic shelves, such as the Laptev Sea, the residence times are very long and often exceed one year as previously reported by Sharples et al. (2017) and by e.g.Schlosser et al. (1994) for the Laptev Sea. Parameterized approaches by Sharples et al. (2017) and Izett and Fennel (2018) were developed with the justification that state-of-the-art global circulation models were not capable of representing complex plume dynamics and therefore the residence times of biogeochemical compounds on the shelves. I however show in Chapter 3 that the residence times approximated with my model using a relatively coarse set-up result in values very similar to those based on the parametrized approaches. The advantage of using HAMOCC is that it also considers important 3-dimensional features such as stratification on the shelves and the full coupling of the dynamical biogeochemical processes taking place within the coastal zone.

The globally averaged residence times in the model (16 months for coastal waters, and 14 months for freshwater) might also be slightly overestimated, since I show lower residence times in Chapter 4 using a model with a finer resolution grid. The shorter residence time is mostly explained by the improved representation of narrow shelf regions, which can only be captured in the finer resolution set-up.

From the computation of coastal water residence time combined with the magnitude of global freshwater inputs, I derive that the inflow from the open ocean is much higher than the freshwater inputs in the model (approximately 40 times higher). This has profound implications for the understanding of the coastal ocean biogeochemistry, since the open ocean inflows and their biogeochemical characteristics have a much larger impact on continental shelves than previously thought. Our results also reveal that box model approaches, which tackle the historical perturbation of the carbon cycle in the coastal ocean while assuming much longer residence times, likely strongly overestimate the biogeochemical processing on the shelves (i.e. remineralization), at the expense of offshore export. For instance, Andersson et al. (2005) used coastal zone residence times ranging from 4 to 11 years, although they acknowledge the strong dependence of their results on this highly uncertain variable. At such a long residence time, more organic matter would be mineralized, leading to lower NEP, higher DIC stocks and higher

CO_2 outgassing fluxes. The discrepancy in coastal water residence times provides likely one of the main explanations on why the pre-industrial CO_2 fluxes in this thesis differ from those reported in the conceptual box model studies.

Another important insight from the simulation of physical ocean variables is that the coastal mixed layer depth rarely reaches the coastal sea floor despite the shallowness of the coastal zone. This is especially the case on shelves dominated by large river inputs, such as the tropical West Atlantic shelf. A shallower mixed layer depth than the sea floor depth implies that the coastal ocean is not fully mixed vertically and that a decoupling between the dominating autotrophic processes in the euphotic zone and the dominating heterotrophic processes below the euphotic layer takes place. Therefore, taken that box model approaches tackling the coastal ocean carbon cycle omit vertical spatial variability, it is expected that key processes such as autotrophic and heterotrophic dynamics, NEP and air-sea CO_2 exchange will differ from those reported in my study.

- *Were continental shelves heterotrophic or autotrophic when considering a range of plausible tDOM and shelf sediment remineralization rates in the model?*

  tDOM is suggested to be an important control factor of the trophic state of the coastal ocean (Cai, 2011). To investigate this research question, I applied a plausible range of tDOM remineralization rate constants, at which tDOM contribute to a few percent of Atlantic and Pacific total dissolved organic material (DOM) concentrations. An important result is that of the 0.23 Pg C yr^{-1} tDOM inputs supplied to the ocean by rivers, 0.12-0.17 Pg yr^{-1} is exported offshore. In addition, sediment organic matter remineralization rates were enhanced by over a factor 2 compared to Chapter 2, leading to higher coastal ocean NPP in agreement to what is reported in the literature. Using this set-up, I found that the coastal ocean is net autotrophic for all plausible (terrestrial and marine) organic matter mineralization rates. Thus, the coastal ocean biology acts as a net sink of DIC in the model, even for the pre-industrial state. The fundamental mechanisms explaining the autotrophic state of the coastal ocean is firstly the efficient cross-shelf export of organic matter delivered by rivers or newly produced on the shelf, as discussed previously. Secondly, the dominant influence of open ocean water inflows brings nutrient enriched waters to many productive coastal regions (e.g. Patagonian

Shelf), thereby inducing enhanced primary production and shifting the NEP towards autotrophy. Indeed, the open ocean inflows usually also have low organic matter concentrations, since they usually originate from subsurface layers, and therefore do not usually strongly enhance heterotrophic processes (Chen and Borges, 2009).

We observe gradients in NEP both in the horizontal and in the vertical planes. For instance, the NPP is very efficient in the tropical coastal regions (e.g. the Sunda shelf), or when open ocean inflows rich with nutrients supply coastal regions (e.g. southern Patagonian shelf). In the vertical, the decoupling of autotrophic and heterotrophic processes due the incomplete mixing of the coastal ocean induces a gradient of NEP, from very positive near the surface to being more negative with increasing depths. Both of these gradients have important implications for the air-sea exchange, as discussed below.

- *Was the coastal ocean a sink or a source of atmospheric CO_2 and which factors exert an important control for the global flux?*

  In the validation step for present-day conditions, we show that our model results are in good agreement with the recent coastal pCO_2 data-product of Laruelle et al. (2017), despite the relatively coarse resolution used in this chapter. This result suggests that representing mean physical features might be sufficient to represent the main pCO_2 distribution features of the global coastal ocean.

  For the pre-industrial state, the simulations reveal that coastal ocean is a slight global CO_2 sink (0.06-0.08 Pg C yr^{-1}), in stark contradiction to the conclusions obtained from box models that the coastal ocean was a relatively strong CO_2 source for this time-period (Mackenzie et al., 2004; Andersson et al., 2005). The global sink mostly occurs in the large extra-tropical shelves such as the Barents Sea, Patagonian Shelf, North Sea and Sea of Okhotsk.

  This discrepancy can on the one hand be explained by the net autotrophic state of the coastal ocean in our simulations. The computed CO_2 sink is however larger than what could be expected from the NEP, in part since a positive NEP also inducing positive changes in alkalinity (Wolf-Gladrow et al., 2007). Furthermore, the vertical decoupling of remineralization and primary production due to the shallow mixed layer depths also favours a CO_2 sink compared to a situation where the coastal ocean is

assumed vertically well mixed as in a "box-model" perspective. Regionally, I also observe that the NEP and the CO_2 flux can be completely decoupled, and even have different signs. In some of these regions with strong decoupling, the physical and biogeochemical properties of the ocean inflows likely dominate the CO_2 signal. For instance, in the Barents Sea, a cooling of North Atlantic inflows takes place, which increases the CO_2 solubility of the water masses. On the Sunda Shelf, a heating of the water masses likely takes place, due to the strong radiative heat transfer from the atmosphere and shallow water depths. In Arctic regions with winter ice-coverage (e.g. in most of the Laptev Sea), the sea-ice likely plays a large role in inhibiting the CO_2 uptake during the cold winter months.

The global sink is thereby mostly caused by the large extra-tropical shelves of the Barents Sea, Patagonian Shelf, North Sea and Sea of Okhost. The coastal ocean sink of 0.06-0.08 Pg C yr^{-1} derived in this chapter implies that the coastal ocean is a less efficient CO_2 sink than the open ocean, assuming the present-day sink of 0.15 Pg C yr^{-1} derived by the transient model simulation.

I acknowledge some uncertainty in the magnitude and sign of the CO_2 flux, for instance due to the omission of shallow shelf carbonate production, or the riverine inputs of soil dissolved CO_2. However, the main mechanism causing this sink, which is the large oceanic inflows that also cause an efficient cross-shelf export of terrestrial and marine organic matter delivered to or produced on the shelves, is also shown to be underestimated in the model configuration of this chapter, as evidenced by the results obtained in the higher resolution configuration of Chapter 4.

Chapter 4: The multifaceted 20th century perturbation of the oceanic carbon cycle: Could coastal ocean and river-induced increases in NPP trump implications of increased open ocean stratification?

- *How strongly do the isolated and combined 20^{th} century perturbation of atmospheric CO_2 concentrations, the physical climate state and changes in riverine nutrient supplies affect the NPP and CO_2 fluxes in the open and coastal ocean?*

In this chapter, sequential model simulations were performed to isolate impacts of anthropogenic perturbations of atmospheric CO_2, changing ocean circulation features and riverine nutrient loads on oceanic NPP and CO_2 fluxes. While the changes in the atmospheric CO_2 concentrations solely impact the ocean's inorganic carbon cycle, changes in the physics and riverine inputs perturb all facets of ocean biogeochemical cycling. When considering the physical oceanic perturbation, the NPP shows a slight decrease in the open ocean. This decrease is spatially variable, with a relatively strong decrease taking place mostly in the open ocean in lower latitudes, whereas in the Southern Ocean a strong NPP increase can be observed due to enhanced vertical mixing. The decrease in open ocean NPP is also compensated by an increase of coastal NPP along Eastern Boundary Upwelling Systems (EBUS), and even in some open ocean upwelling regions such as in the North Pacific. These EBUS regions are likely much better represented in the model configuration used in this chapter (0.4 degrees) than in previous studies such as Laufkötter et al. (2013), who do not observe these regional increases.

In stark contrast with the ocean physics, the enhanced riverine supplies of nitrogen and phosphorus substantially enhance the global oceanic NPP (+4 %), especially in coastal regions (+15 %). This NPP enhancement also trumps the slight decrease in the open ocean NPP induced by changes in ocean physics in the model globally. While previous modelling studies have simulated and discussed changes in NPP due to oceanic physics, my research is the first one to assess the impacts induced by enhanced nutrient supplies from land in a 3-D ocean general circulation model framework (Laufkötter et al., 2013; Laufkötter et al., 2015). Our attribution analysis is consistent with the results of a regional modelling study addressing the effects of increased atmospheric nitrogen deposition during the 20^{th} century, and which reveals a significant stimulation of the NPP in the Pacific Ocean (Yang and Gruber, 2016).

The high sensitivity of NPP to historical changes in the physical state of the ocean in EBUS regions and in enhanced nutrient supplies in both coastal and open oceans globally has important implications for future projections. In Bopp et al. (2013), stratification-induced changes in nutrient availability cause a 21^{st} century decrease in NPP of around 9 % in an ensemble of global models, albeit the models compared show very large differences, with a quantified standard deviation of around 8

%. In the compared models of the Bopp et al. (2013) study, EBUS regions were very poorly represented because of the coarse model resolutions (e.g. as suggested in Milinski et al. (2016)) and increased riverine and atmospheric nutrient supplies were not considered. While it is unclear if the global riverine exports of nitrogen and phosphorus will continue to raise substantially, even maintaining riverine exports at present-day levels will likely cause further enhancement of the NPP, due to the long residence times of nutrients in the ocean (estimated at 10-20 10^3 years for phosphorus by Filippelli (2008)) and the oceanic biogeochemical state is thus not yet in equilibrium with the present-day perturbation. From these findings, I conclude that changes in nutrient supply have a substantial impact on the biological pump and should be considered in models.

- *How are coastal nutrient and carbon cycling fluxes, with the cross-shelf export as a focal point, affected by the net anthropogenic perturbation of the ocean?*

  In the pre-industrial state, I observe a net organic P and N export from the coastal ocean, and a net supply of inorganic N and P from open ocean inflows, which underlines the importance of open-coastal ocean exchanges for the primary production of the coastal ocean. The net export of N and P across the shelf break is relatively inefficient in the model for the 1900-1910 timeframe, due to large inflows of inorganic P and N from the deep that largely compensate the surface exports. The increase in the P and N supplies due to rivers increases both the organic and inorganic export of P and N, and the net offshore export becomes more efficient. For present-day, I estimate that 33 % and 73 % of the P and N riverine anthropogenic perturbation are exported offshore, respectively. Previous assessments from global parametrized approaches by Sharples et al. (2017) and Izett and Fennel (2018) report a vast range for these net exports of P and N (4-90 %) and are thus very inconclusive. Therefore, I advocate that fully resolved physics and biogeochemical models might provide better estimates of the fate of nutrients on the continental shelves globally.

- *Which established regions of the coastal ocean with similar biogeochemical attributes are most affected in their NPP and CO_2 fluxes?*

  In order to assess the global effects of the anthropogenic perturbations on the biogeochemistry of coastal regions, I used the MARCATS coastal

segmentation approach of Laruelle et al. (2013), which fractionates the coastal ocean into regions of similar catchment and continental shelf characteristics. While we find strong increases in NPP in almost all MARCATS (+2 - +58 %), the regions with the highest relative changes in their areal NPP are semi-enclosed coastal seas, most notably the Black Sea, and marginal seas, mostly the eastern Asian shelves. The combined impacts of anthropogenic perturbations (atmospheric CO_2, physical state, riverine nutrient inputs) on the coastal CO_2 flux is much more variable regionally. We find that regions such as the Japanese shelf and the Barents Sea contribute disproportionately to the 20^{th} century anthropogenic CO_2 sink, while several arctic and tropical regions are much less efficient than the average global ocean CO_2 sink. My model results therefore might help reconcile the studies of Laruelle et al. (2018) and Bourgeois et al. (2016), which disagree on whether the coastal ocean is a more efficient CO_2 sink than the global ocean. In my simulations, the coastal ocean is not a more efficient CO_2 sink than the global ocean on average, but consistent with Laruelle et al. (2018), I also find that in many of the regions investigated by these authors on the basis of available observations, the CO_2 sink is more efficient than average. The results described in Laruelle et al. (2018) are also relying on data collected from the late 1980s onwards, thus encompassing a much shorter timeframe than in the Bourgeois et al. (2016) and present studies, which investigate the perturbations since the beginning of the 20^{th} century. It is therefore also plausible that the global coastal ocean has become a more efficient carbon sink only recently, for instance, due to steeper increases in riverine nutrient exports during the late part of the 20^{th} century (Beusen et al., 2016).

- *Is it possible to identify coastal zones of increased 20^{th} century eutrophication and hypoxia using a global model framework?*

  In the literature, coastal eutrophication is related to two main factors: high organic matter fluxes to deeper water layers originating from allochthonous river exports and/or autochthonous primary production in the euphotic layer, and weak ventilation of these deeper layers (Fennel and Testa, 2019). In the model simulations for the 20^{th} century, I observed widespread increases in the NPP of coastal regions due to enhanced nutrient supplies from rivers. This enhanced organic matter supply is to a degree exported to deeper water layers and can potentially

cause oxygen depletion. To assess the ventilation of deeper coastal water layers, I used the mixed layer depth as a proxy for the vertical mixing of deeper layers. The regional changes in the mixed layer depths during the 20th century are spatially strongly variable, notwithstanding a clear global increase in coastal ocean temperatures. Despite the variable signal in coastal ocean mixed layer depths at the regional scale, a widespread decrease in minimum oxygen concentrations can be observed globally. This is particularly the case in regions identified as prominent zones of hypoxia (or "dead zones") as defined in Skogen et al. (2014) and Fennel and Testa (2019), such as the Black Sea, the Baltic Sea and the East China Sea. A quantitative assessment of this oxygen decrease, and its effects on dynamic ecosystems such as sea life, is however difficult to perform, since it is unclear which oxygen levels would be adequately describe "hypoxic conditions" in a relatively coarse model as is used in this chapter. Therefore, while we do observe decreased oxygen concentrations at depths globally, and especially in regions where eutrophication has been reported previously, the results presented in this thesis are inconclusive with respect to how strong of an assessment tool a global ocean model could be for identifying the forecasting zones of increased hypoxia in the future.

Important heterogeneities in the land and ocean systems

Throughout this thesis, important spatial heterogeneities in the factors affecting the carbon and nutrient cycles on land, rivers and ocean have been identified. For instance, weathering is affected by marked spatial patterns of the climate variables runoff and temperature as well as in lithological characteristics (Amiotte Suchet and Probst, 1995; Gaillardet et al., 1999; Hartmann et al., 2009; Hartmann and Moosdorf, 2011; Hartmann et al., 2014). These drivers lead to a much stronger supply of the natural nutrient, carbon and alkalinity fluxes to the wet and warm regions of the ocean. On the land biosphere side, light availability, runoff and temperature, vegetation types and topography all affect the organic carbon and nutrient exports from terrestrial to freshwater systems and, ultimately, to the ocean. In the latter, the biogeochemical dynamics is further controlled by the vertical dimension of the ocean, in particular the mixed layer depth and the bathymetry. Physical ocean features, from ocean circulation and transport, temperature, light availability and salinity, are strongly horizontally and vertically heterogeneous within

the ocean, which all profoundly impact the coastal and global ocean carbon and nutrient cycles. This is especially the case in the coastal ocean where continental shelves are of variable size and widths due to complex coastal ocean bathymetry. Furthermore, residence times of water on the shelves depend not only on the ocean circulation, but also on the freshwater runoff from land. Despite their shallow depths, the vertical structure of the physical variables on the shelves leads to a widespread spatial decoupling between autotrophic biological processes, which only take place in the upper euphotic zone, and heterotrophic processes, which dominate in the deeper layers. Other prominent examples of the importance of spatial features include the inter-hemispheric transfer of carbon needed to compensate the unequal riverine carbon inputs resulting from the uneven global distribution of landmasses. In addition, I have shown that open ocean inflows might have a dominant effect on the coastal zone biogeochemistry and, more specifically, on the magnitude of the pre-industrial CO_2 sink. Lastly, the simulations have revealed the strong inter-regional variability in the efficiency of the coastal ocean CO_2 uptake. While many mid latitude shelves are mostly large sinks for anthropogenic CO_2, tropical shelves and Arctic shelves show much large variations in the magnitude of their anthropogenic CO_2 sinks. Therefore, while conceptual box models such as those developed by Mackenzie et al. (2004) and Andersson et al. (2005) are very useful to advance our conceptual understanding of the physical and biogeochemical processes taking place in the coastal ocean, 3-dimensional models such as those used in this study result are imperatively needed to support the quantitative assessment of the coastal ocean biogeochemical dynamics such as the trophic state or the sign and magnitude of the air-sea CO_2 flux.

While the spatial heterogeneity of land and ocean biogeochemistry and their coupling have largely been ignored in the past, I have shown that state-of-the-art global modelling approaches of land inputs and ocean circulation now permit to capture these spatial heterogeneities at a spatiotemporal resolution compatible with computing power requirements, thus offering more robust conclusions than were made previously, with the coastal ocean being the main focal point.

Outlook

In this thesis, I derived pre-industrial land-ocean exports of important biogeochemical compounds as a function of ESM variables using a novel modelling framework. This framework provides a dynamical description of land-ocean transfers of nutrients, carbon and alkalinity, which can vary with climate state variables, for instance runoff. The framework also offers the opportunity to include recent model developments dedicated to the entire land-ocean-continuum, thereby further improving the analysis of land-ocean couplings over the historical period and in the future. For instance, instead of using DOC exports derived from catchment loads from NEWS2 (Seitzinger et al., 2010), DOC fluxes could be constrained from recent model developments representing DOC leaching in global dynamical terrestrial models (Nakhavali et al., 2018). Similarly, POC fluxes could be derived from a novel erosion module integrated in the land-surface scheme of an ESM (Naipal et al., 2018). Approaches have also recently been developed to simulate P weathering as a phosphorus source to global dynamical vegetation models (Goll et al., 2017a), and its subsequent channelling to soil organic matter. Global approaches quantifying biosphere fluxes of the N cycle have also been recently developed (e.g. Goll et al. (2017b)). For Si, large gaps of knowledge regarding its terrestrial biospheric fluxes and much remains to be done to incorporate this element in an ESM framework. While rivers dynamically transport freshwater to the ocean in many state-of-the-art ESMs, biogeochemical tracers have only been recently implemented at the catchment scale to describe their transport and transformation within inland waters across temporal scales, from seasonal to centennial (Lauerwald et al., 2017). To my knowledge, global scale applications are still to be developed, but such models have already been applied for the Amazon (Lauerwald et al., 2017; Hastie et al., 2019) and the Lena catchments (Bowring et al., 2019). Furthermore, biogeochemical transformations taking place in ecosystems right at the transition between land and ocean such as mangroves, tidal wetlands and estuaries could be included in the future, following regional assessments such as the one reported in Laruelle et al. (2013).

On the temporal scale, I did not take into account the seasonality of riverine exports in my thesis. These intra-annual variations can have strong impacts on the temporal distributions of the riverine loads to the ocean, as shown in, e.g. Le Fouest et al. (2013) for Arctic catchments. Furthermore, in a dynamical ESM setting, the impacts of extreme events in precipitation, runoff and temperature

could be assessed in the future. These extreme events have been suggested to be of particular importance for particulate organic matter exports to the ocean (Hilton et al., 2008; Bauer et al., 2013).

During this thesis, I have performed the implementation of three important features which improve the conceptual and quantitative representation of the coastal ocean physics and biogeochemistry in HAMOCC: the spatially-resolved representation of riverine supplies to the coastal ocean, the description of the fate of terrestrial dissolved organic matter in the ocean and the enhanced mineralization of particulate organic matter in coastal ocean sediments, which induces a stronger coupling between benthic and pelagic processes. While various processes could be further included, such as the shallow shelf benthic calcium carbonate production or the physical re-suspension of sediment particulate matter, the coastal ocean CO_2 dynamics simulated in our global ocean model set-up already shows relatively good agreement with recent pCO_2 data and observationally-based CO_2 flux estimates, which suggests that the current representation of the coastal ocean might already be adequate for the quantification of coastal processes at the global scale. Furthermore, while the results obtained with a relatively coarse model configuration show reasonable agreement of physical indicators such as residence times with regional observation estimates, suggesting that mean circulation features are important factors for the physical processes taking place in the coastal ocean, I nevertheless recommend using at the least a resolution similar to the TPO4 (0.4 degrees) as it provides a significantly improved global representation of bathymetries on the finer scale, especially for EBUS.

This thesis is, to my knowledge, the first one to consider the temporally increasing riverine nutrient supplies at the global scale in a spatially resolved ocean model. While the consequences of anthropogenic perturbations on the biological pump differ from model to model (Bopp et al., 2013; Laufkötter et al., 2015), I have shown that in the single model used here, the enhancement of the riverine supply might lead to a perturbation as large as the one due to increasing open ocean stratification. These results could be further substantiated by implementing the same river nutrient forcing in other models to determine whether such behaviour is reproduced across a larger range of global ocean models. Physically induced changes of the NPP in EBUS regions during the historical period could also be assessed using the current version of other ocean models. Both the changes caused by enhanced upwelling in EBUS regions and increased riverine supplies could furthermore be extended

to the future. Model results for the 21st century could then be compared to the projections synthesized in Bopp et al. (2013) and Laufkötter et al. (2015), which ignore these effects.

Appendix A

Appendix

A.1 Freshwater Fluxes

The freshwater loads from OMIP were already implemented in previous standard HAMOCC versions, in order to close the hydrological cycle. Globally, they add 32,542 km^3 yr^{-1} of freshwater to the ocean. These impact the salinity and the ocean stratification in the proximity of our biogeochemical riverine inputs, and therefore their advection within the ocean.

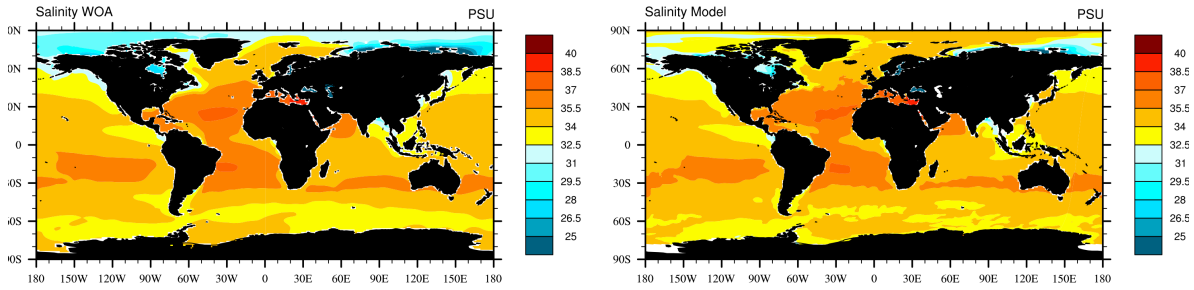

FIGURE A.1: Comparison of salinity from observational data (WOA) and modelled salinity in RIV (Salinity Model).

.

A.2 Coastal Salinity and Nutrient Profiles

Coastal vertical profiles show that despite the coarse resolution of our model, the features of salinity in selected coastal regions is comparable to WOA data, although vertical gradients are often not as strong as in the observational data (Figure A.2). For the Amazon Northward section, we see a vertical the salinity gradient in the WOA data, which is also reproduced albeit not extensively in the modelled data which induces stronger stratification of the water layers. In terms of absolute values the salinity is also well represented for the Ganges river, although the vertical stratification is also not quite as extensive further away from the coast. The bathymetry of the Laptev Sea at the Lena river mouth is poorly represented, as WOA data shows a height increase of the ocean floor at connection of the Sea with the Arctic Ocean, which is not represented in the model bathymetry. The salinity gradient in the East Chinese Sea is very strong due to currents parallel in the model which are also shown in observations (Ichikawa and Beardsley, 2002). Smaller currents in this region and in the Yellow Sea are however not well represented in the model. The Congo river has a very steep coastal shelf, and therefore the salinity relatively strong vertical horizontal gradient, due to little bathymetry induced vertical mixing, as well as heating of the surface waters.

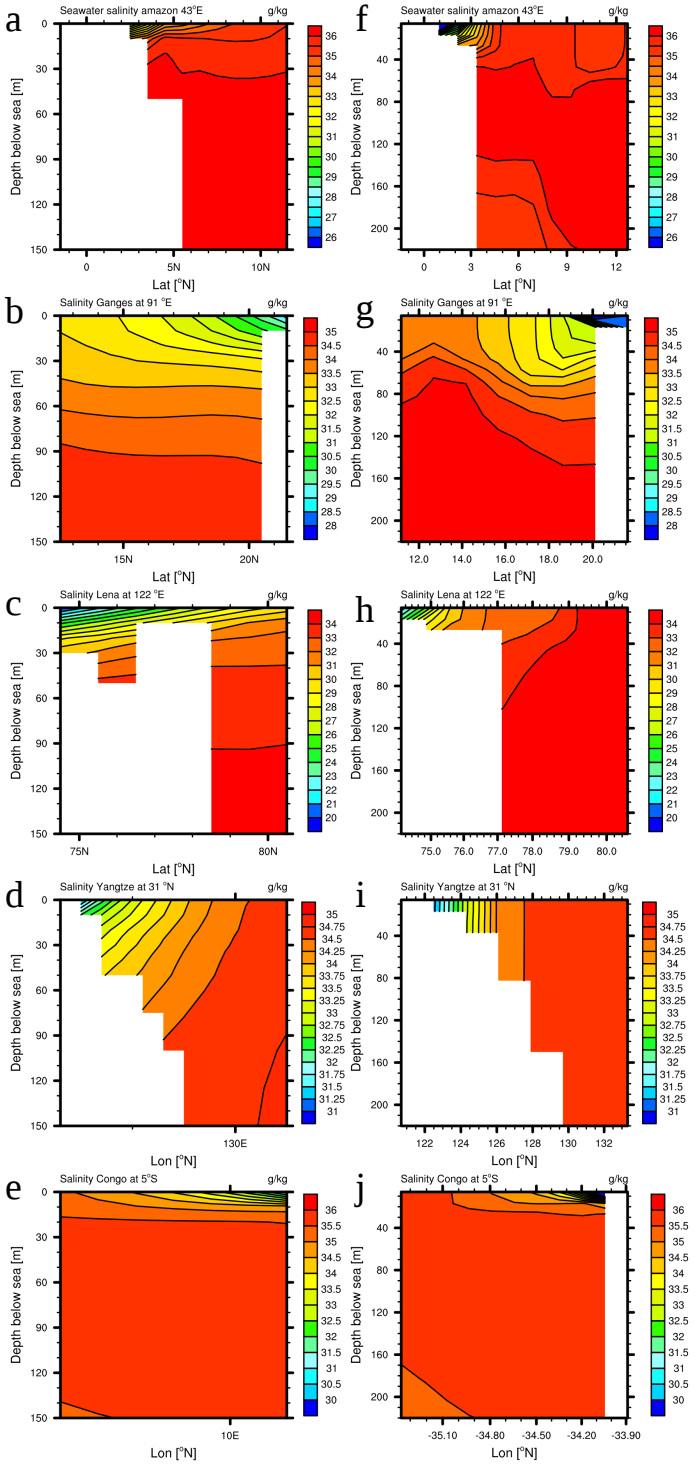

FIGURE A.2: Vertical profiles of the coastal bathymetry and salinity, along specific longitudes and longitudes for chosen river mouths. The left column (a-e) is made of WOA salinity profiles, whereas the right column (f-j) of profiles from model simulation RIV. a & f are shelf and salinity profiles at the Amazon river (TWA), b & g for the Ganges river, c & h Lena river, d & i Yangtze river, e & j Congo river.

A.3 Derivation of carbon fluxes in the simplified coupled system

A.3.1 Terrestrial fluxes

1. Carbonate and silicate weathering cause a land uptake flux of 280 Tg C yr^{-1} from the atmosphere according to the weathering model simulations (Table 2.3).

2. Carbonate mineral weathering causes a lithological carbon release flux of 94 Tg C yr^{-1} DIC, as shown in Section 2.3.2.

3. Carbon from terrestrial organic matter originates from the atmosphere (Meybeck and Vörösmarty, 1999). The net carbon uptake by the terrestrial and riverine biology is therefore the same as the lateral organic carbon export, which we derived from NEWS2 (Seitzinger et al., 2010) DOC and POC exports. The net uptake by the terrestrial biology, while taking into account all respiration processes on land and in rivers, is the sum of the lateral POC and DOC exports (249 Tg C yr^{-1}).

4. The riverine carbon export to the ocean consists of the sum of from weathering and organic matter carbon exports (623 Tg C yr^{-1}), minus a loss term due to endorheic rivers (19 Tg C yr^{-1}), which results in 603 Tg C yr^{-1} (values are rounded).

A.3.2 Long-term ocean fluxes

In the model, riverine loads cause oceanic outgassing through the inputs of inorganic C and tDOM, while the inputs of dissolved inorganic nutrients cause a sink of atmospheric carbon through the biological enhancement of C uptake as well as increasing alkalinity while doing so.

The inorganic C is delivered by rivers as 1 mol DIC and 1 mol alkalinity (HCO_3^-) and exported as 0.5 mol DIC and 1 mol alkalinity ($CaCO_3$), leaving a surplus of 0.5 mol DIC and 0 mol alkalinity. Increasing the DIC pool without increasing the alkalinity directly increases the dissolved CO_2 concentrations, which in its turn causes outgassing:

$$H_2O + Ca^{2+} + 2HCO_3{}^- => CaCO_3 + CO_2 \quad \text{(A.1)}$$

Equilibrium model outgassing caused by inorganic carbon inputs is therefore 0.5 fold of the riverine DIC loads.

tDOM model inputs, in contrary to POM, are not exported to the sediment. Outgassing from organic material results from the high C:P ratio of tDOM. It is mineralized in the ocean providing dissolved inorganic compounds in the C:P ratio of 2584:1, but the subsequent uptake of the released inorganic compounds happens at a C:P ratio of 122:1, resulting in a DIC overshoot. The DIC increase causes a pCO_2 increase (*simplified equation):

$$C_{2584}PN_{16}^* => 2584DIC + DIP + 16DIN+^* => C_{122}PN_{16}^* + 2462CO_2 \quad \text{(A.2)}$$

The organic outgassing caused by organic matter inputs is therefore 2462/2584 multiplied with tDOM carbon loads.

The riverine loads of DIP and DIN on the other hand cause C uptake through their enhancement of biological primary production. DIC is thereby removed, thus sinking pCO_2 (*simplified equation):

$$DIP + 16DIN +^* + 122CO_2 => C_{122}PN_{16}^* \quad \text{(A.3)}$$

The resulting C uptake from the equation is therefore 122-fold the mole DIP inputs. Additionally, alkalinity is produced in equation (16), which enhances C uptake. The uptake of DIN and DIP through primary production causes a net alkalinity increase by a factor of Alk:P = 17:1 (Wolf-Gladrow et al., 2007). The alkalinity is exported in a C:Alk ratio of 1:2 through calcium carbonate production (Eq. A.1). The C uptake enhancement from the alkalinity increase is therefore the 17 * 1/2 - fold of the (bioavailable) DIP loads.

5. According to the $CaCO_3$ export equation (Eq. A.1), half of the DIC input (assuming HCO_3^- is exported to the sediment as $CaCO_3$ and the other half is outgassed as CO_2 in model equilibrium state. The contribution of outgassing caused by inorganic carbon in the ocean is therefore half (0.5-fold) the DIC inputs (366 Tg C yr^{-1}) and therefore 183 Tg C yr^{-1} assuming model equilibrium.

6. tDOM input C:P rations vastly exceed the oceanic sediment export C:P ratios of organic matter, which causes model equilibrium outgassing in the ocean. Equation A.2 shows that for every mol tDOM supplied to the ocean, in model equilibrium 122/2584 of C is exported to the sediment and 2462/2584 of C increases the dissolved CO_2 pool, which is outgassed in the long term. The equilibrium outgassing is therefore the tDOM carbon load (134 Tg C yr^{-1}) multiplied by 2462/2584, which results in 128 Tg C yr^{-1}. In the case of POM, since the C:P ratio of the riverine input (122:1) is the same as the ratio of the export to the sediment in the ocean, there is no effect on the longterm equilibrium outgassing flux.

7. Since P has no further sinks or sources in the model other than riverine inputs and sediment burial as organic matter, in equilibrium the same amount of P supplied by rivers is buried in the sediment. When DIP is taken up by the biology and transformed to organic matter, carbon is also taken up in a mole ratio of C:P = 122:1. Accounting for this uptake through the biological production enhancement by DIP inputs (including bioavailable DIP) from rivers ((1.4 Tg P yr^{-1}) results in the uptake of 67 Tg C yr^{-1} throug the biological enhancement. Furthermore, when DIP and DIN are transformed to organic matter as organic matter, an alkalinity increase of 17 mol per mol DIP uptake takes place (Eq. A.3, Wolf-Gladrow et al., 2007). This increase in alkalinity causes the further uptake uptake and export of 2 Tg C yr^{-1}, resulting in a total sink of 69 Tg C yr^{-1}.

D1. We attribute the difference between the equilibrium CO_2 flux of 242 Tg C yr^{-1} and the modelled net CO_2 flux of 231 Tg C yr^{-1} (=11 Tg C yr^{-1}) to the small surface alkalinity increase over the analysis time period.

8. The simulated global particulate inorganic C sediment deposition flux in the ocean biogeochemistry model is 188 Tg C yr^{-1}.

9. The simulated global organic C sediment deposition flux in the ocean biogeochemistry model is 582 Tg C yr^{-1}.

10. The global modelled DIC flux from the sediment back to the water, which originates from POM remineralization in the sediment, column is 385 Tg C yr^{-1}.

D2. In model equilibrium the net sediment burial C flux is the total riverine C inputs of 603 Tg C yr^{-1} (**4**) subtracted by the equilibrium outgassing of 242 Tg C yr^{-1} (**5**+**6**-**7**), which results in 361 Tg C yr^{-1}. The simulated burial flux in

the model of 385 Tg C yr^{-1} (**8**+**9**-**10**) deviates from the calculated model burial equilibrium flux. Therefore, the drift at the sediment-ocean interface is 24 Tg C yr^{-1} (385 Tg C yr^{-1} - 361 Tg C yr^{-1}).

A.4 Surface Nutrient profiles

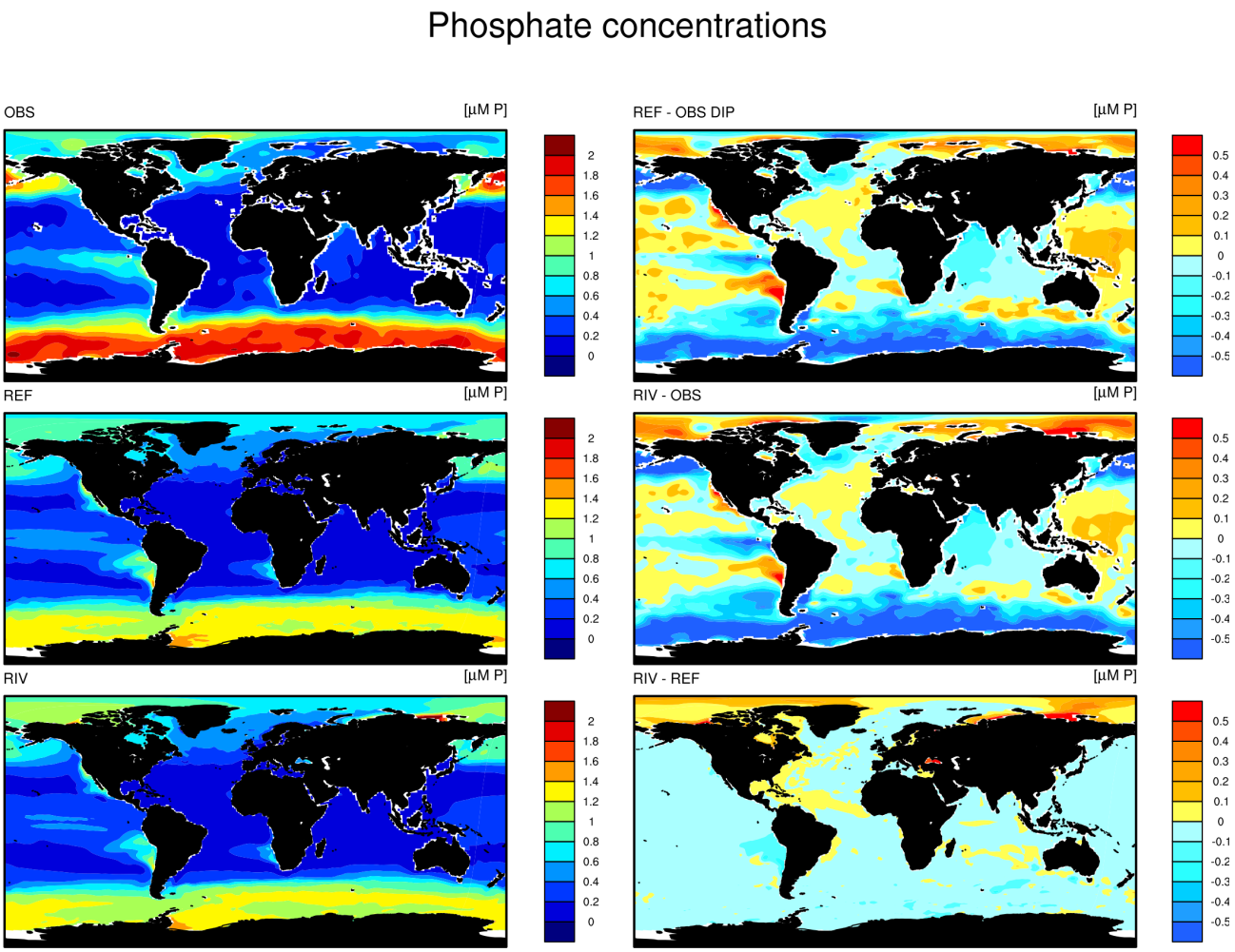

FIGURE A.3: Phosphate (DIP) concentrations in OBS (WOA observations), REF and RIV (Chapter 2).

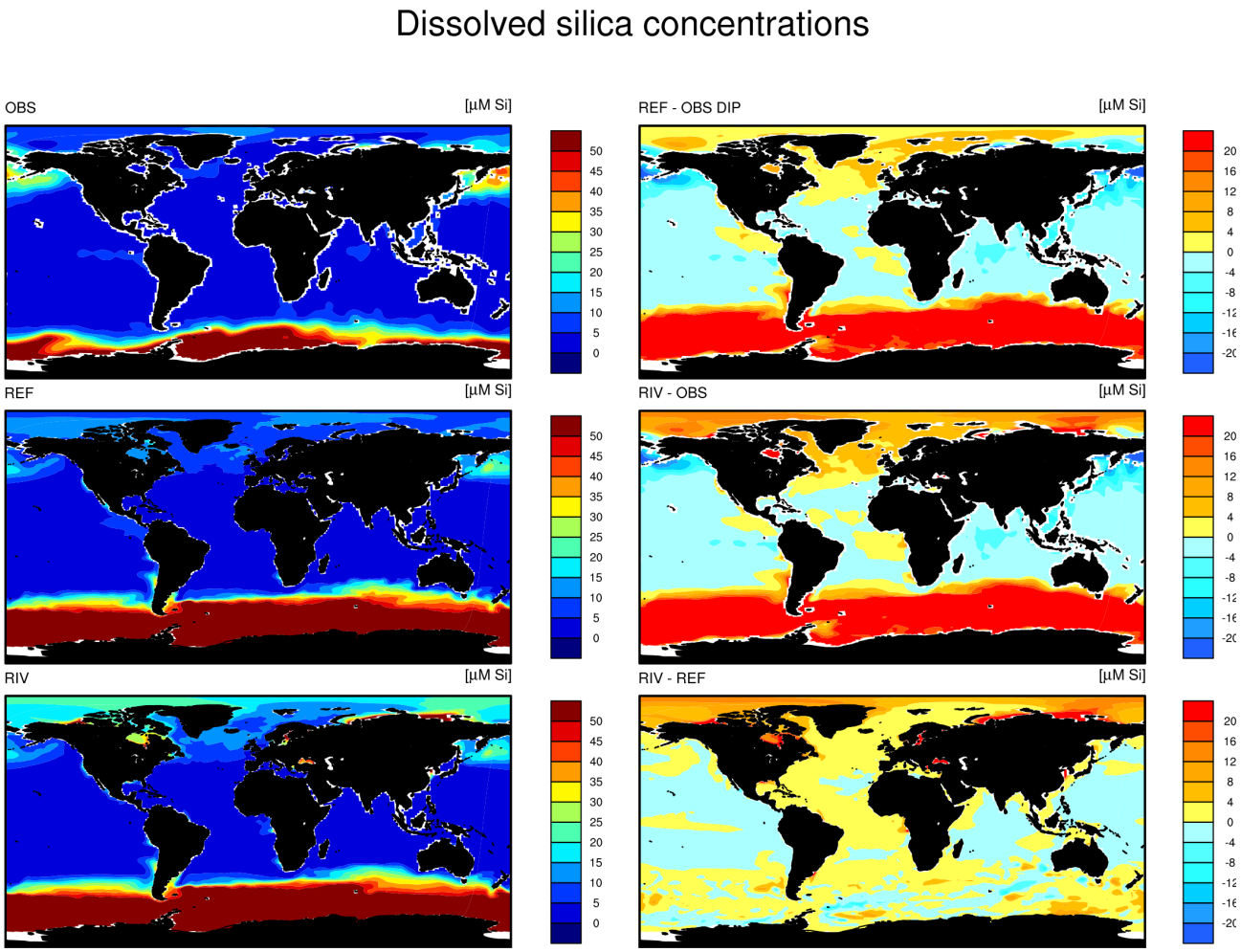

FIGURE A.4: Dissolved silica (DSi) concentrations in OBS (WOA observations), REF and RIV (Chapter 2).

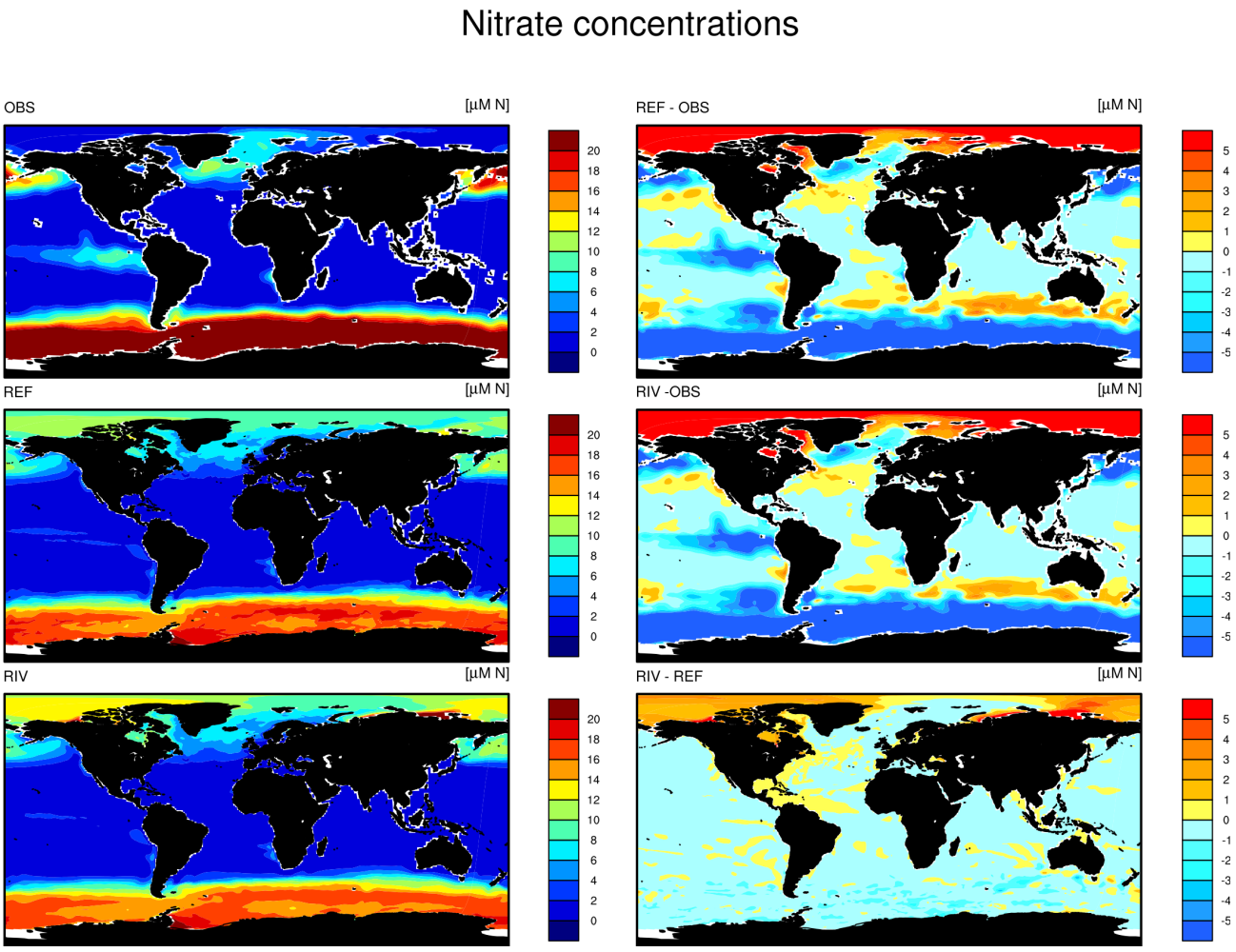

FIGURE A.5: Nitrate (DIN) concentrations in OBS (WOA observations), REF and RIV (Chapter 2).

Bibliography

Aarnos, H., P. Ylöstalo, and A. V. Vähätalo (2012). "Seasonal phototransformation of dissolved organic matter to ammonium, dissolved inorganic carbon, and labile substrates supporting bacterial biomass across the Baltic Sea". In: *Journal of Geophysical Research: Biogeosciences* 117.G1. ISSN: 0148-0227. DOI: 10.1029/2010JG001633.

Aarnos, H., Y. Gélinas, V. Kasurinen, Y. Gu, V.-M. Puupponen, and A. V. Vähätalo (2018). "Photochemical Mineralization of Terrigenous DOC to Dissolved Inorganic Carbon in Ocean". In: *Global Biogeochemical Cycles* 32.2, pp. 250–266. DOI: 10.1002/2017GB005698.

Adler, R. F. et al. (2003). "The Version-2 Global Precipitation Climatology Project (GPCP) Monthly Precipitation Analysis (1979–Present)". In: *Journal of Hydrometeorology* 4.6, pp. 1147–1167. ISSN: 1525-755X. DOI: 10.1175/1525-7541(2003)004<1147:TVGPCP>2.0.CO;2.

Aksenov, Y., S. Bacon, A. C. Coward, and N. P. Holliday (2010). "Polar outflow from the Arctic Ocean: A high resolution model study". In: *Journal of Marine Systems* 83.1, pp. 14–37. ISSN: 0924-7963. DOI: https://doi.org/10.1016/j.jmarsys.2010.06.007.

Amiotte Suchet, P and J.-L. Probst (1995). "A global model for presentday atmospheric/soil CO2 consumption by chemical erosion of continental rocks (GEMCO2)". In: *Tellus B* 47.1-2, pp. 273–280. DOI: 10.1034/j.1600-0889.47.issue1.23.x.

Amiotte Suchet, P., J.-L. Probst, and W. Ludwig (2003). "Worldwide distribution of continental rock lithology: Implications for the atmospheric/soil CO2 uptake by continental weathering and alkalinity river transport to the oceans". In: *Global Biogeochemical Cycles* 17.2. DOI: 10.1029/2002GB001891.

Anderson, L. G., S. Jutterström, S. Hjalmarsson, I. Wåhlström, and I. Semiletov (2009). *Out-gassing of CO2 from Siberian Shelf seas by terrestrial organic matter decomposition*. DOI: 10.1029/2009GL040046. URL: https://agupubs.onlinelibrary.wiley.com/doi/abs/10.1029/2009GL040046.

Andersson, A. J., F Mackenzie, and A. Lerman (2005). *Coastal ocean and carbonate systems in the high CO2 world of the Anthropocene*. Vol. 305, pp. 875–918. DOI: 10.2475/ajs.305.9.875.

Araujo, M., C. Noriega, and N. Lefèvre (2014). "Nutrients and carbon fluxes in the estuaries of major rivers flowing into the tropical Atlantic". In: *Frontiers in Marine Science* 1.May, pp. 1–16. ISSN: 2296-7745. DOI: 10.3389/fmars.2014.00010. arXiv: arXiv:1507.06648v1.

Arndt, S., B. B. Jørgensen, D. E. LaRowe, J. J. Middelburg, R. D. Pancost, and P Regnier (2013). "Quantifying the degradation of organic matter in marine sediments: A review and synthesis". In: *Earth-Science Reviews* 123, pp. 53–86. ISSN: 0012-8252. DOI: https://doi.org/10.1016/j.earscirev.2013.02.008. URL: http://www.sciencedirect.com/science/article/pii/S0012825213000512.

Aumont, O., C. Ethé, A. Tagliabue, L. Bopp, and M. Gehlen (2015). "PISCES-v2: an ocean biogeochemical model for carbon and ecosystem studies". In: *Geoscientific Model Development* 8.8, pp. 2465–2513. DOI: 10.5194/gmd-8-2465-2015. URL: https://www.geosci-model-dev.net/8/2465/2015/.

Aumont, O., J. C. Orr, P. Monfray, W. Ludwig, P. Amiotte Suchet, and J.-L. Probst (2001). "Riverinedriven interhemispheric transport of carbon". In: *Global Biogeochemical Cycles* 15.2, pp. 393–405. DOI: 10.1029/1999GB001238.

Bakker, D. C. E. et al. (2016). "A multi-decade record of high-quality fCO_2 data in version 3 of the Surface Ocean CO_2 Atlas (SOCAT)". In: *Earth System Science Data* 8.2, pp. 383–413. DOI: 10.5194/essd-8-383-2016. URL: https://www.earth-syst-sci-data.net/8/383/2016/.

Bakun, A. (1990). "Global Climate Change and Intensification of Coastal Ocean Upwelling". In: *Science* 247.4939, 198 LP –201. DOI: 10.1126/science.247.4939.198. URL: http://science.sciencemag.org/content/247/4939/198.abstract.

Batjes, N. H. (1997). "A world dataset of derived soil properties by FAO–UNESCO soil unit for global modelling". In: *Soil Use and Management* 13.1, pp. 9–16. DOI: 10.1111/j.1475-2743.1997.tb00550.x.

— (2002). "Revised soil parameter estimates for the soil types of the world". In: *Soil Use and Management* 18.3, pp. 232–235. ISSN: 0266-0032. DOI: doi:10.1111/j.1475-2743.2002.tb00244.x.

Battin, T. J., S. Luyssaert, L. A. Kaplan, A. K. Aufdenkampe, A. Richter, and L. J. Tranvik (2009). "The boundless carbon cycle". In: *Nature Geoscience* 2, p. 598. URL: https://doi.org/10.1038/ngeo618http://10.0.4.14/ngeo618.

Bauer, J. E., W.-J. Cai, P. A. Raymond, T. S. Bianchi, C. S. Hopkinson, and P. A. G. Regnier (2013). "The changing carbon cycle of the coastal ocean". In: *Nature* 504, p. 61.

Beaulieu, C, S. A. Henson, J. L. Sarmiento, J. P. Dunne, S. C. Doney, R. R. Rykaczewski, and L Bopp (2013). "Factors challenging our ability to detect long-term trends in ocean chlorophyll". In: *Biogeosciences* 10.4, pp. 2711–2724. DOI: 10.5194/bg-10-2711-2013. URL: https://www.biogeosciences.net/10/2711/2013/.

Beaulieu, E., Y. Goddéris, Y. Donnadieu, D. Labat, and C. Roelandt (2012). "High sensitivity of the continental-weathering carbon dioxide sink to future climate change". In: *Nature Climate Change* 2.5, pp. 346–349. ISSN: 1758678X. DOI: 10.1038/nclimate1419.

Behrenfeld, M. J. et al. (2006). "Climate-driven trends in contemporary ocean productivity". In: *Nature* 444.7120, pp. 752–755. ISSN: 1476-4687. DOI: 10.1038/nature05317.

Behrenfeld, M. and P. Falkowski (1997). "Photosynthetic rates derived from satellite-based chlorophyll concentration". In: *Limnology and Oceanography* 42, pp. 1479–1491. DOI: 10.4319/lo.1997.42.1.0001.

Bélanger, S., S. A. Cizmeli, J. Ehn, A. Matsuoka, D. Doxaran, S. Hooker, and M. Babin (2013). "Light absorption and partitioning in Arctic Ocean surface waters: impact of multiyear ice melting". In: *Biogeosciences* 10.10, pp. 6433–6452. DOI: 10.5194/bg-10-6433-2013. URL: https://www.biogeosciences.net/10/6433/2013/.

Benner, R., P. Louchouarn, and R. M. W. Amon (2005). "Terrigenous dissolved organic matter in the Arctic Ocean and its transport to surface and deep waters of the North Atlantic". In: *Global Biogeochemical Cycles* 19.2. ISSN: 0886-6236. DOI: 10.1029/2004GB002398.

Bernard, C. Y., H. H. Dürr, C Heinze, J Segschneider, and E Maier-Reimer (2011). "Contribution of riverine nutrients to the silicon biogeochemistry of the global ocean – a model study". In: *Biogeosciences* 8.3, pp. 551–564. DOI: 10.5194/bg-8-551-2011.

Berner, R. A., A. C. Lasaga, and R. Garrels (1983). "The carbonate-silicate geochemical cycle and its effect on atmospheric carbon dioxide over the past 100 million years". In: *American Journal of Science* 283, pp. 641–683. DOI: 10.2475/ajs.283.7.641.

Beusen, A. H. W., A. L. M. Dekkers, A. F. Bouwman, W Ludwig, and J Harrison (2005). "Estimation of global river transport of sediments and associated

particulate C, N, and P". In: *Global Biogeochemical Cycles* 19.4. ISSN: 0886-6236. DOI: 10.1029/2005GB002453.

Beusen, A. H. W., A. F. Bouwman, H Dürr, A. L. M. Dekkers, and J Hartmann (2009). "Global patterns of dissolved silica export to the coastal zone: Results from a spatially explicit global model". In: *Global Biogeochemical Cycles* 23.4. ISSN: 0886-6236. DOI: 10.1029/2008GB003281.

Beusen, A. H. W., A. F. Bouwman, L. P. H. Van Beek, J. M. Mogollón, and J. J. Middelburg (2016). "Global riverine N and P transport to ocean increased during the 20th century despite increased retention along the aquatic continuum". In: *Biogeosciences* 13.8, pp. 2441–2451. DOI: 10.5194/bg-13-2441-2016.

Bird, M. I. et al. (2008). "A preliminary estimate of organic carbon transport by the Ayeyarwady (Irrawaddy) and Thanlwin (Salween) Rivers of Myanmar". In: *Quaternary International* 186.1, pp. 113–122. ISSN: 1040-6182. DOI: https://doi.org/10.1016/j.quaint.2007.08.003.

Björkman, K. M. and D. M. Karl (2003). "Bioavailability of dissolved organic phosphorus in the euphotic zone at Station ALOHA, North Pacific Subtropical Gyre". In: *Limnology and Oceanography* 48.3, pp. 1049–1057. DOI: 10.4319/lo.2003.48.3.1049.

Blaas, M., D Kerkhoven, and H. de Swart (2001). *Large-scale circulation and flushing characteristics of the North Sea under various climate forcings*. Vol. 18. DOI: 10.3354/cr018047.

Blair, N. E. and R. C. Aller (2011). "The Fate of Terrestrial Organic Carbon in the Marine Environment". In: *Annual Review of Marine Science* 4.1, pp. 401–423. ISSN: 1941-1405. DOI: 10.1146/annurev-marine-120709-142717.

Bopp, L. et al. (2013). "Multiple stressors of ocean ecosystems in the 21st century: projections with CMIP5 models". In: *Biogeosciences* 10.10, pp. 6225–6245. DOI: 10.5194/bg-10-6225-2013. URL: https://www.biogeosciences.net/10/6225/2013/.

Borges, A. V., B Delille, and M Frankignoulle (2005). "Budgeting sinks and sources of CO2 in the coastal ocean: Diversity of ecosystems counts". In: *Geophysical Research Letters* 32.14. DOI: 10.1029/2005GL023053. URL: https://agupubs.onlinelibrary.wiley.com/doi/abs/10.1029/2005GL023053.

Bourgeois, T, J. C. Orr, L Resplandy, J Terhaar, C Ethé, M Gehlen, and L Bopp (2016). "Coastal-ocean uptake of anthropogenic carbon". In: *Biogeosciences* 13.14, pp. 4167–4185. DOI: 10.5194/bg-13-4167-2016.

Bouwman, A. F., G Van Drecht, J. M. Knoop, A. H. W. Beusen, and C. R. Meinardi (2005). "Exploring changes in river nitrogen export to the world's

oceans". In: *Global Biogeochemical Cycles* 19.1. ISSN: 0886-6236. DOI: 10.1029/2004GB002314. URL: https://doi.org/10.1029/2004GB002314.

Bouwman, A. F., A. H. W. Beusen, and G Billen (2009). "Human alteration of the global nitrogen and phosphorus soil balances for the period 1970–2050". In: *Global Biogeochemical Cycles* 23.4. ISSN: 0886-6236. DOI: 10.1029/2009GB003576. URL: https://doi.org/10.1029/2009GB003576.

Bowen, R. E. and C. Riley (2003). "Socio-economic indicators and integrated coastal management". In: *Ocean & Coastal Management* 46.3, pp. 299–312. ISSN: 0964-5691. DOI: https://doi.org/10.1016/S0964-5691(03)00008-5. URL: http://www.sciencedirect.com/science/article/pii/S0964569103000085.

Bowring, S. P. K., R. Lauerwald, B. Guenet, D. Zhu, M. Guimberteau, A. Tootchi, A. Ducharne, and P. Ciais (2019). "ORCHIDEE MICT-LEAK (r5459), a global model for the production, transport and transformation of dissolved organic carbon from Arctic permafrost regions, Part 1: Rationale, model description and simulation protocol". In: *Geoscientific Model Development Discussions* 2019, pp. 1–29. DOI: 10.5194/gmd-2018-320. URL: https://www.geosci-model-dev-discuss.net/gmd-2018-320/.

Boyer, T. P. et al. (2013). "World Ocean Database 2013, NOAA Atlas NESDIS 72". In: *S. Levitus, Ed., A. Mishonov, Technical Ed.; Silver Spring* MD, p. 209. DOI: 10.7289/V5NZ85MT.

Brault, M.-O., L. A. Mysak, and H. D. Matthews (2017). "Carbon cycle implications of terrestrial weathering changes since the last glacial maximum". In: *FACETS* 2.1, pp. 267–285. DOI: 10.1139/facets-2016-0040.

Breitburg, D. et al. (2018). "Declining oxygen in the global ocean and coastal waters". In: *Science* 359.6371, eaam7240. DOI: 10.1126/science.aam7240. URL: http://science.sciencemag.org/content/359/6371/eaam7240.abstract.

Bristow, L. A., W. Mohr, S. Ahmerkamp, and M. M.M. Kuypers (2017). *Nutrients that limit growth in the ocean*. Vol. 27, R474–R478. DOI: 10.1016/j.cub.2017.03.030.

Broecker, W. S. and T.-h. Peng (1982). *Tracers in the sea*. English. Includes index. Palisades, Ny : Lamont-Doherty Geological Observatory, Columbia University.

Burton, M. R., G. M. Sawyer, and D. Granieri (2013). "Deep Carbon Emissions from Volcanoes". In: *Reviews in Mineralogy Geochemistry* 75.11, pp. 323–354.

Cai, W.-J. (2011). "Estuarine and Coastal Ocean Carbon Paradox: CO2 Sinks or Sites of Terrestrial Carbon Incineration?" In: *Annual Review of Marine Science* 3.1, pp. 123–145. DOI: 10.1146/annurev-marine-120709-142723.

Cai, W.-J., L. R. Pomeroy, M. A. Moran, and Y. Wang (1999). "Oxygen and carbon dioxide mass balance for the estuarine-intertidal marsh complex of five rivers in the southeastern U.S." In: *Limnology and Oceanography* 44.3, pp. 639–649. ISSN: 0024-3590. DOI: 10.4319/lo.1999.44.3.0639. URL: https://doi.org/10.4319/lo.1999.44.3.0639.

Cauwet, G. (2002). "Chapter 12 - DOM in the Coastal Zone". In: ed. by D. A. Hansell and C. A.B.T.B.o.M.D.O. M. Carlson. Academic Press, pp. 579–609. ISBN: 978-0-12-323841-2. DOI: https://doi.org/10.1016/B978-012323841-2/50014-2. URL: http://www.sciencedirect.com/science/article/pii/B9780123238412500142.

Chavez, F. P., M. Messié, and J. T. Pennington (2010). "Marine Primary Production in Relation to Climate Variability and Change". In: *Annual Review of Marine Science* 3.1, pp. 227–260. ISSN: 1941-1405. DOI: 10.1146/annurev.marine.010908.163917. URL: https://doi.org/10.1146/annurev.marine.010908.163917.

Chen, C and R. C. Beardsley (2006). "An Unstructured Grid, Finite-Volume Coastal Ocean Model (FVCOM) System". In: *Oceanography* 19. URL: https://doi.org/10.5670/oceanog.2006.92.

Chen, C., H. Huang, R. C. Beardsley, H. Liu, Q. Xu, and G. Cowles (2007). "A finite volume numerical approach for coastal ocean circulation studies: Comparisons with finite difference models". In: *Journal of Geophysical Research: Oceans* 112.C3. DOI: 10.1029/2006JC003485. eprint: https://agupubs.onlinelibrary.wiley.com/doi/pdf/10.1029/2006JC003485. URL: https://agupubs.onlinelibrary.wiley.com/doi/abs/10.1029/2006JC003485.

Chen, C.-T. A. and A. Borges (2009). *Reconciling opposing views on carbon cycling in the coastal ocean: Continental shelves as sinks and near-shore ecosystems as sources of atmospheric CO2*. Vol. 56, pp. 578–590. DOI: 10.1016/j.dsr2.2009.01.001.

Chen, C.-T. A. and S.-L. Wang (1999). "Carbon, alkalinity and nutrient budgets on the East China Sea continental shelf". In: *Journal of Geophysical Research: Oceans* 104.C9, pp. 20675–20686. ISSN: 0148-0227. DOI: 10.1029/1999JC900055. URL: https://doi.org/10.1029/1999JC900055.

Church, J. A. et al. (2011). "Revisiting the Earth's sea-level and energy budgets from 1961 to 2008". In: *Geophysical Research Letters* 38.18. ISSN: 0094-8276. DOI: 10.1029/2011GL048794. URL: https://doi.org/10.1029/2011GL048794.

Ciais, P et al. (2013). "Carbon and other biogeochemical cycles". In: *Climate Change 2013: The Physical Science Basis*, pp. 465–570.

Cole, J. J. et al. (2007). "Plumbing the global carbon cycle: Integrating inland waters into the terrestrial carbon budget". In: *Ecosystems* 10.1, pp. 171–184. ISSN: 14329840. DOI: 10.1007/s10021-006-9013-8.

Combes, V. and R. Matano (2018). *The Patagonian shelf circulation: Drivers and variability*. Vol. 167. DOI: 10.1016/j.pocean.2018.07.003.

Commerce, N. O. US Department of and N. G.D. C. Atmospheric Administration (2006). "ETOPO2". In: URL: http://www.ngdc.noaa.gov/mgg/fliers/06mgg01.html.

Compton, J, D Mallinson, C. Glenn, G Filippelli, K Föllmi, G Shields, and Y. Zanin (2000). "Variations in the global phosphorus cycle". In: *IN:Marine Authigenesis: From Global to Microbial, Wiley-Blackwell*, pp. 21–33.

Cooley, S. R., V. J. Coles, A. Subramaniam, and P. L. Yager (2007). "Seasonal variations in the Amazon plume-related atmospheric carbon sink". In: *Global Biogeochemical Cycles* 21.3, pp. 1–15. ISSN: 08866236. DOI: 10.1029/2006GB002831.

Cox, P. M., R. A. Betts, C. D. Jones, S. A. Spall, and I. J. Totterdell (2000). "Acceleration of global warming due to carbon-cycle feedbacks in a coupled climate model". In: *Nature* 408.6809, pp. 184–187. ISSN: 1476-4687. DOI: 10.1038/35041539.

Crossland, C., D. Baird, J.-P. Ducrotoy, H. Lindeboom, R. W. Buddemeier, W. Dennison, B. Maxwell, S. Smith, and D. Swaney (2006). "The Coastal Zone — a Domain of Global Interactions". In: pp. 1–37. DOI: 10.1007/3-540-27851-6_1.

Da Cunha, L., E. T. Buitenhuis, C. Le Quéré, X. Giraud, and W. Ludwig (2007). "Potential impact of changes in river nutrient supply on global ocean biogeochemistry". In: *Global Biogeochemical Cycles* 21.4. DOI: 10.1029/2006GB002718.

Dagg, M, R Benner, S Lohrenz, and D Lawrence (2004). "Transformation of dissolved and particulate materials on continental shelves influenced by large rivers: plume processes". In: *Continental Shelf Research* 24.7, pp. 833–858. ISSN: 0278-4343. DOI: 10.1016/j.csr.2004.02.003.

Dai, A. and K. E. Trenberth (2002). "Estimates of Freshwater Discharge from Continents: Latitudinal and Seasonal Variations". In: *Journal of Hydrometeorology* 3.6, pp. 660–687. ISSN: 1525-755X. DOI: 10.1175/1525-7541(2002)003<0660:EOFDFC>2.0.CO;2.

Deal, C., M. Jin, S. Elliott, E. Hunke, M. Maltrud, and N. Jeffery (2011). "Large-scale modeling of primary production and ice algal biomass within arctic sea ice in 1992". In: *Journal of Geophysical Research: Oceans* 116.C7. DOI: 10.1029/2010JC006409.

Delcroix, T. and R. Murtugudde (2002). "Sea surface salinity changes in the East China Sea during 1997–2001: Influence of the Yangtze River". In: *Journal of Geophysical Research: Oceans* 107.C12, SRF 9–1–SRF 9–11. ISSN: 0148-0227. DOI: 10.1029/2001JC000893. URL: https://doi.org/10.1029/2001JC000893.

Diaz, R. J. and R. Rosenberg (2008). "Spreading Dead Zones and Consequences for Marine Ecosystems". In: *Science* 321.5891, 926 LP –929. DOI: 10.1126/science.1156401. URL: http://science.sciencemag.org/content/321/5891/926.abstract.

Dittmar, T. and G. Kattner (2003). "The biogeochemistry of the river and shelf ecosystem of the Arctic Ocean: a review". In: *Marine Chemistry* 83.3, pp. 103–120. ISSN: 0304-4203. DOI: https://doi.org/10.1016/S0304-4203(03)00105-1.

Doney, S. C., N. Mahowald, I. Lima, R. A. Feely, F. T. Mackenzie, J.-F. Lamarque, and P. J. Rasch (2007). "Impact of anthropogenic atmospheric nitrogen and sulfur deposition on ocean acidification and the inorganic carbon system". In: *Proceedings of the National Academy of Sciences* 104.37, 14580 LP –14585. DOI: 10.1073/pnas.0702218104. URL: http://www.pnas.org/content/104/37/14580.abstract.

Drake, T. W., P. A. Raymond, and R. G. M. Spencer (2018). "Terrestrial carbon inputs to inland waters: A current synthesis of estimates and uncertainty". In: *Limnology and Oceanography Letters* 3.3, pp. 132–142. ISSN: 2378-2242. DOI: 10.1002/lol2.10055.

Dunne, J. P. et al. (2012). "GFDL's ESM2 Global Coupled Climate–Carbon Earth System Models. Part I: Physical Formulation and Baseline Simulation Characteristics". In: *Journal of Climate* 25.19, pp. 6646–6665. ISSN: 0894-8755. DOI: 10.1175/JCLI-D-11-00560.1.

Dürr, H. H., M. Meybeck, J. Hartmann, G. G. Laruelle, and V. Roubeix (2011). "Global spatial distribution of natural riverine silica inputs to the coastal

zone". In: *Biogeosciences* 8.3, pp. 597–620. ISSN: 17264170. DOI: 10.5194/bg-8-597-2011.

Dürr, H. H., M Meybeck, and S. H. Dürr (2005). "Lithologic composition of the Earth's continental surfaces derived from a new digital map emphasizing riverine material transfer". In: *Global Biogeochemical Cycles* 19.4. ISSN: 0886-6236. DOI: 10.1029/2005GB002515.

Edmond, J. M., M. R. Palmer, C. I. Measures, B Grant, and R. F. Stallard (1995). "The fluvial geochemistry and denudation rate of the Guayana Shield in Venezuela, Colombia, and Brazil". In: *Geochimica et Cosmochimica Acta* 59.16, pp. 3301–3325. ISSN: 0016-7037. DOI: 10.1016/0016-7037(95)00128-M.

Eicken, H, I Dmitrenko, K Tyshko, A Darovskikh, W Dierking, U Blahak, J Groves, and H Kassens (2005). "Zonation of the Laptev Sea landfast ice cover and its importance in a frozen estuary". In: *Global and Planetary Change* 48.1, pp. 55–83. ISSN: 0921-8181. DOI: https://doi.org/10.1016/j.gloplacha.2004.12.005. URL: http://www.sciencedirect.com/science/article/pii/S0921818105000585.

Elser, J. J. et al. (2007). "Global analysis of nitrogen and phosphorus limitation of primary producers in freshwater, marine and terrestrial ecosystems". In: *Ecology Letters* 10.12, pp. 1135–1142. DOI: 10.1111/j.1461-0248.2007.01113.x.

Etheridge, D. M., L. P. Steele, R. L. Langenfelds, R. J. Francey, J.-M. Barnola, and V. I. Morgan (1996). "Natural and anthropogenic changes in atmospheric CO2 over the last 1000 years from air in Antarctic ice and firn". In: *Journal of Geophysical Research: Atmospheres* 101.D2, pp. 4115–4128. DOI: 10.1029/95JD03410.

Fanning, K. A., K. L. Carder, and P. R. Betzer (1982). "Sediment resuspension by coastal waters: a potential mechanism for nutrient re-cycling on the ocean's margins". In: *Deep Sea Research Part A. Oceanographic Research Papers* 29.8, pp. 953–965. ISSN: 0198-0149. DOI: https://doi.org/10.1016/0198-0149(82)90020-6. URL: http://www.sciencedirect.com/science/article/pii/0198014982900206.

Fekete, B. M., C. J. Vörösmarty, and W Grabs (2002). "High-resolution fields of global runoff combining observed river discharge and simulated water balances". In: *Global Biogeochemical Cycles* 16.3, pp. 10–15. ISSN: 0886-6236. DOI: 10.1029/1999GB001254.

Fennel, K. and J. M. Testa (2019). "Biogeochemical Controls on Coastal Hypoxia". In: *Annual Review of Marine Science* 11.1, pp. 105–130. ISSN: 1941-1405. DOI: 10.1146/annurev-marine-010318-095138. URL: https://doi.org/10.1146/annurev-marine-010318-095138.

Fennel, K., J. Wilkin, J. Levin, J. Moisan, J. O'Reilly, and D. Haidvogel (2006). "Nitrogen cycling in the Middle Atlantic Bight: Results from a three-dimensional model and implications for the North Atlantic nitrogen budget". In: *Global Biogeochemical Cycles* 20.3. ISSN: 0886-6236. DOI: 10.1029/2005GB002456. URL: https://doi.org/10.1029/2005GB002456.

Ferguson, I. M. and R. M. Maxwell (2011). "Hydrologic and land–energy feedbacks of agricultural water management practices". In: *Environmental Research Letters* 6.1, p. 14006. ISSN: 1748-9326. DOI: 10.1088/1748-9326/6/1/014006. URL: http://dx.doi.org/10.1088/1748-9326/6/1/014006.

Fernández-Martínez, M et al. (2014). "Nutrient availability as the key regulator of global forest carbon balance". In: *Nature Climate Change* 4, p. 471. DOI: 10.1038/nclimate2177.

Fichot, C. G. and R. Benner (2014). "The fate of terrigenous dissolved organic carbon in a river-influenced ocean margin". In: *Global Biogeochemical Cycles* 28.3, pp. 300–318. DOI: 10.1002/2013GB004670.

Field, C. B., M. J. Behrenfeld, J. T. Randerson, and P. Falkowski (1998). "Primary Production of the Biosphere: Integrating Terrestrial and Oceanic Components". In: *Science* 281.5374, 237 LP –240. DOI: 10.1126/science.281.5374.237.

Filippelli, G. M. (2008). "The Global Phosphorus Cycle: Past, Present, and Future". In: *Elements* 4.2, pp. 89–95. ISSN: 1811-5209. DOI: 10.2113/GSELEMENTS.4.2.89.

Friedlingstein, P. et al. (2006). "Climate–Carbon Cycle Feedback Analysis: Results from the C4MIP Model Intercomparison". In: *Journal of Climate* 19.14, pp. 3337–3353. DOI: 10.1175/JCLI3800.1. URL: https://doi.org/10.1175/JCLI3800.1.

Frischknecht, M., M. Münnich, and N. Gruber (2018). "Origin, Transformation, and Fate: The Three-Dimensional Biological Pump in the California Current System". In: *Journal of Geophysical Research: Oceans*. DOI: 10.1029/2018JC013934.

Froelich, P. N. (1988). "Kinetic control of dissolved phosphate in natural rivers and estuaries: A primer on the phosphate buffer mechanism". In: *Limnology and Oceanography* 33.4part2, pp. 649–668. DOI: 10.4319/lo.1988.33.4part2.0649.

Gaillardet, J., B. Dupré, P. Louvat, and C. Allègre (1999). "Global silicate weathering and CO2 consumption rates deduced from the chemistry of large rivers". In: *Chemical Geology* 159.1, pp. 3 –30. ISSN: 0009-2541. DOI: 10.1016/S0009-2541(99)00031-5.

Galloway, J. N. (1995). "Acid deposition: Perspectives in time and space". In: *Water, Air, and Soil Pollution* 85.1, pp. 15–24. ISSN: 1573-2932. DOI: 10.1007/BF00483685. URL: https://doi.org/10.1007/BF00483685.

Gattuso, J.-P., M Frankignoulle, and R Wollast (1998). "CARBON AND CARBONATE METABOLISM IN COASTAL AQUATIC ECOSYSTEMS". In: *Annual Review of Ecology and Systematics* 29.1, pp. 405–434. ISSN: 0066-4162. DOI: 10.1146/annurev.ecolsys.29.1.405. URL: https://doi.org/10.1146/annurev.ecolsys.29.1.405.

Giorgetta, M. A. et al. (2013). "Climate and carbon cycle changes from 1850 to 2100 in MPI-ESM simulations for the Coupled Model Intercomparison Project phase 5". In: *Journal of Advances in Modeling Earth Systems* 5.3, pp. 572–597. DOI: 10.1002/jame.20038.

Giraud, X., C. Le Quéré, and L. C. da Cunha (2008). "Importance of coastal nutrient supply for global ocean biogeochemistry". In: *Global Biogeochemical Cycles* 22.2. ISSN: 0886-6236. DOI: 10.1029/2006GB002717.

Gislason, S. R. et al. (2009). "Direct evidence of the feedback between climate and weathering". In: *Earth and Planetary Science Letters* 277.1, pp. 213–222. ISSN: 0012-821X. DOI: https://doi.org/10.1016/j.epsl.2008.10.018.

Goll, D. S. et al. (2017a). "A representation of the phosphorus cycle for ORCHIDEE (revision 4520)". In: *Geoscientific Model Development* 10.10, pp. 3745–3770. DOI: 10.5194/gmd-10-3745-2017. URL: https://www.geosci-model-dev.net/10/3745/2017/.

Goll, D. S., A. J. Winkler, T. Raddatz, N. Dong, I. C. Prentice, P. Ciais, and V. Brovkin (2017b). "Carbon–nitrogen interactions in idealized simulations with JSBACH (version 3.10)". In: *Geoscientific Model Development* 10.5, pp. 2009–2030. DOI: 10.5194/gmd-10-2009-2017. URL: https://www.geosci-model-dev.net/10/2009/2017/.

Goll, D. S., N. Moosdorf, J. Hartmann, and V. Brovkin (2014). "Climate-driven changes in chemical weathering and associated phosphorus release since 1850: Implications for the land carbon balance". In: *Geophysical Research Letters* 41.10, pp. 3553–3558. DOI: 10.1002/2014GL059471.

Gomes, H. d. R., Q. Xu, J. Ishizaka, E. J. Carpenter, P. L. Yager, and J. I. Goes. In: ISSN: 2296-7745. DOI: 10.3389/fmars.2018.00343.

Gong, D, J. T. Kohut, and S. M. Glenn (2010). "Seasonal climatology of wind-driven circulation on the New Jersey Shelf". In: *Journal of Geophysical Research: Oceans* 115.C4. ISSN: 0148-0227. DOI: 10.1029/2009JC005520. URL: https://doi.org/10.1029/2009JC005520.

Goudie, A. S. and H. A. Viles (2012). "Weathering and the global carbon cycle: Geomorphological perspectives". In: *Earth-Science Reviews* 113.1, pp. 59–71. ISSN: 0012-8252. DOI: 10.1016/j.earscirev.2012.03.005.

Green, P. A., C. J. Vörösmarty, M. Meybeck, J. N. Galloway, B. J. Peterson, and E. W. Boyer (2004). "Pre-industrial and contemporary fluxes of nitrogen through rivers: a global assessment based on typology". In: *Biogeochemistry* 68.1, pp. 71–105. ISSN: 1573-515X. DOI: 10.1023/B:BIOG.0000025742.82155.92.

Gröger, M., E. Maier-Reimer, U. Mikolajewicz, A. Moll, and D. Sein (2013). "NW European shelf under climate warming: implications for open ocean ndash; shelf exchange, primary production, and carbon absorption". In: *Biogeosciences* 10.6, pp. 3767–3792. DOI: 10.5194/bg-10-3767-2013. URL: https://www.biogeosciences.net/10/3767/2013/.

Großkopf, T. et al. (2012). "Doubling of marine dinitrogen-fixation rates based on direct measurements". In: *Nature* 488, p. 361. URL: https://doi.org/10.1038/nature11338http://10.0.4.14/nature11338https://www.nature.com/articles/nature11338{\#}supplementary-information.

Gruber, N. (2014). "Carbon at the coastal interface". In: *Nature* 517, p. 148. URL: https://doi.org/10.1038/nature14082http://10.0.4.14/nature14082.

Gruber, N. and J. N. Galloway (2008). "An Earth-system perspective of the global nitrogen cycle". In: *Nature* 451, p. 293. URL: https://doi.org/10.1038/nature06592http://10.0.4.14/nature06592.

Gruber, N., C. D. Keeling, and N. R. Bates (2002). "Interannual Variability in the North Atlantic Ocean Carbon Sink". In: *Science* 298.5602, 2374 LP –2378. DOI: 10.1126/science.1077077. URL: http://science.sciencemag.org/content/298/5602/2374.abstract.

Gruber, N. et al. (2009). "Oceanic sources, sinks, and transport of atmospheric CO2". In: *Global Biogeochemical Cycles* 23.1. DOI: 10.1029/2008GB003349.

Gruber, N., Z. Lachkar, H. Frenzel, P. Marchesiello, M. Münnich, J. C. McWilliams, T. Nagai, and G.-K. Plattner (2011). "Eddy-induced reduction of biological production in eastern boundary upwelling systems". In: *Nature Geoscience* 4, p. 787. URL: https://doi.org/10.1038/ngeo1273http://10.

0.4.14/ngeo1273https://www.nature.com/articles/ngeo1273{\#}supplementary-information.

Hagemann, S and L Dümenil (1997). "A parametrization of the lateral waterflow for the global scale". In: *Climate Dynamics* 14.1, pp. 17–31. ISSN: 1432-0894. DOI: 10.1007/s003820050205.

Hagemann, S and L. D. Gates (2003). "Improving a subgrid runoff parameterization scheme for climate models by the use of high resolution data derived from satellite observations". In: *Climate Dynamics* 21.3, pp. 349–359. ISSN: 1432-0894. DOI: 10.1007/s00382-003-0349-x.

Hall, C. (2001). "Trends in ocean and coastal tourism: the end of the last frontier?" In: *Ocean & Coastal Management* 44.9, pp. 601–618. ISSN: 0964-5691. DOI: https://doi.org/10.1016/S0964-5691(01)00071-0. URL: http://www.sciencedirect.com/science/article/pii/S0964569101000710.

Hall, R. O., J. L. Tank, M. A. Baker, E. J. Rosi-Marshall, and E. R. Hotchkiss (2016). "Metabolism, Gas Exchange, and Carbon Spiraling in Rivers". In: *Ecosystems* 19.1, pp. 73–86. ISSN: 1435-0629. DOI: 10.1007/s10021-015-9918-1.

Hancock, G., I. Webster, and T. Stieglitz (2006). *Horizontal mixing of Great Barrier Reef waters: Offshore diffusivity determined from radium isotope distribution*. Vol. 111. DOI: 10.1029/2006JC003608.

Hansell, D. A., C. A. Carlson, and R Schlitzer (2012). "Net removal of major marine dissolved organic carbon fractions in the subsurface ocean". In: *Global Biogeochemical Cycles* 26.1. DOI: 10.1029/2011GB004069. URL: https://www.scopus.com/inward/record.uri?eid=2-s2.0-84856755461{\&}doi=10.1029{\%}2F2011GB004069{\&}partnerID=40{\&}md5=c6204e9edf6e9611da77c548c7127666.

Harrison, J. A., N Caraco, and S. P. Seitzinger (2005). "Global patterns and sources of dissolved organic matter export to the coastal zone: Results from a spatially explicit, global model". In: *Global Biogeochemical Cycles* 19.4. ISSN: 0886-6236. DOI: 10.1029/2005GB002480.

Harrison, W. and G. Cota (1991). "Primary production in polar waters-relation to nutrient availability". In: *Polar Research* 10.1, pp. 87–104. DOI: 10.3402/polar.v10i1.6730.

Hart, M., B. Quin, and M Long Nguyen (2004). "Phosphorus Runoff from Agricultural Land and Direct Fertilizer Effects". In: *Journal of environmental quality* 33, pp. 1954–1972.

Hartmann, J. and N. Moosdorf (2011). "Chemical weathering rates of silicate-dominated lithological classes and associated liberation rates of phosphorus on the Japanese Archipelago—Implications for global scale analysis". In: *Chemical Geology* 287.3, pp. 125–157. ISSN: 0009-2541. DOI: https://doi.org/10.1016/j.chemgeo.2010.12.004.

— (2012). "The new global lithological map database GLiM: A representation of rock properties at the Earth surface". In: *Geochemistry, Geophysics, Geosystems* 13.12. ISSN: 1525-2027. DOI: 10.1029/2012GC004370.

Hartmann, J., N. Jansen, H. H. Dürr, S. Kempe, and P. Köhler (2009). "Global CO2-consumption by chemical weathering: What is the contribution of highly active weathering regions?" In: *Global and Planetary Change* 69.4, pp. 185–194. ISSN: 0921-8181. DOI: https://doi.org/10.1016/j.gloplacha.2009.07.007.

Hartmann, J., N. Moosdorf, R. Lauerwald, M. Hinderer, and A. J. West (2014). "Global chemical weathering and associated P-release — The role of lithology, temperature and soil properties". In: *Chemical Geology* 363, pp. 145–163. ISSN: 0009-2541. DOI: https://doi.org/10.1016/j.chemgeo.2013.10.025.

Hastie, A., R. Lauerwald, P. Ciais, and P. Regnier (2019). "Aquatic carbon fluxes dampen the overall variation of net ecosystem productivity in the Amazon basin: An analysis of the interannual variability in the boundless carbon cycle". In: *Global Change Biology* 0.0. DOI: 10.1111/gcb.14620.

Hedges, J. I., R. G. Keil, and R Benner (1997). "What happens to terrestrial organic matter in the ocean?" In: *Organic Geochemistry* 27.5, pp. 195–212. ISSN: 0146-6380. DOI: https://doi.org/10.1016/S0146-6380(97)00066-1.

Heinze, C, E Maier-Reimer, A. M. E. Winguth, and D Archer (1999). "A global oceanic sediment model for longterm climate studies". In: *Global Biogeochemical Cycles* 13.1, pp. 221–250. ISSN: 0886-6236. DOI: 10.1029/98GB02812.

Heinze, M and T Ilyina (2015). "Ocean biogeochemistry in the warm climate of the late Paleocene". In: *Climate of the Past* 11.1, pp. 63–79. DOI: 10.5194/cp-11-63-2015. URL: https://www.clim-past.net/11/63/2015/.

Henson, S. A., J. L. Sarmiento, J. P. Dunne, L. Bopp, I. Lima, S. C. Doney, J. John, and C. Beaulieu (2010). "Detection of anthropogenic climate change in satellite records of ocean chlorophyll and productivity". In: *Biogeosciences* 7.2, pp. 621–640. DOI: 10.5194/bg-7-621-2010.

Hernes, P. J. and R. Benner (2002). "Transport and diagenesis of dissolved and particulate terrigenous organic matter in the North Pacific Ocean".

In: *Deep Sea Research Part I: Oceanographic Research Papers* 49.12, pp. 2119–2132. ISSN: 0967-0637. DOI: https://doi.org/10.1016/S0967-0637(02)00128-0. URL: http://www.sciencedirect.com/science/article/pii/S0967063702001280.

Hilton, R. G., A. Galy, N. Hovius, M.-C. Chen, M.-J. Horng, and H. Chen (2008). In: *Nature Geoscience*, p. 759. DOI: https://doi.org/10.1038/ngeo333.

Holgerson, M. A. and P. A. Raymond (2016). "Large contribution to inland water CO2 and CH4 emissions from very small ponds". In: *Nature Geoscience* 9, p. 222. URL: https://doi.org/10.1038/ngeo2654http://10.0.4.14/ngeo2654https://www.nature.com/articles/ngeo2654{\#}supplementary-information.

Holmes, R. M., J. W. McClelland, P. A. Raymond, B. B. Frazer, B. J. Peterson, and M. Stieglitz (2008). "Lability of DOC transported by Alaskan rivers to the Arctic Ocean". In: *Geophysical Research Letters* 35.3. ISSN: 0094-8276. DOI: 10.1029/2007GL032837. URL: https://doi.org/10.1029/2007GL032837.

Holt, J. et al. (2018). "Climate-Driven Change in the North Atlantic and Arctic Oceans Can Greatly Reduce the Circulation of the North Sea". In: *Geophysical Research Letters* 45.21, pp. 11,811–827,836. DOI: 10.1029/2018GL078878. URL: https://agupubs.onlinelibrary.wiley.com/doi/abs/10.1029/2018GL078878.

Honjo, S et al. (2014). "CITATION Oceanography THE OFFICIAL MAGAZINE OF THE OCEANOGRAPHY SOCIETY C O M M E N TA R Y". In: 27.3. DOI: 10.5670/oceanog.2014.78.

Hsiang, S. M., K. C. Meng, and M. A. Cane (2011). "Civil conflicts are associated with the global climate." In: *Nature* 476.7361, pp. 438–41. ISSN: 1476-4687. DOI: 10.1038/nature10311.

Huthnance, J. M. (1997). "North sea interaction with the north atlantic ocean". In: *Deutsche Hydrografische Zeitschrift* 49.2, pp. 153–162. ISSN: 1616-7228. DOI: 10.1007/BF02764030. URL: https://doi.org/10.1007/BF02764030.

Ichikawa, H. and R. C. Beardsley (2002). "The Current System in the Yellow and East China Seas". In: *Journal of Oceanography* 58.1, pp. 77–92. ISSN: 1573-868X. DOI: 10.1023/A:1015876701363.

Ilyina, T., K. D. Six, J. Segschneider, E. Maier-Reimer, H. Li, and I. Núñez-Riboni (2013). "Global ocean biogeochemistry model HAMOCC: Model architecture and performance as component of the MPI-Earth system model in different CMIP5 experimental realizations". In: *Journal of Advances in Modeling Earth Systems* 5.2, pp. 287–315. DOI: 10.1029/2012MS000178.

IPCC (2013). "Carbon and Other Biogeochemical Cycles". In: *Climate Change 2013 – The Physical Science Basis: Working Group I Contribution to the Fifth Assessment Report of the Intergovernmental Panel on Climate Change*. Ed. by Intergovernmental Panel on Climate Change. Cambridge: Cambridge University Press, pp. 465–570. ISBN: 9781107057999. DOI: DOI:10.1017/CBO9781107415324.015.

Ittekkot, V. (1988). "Global trends in the nature of organic matter in river suspensions". In: *Nature* 332, p. 436.

Ittekkot, V., C. Humborg, and P. Schäfer (2000a). "Hydrological Alterations and Marine Biogeochemistry: A Silicate Issue?" In: *BioScience* 50.9, p. 776. ISSN: 0006-3568. DOI: 10.1641/0006-3568(2000)050[0776:HAAMBA]2.0.CO;2.

Ittekkot, V., C. Humborg, and P. Schäfer (2000b). "Hydrological Alterations and Marine Biogeochemistry: A Silicate Issue?: Silicate retention in reservoirs behind dams affects ecosystem structure in coastal seas". In: *BioScience* 50.9, pp. 776–782. ISSN: 0006-3568. DOI: 10.1641/0006-3568(2000)050[0776:HAAMBA]2.0.CO;2. eprint: http://oup.prod.sis.lan/bioscience/article-pdf/50/9/776/26890470/50-9-776.pdf.

Izett, J. G. and K. Fennel (2018). "Estimating the Cross-Shelf Export of Riverine Materials: Part 1. General Relationships From an Idealized Numerical Model". In: *Global Biogeochemical Cycles* 32.2, pp. 160–175. DOI: 10.1002/2017GB005667. URL: https://agupubs.onlinelibrary.wiley.com/doi/abs/10.1002/2017GB005667.

Jacobson, A. R., S. E. Mikaloff Fletcher, N. Gruber, J. L. Sarmiento, and M. Gloor (2007). "A joint atmosphere-ocean inversion for surface fluxes of carbon dioxide: 1. Methods and global-scale fluxes". In: *Global Biogeochemical Cycles* 21.1. DOI: 10.1029/2005GB002556.

Johannessen, S. C., W. Miller, and J. Cullen (2003). *Calculation of UV attenuation and colored dissolved organic matter absorption spectra from measurement of ocean color*. Vol. 108, 3301, doi:10.1029/2000JC000514. DOI: 10.1029/2000JC000514.

Johnson, K. S., F. P. Chavez, and G. E. Friederich (1999). "Continental-shelf sediment as a primary source of iron for coastal phytoplankton". In: *Nature* 398, p. 697. URL: https://doi.org/10.1038/19511http://10.0.4.14/19511.

Jungclaus, J. H., N Fischer, H Haak, K Lohmann, J Marotzke, D Matei, U Mikolajewicz, D. Notz, and S. J. S. (2013). "Characteristics of the ocean simulations in the Max Planck Institute Ocean Model (MPIOM) the ocean

component of the MPI-Earth system model". In: *Journal of Advances in Modeling Earth Systems* 5.2, pp. 422–446. ISSN: 1942-2466. DOI: 10.1002/jame.20023.

Justić, D., N. N. Rabalais, R. E. Turner, and Q. Dortch (1995). "Changes in nutrient structure of river-dominated coastal waters: stoichiometric nutrient balance and its consequences". In: *Estuarine, Coastal and Shelf Science* 40.3, pp. 339–356. ISSN: 0272-7714. DOI: https://doi.org/10.1016/S0272-7714(05)80014-9.

Kahru, M., R. Kudela, M. Manzano-Sarabia, and B Greg Mitchell (2009). *Trends in primary production in the California Current detected with satellite data*. Vol. 114. DOI: 10.1029/2008JC004979.

Kaiser, K., M. Canedo-Oropeza, R. McMahon, and R. M. W. Amon (2017). "Origins and transformations of dissolved organic matter in large Arctic rivers". In: *Scientific Reports* 7.1, p. 13064. ISSN: 2045-2322. DOI: 10.1038/s41598-017-12729-1.

Kang, Y., D. Pan, Y. Bai, X. He, X. Chen, C.-T. A. Chen, and D. Wang (2013). "Areas of the global major river plumes". In: *Acta Oceanologica Sinica* 32.1, pp. 79–88. ISSN: 1869-1099. DOI: 10.1007/s13131-013-0269-5. URL: https://doi.org/10.1007/s13131-013-0269-5.

Karl, D, R Letelier, L Tupas, J Dore, J Christian, and D Hebel (1997). "The role of nitrogen fixation in biogeochemical cycling in the subtropical North Pacific Ocean". In: *Nature* 388.6642, pp. 533–538. ISSN: 1476-4687. DOI: 10.1038/41474. URL: https://doi.org/10.1038/41474.

Kim, T.-W., K. Lee, R. G. Najjar, H.-D. Jeong, and H. J. Jeong (2011). "Increasing N Abundance in the Northwestern Pacific Ocean Due to Atmospheric Nitrogen Deposition". In: *Science* 334.6055, 505 LP –509. DOI: 10.1126/science.1206583. URL: http://science.sciencemag.org/content/334/6055/505.abstract.

Kronvang, B., I. K. Andersen, C. C. Hoffmann, M. L. Pedersen, N. B. Ovesen, and H. E. Andersen (2007). "Water Exchange and Deposition of Sediment and Phosphorus during Inundation of Natural and Restored Lowland Floodplains". In: *Water, Air, and Soil Pollution* 181.1, pp. 115–121. ISSN: 1573-2932. DOI: 10.1007/s11270-006-9283-y. URL: https://doi.org/10.1007/s11270-006-9283-y.

Krumins, V., M. Gehlen, S. Arndt, P. Van Cappellen, and P. Regnier (2013). "Dissolved inorganic carbon and alkalinity fluxes from coastal marine sediments: Model estimates for different shelf environments and sensitivity

to global change". In: *Biogeosciences* 10.1, pp. 371–398. ISSN: 17264170. DOI: 10.5194/bg-10-371-2013.

Kuhlbrodt, T and J. M. Gregory (2012). "Ocean heat uptake and its consequences for the magnitude of sea level rise and climate change". In: *Geophysical Research Letters* 39.18. ISSN: 0094-8276. DOI: 10.1029/2012GL052952. URL: https://doi.org/10.1029/2012GL052952.

Lacroix, F., T. Ilyina, and J. Hartmann (2019). "Oceanic CO_2 outgassing and biological production hotspots induced by pre-industrial river loads of nutrients and carbon in a global modelling approach". In: *Biogeosciences Discussions* 2019, pp. 1–56. DOI: 10.5194/bg-2019-152. URL: https://www.biogeosciences-discuss.net/bg-2019-152/.

Lalonde, K, A. V. Vähätalo, and Y Gélinas (2014). "Revisiting the disappearance of terrestrial dissolved organic matter in the ocean: a δC13 study". In: *Biogeosciences* 11.13, pp. 3707–3719. DOI: 10.5194/bg-11-3707-2014.

Lange, G.-M. and N. Jiddawi (2009). *Economic value of marine ecosystem services in Zanzibar: Implications for marine conservation and sustainable development*. Vol. 52, pp. 521–532. DOI: 10.1016/j.ocecoaman.2009.08.005.

Laruelle, G. G., H. H. Dürr, R. Lauerwald, J. Hartmann, C. P. Slomp, N. Goossens, and P. A. Regnier (2013). "Global multi-scale segmentation of continental and coastal waters from the watersheds to the continental margins". In: *Hydrology and Earth System Sciences* 17.5, pp. 2029–2051. ISSN: 10275606. DOI: 10.5194/hess-17-2029-2013.

Laruelle, G. G., P Landschützer, N Gruber, J.-L. Tison, B Delille, and P Regnier (2017). "Global high-resolution monthly pCO2 climatology for the coastal ocean derived from neural network interpolation". In: *Biogeosciences* 14.19, pp. 4545–4561. DOI: 10.5194/bg-14-4545-2017.

Laruelle, G. G., H. H. Dürr, C. P. Slomp, and A. V. Borges (2010). "Evaluation of sinks and sources of CO2 in the global coastal ocean using a spatially-explicit typology of estuaries and continental shelves". In: *Geophysical Research Letters* 37.15. ISSN: 0094-8276. DOI: 10.1029/2010GL043691. URL: https://doi.org/10.1029/2010GL043691.

Laruelle, G. G., R. Lauerwald, B. Pfeil, and P. Regnier (2014). "Regionalized global budget of the CO2 exchange at the air-water interface in continental shelf seas." In: *Global Biogeochemical Cycles*, pp. 1199–1214. ISSN: 08866236. DOI: 10.1002/2014GB004832.Received.

Laruelle, G. G., W.-J. Cai, X. Hu, N. Gruber, F. T. Mackenzie, and P. Regnier (2018). "Continental shelves as a variable but increasing global sink for atmospheric carbon dioxide". In: *Nature Communications* 9.1, p. 454. ISSN:

2041-1723. DOI: 10.1038/s41467-017-02738-z. URL: https://doi.org/10.1038/s41467-017-02738-z.

Lauerwald, R., P. Regnier, M. Camino-Serrano, B. Guenet, M. Guimberteau, A. Ducharne, J. Polcher, and P. Ciais (2017). "ORCHILEAK (revision 3875): a new model branch to simulate carbon transfers along the terrestrial–aquatic continuum of the Amazon basin". In: *Geoscientific Model Development* 10.10, pp. 3821–3859. DOI: 10.5194/gmd-10-3821-2017. URL: https://www.geosci-model-dev.net/10/3821/2017/.

Laufkötter, C, M Vogt, and N Gruber (2013). "Long-term trends in ocean plankton production and particle export between 1960–2006". In: *Biogeosciences* 10.11, pp. 7373–7393. DOI: 10.5194/bg-10-7373-2013.

Laufkötter, C et al. (2015). "Drivers and uncertainties of future global marine primary production in marine ecosystem models". In: *Biogeosciences* 12.23, pp. 6955–6984. DOI: 10.5194/bg-12-6955-2015. URL: https://www.biogeosciences.net/12/6955/2015/.

Laursen, A. E. and S. P. Seitzinger (2002). "Measurement of denitrification in rivers: an integrated, whole reach approach". In: *Hydrobiologia* 485.1, pp. 67–81. ISSN: 1573-5117. DOI: 10.1023/A:1021398431995. URL: https://doi.org/10.1023/A:1021398431995.

Lauvset, S. K., M Chierici, F Counillon, A Omar, G Nondal, T Johannessen, and A Olsen (2013). "Annual and seasonal fCO2 and air–sea CO2 fluxes in the Barents Sea". In: *Journal of Marine Systems* 113-114, pp. 62–74. ISSN: 0924-7963. DOI: https://doi.org/10.1016/j.jmarsys.2012.12.011. URL: http://www.sciencedirect.com/science/article/pii/S0924796313000031.

Le Fouest, V, M Babin, and J.-É. Tremblay (2013). "The fate of riverine nutrients on Arctic shelves". In: *Biogeosciences* 10.6, pp. 3661–3677. DOI: 10.5194/bg-10-3661-2013.

Le Quéré, C et al. (2018). "Global Carbon Budget 2018". In: *Earth System Science Data* 10.4, pp. 2141–2194. DOI: 10.5194/essd-10-2141-2018. URL: https://www.earth-syst-sci-data.net/10/2141/2018/.

Lefèvre, N., M. Flores Montes, F. L. Gaspar, C. Rocha, S. Jiang, M. C. De Araújo, and J. S. P. Ibánhez (2017). "Net Heterotrophy in the Amazon Continental Shelf Changes Rapidly to a Sink of CO2 in the Outer Amazon Plume". In: *Frontiers in Marine Science* 4.September, pp. 1–16. ISSN: 2296-7745. DOI: 10.3389/fmars.2017.00278.

Lehner, B. et al. (2011). "High-resolution mapping of the world's reservoirs and dams for sustainable river-flow management". In: *Frontiers in Ecology*

and the Environment 9.9, pp. 494–502. ISSN: 1540-9295. DOI: 10.1890/100125. URL: https://doi.org/10.1890/100125.

Levitus, S, J Antonov, and T Boyer (2005). "Warming of the world ocean, 1955–2003". In: *Geophysical Research Letters* 32.2. ISSN: 0094-8276. DOI: 10.1029/2004GL021592. URL: https://doi.org/10.1029/2004GL021592.

Li, H. and T. Ilyina (2018). "Current and Future Decadal Trends in the Oceanic Carbon Uptake Are Dominated by Internal Variability". In: *Geophysical Research Letters* 45.2, pp. 916–925. DOI: 10.1002/2017GL075370. URL: https://agupubs.onlinelibrary.wiley.com/doi/abs/10.1002/2017GL075370.

Li, S. and R. T. Bush (2015). "Changing fluxes of carbon and other solutes from the Mekong River". In: *Sci. Rep.* 26005.1. ISSN: 1040-6182. DOI: 10.1038/srep16005(2015).

Lind, S., R. B. Ingvaldsen, and T. Furevik (2018). "Arctic warming hotspot in the northern Barents Sea linked to declining sea-ice import". In: *Nature Climate Change* 8.7, pp. 634–639. ISSN: 1758-6798. DOI: 10.1038/s41558-018-0205-y. URL: https://doi.org/10.1038/s41558-018-0205-y.

Liu, K.-K., K. Iseki, and S.-Y Chao (2000). "Continental margin carbon fluxes". In: pp. 187–239.

Longhurst, A. (1995). "Seasonal cycles of pelagic production and consumption". In: *Progress in Oceanography* 36.2, pp. 77–167. ISSN: 0079-6611. DOI: https://doi.org/10.1016/0079-6611(95)00015-1. URL: http://www.sciencedirect.com/science/article/pii/0079661195000151.

Ludwig, W., J.-L. Probst, and S. Kempe (1996). "Predicting the oceanic input of organic carbon by continental erosion". In: *Global Biogeochemical Cycles* 10.1, pp. 23–41. DOI: 10.1029/95GB02925.

Ludwig, W., P. Amiotte Suchet, G. Munhoven, and J.-L. Probst (1998). "Atmospheric CO2 consumption by continental erosion: present-day controls and implications for the last glacial maximum". In: *Global and Planetary Change* 16-17, pp. 107–120. ISSN: 0921-8181. DOI: https://doi.org/10.1016/S0921-8181(98)00016-2.

Ludwig, W., E. Dumont, M. Meybeck, and S. Heussner (2009). "River discharges of water and nutrients to the Mediterranean and Black Sea: Major drivers for ecosystem changes during past and future decades?" In: *Progress in Oceanography* 80.3, pp. 199–217. ISSN: 0079-6611. DOI: https://doi.org/10.1016/j.pocean.2009.02.001. URL: http://www.sciencedirect.com/science/article/pii/S0079661109000020.

Luo, X. S. et al. (2014). "Chinese coastal seas are facing heavy atmospheric nitrogen deposition". In: *Environmental Research Letters* 9.9, p. 95007. ISSN:

1748-9326. DOI: 10.1088/1748-9326/9/9/095007. URL: http://dx.doi.org/10.1088/1748-9326/9/9/095007.

Maavara, T., H. H. Dürr, and P. Van Cappellen (2014). "Worldwide retention of nutrient silicon by river damming: From sparse data set to global estimate". In: *Global Biogeochemical Cycles* 28.8, pp. 842–855. DOI: 10.1002/2014GB004875.

Maavara, T., C. T. Parsons, C. Ridenour, S. Stojanovic, H. H. Dürr, H. R. Powley, and P. Van Cappellen (2015). "Global phosphorus retention by river damming". In: *Proceedings of the National Academy of Sciences* 112.51, 15603 LP –15608. DOI: 10.1073/pnas.1511797112. URL: http://www.pnas.org/content/112/51/15603.abstract.

Maavara, T., R. Lauerwald, P. Regnier, and P. Van Cappellen (2017). "Global perturbation of organic carbon cycling by river damming". In: *Nature Communications* 8, p. 15347. DOI: 10.1038/ncomms15347.

Maavara, T., R. Lauerwald, G. G. Laruelle, Z. Akbarzadeh, N. J. Bouskill, P. Van Cappellen, and P. Regnier (2019). "Nitrous oxide emissions from inland waters: Are IPCC estimates too high?" In: *Global Change Biology* 25.2, pp. 473–488. ISSN: 1354-1013. DOI: 10.1111/gcb.14504. URL: https://doi.org/10.1111/gcb.14504.

Mackenzie, F. T., A Lerman, and A. J. Andersson (2004). "Past and present of sediment and carbon biogeochemical cycling models". In: *Biogeosciences* 1.1, pp. 11–32. DOI: 10.5194/bg-1-11-2004.

Mackenzie, F. T., A. Lerman, and L. M. B. Ver (1998). "Role of the continental margin in the global carbon balance during the past three centuries". In: *Geology* 26.5, pp. 423–426. ISSN: 0091-7613.

Mackenzie, F. T., L. M. Ver, and A. Lerman (2000). "Coastal-Zone Biogeochemical Dynamics under Global Warming". In: *International Geology Review* 42.3, pp. 193–206. ISSN: 0020-6814. DOI: 10.1080/00206810009465077. URL: https://doi.org/10.1080/00206810009465077.

— (2002). "Century-scale nitrogen and phosphorus controls of the carbon cycle". In: *Chemical Geology* 190.1. Geochemistry of Crustal Fluids-Fluids in the Crust and Chemical Fluxes at the Earth's Surface, pp. 13 –32. ISSN: 0009-2541. DOI: https://doi.org/10.1016/S0009-2541(02)00108-0.

Mahowald, N. et al. (2008). "Global distribution of atmospheric phosphorus sources, concentrations and deposition rates, and anthropogenic impacts". In: *Global Biogeochemical Cycles* 22.4. ISSN: 0886-6236. DOI: 10.1029/2008GB003240. URL: https://doi.org/10.1029/2008GB003240.

Mahowald, N. M., D. R. Muhs, S Levis, J Rasch Philip, M Yoshioka, S Zender Charles, and C Luo (2006). "Change in atmospheric mineral aerosols in response to climate: Last glacial period, preindustrial, modern, and doubled carbon dioxide climates". In: *Journal of Geophysical Research: Atmospheres* 111.D10. ISSN: 0148-0227. DOI: 10.1029/2005JD006653.

Maier-Reimer, E and K Hasselmann (1987). "Transport and storage of CO2 in the ocean ——an inorganic ocean-circulation carbon cycle model". In: *Climate Dynamics* 2.2, pp. 63–90. ISSN: 1432-0894. DOI: 10.1007/BF01054491.

Martin, J. H., G. A. Knauer, D. M. Karl, and W. W. Broenkow (1987). "VERTEX: carbon cycling in the northeast Pacific". In: *Deep Sea Research Part A. Oceanographic Research Papers* 34.2, pp. 267–285. ISSN: 0198-0149. DOI: https://doi.org/10.1016/0198-0149(87)90086-0.

Mathis, M, A Elizalde, and U Mikolajewicz (2019). "The future regime of Atlantic nutrient supply to the Northwest European Shelf". In: *Journal of Marine Systems* 189, pp. 98–115. ISSN: 0924-7963. DOI: https://doi.org/10.1016/j.jmarsys.2018.10.002. URL: http://www.sciencedirect.com/science/article/pii/S0924796318300198.

Mauritsen, T. et al. (2019). "Developments in the MPI-M Earth System Model version 1.2 (MPI-ESM 1.2) and its response to increasing CO2". In: *Journal of Advances in Modeling Earth Systems* 0.ja. DOI: 10.1029/2018MS001400.

Mayer, B., T Stacke, I Stottmeister, and T Pohlmann (2015). *Sunda Shelf Seas: flushing rates and residence times*. Vol. 12, pp. 863–895. DOI: 10.5194/osd-12-863-2015.

Mayorga, E., S. P. Seitzinger, J. A. Harrison, E. Dumont, A. A.H. W. Beusen, A. F. Bouwman, B. M. Fekete, C. Kroeze, and G. V. Drecht (2010). "Global Nutrient Export from WaterSheds 2 (NEWS 2): Model development and implementation". In: *Environmental Modelling & Software* 25.7, pp. 837–853. ISSN: 1364-8152. DOI: https://doi.org/10.1016/j.envsoft.2010.01.007.

Men, W. and G. Liu (2015). *Distribution of 226Ra and the residence time of the shelf water in the Yellow Sea and the East China Sea*. Vol. 303, pp. 2333–2344. DOI: 10.1007/s10967-014-3749-y.

Meybeck, M (1993). "C, N, P and S in Rivers: From Sources to Global Inputs". In: *Interactions of C, N, P and S Biogeochemical Cycles and Global Change*. Ed. by R. Wollast, F. T. Mackenzie, and L. Chou. Berlin, Heidelberg: Springer Berlin Heidelberg, pp. 163–193. ISBN: 978-3-642-76064-8.

Meybeck, M. (1982). "Carbon, Nitrogen, and Phosphorus Transport by World Rivers". In: *Am. J. Sci.* 282.

Meybeck, M. and C. Vörösmarty (1999). "Global transfer of carbon by rivers". In: *Global Change News Lett* 26.37.

Meybeck, M., H. H. Dürr, and C. J. Vörösmarty (2006). "Global coastal segmentation and its river catchment contributors: A new look at land-ocean linkage". In: *Global Biogeochemical Cycles* 20.1. ISSN: 0886-6236. DOI: 10.1029/2005GB002540.

Milinski, S., J. Bader, H. Haak, A. C. Siongco, and J. H. Jungclaus (2016). "High atmospheric horizontal resolution eliminates the wind-driven coastal warm bias in the southeastern tropical Atlantic". In: *Geophysical Research Letters*, available online. ISSN: 1944-8007. DOI: 10.1002/2016GL070530.

Millero, F. J. (2007). "The Marine Inorganic Carbon Cycle". In: *Chemical Reviews* 107.2, pp. 308–341. ISSN: 0009-2665. DOI: 10.1021/cr0503557. URL: https://doi.org/10.1021/cr0503557.

Milliman, J. D. and A. W. Droxler (1996). "Neritic and pelagic carbonate sedimentation in the marine environment: ignorance is not bliss". In: *Geologische Rundschau* 85.3, pp. 496–504. ISSN: 1432-1149. DOI: 10.1007/BF02369004.

Milliman, J. D. and K. Farnsworth (2011). *River Discharge to the Coastal Ocean – A Global Synthesis*. ISBN: 9780521879873. DOI: 10.1017/CBO9780511781247.

Moncheva, S., V. Doncheva, G Shtereva, L. Kamburska, A. Malej, and S. Gorinstein (2002). *Application of eutrophication indices for assessment of the Bulgarian Black Sea coastal ecosystem ecological quality*. Vol. 46, pp. 19–28. DOI: 10.2166/wst.2002.0136.

Moore, W. S. and J. de Oliveira (2008). "Determination of residence time and mixing processes of the Ubatuba, Brazil, inner shelf waters using natural Ra isotopes". In: *Estuarine, Coastal and Shelf Science* 76.3, pp. 512–521. ISSN: 0272-7714. DOI: https://doi.org/10.1016/j.ecss.2007.07.042. URL: http://www.sciencedirect.com/science/article/pii/S0272771407003046.

Morée, A. L., A. H. W. Beusen, A. F. Bouwman, and W. J. Willems (2013). "Exploring global nitrogen and phosphorus flows in urban wastes during the twentieth century". In: *Global Biogeochemical Cycles* 27.3, pp. 836–846. DOI: 10.1002/gbc.20072.

Mörner, N.-A. and G. Etiope (2002). "Carbon degassing from the lithosphere". In: *Global and Planetary Change* 33.1, pp. 185–203. ISSN: 0921-8181. DOI: https://doi.org/10.1016/S0921-8181(02)00070-X.

Müller, D, T Warneke, T Rixen, M Müller, A Mujahid, H. W. Bange, and J Notholt (2016a). "Fate of terrestrial organic carbon and associated CO$_2$

and CO emissions from two Southeast Asian estuaries". In: *Biogeosciences* 13.3, pp. 691–705. DOI: 10.5194/bg-13-691-2016.

Müller, D, T Warneke, T Rixen, M Müller, A Mujahid, H. W. Bange, and J Notholt (2016b). "Fate of terrestrial organic carbon and associated CO2 and CO emissions from two Southeast Asian estuaries". In: *Biogeosciences* 13.3, pp. 691–705. DOI: 10.5194/bg-13-691-2016.

Muller-Karger, F. E., R. Varela, R. Thunell, R. Luerssen, C. Hu, and J. J. Walsh (2005). "The importance of continental margins in the global carbon cycle". In: *Geophysical Research Letters* 32.1. ISSN: 0094-8276. DOI: 10.1029/2004GL021346. URL: https://doi.org/10.1029/2004GL021346.

Naipal, V, P Ciais, Y Wang, R Lauerwald, B Guenet, and K Van Oost (2018). "Global soil organic carbon removal by water erosion under climate change and land use change during AD\,1850–2005". In: *Biogeosciences* 15.14, pp. 4459–4480. DOI: 10.5194/bg-15-4459-2018. URL: https://www.biogeosciences.net/15/4459/2018/.

Nakhavali, M et al. (2018). "Representation of dissolved organic carbon in the JULES land surface model (vn4.4_JULES-DOCM)". In: *Geoscientific Model Development* 11.2, pp. 593–609. DOI: 10.5194/gmd-11-593-2018. URL: https://www.geosci-model-dev.net/11/593/2018/.

Nixon, S. W. et al. (1996). "The fate of nitrogen and phosphorus at the land-sea margin of the North Atlantic Ocean". In: *Nitrogen Cycling in the North Atlantic Ocean and its Watersheds*. Ed. by R. W. Howarth. Dordrecht: Springer Netherlands, pp. 141–180. ISBN: 978-94-009-1776-7.

Noriega, C. and M. Araujo (2011). *Nutrient budgets (C, N and P) and trophic dynamics of a Brazilian tropical estuary: Barra das Jangadas*. Vol. 83, pp. 441–456. DOI: 10.1590/S0001-37652011000200007.

Nozaki, Y., V. Kasemsupaya, and H. Tsubota (1989). "Mean residence time of the shelf water in the East China and the Yellow Seas determined by 228Ra/226Ra measurements". In: *Geophysical Research Letters* 16.11, pp. 1297–1300. ISSN: 0094-8276. DOI: 10.1029/GL016i011p01297. URL: https://doi.org/10.1029/GL016i011p01297.

Ohta, K., Y. Inomata, A. Sano, and K. Sugimura (2000). "Photochemical Degradation of Dissolved Organic Carbon to Carbon Monoxide in Coastal Seawater BT - Dynamics and Characterization of Marine Organic Matter". In: ed. by N. Handa, E. Tanoue, and T. Hama. Dordrecht: Springer Netherlands, pp. 213–229. ISBN: 978-94-017-1319-1. DOI: 10.1007/978-94-017-1319-1_10. URL: https://doi.org/10.1007/978-94-017-1319-1{_}10.

Opsahl, S. and R. Benner (1997). "Distribution and cycling of terrigenous dissolved organic matter in the ocean". In: *Nature* 386.6624, pp. 480–482. ISSN: 1476-4687. DOI: 10.1038/386480a0. URL: https://doi.org/10.1038/386480a0.

Orr, J. C. et al. (2017). "Biogeochemical protocols and diagnostics for the CMIP6 Ocean Model Intercomparison Project (OMIP)". In: *Geoscientific Model Development* 10.6, pp. 2169–2199. DOI: 10.5194/gmd-10-2169-2017.

Pailler, K, B Bourlès, and Y Gouriou (1999). "The barrier layer in the western tropical Atlantic Ocean". In: *Geophysical Research Letters* 26.14, pp. 2069–2072. ISSN: 0094-8276. DOI: 10.1029/1999GL900492. URL: https://doi.org/10.1029/1999GL900492.

Painter, S. C., D. J. Lapworth, E. Woodward, S. Kroeger, C. D. Evans, D. Mayor, and R. Sanders (2018). "Terrestrial dissolved organic matter distribution in the North Sea". In: *Science of The Total Environment* 630, pp. 630–647. ISSN: 0048-9697. DOI: https://doi.org/10.1016/j.scitotenv.2018.02.237.

Paulsen, H., T. Ilyina, J. H. Jungclaus, K. D. Six, and I. Stemmler (2018). "Light absorption by marine cyanobacteria affects tropical climate mean state and variability". In: *Earth System Dynamics* 9.4, pp. 1283–1300. DOI: 10.5194/esd-9-1283-2018. URL: https://www.earth-syst-dynam.net/9/1283/2018/.

Paulsen, H., T. Ilyina, K. D. Six, and I. Stemmler (2017). "Incorporating a prognostic representation of marine nitrogen fixers into the global ocean biogeochemical model HAMOCC". In: *Journal of Advances in Modeling Earth Systems* 9.1, pp. 438–464. ISSN: 1942-2466. DOI: 10.1002/2016MS000737.

Pfeil, B et al. (2013). "A uniform, quality controlled Surface Ocean CO$_{2}$ Atlas (SOCAT)". In: *Earth System Science Data* 5.1, pp. 125–143. DOI: 10.5194/essd-5-125-2013. URL: https://www.earth-syst-sci-data.net/5/125/2013/.

Pipko, I. I. et al. (2017). "The spatial and interannual dynamics of the surface water carbonate system and air–sea CO_2 fluxes in the outer shelf and slope of the Eurasian Arctic Ocean". In: *Ocean Science* 13.6, pp. 997–1016. DOI: 10.5194/os-13-997-2017. URL: https://www.ocean-sci.net/13/997/2017/.

Plummer, L. and E. Busenberg (1982). "The solubilities of calcite, aragonite and vaterite in CO2-H2O solutions between 0 and 90C, and an evaluation of the aqueous model for the system CaCO3-CO2-H2O". In: *Geochimica et Cosmochimica Acta* 46.6, pp. 1011–1040. ISSN: 0016-7037. DOI: 10.1016/0016-7037(82)90056-4.

Poli, P. et al. (2016). "ERA-20C: An Atmospheric Reanalysis of the Twentieth Century". In: *Journal of Climate* 29.11, pp. 4083–4097. ISSN: 0894-8755. DOI: 10.1175/JCLI-D-15-0556.1. URL: https://doi.org/10.1175/JCLI-D-15-0556.1.

Qiao, F., Y. Yang, X. Lü, C. Xia, X. Chen, B. Wang, and Y. Yuan (2006). "Coastal upwelling in the East China Sea in winter". In: *Journal of Geophysical Research: Oceans* 111.C11. DOI: 10.1029/2005JC003264. URL: https://agupubs.onlinelibrary.wiley.com/doi/abs/10.1029/2005JC003264.

Rabalais, N. N., R. E. Turner, and W. J. Wiseman (2002). "Gulf of Mexico Hypoxia, A.K.A. "The Dead Zone"". In: *Annual Review of Ecology and Systematics* 33.1, pp. 235–263. ISSN: 0066-4162. DOI: 10.1146/annurev.ecolsys.33.010802.150513. URL: https://doi.org/10.1146/annurev.ecolsys.33.010802.150513.

Rabouille, C., F. T. Mackenzie, and L. M. Ver (2001). "Influence of the human perturbation on carbon, nitrogen, and oxygen biogeochemical cycles in the global coastal ocean". In: *Geochimica et Cosmochimica Acta* 65.21, pp. 3615–3641. ISSN: 0016-7037. DOI: https://doi.org/10.1016/S0016-7037(01)00760-8. URL: http://www.sciencedirect.com/science/article/pii/S0016703701007608.

Radach, G. and J. Pätsch (2007). "Variability of continental riverine freshwater and nutrient inputs into the North Sea for the years 1977–2000 and its consequences for the assessment of eutrophication". In: *Estuaries and Coasts* 30.1, pp. 66–81. ISSN: 1559-2731. DOI: 10.1007/BF02782968. URL: https://doi.org/10.1007/BF02782968.

Ramirez, A. J. and A. W. Rose (1992). "Analytical geochemistry of organic phosphorus and its correlation with organic carbon in marine and fluvial sediments and soils". In: *American Journal of Science* 292, pp. 421–454. DOI: 10.2475/ajs.292.6.421.

Raymond, P. A., J. W. McClelland, R. M. Holmes, A. V. Zhulidov, K Mull, B. J. Peterson, R. G. Striegl, G. R. Aiken, and T. Y. Gurtovaya (2007). "Flux and age of dissolved organic carbon exported to the Arctic Ocean: A carbon isotopic study of the five largest arctic rivers". In: *Global Biogeochemical Cycles* 21.4. DOI: 10.1029/2007GB002934.

Raymond, P. A. et al. (2013). "Global carbon dioxide emissions from inland waters". In: *Nature* 503, p. 355. URL: https://doi.org/10.1038/nature12760http://10.0.4.14/nature12760https://www.nature.com/articles/nature12760{\#}supplementary-information.

Regnier, P. et al. (2013). "Anthropogenic perturbation of the carbon fluxes from land to ocean". In: *Nature Geoscience* 6, p. 597.

Ren, J. L., J Zhang, J. B. Li, X. Y. Yu, S. M. Liu, and E. R. Zhang (2006). "Dissolved aluminum in the Yellow Sea and East China Sea – Al as a tracer of Changjiang (Yangtze River) discharge and Kuroshio incursion". In: *Estuarine, Coastal and Shelf Science* 68.1, pp. 165–174. ISSN: 0272-7714. DOI: https://doi.org/10.1016/j.ecss.2006.02.004. URL: http://www.sciencedirect.com/science/article/pii/S0272771406000539.

Resplandy, L, R. F. Keeling, C Rödenbeck, B. B. Stephens, S Khatiwala, K. B. Rodgers, M. C. Long, L Bopp, and P. P. Tans (2018). "Revision of global carbon fluxes based on a reassessment of oceanic and riverine carbon transport". In: *Nature Geoscience* 11.7, pp. 504–509. ISSN: 1752-0908. DOI: 10.1038/s41561-018-0151-3.

Rhein, M., S. Rintoul, S Aoki, E. Campos, D Chambers, R. Feely, and F. Wang (2013). *Observations: Ocean. In: Climate Change 2013: The Physical Science Basis. Contribution of Working Group I to the Fifth Assessment Report of the Intergovernmental Panel on Climate Change*, pp. 255–315.

Ricker-Gilbert, J. and T. S. Jayne (2017). "Estimating the Enduring Effects of Fertiliser Subsidies on Commercial Fertiliser Demand and Maize Production: Panel Data Evidence from Malawi". In: *Journal of Agricultural Economics* 68.1, pp. 70–97. ISSN: 0021-857X. DOI: 10.1111/1477-9552.12161. URL: https://doi.org/10.1111/1477-9552.12161.

Roelandt, C, Y Goddéris, M.-P. Bonnet, and F. Sondag (2010). "Coupled modeling of biospheric and chemical weathering processes at the continental scale". In: *Global Biogeochemical Cycles* 24.2. ISSN: 0886-6236. DOI: 10.1029/2008GB003420.

Romero-Mujalli, G, J Hartmann, and J Börker (2018). "Temperature and CO2 dependency of global carbonate weathering fluxes – Implications for future carbonate weathering research". In: *Chemical Geology*. ISSN: 0009-2541. DOI: https://doi.org/10.1016/j.chemgeo.2018.08.010.

Röske, F. (2006). "A global heat and freshwater forcing dataset for ocean models". In: *Ocean Modelling* 11.3, pp. 235–297. ISSN: 1463-5003. DOI: https://doi.org/10.1016/j.ocemod.2004.12.005.

Saba, V. S. et al. (2011). "An evaluation of ocean color model estimates of marine primary productivity in coastal and pelagic regions across the globe". In: *Biogeosciences* 8.2, pp. 489–503. DOI: 10.5194/bg-8-489-2011. URL: https://www.biogeosciences.net/8/489/2011/.

Saba, V. S. et al. (2010). "Challenges of modeling depth-integrated marine primary productivity over multiple decades: A case study at BATS and HOT". In: *Global Biogeochemical Cycles* 24.3. ISSN: 0886-6236. DOI: 10.1029/2009GB003655. URL: https://doi.org/10.1029/2009GB003655.

Sabine, C. L. (2004). "The Oceanic Sink for Anthropogenic CO$_2$". In: *Science* 305.5682, pp. 367–371. ISSN: 0036-8075. DOI: 10.1126/science.1097403. arXiv: 9809069 [gr-qc].

Sarin, M. M., R. Rengarajan, and B L. K. Somayajulu (1994). *Natural radionuclides in the Arabian Sea and Bay of Bengal: Distribution and evaluation of particle scavenging processes*. Vol. 103, pp. 211–235. DOI: 10.1007/BF02839537.

Sarmiento, J. L., P. Monfray, E. Maier-Reimer, O. Aumont, R. J. Murnane, and J. C. Orr (2000). "Sea-air CO2 fluxes and carbon transport: A comparison of three ocean general circulation models". In: *Global Biogeochemical Cycles* 14.4, pp. 1267–1281. DOI: 10.1029/1999GB900062.

Sarmiento, J. and E. Sundquist (1992). "Revised budget for the oceanic uptake of anthropogenic carbon dioxide". In: *Nature* 356, pp. 589–593. DOI: 10.1038/356589a0.

Sarmiento, J. L. and N. Gruber (2006). *Ocean Biogeochemical Dynamics. xiii + 503 pp. Princeton, Woodstock: Princeton University Press.* Vol. 144. 06. DOI: 10.1017/s0016756807003755.

Sarmiento, J. L. and C. Le Quéré (1996). "Oceanic Carbon Dioxide Uptake in a Model of Century-Scale Global Warming". In: *Science* 274.5291, 1346 LP –1350. DOI: 10.1126/science.274.5291.1346.

Schlesinger, W. H. (1977). "Carbon Balance in Terrestrial Detritus". In: *Annual Review of Ecology and Systematics* 8.1, pp. 51–81. DOI: 10.1146/annurev.es.08.110177.000411. URL: https://doi.org/10.1146/annurev.es.08.110177.000411.

Schlosser, P., D. Bauch, R. Fairbanks, and G. Bönisch (1994). *Arctic river-runoff: mean residence time on the shelves and in the halocline*. Vol. 41, pp. 1053–1068. DOI: 10.1016/0967-0637(94)90018-3.

Seidel, M., M. Manecki, D. P. R. Herlemann, B. Deutsch, D. Schulz-Bull, K. Jürgens, and T. Dittmar (2017). "Composition and Transformation of Dissolved Organic Matter in the Baltic Sea". In: *Frontiers in Earth Science* 5.May, pp. 1–20. DOI: 10.3389/feart.2017.00031.

Seitzinger, S., J. A. Harrison, J. K. Böhlke, A. F. Bouwman, R. Lowrance, B. Peterson, C. Tobias, and G. V. Drecht (2006). "Denitrification across landscapes and waterscapes: A synthesis". In: *Ecological Applications* 16.6,

pp. 2064–2090. DOI: 10.1890/1051-0761(2006)016[2064:DALAWA]2.0.CO;2.

Seitzinger, S. P. and R. W. Sanders (1997). "Contribution of dissolved organic nitrogen from rivers to estuarine eutrophication". In: *Marine Ecology Progress Series* 159, pp. 1–12. ISSN: 01718630, 16161599.

Seitzinger, S. P., C Kroeze, A. F. Bouwman, N Caraco, F Dentener, and R. V. Styles (2002). "Global patterns of dissolved inorganic and particulate nitrogen inputs to coastal systems: Recent conditions and future projections". In: *Estuaries* 25.4, pp. 640–655. ISSN: 0160-8347. DOI: 10.1007/BF02804897. URL: https://doi.org/10.1007/BF02804897.

Seitzinger, S. P., J. A. Harrison, E. Dumont, A. H. W. Beusen, and A. F. Bouwman (2005). "Sources and delivery of carbon, nitrogen, and phosphorus to the coastal zone: An overview of Global Nutrient Export from Watersheds (NEWS) models and their application". In: *Global Biogeochemical Cycles* 19.4. DOI: 10.1029/2005GB002606.

Seitzinger, S. P. et al. (2010). "Global river nutrient export: A scenario analysis of past and future trends". In: *Global Biogeochemical Cycles* 24.4. DOI: 10.1029/2009GB003587.

Semiletov, I. P., N. E. Shakhova, I. I. Pipko, S. P. Pugach, A. N. Charkin, O. V. Dudarev, D. A. Kosmach, and S. Nishino (2013). "Spaceâ"time dynamics of carbon and environmental parameters related to carbon dioxide emissions in the Buor-Khaya Bay and adjacent part of the Laptev Sea". In: *Biogeosciences* 10.9, pp. 5977–5996. DOI: 10.5194/bg-10-5977-2013. URL: https://www.biogeosciences.net/10/5977/2013/.

Sharples, J., J. J. Middelburg, K. Fennel, and T. D. Jickells (2017). "What proportion of riverine nutrients reaches the open ocean?" In: *Global Biogeochemical Cycles* 31.1, pp. 39–58. DOI: 10.1002/2016GB005483.

Sigman, D. and M. Hain (2012). "The biological productivity of the Ocean," in: *Nature Education Knowledge* 3.10, p. 21. URL: https://www.nature.com/scitable/knowledge/library/the-biological-productivity-of-the-ocean-70631104.

Six, K. D. and E. Maier-Reimer (1996). "Effects of plankton dynamics on seasonal carbon fluxes in an ocean general circulation model". In: *Global Biogeochemical Cycles* 10.4, pp. 559–583. DOI: 10.1029/96GB02561.

Skogen, M. D., K. Eilola, J. L. Hansen, H. M. Meier, M. S. Molchanov, and V. A. Ryabchenko (2014). "Eutrophication status of the North Sea, Skagerrak, Kattegat and the Baltic Sea in present and future climates: A model study".

In: *Journal of Marine Systems* 132, pp. 174 –184. ISSN: "0924-7963". DOI: https://doi.org/10.1016/j.jmarsys.2014.02.004.

Smith, R. C., R. R. Bidigare, B. B. Prézelin, K. S. Baker, and J. M. Brooks (1987). "Optical characterization of primary productivity across a coastal front". In: *Marine Biology* 96.4, pp. 575–591. ISSN: 1432-1793. DOI: 10.1007/BF00397976. URL: https://doi.org/10.1007/BF00397976.

Smith, S. V. and J. T. Hollibaugh (1993). "Coastal metabolism and the oceanic organic carbon balance". In: *Reviews of Geophysics* 31.1, pp. 75–89. ISSN: 8755-1209. DOI: 10.1029/92RG02584. URL: https://doi.org/10.1029/92RG02584.

Søndergaard, M. and M. Middelboe (1995). "A cross-system analysis of labile dissolved organic carbon". In: *Marine Ecology Progress Series* 118.1/3, pp. 283–294. ISSN: 01718630, 16161599. URL: http://www.jstor.org/stable/24849785.

Song, H., J. Marshall, M. J. Follows, S. Dutkiewicz, and G. Forget (2016). "Source waters for the highly productive Patagonian shelf in the southwestern Atlantic". In: *Journal of Marine Systems* 158, pp. 120–128. ISSN: 0924-7963. DOI: https://doi.org/10.1016/j.jmarsys.2016.02.009.

Sørensen, H. L., B. Thamdrup, E. Jeppesen, S. Rysgaard, and R. N. Glud (2017). "Nutrient availability limits biological production in Arctic sea ice melt ponds". In: *Polar Biology* 40.8, pp. 1593–1606. ISSN: 1432-2056. DOI: 10.1007/s00300-017-2082-7.

St-Laurent, P, M. A. M. Friedrichs, R. G. Najjar, D. K. Martins, M Herrmann, S. K. Miller, and J Wilkin (2017). "Impacts of Atmospheric Nitrogen Deposition on Surface Waters of the Western North Atlantic Mitigated by Multiple Feedbacks". In: *Journal of Geophysical Research: Oceans* 122.11, pp. 8406–8426. ISSN: 2169-9275. DOI: 10.1002/2017JC013072. URL: https://doi.org/10.1002/2017JC013072.

Stallard, R. F. (1995). "Tectonic, Environmental, and Human Aspects of Weathering and Erosion: A Global Review using a Steady-State Perspective". In: *Annual Review of Earth and Planetary Sciences* 23.1, pp. 11–39. DOI: 10.1146/annurev.ea.23.050195.000303.

Stepanauskas, R, N. O. G. Jørgensen, O. R. Eigaard, A. Žvikas, L. J. Tranvik, and L. Leonardson (2002). "Summer Inputs of riverine nutrients to the Baltic Sea: bioavailability and eutrophication relevance". In: *Ecological Monographs* 72.4, pp. 579–597. ISSN: 0012-9615. DOI: 10.1890/0012-9615(2002)072[0579:SIORNT]2.0.CO;2.

Stevens, B. et al. (2013). "Atmospheric component of the MPIM earth system model: ECHAM6". In: *Journal of Advances in Modeling Earth Systems* 5.2, pp. 146–172. ISSN: 19422466. DOI: 10.1002/jame.20015.

Stramski, D., E. Boss, D. Bogucki, and K. J. Voss (2004). "The role of seawater constituents in light backscattering in the ocean". In: *Progress in Oceanography* 61.1, pp. 27–56. ISSN: 0079-6611. DOI: 10.1016/j.pocean.2004.07.001.

Stranne, C. et al. (2018). "Acoustic mapping of mixed layer depth". In: *Ocean Science* 14.3, pp. 503–514. DOI: 10.5194/os-14-503-2018. URL: https://www.ocean-sci.net/14/503/2018/.

Stumm, W. (1973). "The acceleration of the hydrogeochemical cycling of phosphorus". In: *Water Research* 7.1, pp. 131–144. ISSN: 0043-1354. DOI: https://doi.org/10.1016/0043-1354(73)90158-9. URL: http://www.sciencedirect.com/science/article/pii/0043135473901589.

Takahashi, T., S. B. Wallace, and S. Langer (1985). "Redfield ratio based on chemical data from isopycnal surfaces". In: *Journal of Geophysical Research: Oceans* 90.C4, pp. 6907–6924. ISSN: 0148-0227. DOI: 10.1029/JC090iC04p06907.

Tank, S. E., P. A. Raymond, R. G. Striegl, J. W. McClelland, R. M. Holmes, G. J. Fiske, and B. J. Peterson (2012). "A land-to-ocean perspective on the magnitude, source and implication of DIC flux from major Arctic rivers to the Arctic Ocean". In: *Global Biogeochemical Cycles* 26.4. DOI: 10.1029/2011GB004192.

Tao, Y., M. Wei, E. Ongley, L. Zicheng, and C. Jingsheng (2010). "Estuarine , Coastal and Shelf Science Long-term variations and causal factors in nitrogen and phosphorus transport in the Yellow River , China". In: *Estuarine, Coastal and Shelf Science* 86.3, pp. 345–351. ISSN: 0272-7714. DOI: 10.1016/j.ecss.2009.05.014.

Thomas, H, Y Bozec, H. J. W. de Baar, K Elkalay, M Frankignoulle, L.-S. Schiettecatte, G Kattner, and A. V. Borges (2005). "The carbon budget of the North Sea". In: *Biogeosciences* 2.1, pp. 87–96. DOI: 10.5194/bg-2-87-2005. URL: https://www.biogeosciences.net/2/87/2005/.

Thullner, M., A. W. Dale, and P. Regnier (2009). "Global-scale quantification of mineralization pathways in marine sediments: A reaction-transport modeling approach". In: *Geochemistry, Geophysics, Geosystems* 10.10. ISSN: 1525-2027. DOI: 10.1029/2009GC002484. URL: https://doi.org/10.1029/2009GC002484.

Tranvik, L. J. et al. (2009). "Lakes and reservoirs as regulators of carbon cycling and climate". In: *Limnology and Oceanography* 54.6part2, pp. 2298–2314. ISSN: 0024-3590. DOI: 10.4319/lo.2009.54.6_part_2.2298.

Tréguer, P. J. and C. L. De La Rocha (2013). "The World Ocean Silica Cycle". In: *Annual Review of Marine Science* 5.1, pp. 477–501. DOI: 10.1146/annurev-marine-121211-172346.

Trenberth, K. E. (1995). "Atmospheric circulation climate changes". In: *Climatic Change* 31.2, pp. 427–453. ISSN: 1573-1480. DOI: 10.1007/BF01095156.

Turi, G, Z Lachkar, N Gruber, and M Münnich (2016). "Climatic modulation of recent trends in ocean acidification in the California Current System". In: *Environmental Research Letters* 11.1, p. 14007. ISSN: 1748-9326. DOI: 10.1088/1748-9326/11/1/014007. URL: http://dx.doi.org/10.1088/1748-9326/11/1/014007.

Turner, R. E., N. N. Rabalais, D Justic', and Q Dortch (2003). "Global patterns of dissolved N, P and Si in large rivers". In: *Biogeochemistry* 64.3, pp. 297–317. ISSN: 1573-515X. DOI: 10.1023/A:1024960007569.

Turney, C. S. M. et al. (2017). "Tropical forcing of increased Southern Ocean climate variability revealed by a 140-year subantarctic temperature reconstruction". In: *Climate of the Past* 13.3, pp. 231–248. DOI: 10.5194/cp-13-231-2017. URL: https://www.clim-past.net/13/231/2017/.

Tyrrell, T. (1999). "The relative influences of nitrogen and phosphorus on oceanic primary production". In: *Nature* 400, pp. 525–531. DOI: 10.1038/22941.

Van Drecht, G, A. F. Bouwman, E. W. Boyer, P Green, and S Siebert (2005). "A comparison of global spatial distributions of nitrogen inputs for nonpoint sources and effects on river nitrogen export". In: *Global Biogeochemical Cycles* 19.4. ISSN: 0886-6236. DOI: 10.1029/2005GB002454. URL: https://doi.org/10.1029/2005GB002454.

Ver, L. M. B., F. T. Mackenzie, and A. Lerman (1999). "Carbon cycle in the coastal zone: effects of global perturbations and change in the past three centuries". In: *Chemical Geology* 159.1, pp. 283–304. ISSN: 0009-2541. DOI: https://doi.org/10.1016/S0009-2541(99)00042-X. URL: http://www.sciencedirect.com/science/article/pii/S000925419900042X.

Vodacek, A., N. V. Blough, M. D. DeGrandpre, M. D. DeGrandpre, and R. K. Nelson (2003a). "Seasonal variation of CDOM and DOC in the Middle Atlantic Bight: Terrestrial inputs and photooxidation". In: *Limnology and Oceanography* 42.4, pp. 674–686. DOI: 10.4319/lo.1997.42.4.0674. URL: https://aslopubs.onlinelibrary.wiley.com/doi/abs/10.4319/lo.1997.42.4.0674.

— (2003b). "Seasonal variation of CDOM and DOC in the Middle Atlantic Bight: Terrestrial inputs and photooxidation". In: *Limnology and Oceanography* 42.4, pp. 674–686. DOI: 10.4319/lo.1997.42.4.0674.

Volk, T and M. I. Hoffert (1985). "Ocean carbon pumps: analysis of relative strengths and efficiencies in ocean-driven atmospheric CO2 changes." In: *The carbon cycle and atmospheric CO₂: natural variations Archean to present. Chapman conference papers, 1984*, pp. 99–110.

"Inside Front Cover" (1992). In: ed. by R. A. Vollenweider, R Marchetti, and R. B.T.M.C. E. Viviani. Amsterdam: Elsevier, p. v. ISBN: 978-0-444-89990-3. DOI: https://doi.org/10.1016/B978-0-444-89990-3.50003-1. URL: http://www.sciencedirect.com/science/article/pii/B9780444899903500031.

Walsh, J. J. (1991). "Importance of continental margins in the marine biogeochemical cycling of carbon and nitrogen". In: *Nature* 350.6313, pp. 53–55. ISSN: 1476-4687. DOI: 10.1038/350053a0. URL: https://doi.org/10.1038/350053a0.

Wang, J., W. Yan, N. Chen, X. Li, and L. Liu (2015). "Modeled long-term changes of DIN:DIP ratio in the Changjiang River in relation to Chl-α and DO concentrations in adjacent estuary". In: *Estuarine, Coastal and Shelf Science* 166, pp. 153–160. ISSN: 0272-7714. DOI: https://doi.org/10.1016/j.ecss.2014.11.028.

Wang, Y. P., R. M. Law, and B. Pak (2010). "A global model of carbon, nitrogen and phosphorus cycles for the terrestrial biosphere". In: *Biogeosciences* 7.7, pp. 2261–2282. ISSN: 17264170. DOI: 10.5194/bg-7-2261-2010.

Wanninkhof, R et al. (2013). "Global ocean carbon uptake: magnitude, variability and trends". In: *Biogeosciences* 10.3, pp. 1983–2000. DOI: 10.5194/bg-10-1983-2013.

Weaver, A. J. et al. (2001). "The UVic earth system climate model: Model description, climatology, and applications to past, present and future climates". In: *Atmosphere-Ocean* 39.4, pp. 361–428. DOI: 10.1080/07055900.2001.9649686. URL: https://doi.org/10.1080/07055900.2001.9649686.

Wolf-Gladrow, D., R. Zeebe, C. Klaas, A. Körtzinger, and A. G. Dickson (2007). "Total alkalinity: the explicit conservative expression and its application to biogeochemical processes". In: *Marine Chemistry* 106, pp. 287–300. DOI: 10.1016/j.marchem.2007.01.006.

Wollast, R (1998). "Evaluation and comparison of the global carbon cycle in the coastal zone and in the open ocean". In: *The Sea* 10.

Wollast, R. and L. Chou (1998). "Distribution and Fluxes of Calcium Carbonatealong the Continental Margin in the Gulf of Biscay". In: *Aquatic Geochemistry* 4.3, pp. 369–393. ISSN: 1573-1421. DOI: 10.1023/A:1009640432692.

Woodroffe, C. D., J. W. Farell, F. R. Hall, and H. P. T. (2017). "Calcium Carbonate Production and Contribution to Coastal Sediments". In: *The First Global Integrated Marine Assessment: World Ocean Assessment I*, pp. 149–158. DOI: DOI:10.1017/9781108186148.010. URL: https://www.cambridge.org/core/books/first-global-integrated-marine-assessment/calcium-carbonate-production-and-contribution-to-coastal-sediments/6AED797D40D9EDBE6C080AFCB9C093B7.

Yan, W., S. Zhang, P. Sun, and S. P. Seitzinger (2003). "How do nitrogen inputs to the Changjiang basin impact the Changjiang River nitrate: A temporal analysis for 1968–1997". In: *Global Biogeochemical Cycles* 17.4. ISSN: 0886-6236. DOI: 10.1029/2002GB002029. URL: https://doi.org/10.1029/2002GB002029.

Yang, S. and N. Gruber (2016). "The anthropogenic perturbation of the marine nitrogen cycle by atmospheric deposition: Nitrogen cycle feedbacks and the 15N Haber-Bosch effect". In: *Global Biogeochemical Cycles* 30.10, pp. 1418–1440. ISSN: 0886-6236. DOI: 10.1002/2016GB005421. URL: https://doi.org/10.1002/2016GB005421.

Yasuda, I., S. Kouketsu, K. Katsumata, M. Ohiwa, Y. Kawasaki, and A. Kusaka (2002). "Influence of Okhotsk Sea Intermediate Water on the Oyashio and North Pacific Intermediate Water". In: *Journal of Geophysical Research: Oceans* 107.C12, pp. 11–30. ISSN: 0148-0227. DOI: 10.1029/2001JC001037. URL: https://doi.org/10.1029/2001JC001037.

Yoshimura, C., M. Zhou, A. S. Kiem, K. Fukami, H. H. A. Prasantha, H. Ishidaira, and K. Takeuchi (2009). "Science of the Total Environment 2020s scenario analysis of nutrient load in the Mekong River Basin using a distributed hydrological model". In: *Science of the Total Environment, The* 407.20, pp. 5356–5366. ISSN: 0048-9697. DOI: 10.1016/j.scitotenv.2009.06.026.

Álvarez, E., J. Zanella, A. Pescio, and W. Dragani (2016). "An estimation of the effect of a possible wind speed increase on the ocean mixed layer depth at the northern Patagonian continental shelf". English. In: *Regional Studies in Marine Science* 6.Complete, pp. 87–95. DOI: 10.1016/j.rsma.2016.03.004.

Acknowledgements

I would first like to thank to thank my supervisors Dr. Tatiana Ilyina and Prof. Pierre Regnier for their support and feedbacks. I thank the ocean biogeochemistry group of the Max Planck Institute for Meteorology and the Biogeochemistry and Modeling of the Earth System at the Université Libre de Bruxelles, in particular Dr. Katharina Six, Irene Stemmler and Goulven Laruelle for their close support and vast inputs of ideas. I would like to thank Prof. Jochem Marotzke for enabling my stay at the Max Planck Institute for Meteorology and benefiting from the great infrastructure of the institute.

I thank all of the C-CASCADES network, in particular the project Chair Prof. Pierre Regnier and the Early Stage Researchers. I really enjoyed the time spent together (even sharing rooms) and the trainings and conferences inspired many of my ideas.

I would like to thank the company football group, our lunch squash group and the whole Elbstrand beachvolleyball group for keeping me fresh and great sport sessions.

I would like to thank my parents Prof. Christophe Lacroix and Dr. Janice Sych for supporting and motivating me throughout my thesis with their immense scientific experience.

Eidesstattliche Versicherung / *Declaration on oath*

Hiermit erkläre ich an Eides Statt, dass ich die vorliegende Dissertationsschrift selbst verfasst und keine anderen als die angegebenen Quellen und Hilfsmittel benutzt habe.

I hereby declare, on oath, that I have written the present dissertation by my own and have not used other than the acknowledged resources and aids.

Hamburg _____ Unterschrift / Signature _____

(Datum / Date)

Hinweis / Reference

Die gesamten Veröffentlichungen in der Publikationsreihe des MPI-M
„Berichte zur Erdsystemforschung / Reports on Earth System Science“,
ISSN 1614-1199

sind über die Internetseiten des Max-Planck-Instituts für Meteorologie erhältlich:
http://www.mpimet.mpg.de/wissenschaft/publikationen.html

All the publications in the series of the MPI -M
„Berichte zur Erdsystemforschung / Reports on Earth System Science“,
ISSN 1614-1199

are available on the website of the Max Planck Institute for Meteorology:
http://www.mpimet.mpg.de/wissenschaft/publikationen.html